INCIPIENT MOTION OF ARMORFLEX ARTICULATING CONCRETE BLOCKS ON STEEP SLOPES

by
Kobus Delport

Thesis presented in fulfilment of the requirements for the degree of Master of Engineering in the Faculty of Engineering at Stellenbosch University

Supervisor: Prof. G.R. Basson
Co-supervisor: Mrs. A. Bosman

December 2019

Declaration

By submitting this thesis electronically, I declare that the entirety of the work contained therein is my own, original work, that I am the sole author thereof (save to the extent explicitly otherwise stated), that reproduction and publication thereof by Stellenbosch University will not infringe any third party rights and that I have not previously in its entirety or in part submitted it for obtaining any qualification.

December 2019

Kobus Delport

ABSTRACT

Armorflex is an articulating concrete block erosion protection measure that has been used as an alternative to riprap (dumped rock) for many years. Even though extensive research and hydraulic testing have been conducted on Armorflex, the principal constraint on the use of concrete blocks has been the lack of information on prototype performance. Furthermore, there are no standards for Armorflex or articulating concrete block revetments in SANS.

The aim of this study is to improve the understanding of the critical flow conditions under which Armorflex blocks are lifted up and removed by flowing water in open channel flow applications. Armorflex 140 and Armorflex 180 blocks are studied in particular.

Liu's theory (1957) of incipient motion is of primary interest and is applied in an attempt to define the point where block movement is initiated. Scaled laboratory tests were conducted to determine whether Liu's theory holds for Armorflex blocks. For particle Reynolds numbers between 11025 and 131397, the results from the study indicate respective Movability Numbers of 0.249 and 0.220 for Armorflex 140 and 180 installed on bed slopes. Dimensionless stability factors of 1.47 and 1.33 can respectively be applied to Armorflex 140 and 180 blocks installed on side slopes.

The results from the laboratory tests were compared with the manufacturer design guidelines of Technicrete (2016) and Contech Construction Products inc. (Armortec Incorporated, 1981). Technicrete (2016) provides a maximum desired slope of 1V:1.5H and limiting flow velocities only, while Contech Construction Products inc. (Armortec Incorporated, 1981) includes flow velocities and hydraulic radius at varying bed slopes as limiting parameters.

The results proposed that Technicrete's respective limiting flow velocities of 3.5 m/s and 5.5 m/s for Armorflex 140 and 180 blocks may be an overestimation for blocks installed on bed slopes. On side slopes, however, failure was observed at flow velocities similar to the limits stated by Technicrete. Comparing the laboratory findings to the limiting velocity guideline of Contech Construction Products inc. (Armortec Incorporated, 1981), no block failures were achieved at flow velocities lower than the design guideline velocities. According to incipient motion theory, however, flow velocity is not a suitable parameter for defining incipient motion. Therefore, the limiting flow velocity guidelines of Technicrete (2016) and Contech Construction Products inc. (Armortec Incorporated, 1981) alone cannot be used to design Armorflex lined structures in practice. Instead, this thesis recommends the use of Liu's Movability Number to determine the point of incipient motion of Armorflex. The results from the study were used to develop a Microsoft Excel model for the safe design of Armorflex-lined drainage channels.

The Movability Numbers of Armorflex blocks obtained in this study are greater than the Movability Numbers recommended by researchers for riprap (dumped rock) and Reno-mattresses. Unlike riprap and Reno-mattresses, Armorflex has no particles smaller than the design weight that can be washed away by forces of flowing water, undermining the larger particles. The Movability Numbers presented in this thesis are also greater than Rooseboom & van Vuuren's (2013) recommended Movability Number of 0.12 for articulating concrete blocks.

OPSOMMING

Armorflex is ‘n metode wat as ‘n alternatief vir stortklip vir baie jare gebruik word om erosie te voorkom. Ondanks die omvattende navorsing en hidrouliese toetse was reeds op Armorflex gedoen is, bly daar steeds ‘n mate van onsekerheid in die limiete van Armorflex in kanaalvloei toepassings. Boonop is daar geen standaarde wat gespesifiseer is vir die gebruik van Armorflex in SANS nie.

The hoofdoelwit van hierdie studie is om die kritieke faktore wat beweging van Armorflex-blokke in kanaalvloei toepassings veroorsaak, beter te verstaan. Armorflex 140 en Armorflex 180 word spesifiek bestudeer.

Verskillende metodes wat die begin van beweging voorspel en beskryf word ondersoek, met Liu se teorie van 1957 wat van spesifieke belang is. Geskaalde laboratoriumtoetse is gedoen om die toepaslikheid van Liu se teorie op Armorflex-blokke te bepaal. Vir partikel Reynolds getalle tussen 11025 en 131397, dui die resultate van die studie op Mobiliteitsgetalle van 0.249 en 0.220 vir Armorflex 140 en 180 op bodemhellings. ‘n Dimensielose stabiliteitsfaktor van 1.47 en 1.33 kan onderskeidelik op Armorflex 140 en 180 toegepas word vir blokke op kanthellings.

Die resultate verkry vanaf die laboratoriumtoetse is vergelyk met die ontwerpriglyne van die Armorflex vervaardigers Technicrete (2016) en Contech Construction Products inc. (Armortec Incorporated, 1981). Die Armorflex produkbrosjure van Technicrete (2016) bied ‘n maksimum helling van 1V:1.5H en vloeisnelheidslimiete as ontwerpriglyne, terwyl Contech Construction Products inc. (Armortec Incorporated, 1981) vloeisnelheid asook hidrouliese radius by verskillende bodemhellings gebruik om die limiete van Armorflex te beskryf.

Die resultate van die studie toon dat Technicrete se ontwerpriglyne van 3.5 m/s en 5.5 m/s vir Armorflex 140 en 180 blokke moontlik oorgeskatte waardes is vir blokke op bodemhellings. Blokke op kanthellings het wel kritiese vloeisnelhede getoon wat soortgelyk is aan die limiete van Technicrete. Die vergelyking van die laboratoriumtoetsresultate met die ontwerpriglyne van Contech Construction Products inc. (Armortec Incorporated, 1981) toon dat geen blokfalings bereik is teen vloeisnelhede laer as die ontwerpriglyne nie. Literatuur toon dat vloeisnelheid nie ‘n gepaste parameter is om die voorwaardes vir beweging van kohesielose partikels te voorspel nie. Die Armorflex ontwerpriglyne van Technicrete (2016) en Contech Construction Products inc. (Armortec Incorporated, 1981) in terme van ‘n maksimum vloeisnelheid alleen kan dus nie gebruik word vir die ontwerp van Armorflex strukture nie. Hierdie tesis skryf Liu se Mobiliteitsgetal voor as die gekose metode om die punt van beweging

van Armorflex-blokke te bepaal. Die resultate van die studie is gebruik om ‘n Microsoft Excel model te ontwikkel vir die veilige ontwerp van Armorflex kanale.

Die berekende Mobiliteitsgetalle van Armorflex-blokke is hoër as die Mobiliteitsgetalle van stortklip en Reno-matrasse wat deur navorsers voorgeskryf word. Anders as Armorflex, bevat stortklip en Reno-matrasse partikels wat kleiner is as die ontwerpsgrootte wat makliker weggespoel kan word deur vloeiende water en wat moontlik kan lei tot die ondermyning van die groter partikels. Die Mobiliteitsgetalle voorgestel in hierdie tesis is ook hoër as Rooseboom & van Vuuren (2013) se Mobiliteitsgetal van 0.12 vir betonblokkanale.

ACKNOWLEDGEMENTS

Firstly, I would like to thank my God and Saviour, Jesus Christ, for covering me in His righteousness so that I could have everlasting life, not because of what I have done, but because of what He did.

Furthermore, I would like to thank the following people who helped to make this thesis possible:

- My wife Joanie, for her love and patience throughout my time of studying part-time. Many long nights and weekends were sacrificed. Thank you for being my helper.
- My employer, AECOM SA, for the financial support in funding my studies, as well as for their understanding and consideration with regards to study leave.
- Professor Gerrit Basson of the Civil Engineering Department at the University of Stellenbosch, for his assistance and guidance throughout the execution of this thesis.
- Mrs. Adele Bosman of the Civil Engineering Department at the University of Stellenbosch, for her guidance throughout and for reviewing this thesis.
- Ning Ma, “oom” Johann Nieuwoudt and the rest of the laboratory staff, for their efforts in the construction of the various test channel setups.
- Mr. Eddie Bosman, retired lecturer from the University of Stellenbosch, for his assistance with the analyses and processing of the results.
- Mr. Marius Cloete, from Badger Moulds, for the manufacturing of the polyurethane moulds in which the model Armorflex blocks were cast. The precision with which the moulds were made allowed for consistent block shape and volume throughout the manufacturing of the scaled blocks.

TABLE OF CONTENTS

LIST OF FIGURES

LIST OF TABLES

LIST OF ABBREVIATIONS, SYMBOLS AND ACRONYMS

A_p = Exposed surface area of particle (m^2)

a = Longest dimension of a particle (m)

a_θ = Coefficient of the weight force acting in the direction normal to the side-slope plane

B = Width at water surface (m)

C = Chezy coefficient ($m^{1/2}/s$)

C_D = Drag force coefficient

C_r = Stability coefficient varying with turbulence intensity

C_{st} = Stability coefficient for rock

C_T = Blanket thickness coefficient

C_v = Velocity distribution coefficient

c = Cohesion

c' = Effective cohesion

D = Depth of flow (m)

d = Particle diameter (mean- or median diameter) (m)

d_{50} = Median sieve size (m)

d_m = Maximum flow depth at uniform flow condition (m)

d_n = Block thickness (m)

d_s = Surface area equivalent sphere diameter (m)

d_v = Volume-equivalent sphere diameter (m)

d_y = Sieve size of particle that exceeds y% of stone size (m)

EGL_i = Energy grade line elevation at station i in a defined channel (m)

F_D = Drag force (kg)

$F_{D,cr,\beta}$ = Critical drag force for longitudinal slope (N)

$F_{D,cr,\gamma}$ = Critical drag force for transverse slope (N)

$F_{D,cr,0}$ = Critical drag force for a horizontal bed (N)

F_D' = Additional drag force (kg)

F_L = Lift force (kg)

F_L' = Additional lift force (kg)

f = Darcy-Weisbach friction factor

f_g = Grading width, gradation factor

g = Gravitational acceleration (m/s^2)

H_s = Significant wave height or the average wave height of the highest third of waves in a given period (m)

H_i = Maximum wave height (m)

h_i = Water-surface elevation at station i in a defined channel (m)

Δh = Change in water level (m)

I_r = Iribarren number

i = Station number in a defined channel (1, 2, 3, etc.)

K = Von Karman's constant = 0.4 for clear water

K_b = Bend coefficient

K_h = Depth factor

K_T = Turbulence factor

K_w = Wave amplification factor

k_h = Velocity profile factor

k_s = Chezy's roughness coefficient (m)

k_{sl} = Side slope factor

k_t = Turbulence amplification factor

k_β = Ratio of the critical drag force for any longitudinal slope to the critical drag force for a horizontal bed

k_γ = Ratio of the critical drag force for any transverse slope to the critical drag force for a horizontal bed

L = Length of the control volume along slope (m)

l_x = Block specific moment arms (m)

l_{xT} = Moment arms of tested block (m)

l_{xU} = Moment arms of untested block (m)

l_1 = Moment arm for the submerged weight force component parallel to the side-slope plane (m)

l_2 = Moment arm for the submerged weight force component normal to the side-slope plane (m)

l_3 = Moment arm for the drag force component along the path of motion (m)

l_4 = Moment arm for the lift force (m)

m = Number of particles displaced

N = Total number of surface particles across sample area

n = Porosity of the revetment, i.e. the open area of the blocks (25% open area: n = 0.25)

n_l = Ratio of applied unit stream power to unit stream power required to suspend a particle in a laminar boundary

n_t = Ratio of applied unit stream power to unit stream power required to suspend a particle in a turbulent boundary

P_a = Unit stream power applied

$P_{a(l)}$ = Applied unit stream power in the linear layer (W/m^3)

$P_{a(t)}$ = Applied unit stream power in the log-law layer (W/m³)

P_{avg} = Average stream power

P_d = Unit stream power dissipated

P_r = Unit stream power required

p = Porosity of rock particle

Q = Total discharge (m³/s)

$Q_{p,i}$ = Discharge at specific station in a defined channel (m³/s)

q = Unit discharge (m³/s per meter width)

R = Hydraulic radius (m)

R_b = Centreline radius of curvature/bend (m)

R_{ed} = Particle fall Reynolds number

R_e^* = Particle Reynolds number

r = Turbulence intensity

S = Energy gradient in direction of flow (m/m)

S_f = Energy grade line slope (m/m)

$S_{f,i}$ = Energy grade line slope at station i in a defined channel (m/m)

S_r = Degree of saturation

S_w = Water surface slope (m/m)

S_o = Bed slope (m/m)

SF = Shape Factor

SF_B = Base factor of safety

SF_T = Target factor of safety

TI = Transport intensity (s^{-1})

T_z = Wave period

t = Time interval (s)

u = Pore water pressure

V = Local flow velocity (m/s)

V_{avg} = Average velocity (m/s)

V_b = Bed velocity (m/s)

V_{cr} = Critical flow velocity (m/s)

$V_{cr,avg}$ = Average critical flow velocity (m/s)

V_d = Depth-averaged velocity (m/s)

V_i = Flow velocity at station i in a defined channel (m/s)

$V_{p,i}$ = Average of point flow velocities measured at 20%, 60% and 80% of flow depth or, where three velocity measurements are not available, the point flow velocity at 60% of flow depth (m/s)

V_{ss} = Particle settling velocity (m/s)

V^* = Shear velocity (m/s)

$V_{0,cr,0}$ = Critical bed shear velocity on a sloped bed (m/s)

$V_{0,cr}$ = Critical bed shear velocity on a horizontal bed (m/s)

V_L' = Longitudinal turbulent velocity component (m/s)

V_V' = Vertical turbulent velocity component (m/s)

$W_{S,U}$ = Submerged weight of untested block (kg)

$W_{S,T}$ = Submerged weight of tested block (kg)

W_s = Submerged weight of block (kg)

w = Width of the projecting surface normal to the direction of flow (m)

X_C = Multiplier based on consequence of failure

X_M = Multiplier based on hydraulic model uncertainty

y = Flow depth (m)

y_i = Flow depth at station i in a defined channel (measured perpendicular to embankment) (m)

y_t = Water depth at the toe of the bank (m)

y_0 = Reference level near the bed (m)

ΔZ = Height of the projecting surface normal to the direction of flow (m)

z = Shortest dimension of a particle (m)

z_i = Bed elevation at station i in a defined channel (m)

β = Longitudinal slope (in the direction of flow in a channel or river)

Δ = Relative submerged density = $\frac{\rho_s - \rho}{\rho}$

γ = Transverse slope (normal to the direction of flow) (degrees)

Λ_h = Velocity profile factor

λ = Darcy coefficient

μ = Dynamic viscosity of water (Pa.s)

ν = Kinematic viscosity of water = 1.13 x 10^{-6} m²/s at 15˚C

Φ = Angle of repose of particle (degrees)

φ_f = Angle of internal friction (degrees)

φ_f' = Effective angle of internal friction (degrees)

φ_s = Stability correction factor

ψ = Shields's parameter

ψ_{cr} = Critical Shields's parameter

ψ_s = Slope correction factor

ρ = Fluid density (kg/m³)

ρ_r = Rock density (kg/m³)

ρ_s = Particle density (kg/m³)

σ_n = Normal stress (Pa)

σ'_n = Effective normal stress (Pa)

τ_{des} = Design shear stress (kg/m²)

τ_0 = Bed shear stress (Pa)

$\tau_{0,cr}$ = Critical bed shear stress on a given sloped bed (Pa)

$\tau_{0,cr,0}$ = Critical bed shear stress on a horizontal bed (Pa)

τ_{cr} = Critical bed shear stress (Pa)

$\tau_{cr,T}$ = Critical shear stress for tested block (kg/m²)

$\tau_{cr,U}$ = Critical shear stress for untested block (kg/m²)

τ_{cr,θ_T} = Critical shear stress for tested bed slope (kg/m²)

τ_{cr,θ_U} = Critical shear stress for untested bed slope (kg/m²)

τ' = Effective shear strength (Pa)

θ = Resulting angle of the combined weight force components acting in the side-slope plane measured from a vertical line projected onto the side-slope plane

θ_T = Tested bed slope (degrees)

θ_U = Untested bed slope (degrees)

1. INTRODUCTION

1.1 Problem statement

Many hydraulic engineering projects demand the design and construction of measures to combat possible erosion of sections of a watercourse. Revetments lessen or prevent soil erosion by reducing the hydraulic load imposed on the soil. Some of the most popular erosion protection systems for channel beds and banks include riprap, gabions, Reno-mattresses, concrete linings, articulating concrete blocks (ACB's), soil reinforcement systems and stone pitching.

Riprap and Reno-mattresses have been extensively researched and tested by many renowned researchers. As an alternative to riprap in low- to intermediate energy wave environments, ACB's have widely been used for many years (Leidersdorf, et al., 1988). Extensive research and physical model testing have previously been conducted on ACB's (Armorflex in particular) for overtopping flow applications. However, there are no SANS standards for Armorflex or ACB revetments.

Technicrete, a manufacturer of Armorflex blocks in South Africa, provides the following design guidelines of Armorflex revetments (Technicrete, 2016):

- Slope limits:
  - Angle of repose of in-situ material should not be exceeded;
  - Maximum desired slope = 1V:1.5H (but never exceeding the angle of repose of the in situ material)
- Armorflex 140 maximum flow velocity = 3.5 m/s; and
- Armorflex 180 maximum flow velocity = 5.5 m/s.

Technicrete (2016) does not specify which slope the maximum desired slope of 1V:1.5H refers to, either longitudinal- or side slope.

Contech Construction Products inc., another manufacturer of Armorflex, also uses maximum flow velocity as a limiting condition for block movement but does so for a range of different bed slopes. Additional to flow velocity, Contech Construction Products inc. includes the hydraulic radius of flow in a trapezoidal channel at various bed slopes as another limiting condition of Armorflex (Armortec Incorporated, 1981). These design guidelines were developed for Armorflex Class 30 blocks, which are similar but not identical to Armorflex 180 blocks.

Neither of the abovementioned manufacturers of Armorflex refers to Froude number nor Movability Number. A limiting velocity alone does not allow the designer of any revetment system to make positive claims regarding the stability of the revetment against erosion. There is, therefore, a high level of uncertainty in the performance of Armorflex ACB's in channelized applications, especially on channel side slopes.

Figure 1-1 shows an Armorflex 180 revetment structure that failed under hydraulic loading in a channel, resulting in the blocks being washed out.

Figure 1-1: Armorflex 180 washed out by flow (Photograph by Justin Kretzmar, Technicrete)

Figure 1-2 shows an Armorflex revetment that failed under overtopping flow conditions downstream of a weir. Technicrete reported that the revetment ended too short and, due to high turbulence flow in the area, the subgrade below the blocks washed away.

Figure 1-2: Overtopping flow failure of Armorflex revetment downstream of a weir (Photograph by Justin Kretzmar, Technicrete)

1.2 Objectives of the study

Given the problem statement in Section 1.1, the objectives of this study were to:

i. Provide reliable limiting conditions for Armorflex blocks in channelized applications;
ii. Review the design guidelines of Armorflex manufacturers Technicrete (2016) and Contech Construction Products inc. (Armortec Incorporated, 1981);
iii. Investigate the use of the modified Liu Diagram for determining when Armorflex blocks would be lifted up and removed by flowing water in channelized applications; and
iv. Compare the findings of the study to the design guidelines for riprap and Reno-mattresses in terms of Movability Number.
v. Develop a dimensionless stability factor which can be applied when designing for Armorflex revetments at steep side slopes in channelized applications.
vi. Develop a Microsoft Excel model that can be used for the safe design of Armorflex-lined channels.

1.3 Study limitations

The limitations of this study are as follows:

- The maximum discharge capacity of the hydraulics laboratory was just under 600 L/s, which ruled out the possibility of full scale (prototype) testing. A scale factor of 1:3 was used.
- This study is only applicable to cellular Armorflex blocks, specifically Armorflex 140 and Armorflex 180.
- This study is limited to fully turbulent flow conditions with Reynolds numbers > 3000.
- This study is limited to particle Reynolds numbers (Re*) ranging between 11025 and 131397.
- The test channel sidewall is not included in the calculation of the wetted perimeter and its roughness is therefore ascribed to the rougher area that is lined with Armorflex blocks.
- This study is limited to a bed slope range of 1V:30H to 1V:10H and a side slope of 1V:1.5H.
- No slope correction factors were applied to the recommended Movability Numbers for Armorflex 140 and 180 as the angle of repose of Armorflex blocks was not determined. The determination of the angle of repose of Armorflex blocks is recommended for future incipient motion studies on Armorflex blocks.

1.4 Report structure

The report is divided into four parts:

i. Part 1 (Chapter 2) entails the literature study. This chapter includes a review of incipient motion theory, a study of Armorflex ACB's and a discussion on the relevant previous performance testing studies conducted on Armorflex ACB's. Furthermore, the literature study includes a brief review of the physical characteristics and design guidelines of riprap and Reno-mattresses. The chapter ends with a summary and a list of conclusions drawn from the literature study.

ii. Part 2 (Chapter 3) presents the physical model study, scale effects, test channel setup and testing methodology.

iii. Part 3 (Chapter 4) presents the physical model data analysis that includes the laboratory data, the data analysis and the incipient motion criteria of Armorflex. The chapter also includes a comparison of the results with design guidelines of Armorflex manufacturers and the comparison of the recommended Movability Numbers with those for riprap and Reno-mattresses.

iv. Part 4 (Chapters 5 and 6) presents the general conclusions drawn from the study and a list of recommendations for future studies.

2. LITERATURE STUDY

One of the main objectives of this study is providing reliable limiting flow conditions for Armorflex blocks in channelized applications. As incipient motion refers to some threshold of motion, i.e. the boundary condition between one state of affairs and another, an investigation into incipient motion theory is appropriate.

The physical characteristics of Armorflex are presented, together with a discussion on the previous hydraulic testing and manufacturer design guidelines of Armorflex. The literature study includes a section on the design guidelines of riprap and Reno-mattress revetments as these guidelines are compared to the findings from this study conducted on Armorflex.

2.1 Incipient Motion Theory

Many renowned researchers in the field of particle movement, such as Armitage (2002), Rooseboom (1992) and Yang (1973), have done ample studies examining the incipient motion theories most commonly used by design engineers. In this section, these incipient motion theories are reviewed, concluding with a recommendation of the preferred theory.

2.1.1 Types- and intensities of motion

“Motion” in the term “incipient motion” can occur in the form of sliding, rolling, saltating (hop/leap) and suspension. Generally, particles slide and roll before saltating, and saltate before being carried into suspension (Armitage & McGahey, 2003).

According to Vanoni (1975), Kramer (1935) defined three intensities of particle motion:

i. Weak movement: The few particles in motion can be counted.
ii. Medium movement: Particles of mean diameter begin to move; impossible to count moving particles; bed configuration remains unaffected.
iii. General movement: The movement of a whole mixture of particles, including the largest particles, occurring everywhere and at all times.

Henderson (1966) argued that there is no point at which movement suddenly becomes general. Rather, particle movement gradually becomes more frequent until it is general over the whole bed.

2.1.2 Physical characteristics influencing particle movement

The physical characteristics of the particle under consideration are studied in this section. These physical characteristics include particle size, shape, uniformity, settling velocity,

cohesiveness and angle of repose, all of which greatly affects particle movement and the prediction thereof.

2.1.2.1 Particle size

Particle size is perhaps the most important parameter when defining incipient motion (Stoffberg, 2005). Smaller particles are generally washed away more easily than larger sized particles. Particle density, and in effect its weight, greatly impacts the chances of a particle washing away.

2.1.2.2 Particle shape

Even though sediment theory commonly assumes particles to be spherical in shape, in reality it is not the case. Tests performed at the Delft Hydraulics Laboratory in The Netherlands argued that no direct relationship between particle shape and threshold velocity exists (Pilarczyk, 1984). Armitage and McGahey (2003), on the other hand, argued that the shape of a particle greatly affects its drag coefficient. According to Abt & Johnson (1991) and Robinson, et al. (1998), the shape of a particle can impact its movability by as much as 40%. The shape of a particle is defined by a suitable shape factor (S_p) indicating its deviation from the spherical. The most common shape factor is that of Corey (Schulz, et al., 1954):

$$S_p = \frac{c}{\sqrt{ab}} \qquad \text{Equation 2.1}$$

Where:

a = Longest dimension (m)

c = Shortest dimension (m).

A perfect sphere has a shape factor of 1. However, a cube also has a shape factor of 1. Therefore, Equation 2.2 was altered to account for the diameter of the sphere (d_s) having the same surface area as that of the particle, and the diameter of the sphere (d_v) having the same volume as that of the particle (Armitage & McGahey, 2003):

$$SF = \frac{d_s c}{d_v \sqrt{ab}} \qquad \text{Equation 2.2}$$

Round particles have less interlocking ability compared to angular particles. Long flat particles are generally considered less stable than particles that have similar dimensions of a, b and c (Langmaak, 2013).

2.1.2.3 Uniformity of material

Uniformity is the distribution of particle sizes. By means of a simple sieve analysis, statistical parameters such as the median diameter (d_{50}), mean diameter ($\bar{d}$), standard deviation (σ), and skewness can be determined (Armitage & McGahey, 2003). The grading of rocks for use in riprap and Reno-mattress structures are discussed in Section 2.3.1.2.

2.1.2.4 Settling velocity

The settling velocity (or fall velocity) is the average velocity achieved by a particle falling alone in quiescent distilled water of infinite extent. Settling velocity is influenced by the particle size, -shape, -surface roughness and -density, as well as the density and viscosity of the fluid (Armitage & McGahey, 2003). Settling velocity is defined by the following equation (Raudkivi, 1998):

$$V_{ss} = \sqrt{\frac{4}{3}\left(\frac{\rho_s - \rho}{\rho}\right)\frac{gd}{C_D}} \qquad \text{Equation 2.3}$$

Where:

V_{ss} = Particle settling velocity (m/s)

ρ_s = Particle density (kg/m³)

ρ = Fluid density (kg/m³)

g = Gravitational acceleration (m/s²)

d = Particle diameter (mean- or median diameter can be used) (m)

C_D = Drag coefficient.

The term $\frac{\rho_s - \rho}{\rho}$ is defined as the relative submerged density, Δ.

The accurate determination of the drag coefficient makes Equation 2.3 difficult to compute. Drag coefficient is a function of particle shape and the particle fall Reynolds number, R_{ed} which is defined by Equation 2.4 (Armitage & McGahey, 2003):

$$R_{ed} = \frac{V_{ss}d}{\nu} \qquad \text{Equation 2.4}$$

Where:

ν = Kinematic viscosity of water = 1.13 x 10^{-6} m²/s at 15˚C

Figure 2-1 is a graph adapted from Concha (2009), which affirms that particle movement is indeed influenced by particle shape. As illustrated in Figure 2-1, Concha (2009) presents C_D values between 0.4 and 2 for $R_{ed} > 10^3$, depending on the particle shape. For spheres, the drag coefficient is high at low values of R_{ed}, drops promptly as R_{ed} rises to about 10^3 (indicated

by the blue line), after which it remains constant until R_{e_d} equals 10^5. For a perfect sphere, C_D equals 0.45 over a range of $10^3 < R_{e_d} < 10^5$ (Armitage & McGahey, 2003). Several researchers found that non-spherical particles rotate and vibrate at large Reynolds numbers, causing complex interactions between the particle and the water, which affects the velocity of the particle (Concha, 2009; Simons & Sentürk, 1992).

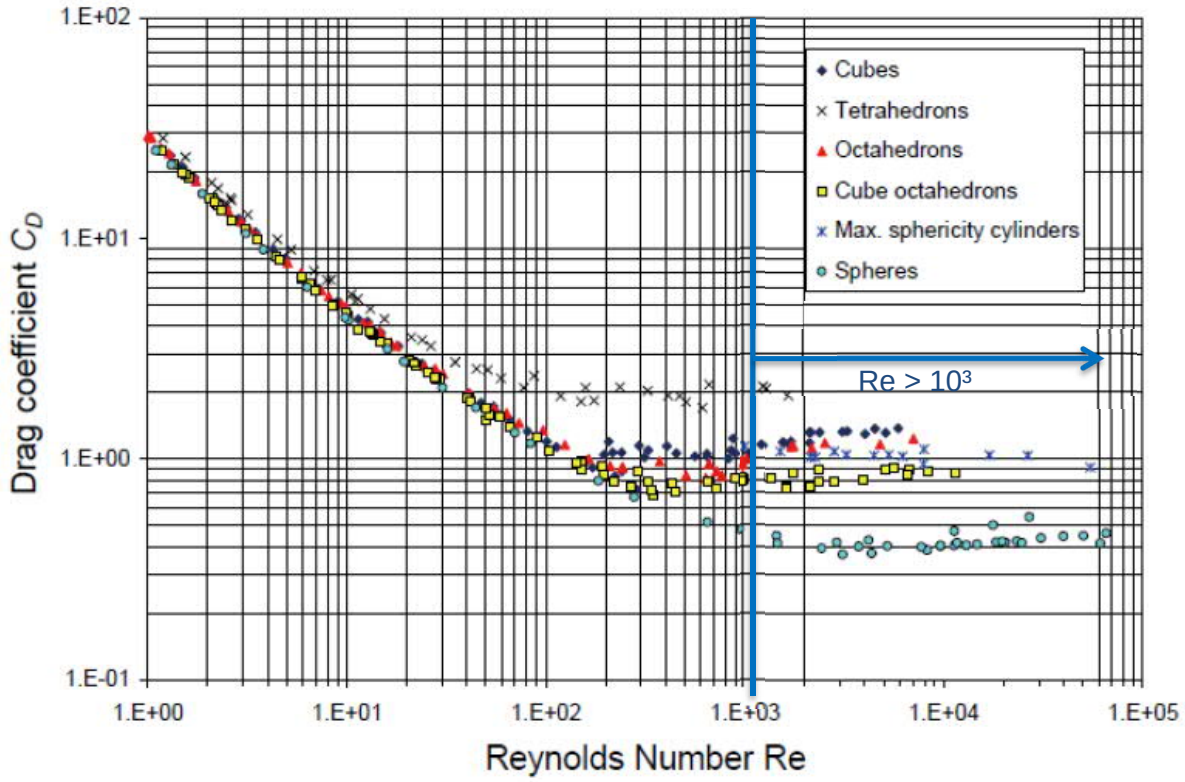

Figure 2-1: Drag coefficient versus Reynolds number (adapted from Concha, 2009)

2.1.2.5 Cohesiveness of material

Material can either be cohesive or non-cohesive. The weight of non-cohesive particles is the dominant force in determining its movability (Armitage & McGahey, 2003). This thesis, being a study on Armorflex blocks, focusses on non-cohesive particles.

2.1.2.6 Angle of repose

Incipient motion is obtained when the particle centre of mass is vertically above the point of contact. The angle of repose (φ) can be defined as the maximum angle to the horizontal at which an unsupported heap of material would stand. The critical angle of repose is the angle at which motion starts to occur. Julien (2010) argued that the angle of repose increases with particle angularity. Rooseboom & van Vuuren (2013) affirmed Julien's theory by presenting a

plot of the angle of repose (referred to as “slope angles”) for a given particle angularity and particle size.

2.1.2.7 Other factors influencing particle movement

Armitage (2002) lists some other factors that could influence the movement of a particle:

- Boundary conditions and contact points: Surrounding particles may support another particle, preventing it from moving. It could be that the particle would ordinarily have moved if not for the contact points with surrounding particles.
- Armouring: The process by which the smaller particles on the surface bed are eroded, leaving behind the coarser material which then acts as protection of the underlying sediments.
- Various forms of coherent flow structures: Large scale structures such as secondary currents are somewhat constant over short periods of time. Secondary currents might form part of the general flow over the particle. Smaller scale coherent structures tend to exert rapidly varying forces on individual particles.
- Particle on a slope: The particle may be on a side slope in a channel or on an embankment, affecting the gravitational force component.
- Momentum interchange between slow- and fast-moving particles: When moving particles collide, a dispersive force is created between them. The change in momentum between a fast-moving particle and a slow-moving particle results in a dispersive shear stress.
- Seepage pressure: Seepage into or out of the riverbed may result in seepage pressures.

2.1.3 Models of incipient motion

2.1.3.1 Introduction

Incipient motion is initiated by oscillating eddy currents in the vicinity of the particles (Armitage & McGahey, 2003). Eddy currents are complex and close to impossible to describe mathematically. Instead, in an effort to simplify the theory of incipient motion, researchers made use of a single flow related parameter in the vicinity of the particle under consideration to define incipient motion. Some of the most recognised researchers in the field of incipient motion include Shields (1936), Liu (1957), Rooseboom (1992) and Armitage (2002).

The three most-used models of incipient motion are:

i. Critical flow velocity approach;
ii. Shields’s critical shear stress approach; and
iii. Liu’s stream power approach.

2.1.3.2 Critical flow velocity approach

Flow velocity, specifically average flow velocity, is relatively easy to measure. It is therefore no surprise, given the convenience, that many researchers have tried to link incipient motion to some flow velocity (Armitage & McGahey, 2003).

The problem, though, with using average flow velocity to describe incipient motion is that lift- and drag forces are dependent on the velocity distribution rather than the average velocity. For the same average velocity, a shallow flowing channel would have higher velocity gradients than a deeper flowing channel. Therefore, to promote particle movement, a higher average velocity would be required in a deep channel compared to an otherwise identical shallow channel. It makes more sense to use local flow velocity, i.e. the velocity in the vicinity of the particle under consideration. However, local flow velocity is extremely difficult to measure, if at all possible, as particles often lie in regions of high velocity gradients (Armitage & McGahey, 2003).

Liu's (1957) theory of incipient motion (discussed in Section 2.1.3.4) was based on the assumption that local flow velocity is the energy behind particle movement. He determined that local flow velocities and drag coefficients were all functions of the particle Reynolds Number. Liu (1957) determined that there is a unique relationship between the ratio of shear velocity to the particle settling velocity (V^*/V_{ss}) and particle Reynolds number (Re^*). Liu (1957) termed the ratio of $\frac{V^*}{V_{ss}}$ the "Movability Number". The resulting curve, however, does not explicitly include average or local flow velocity. Particle Reynolds number is defined as:

$$R_e{}^* = \frac{V^* d}{\nu} \qquad \text{Equation 2.5}$$

A detailed discussion on Liu's (1957) theory is presented in Section 2.1.3.4, as the relationship between Movability Number and particle Reynolds number follows logically from the theory of stream power. Yang (1973) had similar arguments to Liu (1957), but formulated equations in terms of the critical average flow velocity for incipient motion:

For $0 < R_e{}^* \leq 70$

$$\frac{V_{cr,avg}}{V_{ss}} = \frac{2.5}{\log(R_e{}^*) - 0.06} + 0.66 \qquad \text{Equation 2.6}$$

For $R_e{}^* > 70$

$$\frac{V_{cr,avg}}{V_{ss}} = 2.05 \qquad \text{Equation 2.7}$$

Where:

$V_{cr,avg}$ = Critical average flow velocity (m/s)

Although the work of Yang (1973) had been confirmed by laboratory flume tests, some researchers expressed doubt in its applicability to natural rivers that generally have greater depth of flow (Armitage & McGahey, 2003).

Although there is substantial amount of theoretical support for using local flow velocity to predict incipient motion, it is extremely difficult to estimate.

2.1.3.3 Critical bed shear stress approach

Shields (1936) is arguably the most cited reference in the field of sediment transport and river hydraulics given his extensive research contributions toward the fields. Shields developed his widely accepted theory by arguing that a particle will start to move when the drag force (F_D) exerted on the particle exceeds the resistive force. Shields determined that drag force was influenced by the particle size, particle shape, bed form, particle Reynolds number and bed shear stress. Shields assumed that a particle's resistance to motion is only dependent on the bed form and submerged weight of the particle (Raudkivi, 1998).

From his findings and assumptions, Shields (1936) derived the "Shields's parameter" (ψ), also referred to as the "entrainment function" or the "dimensionless mobility factor", as follows:

$$\psi = \frac{\tau_o}{(\rho_s - \rho)gd} = \frac{\rho V^{*2}}{(\rho_s - \rho)gd} \qquad \text{Equation 2.8}$$

Equation 2.8 shows that Shields's parameter is, among others, a function of shear velocity (V^*) (Langmaak, 2013). V^* is related to the real fluid velocity that gives rise to a shear stress (τ_0) (Henderson, 1966). Many researchers (Armitage, 2002; CIRIA, CUR & CETMEF, 2007; Simons & Sentürk, 1976) have expressed V^* as follows:

$$V^* = \sqrt{\frac{\tau_0}{\rho}} \approx \sqrt{gDS_f} \qquad \text{Equation 2.9}$$

Where:

S_f = Energy slope (m/m)

At incipient motion the critical bed shear stress (τ_{cr}), is used to calculate the critical Shields's parameter (ψ_{cr}) (Langmaak, 2013):

$$\psi_{cr} = \frac{\tau_{cr}}{(\rho_s - \rho)gd} \qquad \text{Equation 2.10}$$

Figure 2-2 presents Shields's incipient motion diagram used for determining the flow conditions at which non-cohesive particles begin to move (Stoffberg, 2005). Henderson (1966) explained the initial decline in the Shields's curve by arguing that the resultant drag force is

higher in laminar flow than in turbulent flow. In fully turbulent flow ($R_e^* > 1000$) the drag force is constant, hence ψ remains constant at 0.056.

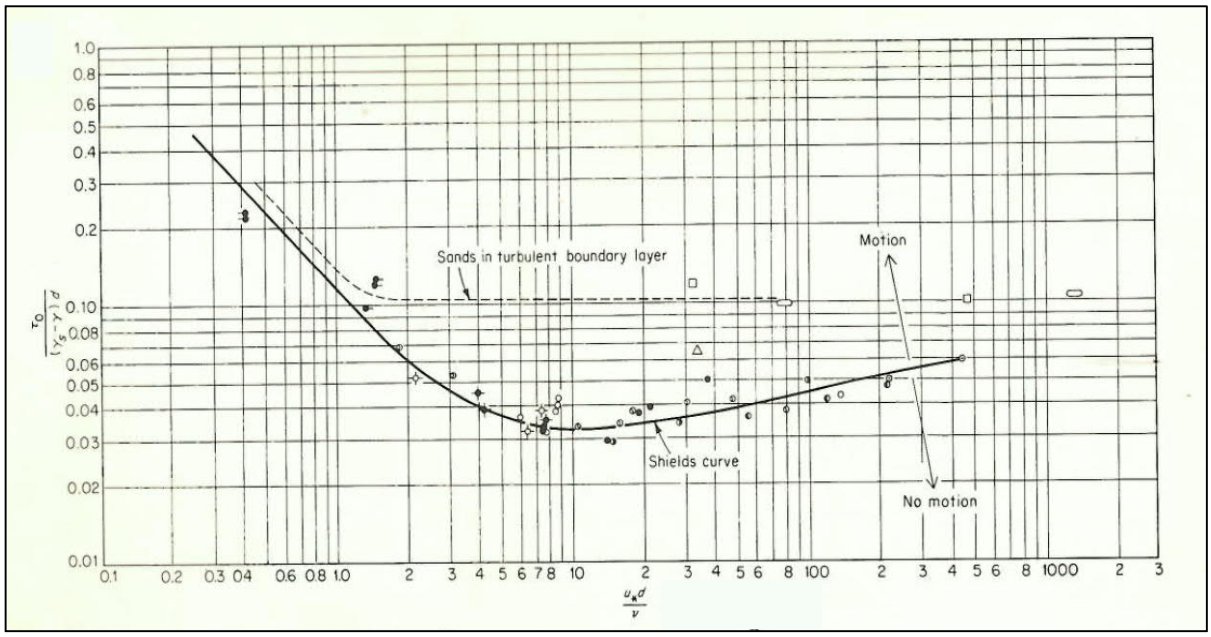

Figure 2-2: Incipient motion diagram of Shields (adapted from Graf, 1971)

The primary criticism against the use of Shields's theory is that particle movement is not uniquely determined by shear stress (Yang, 1973). Yang (1973) also argued that at high particle Reynolds numbers the vertical lift force cannot simply be ignored from the stability calculations, as Shields only took into account the tangential force. It is noted that V^* is present on both axes on Shields's incipient motion diagram, resulting in trial-and-error solutions being required (Armitage & McGahey, 2003). Furthermore, Rooseboom (1992) argued that median particle size is not a sufficient parameter to adequately describe incipient motion and that settling velocity should be used instead.

In deriving his theory, Shields did not take into account that some particles may be more exposed to flow than others, leading to questions being raised by Przedwojski *et al.* (1995), Simons & Sentürk (1992) and van der Walt (2005).

2.1.3.4 Stream power approach

As briefly introduced in Section 2.1.3.2, Liu (1957) agrees that local velocity is the energy behind particle movement and that drag force is a function of the particle Reynolds Number (R_e^*). Furthermore, Liu (1957) denoted a unique relationship between the Movability Number (V^*/V_{ss}) and R_e^*. The resulting curve, referred to as the Liu-diagram, does not include local or average flow velocity.

Stream power, which is related to flow rate, is defined as the rate of the dissipation of energy. For water to flow, or particles to move, the expenditure of energy is required (Armitage & McGahey, 2003). For uniform flow with average velocity down a bed slope S_0, the average stream power P_{avg} per unit volume is:

$$P_{avg} = (\rho_s - \rho)gV_{ss} \qquad \text{Equation 2.11}$$

Being one of the first researchers to use stream power as an indicator of particle movement, Bagnold (1960) showed that a minimum critical unit stream power is required to initiate particle movement. Similarly, Yang (1973) expressed a "dimensionless unit stream power" given by Equation 2.12:

$$\text{Dimensionless unit stream power} = \frac{S_0 V}{V_{ss}} \qquad \text{Equation 2.12}$$

The problem with Equation 2.11 and Equation 2.12 is that average flow velocity is used, rendering it only useful in one-dimensional models. Stream power, however, varies with height above the bed. The unit stream power applied is zero at the channel bed and a maximum at the surface. In the process of overcoming shear stresses, stream power is dissipated into heat (Armitage & McGahey, 2003).

Stream power applied P_a and unit stream power dissipated P_d at any depth above the bed, in the water column in a stream with flow depth D, can be determined with Equation 2.13 and Equation 2.14, respectively (Rooseboom, 1974):

$$P_a = \rho g S_0 V_{avg} \qquad \text{Equation 2.13}$$

$$P_d = \tau_{yx} \frac{dV}{dy} \qquad \text{Equation 2.14}$$

Where:

$\frac{dV}{dy}$ = Change in velocity with change in depth (m/s/m)

y = Depth above the bed in the water column (m)

τ_{yx} = Shear stress in the case of uniform flow in a wide channel = $\rho g(D - y)S_0$.

The velocity gradient is dependent on whether laminar- or turbulent flow exists. Near the boundary, where the flow is always laminar, the velocity is calculated by:

$$V = \frac{(V^*)^2 . y}{\nu} \qquad \text{Equation 2.15}$$

For particles in the linear layer (laminar flow) exposed to steady uniform flow in a deep, wide channel, $\tau_{yx} = \tau_o = \rho g D S_o$ and $V^* = \sqrt{gDS_o}$. By differentiating Equation 2.15 with respect to y

and multiplying with the bed shear stress $\tau_{yx} = \tau_0 = \rho V^{*2}$, the applied unit stream power in the linear layer is expressed by Equation 2.16.

$$P_{t(l)} = \frac{(\rho g D S_0)^2}{\mu} \qquad \text{Equation 2.16}$$

Where:

$P_{t(l)}$ = Applied unit stream power in the linear layer (W/m³)

μ = Dynamic viscosity of water (Pa.s).

Prandtl (1925) expressed the velocity gradient in the turbulent zone of the inner boundary as:

$$\frac{dV}{dy} = \frac{V^*}{Ky} \qquad \text{Equation 2.17}$$

Where:

K = Von Karman constant = 0.4 for clear water

By multiplying Equation 2.17 by $\tau_{yx} = \tau_0 = \rho V^{*2}$, the applied unit stream power for the log-law layer could be obtained and is given in Equation 2.18.

$$P_{t(t)} = \frac{\rho(gDS_0)^{3/2}}{Ky} \qquad \text{Equation 2.18}$$

Where:

$P_{t(t)}$ = Applied unit stream power in the log-law layer (W/m³)

Away from the boundary, $\tau_{yx} \neq \tau_0$ as the unit stream power dissipation is a maximum at the channel bed and zero at the surface, complicating the situation.

The stream power required to keep a particle in suspension, P_r, is similar to the power dissipated by a particle free-falling at terminal velocity, with only minor differences in the drag coefficient. The expression for P_r was defined by Rooseboom (1992) as given by Equation 2.19. For a particle to remain suspended, the instantaneous vertical velocities in the vicinity of the particle regularly need to exceed the settling velocity of the particle. V_{ss} differs in laminar and turbulent flow.

$$P_r = (\rho_s - \rho) g V_{ss} \qquad \text{Equation 2.19}$$

For a particle to be lifted out of its existing state in the bed, the power dissipated on the particle must be equal to or greater than the applied power required to suspend the particle (Armitage & McGahey, 2003):

$$P_t \geq P_r \qquad \text{Equation 2.20}$$

However, it is known that particle movement is not limited only to particles that are lifted out of plane. The initial movement of a particle might be in the form of rolling/sliding. Rooseboom (1992) deemed it unnecessary to differentiate between suspended and bed load and argued that bed load could simply be regarded as a concentrated layer of suspended particles moving close to the bed (Armitage & McGahey, 2003). Equation 2.20 was therefore altered to the following equation:

$$P_t \propto P_r \qquad \text{Equation 2.21}$$

Depending on whether the particle under consideration is in the linear (laminar flow) or log-law (turbulent flow) layer, P_t is calculated using either Equation 2.16 or Equation 2.18. The stream power required to initiate movement, P_r, either in the form of rolling/sliding, saltating or suspending, is calculated using Equation 2.19.

For laminar flow, the settling velocity of natural sediment particles was presented by Rooseboom (1974 & 1992) as:

$$\text{Settling velocity}, V_{ss} = \frac{4}{3}\frac{(\rho_s-\rho)}{\rho}\frac{gd^2}{32v} \qquad \text{Equation 2.22}$$

Many researchers have proposed values for the Movability Number for particles in laminar flow conditions, as presented in Table 2-1. The amount of stream power required to initiate particle movement is less than that required to keep it in suspension (P_r) as particles do not necessarily have to be suspended to commence motion (for instance rolling or sliding). Therefore, Armitage & McGahey (2003) argued that it is not the motion of a single particle that is of interest, but rather the intensity of motion:

$$\frac{V^*}{V_{ss}} = \frac{\alpha_1}{R_e{}^*} \qquad \text{Equation 2.23}$$

Where:

α_1 = Function of the intensity of motion that needs to be measured

For turbulent flow conditions, in the vicinity of the particle, particle settling velocity is constant. By assuming that the flow is uniform and homogeneous, Rooseboom (1992) showed that Movability Number plots along a horizontal line for a certain flow condition and particle size (Langmaak, 2013):

$$\frac{\sqrt{gDS_f}}{V_{ss}} = \text{Constant} \qquad \text{Equation 2.24}$$

The empirical constant representing intensity of motion in turbulent flow is given by Equation 2.25, where α_2 needs to be measured.

$$\frac{V^*}{V_{ss}} = \alpha_2 \qquad \text{Equation 2.25}$$

Where:

α_2 = Function of the intensity of motion that needs to be measured

It is already known that a particle would likely roll/slide prior to being lifted out of the bed matrix. Assuming that the average unit stream power required to initiate rolling/sliding is a constant fraction, η, of the unit stream power required to suspend it, the following form of Equation 2.20 yields (Armitage & McGahey, 2003):

$$P_t = \eta P_r \qquad \text{Equation 2.26}$$

Therefore, the laminar boundary condition of Equation 2.23 changes to:

$$\frac{V^*}{V_{ss}} = (\eta_l{}^{1/2})\frac{\alpha_1}{R_e{}^*} \qquad \text{Equation 2.27}$$

Where:

η_l = Power fraction for the laminar boundary

The turbulent boundary condition of Equation 2.25 changes to:

$$\frac{V^*}{V_{ss}} = (\eta_t{}^{1/3})\alpha_2 \qquad \text{Equation 2.28}$$

Where:

η_t = Power fraction for the turbulent boundary

Many researchers have proposed values for the Movability Number, as presented in Table 2-1. The analytical solutions in Table 2-1 are presented graphically in Figure 2-3. Shields and Liu assume uniform flow, i.e. the water surface slope S_w, bed slope S_o and friction slope S_f are all parallel. Even so, researchers such as Yang (1973), Rooseboom (1992), Przedwojski, Błażejewski & Pilarczyk (1995), Stoffberg (2005) and Langmaak (2013) support Liu's (1957) stream power model for providing the soundest theoretical base of incipient motion theory for non-cohesive particles in natural rivers.

Table 2-1: Analytical solutions of the Movability Number as presented by various researchers

Researcher	Laminar flow boundaries	Turbulent flow boundaries
Rooseboom (1992), after data from Yang (1973)	$R_e{}^* < 13$: $\frac{V^*}{V_{ss}} = \frac{1.6}{R_e{}^*}$	$R_e{}^* > 13$: $\frac{V^*}{V_{ss}} = 0.12$
Armitage (2002)	$R_e{}^* < 11.8$: $\frac{V^*}{V_{ss}} = \frac{2.0}{R_e{}^*}$	$R_e{}^* > 11.8$: $\frac{V^*}{V_{ss}} = 0.17$
Armitage and McGahey (2003)	$R_e{}^* \leq 6.23$: $\frac{V^*}{V_{ss}} = \frac{2.2}{R_e{}^{*1.4}}$	$R_e{}^* > 6.23$: $\frac{V^*}{V_{ss}} = 0.17$

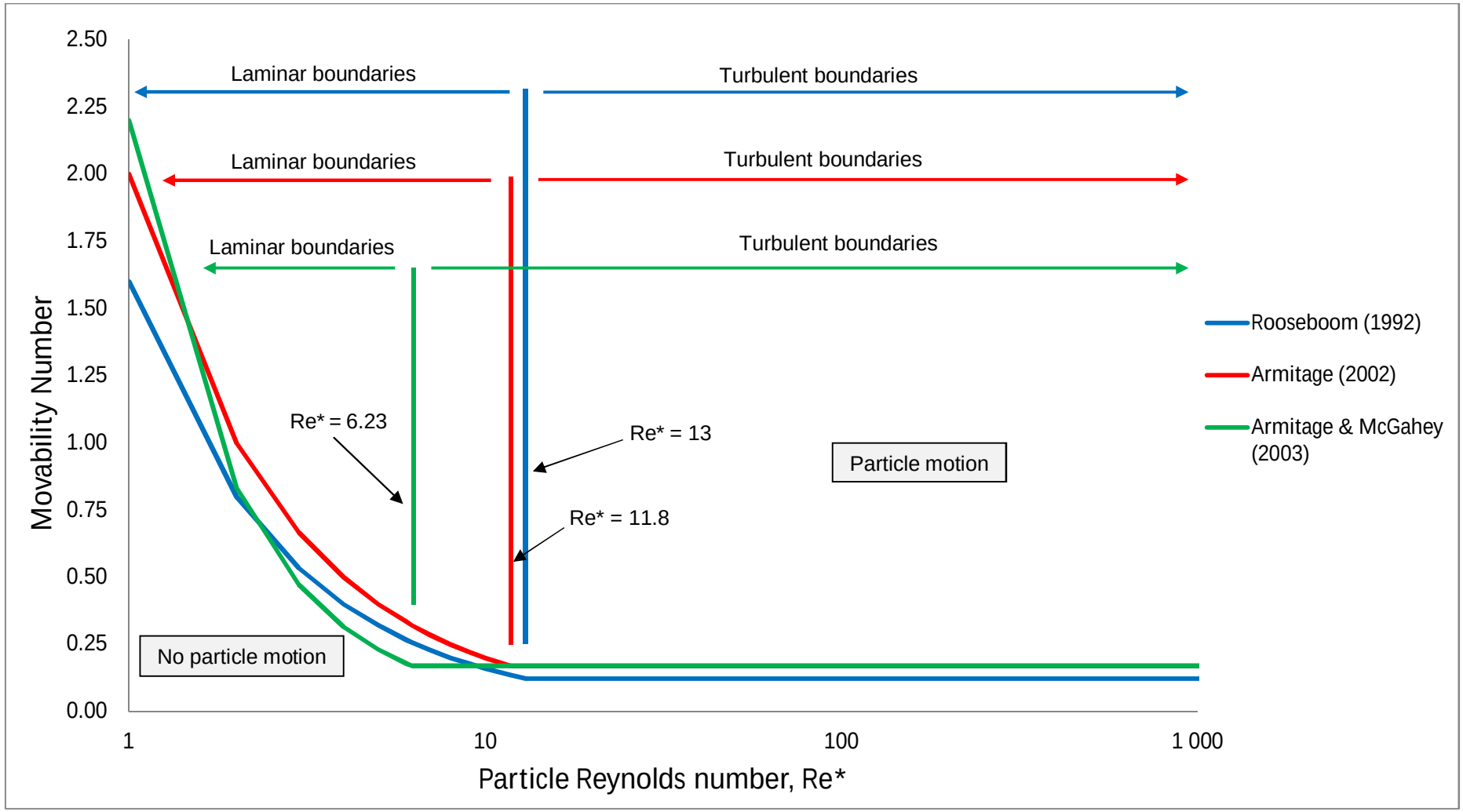

Figure 2-3: **Incipient motion criteria of Rooseboom (1992), Armitage (2002) and Armitage & McGahey (2003)**

2.1.4 Incipient motion on slopes

As one of the main contributions of this study is developing design criteria for ACB's placed on steep slopes, an understanding of incipient motion on slopes is required. The criteria for incipient motion on slopes vary somewhat from that which is presented in the previous sections.

Generally, a distinction is made between two slope types:

i. Longitudinal slope (β): A slope in the direction of flow in a channel or river. A fall in slope is regarded as a positive slope while a rise is regarded as a negative slope.
ii. Transverse slope (γ): A slope indicating a fall of the bed normal to the direction of flow.

To account for slope, either longitudinal, transverse or both, a correction factor derived from the drag force (F_D) is applied to the horizontal bed shear stress (Henderson, 1966; Armitage, 2002). Table 2-2 presents the equations of bed shear stress for sloping beds. The definition of all symbols used is given in Table 2-2. The steeper the slope, the less stable the particle.

Table 2-2: Bed shear stress for sloped channel beds (Henderson, 1966; Armitage, 2002)

Type of slope	Correction factor	Bed shear stress (Pa)
Longitudinal	$k_\beta = \frac{F_{D,cr,\beta}}{F_{D,cr,0}} = \frac{\sin(\varphi-\beta)}{\sin\varphi} = \cos\beta(1-\frac{\tan\beta}{\tan\varphi})$	$\tau_{0,cr} = k_\beta \tau_{0,cr,0}$
Transverse	$k_\gamma = \frac{F_{D,cr,\gamma}}{F_{D,cr,0}} = \cos\gamma\sqrt{1-\frac{\tan^2\gamma}{\tan^2\varphi}}$	$\tau_{0,cr} = k_\gamma \tau_{0,cr,0}$
Combination of both longitudinal and transverse	-	$\tau_{0,cr} = k_\beta k_\gamma \tau_{0,cr,0}$

Where:

k_β = Ratio of the critical drag force for any longitudinal slope to the critical drag force for a horizontal bed

k_γ = Ratio of the critical drag force for any transverse slope to the critical drag force for a horizontal bed

$F_{D,cr,\beta}$ = Critical drag force for longitudinal slope (N)

$F_{D,cr,\gamma}$ = Critical drag force for transverse slope (N)

$F_{D,cr,0}$ = Critical drag force for a horizontal bed (N)

$\tau_{0,cr}$ = Critical bed shear stress on a given sloped bed (Pa)

$\tau_{0,cr,0}$ = Critical bed shear stress on a horizontal bed (Pa)

φ = Angle of repose of particle (degrees).

A slope correction factor, ψ_s, is defined as follows:

$$\psi_s = \sqrt{k_\beta k_\gamma} = \sqrt{\cos\beta\left(1-\frac{\tan\beta}{\tan\varphi}\right)\cos\gamma\left(1-\frac{\tan^2\gamma}{\tan^2\varphi}\right)}^{\frac{1}{2}} \quad \text{Equation 2.29}$$

The slope correction factor can be used with the three models of incipient motion discussed in Section 2.1.3:

- From the critical flow velocity approach (Stoffberg, 2005):

$$V_{0,cr} = \psi_s V_{0,cr,0} \quad \text{Equation 2.30}$$

$$\left(\frac{V^*}{V_{ss}}\right)_{\beta,\gamma} = \psi_s \left(\frac{V^*}{V_{ss}}\right)_0 \quad \text{Equation 2.31}$$

Where:

$V_{0,cr}$ = Critical bed shear velocity on a horizontal bed (m/s)

$V_{0,cr,0}$ = Critical bed shear velocity on a sloped bed (m/s)

$\left(\frac{V^*}{V_{ss}}\right)_{\beta,\gamma}$ = Movability Number for any given slope

$\left(\frac{V^*}{V_{ss}}\right)_0$ = Movability Number for a horizontal bed.

- From the critical bed shear stress approach (Armitage, 2002):

$$\tau_{0,cr} = \psi_s{}^2 \tau_{0,cr,0} \quad \text{Equation 2.32}$$

- From the stream power approach (Armitage, 2002):

For laminar boundaries: $P_t = \psi_s{}^2 \eta_l P_r$ Equation 2.33

For turbulent boundaries: $P_t = \psi_s{}^3 \eta_t P_r$ Equation 2.34

Where:

η_l, η_t = Ratio of the average unit stream power required to initiate rolling/sliding of a particle to the unit stream power required to suspend particle in a laminar and turbulent boundary, respectively.

Extrapolation of results from a tested bed slope to an untested slope is discussed in Section 2.2.3.8.

As there is no scientific way of accurately determining the angle of repose of articulating concrete blocks, no slope adjustment factors were applied to the results obtained from this model study. Instead, test results were referenced to the channel bed- and/or side slope at which they were tested.

2.1.5 The impact of excessive turbulence on incipient motion

Turbulence is associated with large velocity gradients. It therefore has a significant effect on the stability of sediment or revetments (Langmaak, 2013). In most model studies, it seems to be common practice to not take turbulence into account. Normal levels of turbulence are generally assumed (Langmaak, 2013). However, when turbulence levels are high, an amplification factor (k_t), relating to velocity and not shear stress, should be applied (CIRIA *et al.*, 2007):

$$k_t = \frac{1 + 3r}{1.3} \qquad \text{Equation 2.35}$$

Where:

r = Turbulence intensity

Turbulence intensity has become the most common term used to define the level of turbulence present in flow (CIRIA *et al.*, 2007). Turbulence intensity is defined as the ratio of the variation in flow velocity around the mean to either the mean flow velocity or the shear velocity. Vanoni (1975) defined turbulence intensity quantitatively as the ratio of the root mean square of the longitudinal and vertical turbulent velocity components to the shear velocity V^*:

$$r = \frac{\sqrt{V_L'^2}}{V^*} \text{ and } \frac{\sqrt{V_V'^2}}{V^*} \qquad \text{Equation 2.36}$$

Where:

V_L' = Longitudinal turbulent velocity component

V_V' = Vertical turbulent velocity component.

Turbulence intensity near the bed is not the same in all directions. Its longitudinal component approaches 1.8 in the inner boundary layer, peaking in excess of 2.0 before falling to around 0.6 near the surface. Following the same trend, vertical turbulence intensity peaks in excess of 1.0 before falling down to 0.6 near the surface (Graf, 1998).

Typical values of turbulence intensity for flow over rough beds or uniform flow in flat rivers with a low flow regime are 0.15 and 0.1, respectively (CIRIA *et al.*, 2007). It is obvious that an accurate comprehension of the in-situ site conditions is necessary for turbulence intensity to

be determined accurately. However, site specific information is not always available, making it nearly impossible to determine the turbulence intensity quantitatively. As a result, CIRIA *et al.* (2007) defined turbulence intensity subjectively as high, medium or low, with "low" referring to normal turbulence levels. For each qualitative turbulence intensity, CIRIA *et al.* (2007) specified an associated condition and a range of recommended r values for design purposes, which are presented in Table 2-3. Considering the broad range of the r values, Table 2-3 should be used with caution (Escarameia, 1998; CIRIA *et al.*, 2007).

Table 2-3: Recommended r values at 0.1y above bed (CIRIA et al., 2007)

Condition	Turbulence intensity	
	Qualitative	r
Straight channel reaches and wide natural bends ($\mathbf{r_c/W} > 26$)	Normal (low)	0.12
Edges of revetments in straight reaches	Normal (higher)	0.2
Bridge piers, caissons and groynes; transitions	Medium to high	0.35 – 0.50
Downstream of hydraulic structures such as weirs, culverts, stilling basins	Very high	0.60

Reference is made to Section 2.2.4 which presents design guidelines of ACB's exposed to turbulent flow conditions.

2.1.6 The effect of the velocity profile on incipient motion

For a hydraulically rough boundary ($\frac{V^* k_s}{\nu} > 70$) and fully developed flow, the logarithmic velocity distribution is determined by the following equation (CIRIA et al., 2007):

$$V = \frac{V^*}{K} \ln\left(\frac{y}{y_0}\right) \qquad \text{Equation 2.37}$$

Where:

- y = Depth above bed (m)
- y_0 = Reference level near the bed = $0.033k_s$, where k_s = Chezy's roughness coefficient (m).

A plotted profile of Equation 2.37 is depicted in Figure 2-4. Equation 2.37 and Figure 2-4 show that the maximum velocities occur at the water surface.

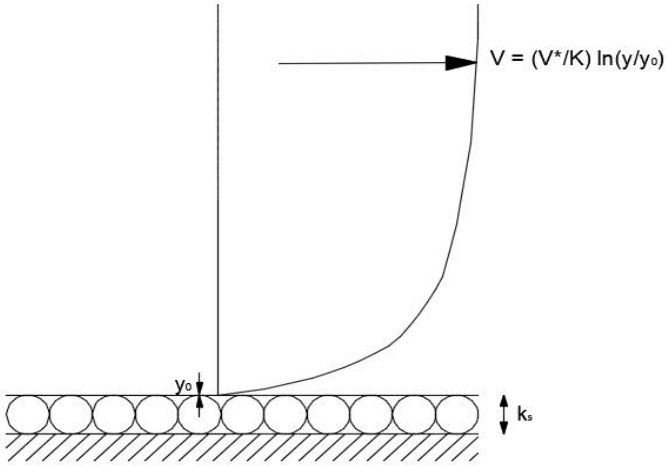

Figure 2-4: Vertical velocity profile (adapted from CIRIA et al., 2007)

The general expression that is used to convert velocity to bed shear stress is given by Equation 2.9 in Section 2.1.3.3, and can be also be presented in the following form:

$$\tau_0 = \rho V^{*2} \qquad \text{Equation 2.38}$$

Table 2-4 presents equations for determining the velocity profile factor ($\Lambda_h = 33/k_h$). According to Maynord et al. (1989), however, this approach proved unreliable when the logarithmic relationship was applied to rough surfaces such as riprap.

Table 2-4: Velocity profile factors for rough boundaries (CIRIA *et al.*, 2007)

Velocity profile	Applicability	Velocity profile factor, Λ_h	Equation number
Fully developed	Large relative water depths ($\frac{D}{k_s} > 2$)	$\Lambda_h = \frac{18^2}{2g}\log^2(\frac{12D}{k_s})$	Equation 2.39
Fully developed	Small relative water depths ($\frac{D}{k_s} < 2$)	$\Lambda_h = \frac{18^2}{2g}\log^2(1+\frac{12D}{k_s})$	Equation 2.40
Not fully developed	Short flow lengths	$\Lambda_h = \frac{33}{(1+\frac{D}{d_y})^{0.2}}$	Equation 2.41

2.1.7 The effect of flow around bends

Even though this study does not include flow around a bend, it's effect on the movability of a particle should be noted.

Flow around bends generates secondary currents due to the centrifugal force acting on the filaments of fluids producing the super-elevation of the water surface level on the outside (concave) bank, and a decreased water surface level on the inside (convex) bank (Pacheco-

Ceballos, 1983). Figure 2-5 illustrates the super-elevation of the water surface level around a bend.

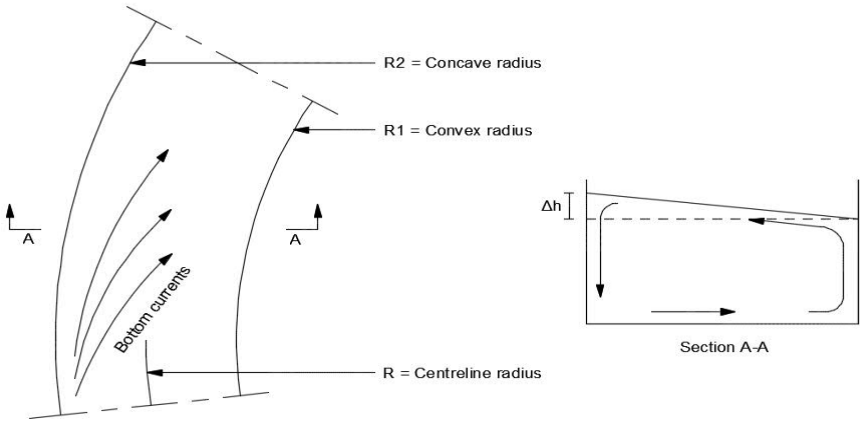

Figure 2-5: Curvilinear flow and super-elevation of the water surface in an open channel bend (adapted from Bouvard, 1992)

The change in water surface level (Δh) in a bend is calculated by:

$$\Delta h = \frac{V^2 B}{g R_c} \qquad \text{Equation 2.42}$$

Where:

B = Width at water surface (m)

R_c = Centreline radius of curvature (m).

Pacheco-Ceballos (1983) confirmed that the velocity- and shear stress distributions in bends differ considerably from those in straight channels because of secondary currents. The velocity distribution around bends gives rise to a transverse pressure gradient which increases the hydrostatic pressure towards the concave bank. This pressure is a maximum at the concave bank and a minimum at the convex bank, explaining why scouring typically occurs on the concave bank of a bend while sediment deposition occurs on the convex bank of a bend (Brink, 2004).

Figure 2-6 is a schematic drawing of a meandering channel which illustrates the movement of the thalweg from the convex- to the concave of a bend in a downstream direction. Therefore, maximum velocity is found near the outside of the bend, just downstream of its apex. However, in the event of extreme floods, the highest velocity in the channel is located near the convex bank of a bend (Christian, 1988).

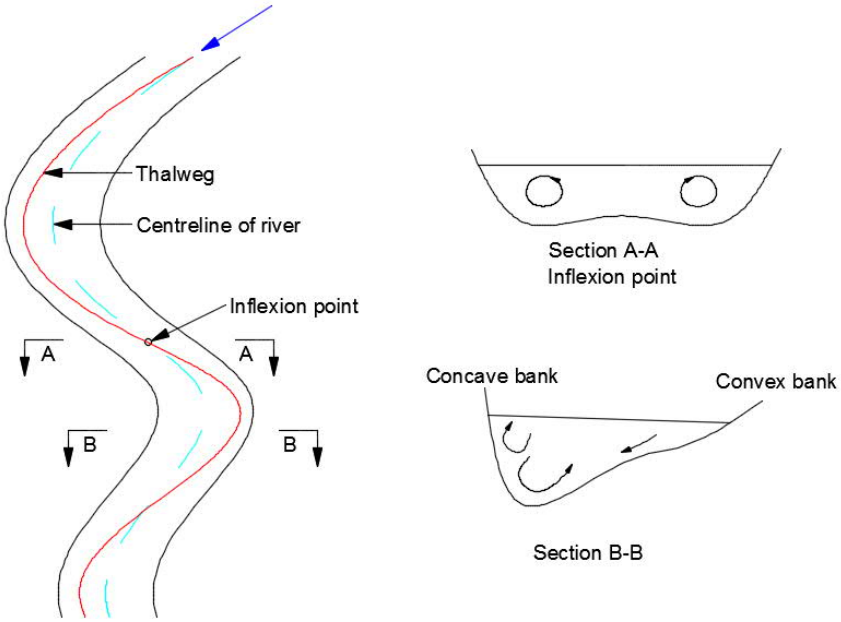

Figure 2-6: Schematic illustration of flow patterns in a meandering river (adapted from Christian, 1988)

Rooseboom & van Vuuren (2013) recommended that the amplification factors presented in Table 2-5 be applied to the calculated required particle size when designing for riprap or stone pitching to prevent scour on the concave bank of a bend.

Table 2-5: Amplification factor for required particle sizes around a channel bend

Channel bend characteristic	Amplification factor
Gentle	1.3
Sharp	1.6

U.S. Army Corps of Engineers (1981) defines a sharp bend as follows:

$$\frac{r_c}{B} < 26 \qquad \text{Equation 2.43}$$

Where:

r_c = Centreline radius of the bend (m)

B = Water surface width (m).

For bends with a $\frac{r_c}{B}$-ratio of 2.3, revetments should extend upstream to a minimum of one mean water surface width (B) and downstream to a minimum of 1.5B (U.S. Army Corps of Engineers, 1981).

2.2 Armorflex ACB's

2.2.1 Background

Armorflex is machine-compressed concrete blocks of uniform size, shape and weight (Armortec Incorporated, 1981). Armorflex was originally designed, developed and patented by the Dutch company Nicolon Corporation with the aim of combining the favourable aspects of a flexible lining, such as porosity, vegetation and habitat enhancement and ease of installation, with the high force resistance of rigid linings. When licensed internationally, it was done so in the form of two Armorflex types: Armorflex 140 and Armorflex 180, with the number referring to the weight of a packed block matrix per square metre (kg/m²). Armorflex 140 and 180 blocks are of primary interest in this study.

2.2.2 Physical characteristics and installation guidelines

Figure 2-7 and Figure 2-8 are photographs (top and isometric views, respectively) of single prototype Armorflex 140 and 180 blocks. These sample blocks were provided by Technicrete for this study. The puzzle-like shape of Armorflex allows for better articulation of the joints while its tapered sides allow for increased flexibility between adjacent blocks, especially for installation at bends and sloping grade control structures. Armorflex mats are free to conform to the contours of the subgrade, even if settlement were to occur after installation (Schweiger & Holderbaum, 2001). However, like many other revetments, Armorflex is not intended for slope stabilisation.

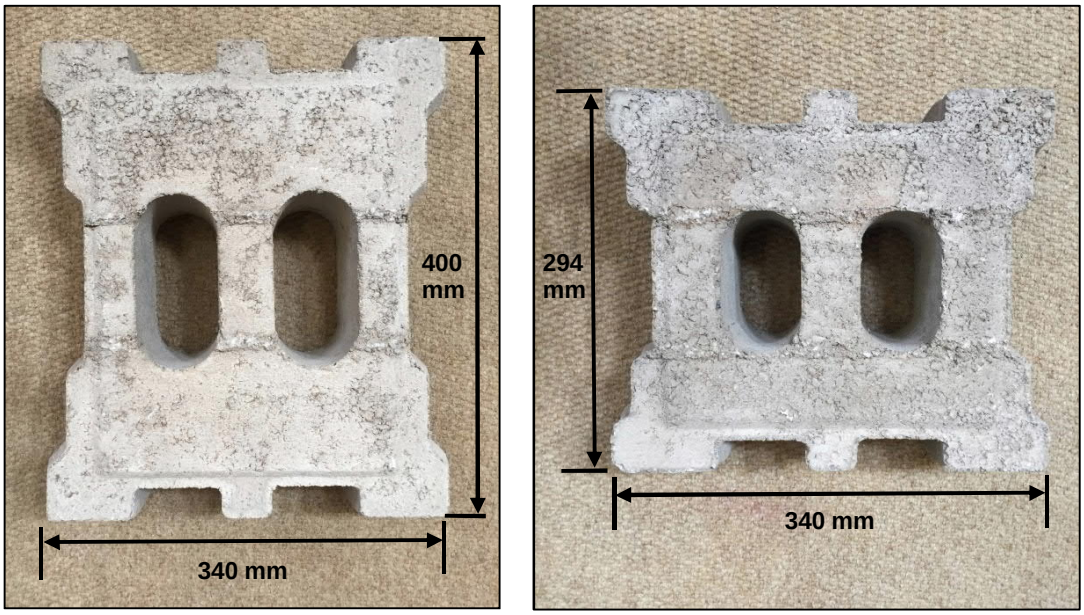

Figure 2-7: Top view of Armorflex 140 (left) and Armorflex 180 (right) prototype blocks

Figure 2-8: Isometric views of Armorflex 140 (left) and Armorflex 180 (right) prototype blocks

Table 2-6 presents the physical characteristics of Armorflex 140 and 180.

Table 2-6: Physical characteristics of Armorflex 140 and 180 blocks (Technicrete, 2016)

Block class	Dimensions L x B x H (mm)	Plan size of block (mm)	Block weight (kg)	Unit weight (kg/m²)	Solid or cellular
Armorflex 140	340 x 400 x 95	309 x 400	17.5	140	Cellular
Armorflex 180	340 x 294 x 115	309 x 294	16.4	180	Cellular

The open cells in the blocks, causing the blocks to be referred to as “cellular”, offer hydraulic relief as it limits the build-up of hydrostatic pressure behind the blocks. Water passes freely through the Armorflex system, forming eddy currents in the open cells. These currents act as energy dissipators, reducing the erosive velocity of the water (Armortec Incorporated, 1981). Technicrete (2016) specifies that the area of the open cells in Armorflex 140 and 180 blocks are only 18% of the respective block surface area. According to Armortec (2016a), however, the area of the open cells should not exceed 35% of the block surface area.

In practice, after the blocks have been installed, the revetment structure would generally be screeded with gravel or topsoil, filling the open cells and gaps between adjacent blocks. This not only increases the friction between adjacent blocks, but it also provides for the establishment of vegetation. Vegetative growth forms a plug effect which, in effect, reinforces the block structure. In terms of an ACB system’s allowable shear stress, vegetated ACB systems are 41% more stable than ACB systems with no vegetative growth (Lipscomb, et al., 2001). Furthermore, vegetative growth increases the ecological and aesthetic appearance of the revetment, making it appear natural.

According to Technicrete (2016), the maximum scour depth inside the open cells is approximately equal to the width of the opening. Figure 2-9 is a schematic illustration which shows the maximum scour depth (A) being equal to the width of the open cells (L).

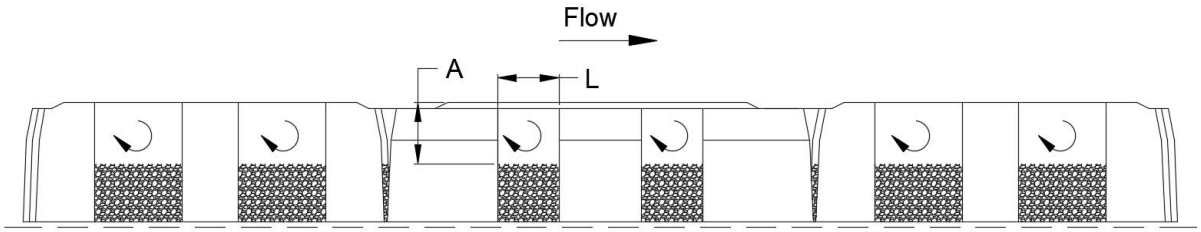

Figure 2-9: Maximum scour depth in open cells of Armorflex blocks (adapted from Armortec Incorporated, 1981)

Armorflex blocks are manufactured with holes on either side of the open cells to allow blocks to be linked longitudinally with either galvanised wire cables or polyester ropes. Even though the NCMA (2010) argues that cables do not increase the hydraulic stability of an Armorflex revetment system, it aids in making installation less labour intensive. Furthermore, it makes the use of soil anchors more effective (Schweiger & Holderbaum, 2001). Cabled systems are, however, known to roll up during failure. For this reason, the City of Tshwane municipality recommends that for long length cabled Armorflex installations anchor beams are cast at 50 m intervals (unless otherwise specified by the Engineer). This ensures that failure occurs only locally (within the 50 m section) instead of resulting in the catastrophic failure of the entire structure. City of Tshwane (2018) also specifies intermediate anchoring in the form of Y-fencing bars driven into the ground at 2 m spacing through the block openings before encasing it with concrete. For loose Armorflex block installation, these guidelines are obviously not applicable.

Armorflex blocks are typically installed on a filter layer to aid the open cells of the blocks in relieving hydrostatic pressure build-up behind the blocks. Geotextile filters may be used as a simplified alternative to a graded filter, although not all roots may be able to penetrate the geotextile, constricting the establishment of vegetation (Technicrete, 2016). The purpose of the filter layer is to prevent fines from being washed out from underneath the Armorflex blocks, undermining the revetment. This could potentially cause the revetment to fail as intimate contact between the subgrade, the filter and the blocks is compromised. The filter should therefore be designed to retain the fine material in the subgrade but should also permit seepage to occur freely.

According to the original manufacturer, Nicolon Corporation, Armorflex mats have a minimum radius of 0.61 m. Sharp turns/corners in a channel should therefore be prevented.

According to Scholl *et al.*, (2010), the Armorflex revetment should extend a longitudinal distance equal to at least the channel width upstream and at least 1.5 times the channel width downstream of the region exposed to severe hydraulic loading. In complex conditions, however, the extent of the installation should be determined through laboratory studies.

Figure 2-10 illustrates the flexibility of an Armorflex 180 structure installed along a section of the right bank of the Blyde River in Hoedspruit. It is clear that Armorflex blocks can conform to large changes in the subgrade. In this case, it was deemed fair to assume that the preparation of the subgrade was substandard, exposing the Armorflex revetment to failure in the case of a flood. According to Technicrete (2016), the quality of the subgrade preparation will be reflected in the finished surface. Furthermore, given the lack of established vegetation through the openings of the blocks, it questions whether the structure had been screeded with gravel or topsoil after installation.

Figure 2-10: Loose Armorflex 180 blocks installed along the Blyde River, Hoedspruit

In contrast to Figure 2-10, Figure 2-11 is an open drainage channel lined with Armorflex 140 blocks. The straight lines and even bed suggest that the subgrade was prepared according to specifications. The channel shown in Figure 2-11 is located in the Klein-Kariba Holiday Resort in Bela-Bela, Limpopo.

Figure 2-11: Channel constructed with Armorflex 140 in ATKV Klein-Kariba, Limpopo

2.2.3 Performance testing of Armorflex

2.2.3.1 Introduction

Several research projects and laboratory studies have been conducted to evaluate the performance of Armorflex and other ACB systems under hydraulic flow. This section discusses the relevant tests conducted on ACB's and presents the relevant results of each study. Also included in this section are the standards for testing and analysing results of ACB revetments.

In 1986, the Construction Industry and Research Information Association (CIRIA) conducted tests on concrete block revetments in the United Kingdom (Hewlett, Boorman & Bramley, 1987). The Federal Highway Administration (FHWA) followed CIRIA with controlled laboratory testing of embankment erosion protection systems in 1988 and 1989. Leech, Abt, Thornton & Combs (1999) then developed test protocols for ACB revetments for overtopping and channelized flow conditions. In compliance with these protocols, Abt, Leech, Thornton & Lipscomb (2001) tested a generic block in overtopping and channelized flow conditions. Separate standards were published by ASTM (2008a, 2008b) for the testing of ACB revetments, and for the analysing and interpretation of ACB test data.

2.2.3.2 CIRIA embankment testing

The embankment tests performed by CIRIA in the UK examined ACB's (including Armorflex 30S) as concrete-reinforced systems for grass erosion protection. Armorflex 30S, having

dimensions of 330 x 295 x 120 mm and a unit weight of 166 kg/m², is similar to Armorflex 180. CIRIA tested five types of concrete block revetments in high-velocity, steep-slope channelized applications (Clopper & Chen, 1988). All tests were conducted on a 10 m high embankment with a 1V: 2.5H slope.

CIRIA's criteria for failure was the erosion of the subsoil. According to Clopper & Chen (1988), the study reported a limiting flow velocity of 7 - 8 m/s. The CIRIA tests, however, included well established grass growth within the block matrix, rendering a system with enhanced stability. However, in the semi-arid climate of South Africa one cannot always rely on grass during extended droughts, which could become even more problematic with future climate change impacts.

2.2.3.3 FHWA overtopping flow testing

a) Clopper & Chen (1988) laboratory testing

Following the CIRIA study, the FHWA funded research and laboratory testing of different revetment systems exposed to overtopping flow conditions, with the aim of developing preliminary design guidelines (Clopper & Chen, 1988). Full scale cabled concrete blocks were included in their study.

A 1.8 m high embankment with a horizontal crest length of 6.1 m was constructed in a 1.2 m wide flume. The downstream slope of the embankment was constructed on either a 1V:2H, 1V:3H or 1V:4H slope, with Armorflex only tested on the 1V:2H slope. Armorflex class 30 was subjected to three overtopping depths: 0.3 m, 0.61 m and 1.22 m, all with freeflow downstream conditions.

Cabled Armorflex class 30 was stable at 0.3 m and 0.61 m overtopping depths but failed under the 1.2 m overtopping depth due to an apparent shallow-seated liquifaction of the subsoil material. Apparent uplift of the blocks, because of negative pressure, allowed water under the system which led to the saturation of the subsoil. Clopper and Chen (1988) presented critical velocities and bed shear stresses for Armorflex, given in Table 2-7.

Table 2-7: Critical shear stress of Armorflex class 30 (Clopper & Chen, 1988)

ACB type	Critical velocity, V_c (m/s)	Critical bed shear stress, τ_{cr} (kg/m²)**
Armorflex class 30*	3.7 – 4.6	58.6 – 97.7

** Armorflex class 30 is similar to Armorflex 180, although not 100% identical.*

*** 1 kg/m² = 9.81 N/m².*

Clopper and Chen (1988) concluded that further investigation into the capabilities of ACB systems in overtopping flow was needed.

b) Clopper (1989) laboratory testing

Clopper (1989) performed detailed tests on ACB's to determine the causes of failure during overtopping flow. Armorflex class 30 blocks were once again included in the tests and were tested with and without cables. The tests were conducted in the same flume used in the Clopper and Chen (1988) study. The tests were also structured the same in terms of overtopping depths (0.3 m, 0.61 m and 1.22 m). Clopper (1989), however, included a rigid embankment (concrete surfaced) into the laboratory tests. Eight full-scale hydraulic tests were conducted on the rigid embankment and nine on an erodible embankment. The erodible embankment was constructed with soil placed and compacted according to the U.S. Department of Transportation and U.S. Bureau of Reclamation procedures and standards. The complete description of the test setup and procedure followed is given in Clopper (1989).

Armorflex class 30 proved to be stable for all hydraulic conditions tested on the rigid embankment tests. Upon completion of the erodible embankment tests, Clopper (1989) observed that failure of the blocks occurred during the 1.22 m overtopping test at freefall conditions (run for a period of 4 hours) followed by another 4 hours using a tailwater depth of 1.5 m. Clopper (1989) concluded, however, that faulty installation was to blame rather than block characteristics. Clopper (1989) therefore deemed the Armorflex system to be stable at all tested overtopping depths. The results from the erodible embankment tests are given in Table 2-8. For these tests the Armorflex structure was screeded with gravel, which lead to increased system stability.

Table 2-8: Critical velocity and bed shear stress of Armorflex class 30 on rigid and erodible embankments (Clopper, 1989)

ACB type	Embankment type	Critical velocity, V_c (m/s)	Critical bed shear stress, τ_{cr} (kg/m²)
Armorflex class 30	Rigid	> 5.12	> 169.9
Armorflex class 30	Erodible	> 4.75	> 198.2

Clopper's (1989) study concluded that ACB revetments, when installed properly on a well-prepared subgrade, can maintain hydraulic stability under high flow velocities of 6.1 m/s or more, with corresponding bed shear stresses of 144 to 192 kg/m². Clopper (1989) furthermore argued that the effect of cabling on the hydraulic stability is probably insignificant, but that it offers ease of installation and may assist in keeping the system tied together when properly installed. Clopper (1989) also pointed out the importance of the capacity of the filter layer, in that it should be sufficient to accommodate the flow entering the sub-block environment in order to relieve uplift pressures.

2.2.3.4 High turbulence testing of ACB's

In the period between 1990 and 1992, HR Wallingford investigated the stability of riprap and concrete block revetments in high turbulent flow conditions. Laboratory tests were conducted for flows with various levels of turbulence, ranging from normal levels in uniform channels to high levels downstream of hydraulic structures (Escarameia & May, 1992).

Using the results from the tests, Escarameia & May (1992) developed a design equation for riprap and concrete block revetments subjected to various levels of turbulence. Escarameia & May (1992) incorporated a stability coefficient varying with turbulence intensity. However, only turbulence intensity in the streamwise direction was considered. Their design equation uses flow velocity measured at 10% of the flow depth above the bed. Escarameia & May (1992) deemed it sufficiently close to represent the flow conditions experienced by the bed. The design equation developed was of the following form:

$$d_n = C_r \frac{V_b^2}{2g\Delta} \qquad \text{Equation 2.44}$$

Where:

d_n = Block thickness (m)

C_r = Stability coefficient varying with turbulence intensity (refer to Table 2-9 and Table 2-3 for turbulence intensity r)

V_b = Bed velocity (measured at 10% of the water depth above the bed) (m/s)

Δ = Relative submerged density = $\frac{\rho_s - \rho}{\rho}$.

Table 2-9: Stability coefficient varying with turbulence intensity for loose- and cabled ACB's

	Criteria	Equation	Equation number
Loose blocks:	r ≥ 0.05 & slopes of 1V:2.5H or flatter	$C_r = 9.22r - 0.15$	Equation 2.45
Cabled blocks:	r ≤ 0.43	$C_r = 0.05$	Equation 2.46
	0.43 < r ≤ 0.90	$C_r = 1.79r - 0.72$	Equation 2.47

After completing the study, HR Wallingford was commissioned to conduct a follow-up project to the one completed in 1992. The aim of this project was to include field data on typical turbulence levels in rivers for use in the design equations presented in the first study, and to extend the laboratory study to include a wider range of channel protection materials which included gabions and more concrete block revetments (Escarameia, 1995).

Using data from the initial study, Escarameia (1995) aimed to determine adequate stability coefficients for the channel revetment systems considered under both rapid- and highly turbulent flow. The full description of the test setup and procedure is explained in Escarameia (1995). The findings and recommendations on gabion mattresses are included in Section 2.3.2.1 of this report.

Escarameia (1995) performed tests on cabled Armorflex 140 blocks scaled at 1:8. Flow depths were monitored using scales fixed to transparent sections of the walls of the 28 m long flume. Flow velocities were measured using an electromagnetic current meter at approximately 10% of the water depth above the bed. Tests were conducted without a filter layer beneath the mattress. Escarameia (1995) argued that a granular filter layer can in fact destabilise the revetment in highly turbulent flows.

To produce normal (rapid) flow conditions, a downstream tailwater gate was kept fully open to ensure that tailwater levels do not affect the flow upstream. To produce high turbulent flows in the test section, the tailwater gate was gradually lowered until block movement was observed.

Tests were conducted at three levels of tension in the cables linking the Armorflex blocks:

- Tension level A: Cables tightly stretched;
- Tension level B: Cables stretched to a lesser extent; and
- Tension level C: No tension applied but blocks still tied together.

Escarameia (1995) regarded tension level C to best represent field conditions, as tension does not last long in practice.

Table 2-10 presents the results in terms of bed flow velocity and Froude number at the point of movement for all tests conducted.

Table 2-10: Bed flow velocity and Froude number at failure of Armorflex blocks (Escarameia, 1995)

Flow condition	Loose blocks	Cabled blocks: Cable tension level		
		A	B	C
High turbulent flow	V = 1.29 m/s; Fr = 0.337	No movement	No movement	V = 0.311 m/s; Fr = 0.541
Rapid flow (low turbulence)	-	Failure 1: V = 5.34 m/s; Fr = 2.52 Failure 2: V = 5.37 m/s; Fr = 2.61 Failure 3: V = 6.99 m/s; Fr = 2.27	Failure 1: V = 5.57 m/s; Fr = 2.38 Failure 2: V = 6.08 m/s; Fr = 2.68 Failure 3: V = 6.16 m/s; Fr = 2.60	No movement

The following conclusions and recommendations were drawn from the study of Escarameia (1995):

- Cabled ACB's collapse earlier under rapid flow conditions than under highly turbulent flows. Mean and local flow velocities can be relatively low where the turbulence is high.
- The amount of tension applied to the mattress does not greatly affect the stability of Armorflex.
- A slightly higher stability was achieved when the cable direction was transverse to the flow direction.

In 1998, Escarameia presented an approximate guide detailing the range of applicability of non-vegetated loose- and cabled ACB revetments in normal- to medium turbulence flow conditions. This guide is presented in Table 2-11 and can be used in the early stages of design (Escarameia, 1998). It should be noted that the velocities in Table 2-11 are mean flow velocities and not bed flow velocities as given in Table 2-10. The velocities presented by Escarameia (1998) in Table 2-11 propose that cables do offer some assistance in terms of stability. This is in contrast to the statements of Clopper (1989) and the NCMA (2010) that argued that cables do not increase block stability. Therefore, there remains uncertainty about the impact cables have on the stability of ACB revetments.

Table 2-11: Applicability of ACB's in normal- to medium turbulence conditions (Escarameia, 1998)

	Mean flow velocity (m/s)	Weight of block per unit area (kg/m²)	Resistance to wave attack: Wave height (m)
Loose blocks	≤ 1.5	< 160	≤ 0.15
	≤ 2	> 160	≤ 0.5
Cabled blocks	≤ 4.5	< 250	≤ 1.5
	≤ 5	> 250	≤ 1.5

2.2.3.5 Testing protocols of ACB systems

Leech *et al.* (1999) published a set of protocols for the testing of ACB's in overtopping- and channelized flow conditions, to allow designers to compare their findings. The protocols were based on the FHWA studies documented by Clopper & Chen (1988) and Clopper (1989).

Leech *et al.* (1999) defined failure of a block revetment as any of the following occurrences:

i. The loss of a block or group of blocks, leaving the subgrade exposed to the flow;
ii. The loss of contact between the block and the embankment due to erosion along the slope or the washout of material through joints; and
iii. The loss of system integrity due to the movement of blocks.

Table 2-12 summarises the test protocols developed by Leech *et al.* (1999) for overtopping and channelized flow conditions.

Table 2-12: Test protocols for overtopping and channelized flow (Leech et al., 1999)

Test protocols for overtopping flow:	Test protocols for channelized flow:
• Width of channel ≥ 1.22 m; • Embankment height ≥ 1.83 m; • Horizontal crest approach ≥ 6.1 m; • Variable embankment slopes (1V:2H, 1V:3H, etc.).	• Channel length ≥ 20 m; • Channel to have a trapezoidal cross-section with half-channel configuration; • Channel bed width = 0.3 m or the width of one concrete block, whichever is greater; • Channel bed thickness = 0.3 m; • Channel side slopes = 1V:2H.

Test setup and testing procedure:
• Embankment constructed of sand or silty-sand, compacted in 150 mm to 230 mm layers at 90% Standard Proctor density.
• Embankment to be surveyed after layer works are completed.
• Install blocks as recommended by the manufacturer.
• Full-size prototype blocks to be used rather than scaled blocks.
• Blocks to be anchored at embankment toe to ensure the evaluation of the block system and not toe stability.
• Increase flow until flow depth at the leading edge of the embankment is 0.3 m.
• Sustain each tested discharge for 4 hours, or until failure. • Flow velocities and depths to be recorded on an hourly basis along the centreline of the slope at predetermined cross sections (near entrance, mid-channel and near exit).
• No tailwater to be present on the embankment (flow to discharge freely through the test section).

Leech *et al.* (1999), however, recommended that the test protocols for channelized flow applications need to be considered as preliminary and that more research was required.

In an attempt to evaluate these test protocols, Abt *et al.* (2001) performed a detailed study using a generic concrete block, termed the “Corps Block”. This block was developed by the United States Army Corps of Engineers (USACE).

Overtopping tests were conducted on embankment slopes of 1V:5H and 1V:7H, while channelized tests were conducted in a half-trapezoidal channel with a bottom width of 0.37 m and side slopes of 1V:2H. The study yielded similar results in overtopping and channelized flow conditions. The “Corps Block” achieved a critical flow velocity of 4.11 m/s and shear stress of 21.92 kg/m². Abt *et al.* (2001) argued that the overtopping test protocol is more efficient and cost effective, compared to the channelized test protocol. Therefore, the overtopping test protocol was recommended for the evaluation of all applications of ACB revetments (Abt *et al.*, 2001).

2.2.3.6 Standard for ACB testing

The ASTM published a standard for full scale ACB laboratory performance testing (ASTM, 2008a). This standard aims to provide guidelines for determining the stability threshold values of shear stress and flow velocity of ACB revetment systems under controlled laboratory conditions. The standard was developed specifically for testing in rectangular open channels with high flow velocities and steep slopes.

ASTM (2008a) defined the stability threshold as any of the following occurrences:

i. Vertical displacement or loss of a block or group of blocks;
ii. Loss of soil beneath the geotextile, resulting in voids; and
iii. Liquefaction and mass slumping/sliding of the subsoil.

The standard's requirements in terms of the test flume, embankment preparation, block installation and test methodology are presented in Table 2-13.

Table 2-13: ASTM (2008a) standard for ACB testing

Test flume requirements and embankment preparation:
• Flume width ≥ 1.2 m; • Soil subgrade to consist of silty-sand, placed in lifts of 100 to 150 mm and compacted to 90 – 95% of Standard Proctor Density; • Horizontal crest length ≥ 1.83 m, followed by a 1V:2H sloped embankment.
Installation requirements:
• A designed filter to be placed between subgrade and blocks; • Full-size prototype blocks to be used; • The blocks to be installed as per manufacturer recommendations.
Test methodology:
• Maintain continuous uniform flow for 4 hours; should revetment not fail, repeat test at the next higher target discharge (until flow capacity of test facility); • Hourly measurements of water surface elevations at 0.6 m intervals along centreline of flume (measurements to the nearest 3 mm); • Bed elevation (top of ACB) measurements before and after each test at 0.6 m intervals along flume centreline (measurements to the nearest 3 mm); • Using an electromagnetic current meter, Price-type pygmy (mini) current meter or a pitot tube flow meter, take hourly measurements of point velocities at 20%, 60% and 80% of flow depth (measured from the water surface) at 1.2 m intervals along the centreline.

ASTM (2008a) recommends that flow depth measurements be corrected for the embankment slope by multiplying the flow depth measurements with the cosine of the bed slope angle. Furthermore, ASTM (2008a) recommends that the discharge at each of the measurement cross-sections be determined using the continuity equation, given as Equation 2.48.

$$Q_{p,i} = A(V_{p,i})$$ Equation 2.48

Where:

$Q_{p,i}$ = Discharge at specific station (m³/s)

$V_{p,i}$ = Average of point flow velocities measured at 20%, 60% and 80% of flow depth or, where three velocity measurements are not available, the point flow velocity at 60% of flow depth (m/s)

i = Station number (1, 2, 3, etc.).

2.2.3.7 Standard for analysis and interpretation of ACB testing

The standard for the analysis and interpretation of ACB performance test data (ASTM, 2008b) was developed to be used in conjunction with ASTM (2008a). Figure 2-12 serves as a definition sketch for the parameters used.

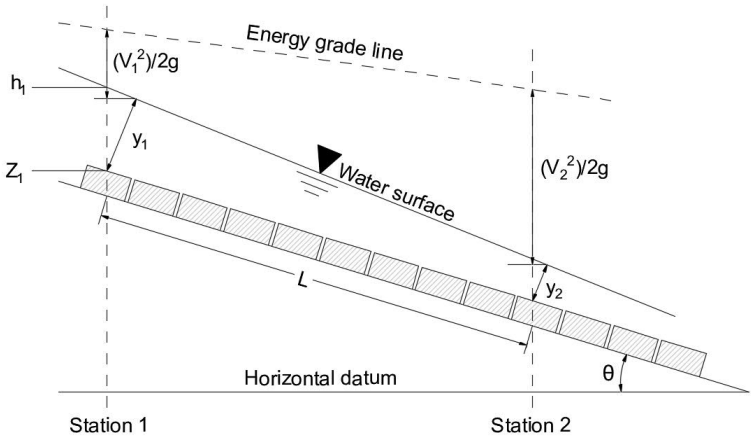

Figure 2-12: Definition sketch (adapted from ASTM, 2008b)

ASTM (2008b) recommends that the following hydraulic conditions have to be quantified in order to accurately establish stability threshold (with reference made to):

- Total discharge, Q;
- Flow depth at each measurement station, y_i;
- Section-averaged velocity at each measurement station, $V_{ave,i} = \frac{Q}{A}$;
- Energy grade line slope at each measurement station, $S_{f,i}$, determined using Equation 2.49:

$$S_{f,i} = \frac{[n(V_i)]^2}{y_i^{4/3}}$$ Equation 2.49

Where:

$S_{f,i}$ = Energy grade line slope at station i (m/m)

n = Optimal Manning's n-value

V_i = Velocity at station i (m/s).

- Optimal Manning's n-value, determined by a step-forewater calculation:
  - For supercritical flow, the water surface profile should be determined by solving the momentum equation, proceeding in a downstream direction:

$$h_2 = h_1 + \frac{1}{2g}(V_1 + V_2)(V_1 - V_2) - \frac{L}{2}\left(S_{f,1} + S_{f,2}\right) \quad \text{Equation 2.50}$$

Where:

h_1, h_2 = Upstream and downstream water surface elevations at stations 1 and 2 (m)

L = Slope length between stations 1 and 2 (m).

  - The optimal Manning's n-value is that value that minimises the objective function, which is defined as:

$$\xi = \sum_{i=i_1}^{i_n} \text{abs}\left(h_{\text{pred}} - h_{\text{obs}}\right) \quad \text{Equation 2.51}$$

Where:

i_1, i_n = Starting and ending station for analysis, respectively

$h_{\text{pred}}, h_{\text{obs}}$ = Predicted and observed water surface elevation at station i (m).

The optimal Manning's n-value is then used to determine the water surface elevation profile that best fits the observed profile.

- Energy grade line elevation (EGL) at each measurement station:

$$EGL_i = z_i + y_i(\cos\beta) + \frac{V_i^2}{2g} \quad \text{Equation 2.52}$$

Where:

EGL_i = Energy grade line elevation at station i (m)

- Bed shear stress, τ_0:

$$\tau_0 = \rho g y S_f \quad \text{Equation 2.53}$$

Where:

y = Average of measured flow depths from stations (perpendicular to bed) (m)

Equation 2.53 represents the maximum boundary shear stress at the bed for gradual varied flow. Alternatively, the momentum equation may be used to determine bed shear stress across a representative control volume (for instance between station 1 and 2) (ASTM, 2008b).

$$\tau_0 = \frac{\rho g}{2}(y_1 + y_2)(\sin\theta) + \frac{1}{L}[\frac{\rho g}{2}(y_1^2 - y_2^2)\cos\theta - \rho q^2(\frac{1}{y_2} - \frac{1}{y_1})] \qquad \text{Equation 2.54}$$

Where:

L = Length of the control volume along slope (m)

q = Unit discharge (m^3/s per meter width).

Included in ASTM (2008b) are the reporting requirements of the revetment testing program.

2.2.3.8 Colorado State University Testing (2000 - 2013)

Over an approximate 14-year period, the Colorado State University (CSU) conducted laboratory hydraulic tests at its Engineering Research Centre (ERC) and performed a thorough analysis of the results of previous ACB hydraulic performance testing. Overtopping tests were conducted over a steep embankment. The facility provided for a headbox capable of holding ±1.83 m of static head above the test embankment. The test embankment was 1.22 m wide with a 3.05 m long horizontal approach section followed by a 30.5 m long 1V:2H slope.

All tests were conducted in accordance with ASTM (2008a). The ACB products were analysed by running a direct step hydraulic model (DSHM), as recommended in ASTM (2008b). The DSHM determines the best-fit S-2 flow profile and Manning's n-value. Numerical data obtained from the analysis included flow depth, EGL slope, average flow velocity and bed shear stress. Table 2-14 summarises the results of four Armorflex block types tested. It should be noted that Armorflex class 30 is similar to Armorflex 180, and Armorflex class 40 is similar to Armorflex 140, although not identical.

Table 2-14: Summary of performance tests in terms of V_{cr} and τ_{cr}

Block type	Year of test	V_{cr} (m/s)	τ_{cr} (kg/m²)
Armorflex class 30S*	2000	3.7	19.5
Armorflex class 40	2000	5.5	43.9
Armorflex class 40L*	2001	6.7	78.1
Armorflex class 40T*	2013	10.7	97.6

** S and L denote different block footprint sizes.*

T refers to a "Tapered" block typically used in high velocity applications.

2.2.4 Manufacturer design guidelines

The design guidelines of manufacturers of Armorflex are provided and discussed in this section. This section, however, does not include guidelines related to subgrade preparation

nor installation of the blocks itself. This section is split in two parts; 1) design guidelines in terms of limiting flow characteristics, and 2) design guidelines by means of moment stability analyses, i.e. factor of safety (FoS) methods. Limiting flow characteristics may include parameters such as flow velocity, bed shear stress, flow depth, Froude number, and Movability Number, even though no manufacturers use Froude number nor Movability Number as a design guideline. Factor of safety methods include the determination of overturning- and resisting (stabilising) moments about a single block.

2.2.4.1 Limiting flow characteristic design guidelines

a) Technicrete

The Armorflex product brochure of Technicrete (2016) specifies a critical flow velocity and a maximum desired slope as the hydraulic limitations of Armorflex blocks. Technicrete (2016) does not specify whether the slope stated refers to a longitudinal- or side slope. These limitations are provided in Table 2-15:

Table 2-15: Armorflex design guidelines according to Technicrete (2016)

Block type	Maximum permissible flow velocity (m/s)	Maximum desired slope (m/m)
Armorflex 140	Up to 3.5 m/s	1:1.5 (but not exceeding the angle of repose of in situ material)
Armorflex 180	Up to 5.5 m/s	

b) Contech Construction Products inc.

Contech Construction Products inc. also uses flow velocity as a limiting condition but does so for a wide range of bed slopes, as plotted on the logarithmic scale graph in Figure 2-13. Armortec presents plots for Armorflex class 30, 50 and 70. Only Armorflex class 30 is of interest in this study as it is similar to Armorflex 180 in dimensions and unit weight per area.

Using the data from Figure 2-13, the following regression function for determining the critical mean velocity of Armorflex class 30 blocks installed at various bed slopes could be obtained:

$$V = 1.2543(So^{-0.163}) \qquad \text{Equation 2.55}$$

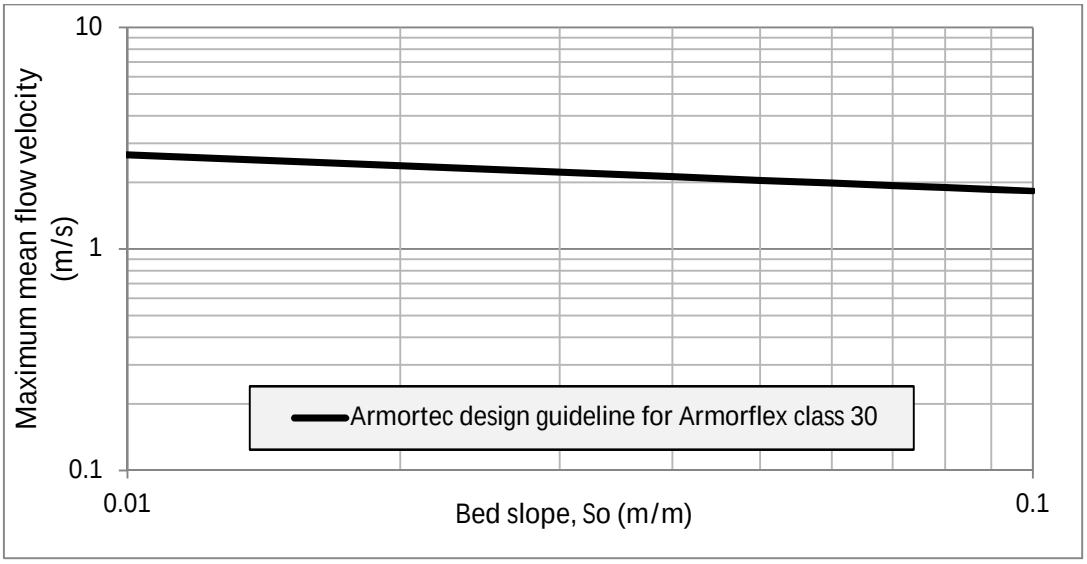

Figure 2-13: Limiting mean flow velocity for Armorflex class 30 in trapezoidal channels with various bed slopes (replotted from Armortec Incorporated, 1981)

Furthermore, Contech includes the hydraulic radius of flow in a trapezoidal channel at various bed slopes as another limiting condition of Armorflex class 30 blocks (Armortec Incorporated, 1981). Again, Armortec plots values for Armorflex class 30, 50 and 70, with only class 30 being of interest to this study. As hydraulic radius R is defined as the flow area A divided by the wetted perimeter P (i.e. A/P), flow depth is rendered a parameter which impacts the incipient motion of Armorflex blocks. The logarithmic scale graph plotted in Figure 2-14 illustrates the limiting hydraulic radius for Armorflex class 30 blocks installed in a trapezoidal channel for a range of bed slopes.

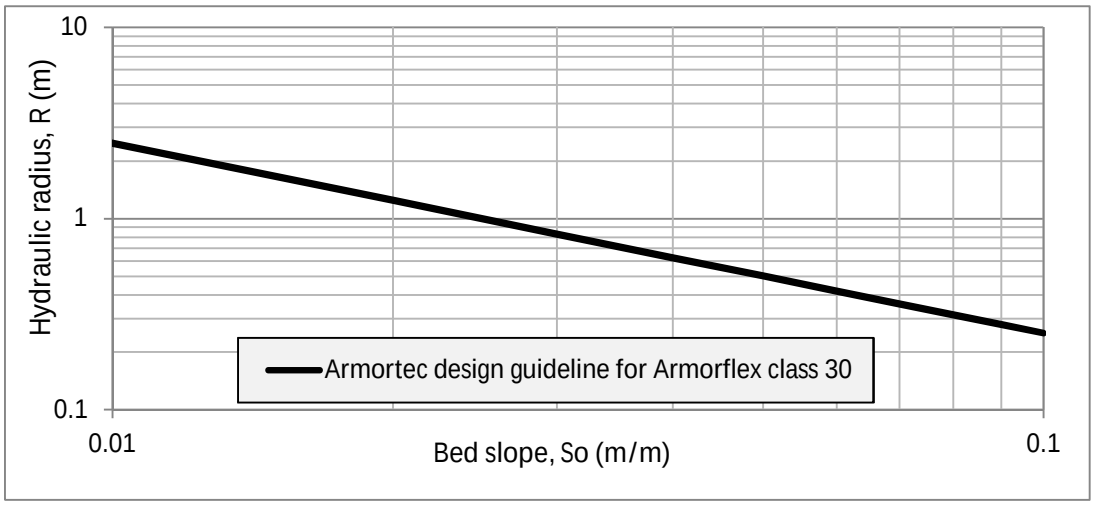

Figure 2-14: Hydraulic radius for Armorflex class 30 in trapezoidal channels with various bed slopes (replotted from Armortec Incorporated, 1981)

Using the data from Figure 2-14, the following regression function can be used to determine the limiting hydraulic radius of Armorflex class 30 blocks installed at various bed slopes in a trapezoidal channel:

$$R = 0.0254(So^{-0.995}) \qquad \text{Equation 2.56}$$

A technical report from Armortec Erosion Control Systems (Koutsourais, 1994) presented limiting hydraulic conditions of Armorflex class 30 and 40 blocks, based on results of flume studies conducted by Clopper (1989). Armorflex class 40 is comparable to Armorflex 140, although a bit larger in dimension and unit weight per area. The dimensions of Armorflex class 40 is 440 x 395 x 120 mm, compared to the smaller dimensions of Armorflex 140 of 340 x 400 x 95 mm. Table 2-16 presents the limiting hydraulic conditions of Armorflex class 30 and 40.

Table 2-16: Armorflex class 30 and 40 limiting velocity and shear stress (Clopper, 1989)

Block type	Critical flow velocity V_{cr} (m/s)	Critical Shear stress τ_{cr} (kg/m²)
Armorflex 30S	4.5	73.4
Armorflex 40	4.5	166.2*

** Shear stress at maximum flume capacity; no failure of blocks*

2.2.4.2 Moment stability analyses

Reference is made to “Appendix A: Moment stability analyses of ACB’s”. Clopper (1991) and the NCMA (2010) adapted the factor of safety (FoS) methods presented by Stevens & Simons (1971), Julien and Anthony (2002) and Julien (2010) to consider the properties of ACB’s. Clopper (1991) and the NCMA (2010) used the Shields relationship to determine the critical shear stress. Several assumptions and simplifications were applied during the original and extrapolated safety factor derivations.

Manufacturers of Armorflex have adopted the equations of Clopper (1991) and the NCMA (2010) as design guidelines for Armorflex revetments in channelized conditions. The design manuals published by Nicolon (n.d.) were based on the safety factor derivation of Clopper (1991), while Contech (Armortec Erosion Control Solutions, 2002) based their design on the derivation of the NCMA (2010). Therefore, small differences in the two safety factor equations exist.

Appendix A1 and A2 present the variables used in the safety factor derivations of Clopper (1991) and the NCMA (2010), and the respective safety factor equations adopted by Nicolon (n.d.) and Contech (Armortec Erosion Control Solutions, 2002). Appendix A3 shows how ACB test results can be extrapolated, either in terms of bed shear stress (from a tested bed slope

to a more mild slope) or block class. Appendix A4 presents an ACB safety factor design example.

As this study provides critical flow characteristics for Armorflex 140 and 180 blocks, it is recommended that the designer of the revetment apply a suitable safety factor to the design.

2.2.5 Practical design equations from other sources

The design of concrete block revetments generally follows the same approach as riprap design, except for changes in some equations and coefficients. The commonly used and accepted methods are presented in this section.

2.2.5.1 Escarameia & May's (1992) design equation

Escarameia & May (1992) modified Izbash & Khaldre's (1970) design equation to include the effect of turbulence. The calculation of all parameters of the design equation has been discussed in Section 2.2.3.4. The equation is given again as Equation 2.57.

$$d_n = C_r \frac{V_b^2}{2g\Delta} \qquad \text{Equation 2.57}$$

2.2.5.2 Pilarczyk's (1995) design equation

Pilarczyk (1995) modified the Izbash- and Shields equations by adding correction factors for turbulence, bed/side slope and velocity distribution. The design equation is recommended for cabled concrete block revetments:

$$d_n = \frac{\varphi_s}{\Delta}\frac{0.035}{\psi_{cr}} K_T^2 K_h (\psi_s{}^2)^{-1} \frac{V_d{}^2}{2g} \qquad \text{Equation 2.58}$$

Where:

- φ_s = Stability correction factor = 0.5 for ACB's (CIRIA *et al.*, 2007)
- ψ_{cr} = Critical Shields's parameter
- K_T = Turbulence factor = 1 for normal river turbulence and 1.5 to 2 for high turbulence
- K_h = Depth factor = $(d/y)^{0.2}$, where y = water depth (m)
- ψ_s = Slope correction factor = $\sqrt{k_\gamma k_\beta}$ (refer to Equation 2.29), where:

  $k_\gamma = \cos\gamma\sqrt{1-\left(\frac{\tan\gamma}{\tan\varphi}\right)^2}$ and $k_\beta = \cos\beta(1-\frac{\tan\beta}{\tan\varphi})$

  where γ = transverse slope (degrees), φ = internal friction angle of the particles (degrees) and β = longitudinal slope of the channel (degrees).

2.2.5.3 Escarameia (1998)

Escarameia (1998) presented design equations for loose- or interlocking block revetments exposed to specific hydraulic loadings such as current attack and wave induced loading, both of which are discussed in the subsequent sections:

a) ACB's under current attack

Hydraulic loadings induced by currents include streamwise current attack, secondary currents, ship-induced currents, wind-induced currents, and tidal currents.

The stability of loose concrete blocks under current attack, in the absence of waves and high turbulence, is dependent primarily on flow velocity, concrete density and block thickness (Escarameia, 1998).

Loose- or interlocking ACB revetments installed in straight stretches on slopes equal to or milder than 1V:2.5H and/or exposed to normal turbulence levels can be designed using Equation 2.59 and Equation 2.60 (Escarameia, 1998):

For continuous protection: $d_n = 0.037V_d^2/\Delta$ Equation 2.59

At edges of revetments: $d_n = 0.048V_d^2/\Delta$ Equation 2.60

For cabled concrete block mattresses under current attack, in the absence of waves and high turbulence, a simplified version of Pilarczyk's (1995) design equation (Equation 2.58) can be used:

$$d_n = \frac{0.026V_d^2}{(1-n)\Delta[\log(12y_t/d_n)]^2{\psi_s}^2} \quad \text{Equation 2.61}$$

Where:

- n = Porosity of the revetment, i.e. the open area of the blocks (25% open area: n = 0.25)
- y_t = Flow depth at the toe of the bank (m)
- ψ_s = Slope correction factor (refer to Equation 2.29 in Section 2.1.4).

b) ACB's under wave induced loading

Wave induced loading may occur due to wind, sudden releases from dams/reservoirs, surge waves and/or the movement of boats and ships. Two techniques are used to make provision for wave induced loadings during the design of revetments (Escarameia, 1998):

- Spectral analysis (random collection of waves of different heights and periods); and
- Determination of the significant wave height H_s, with period T_z.

Engineers have generally favoured the significant wave height approach due to its simplicity. Statistically, H_s represents the average wave height of the highest third of waves in a given period.

The thickness of plain, solid concrete block revetments exposed to moderate wave conditions can be determined by:

$$d_n = G\frac{H_i}{\Delta\cos\beta}I_r^{0.5} \qquad \text{Equation 2.62}$$

Where:

G = 0.19 – 0.26 for loose blocks and 0.15 – 0.19 for cabled block mats

H_i = Maximum wave height (m)

I_r = Iribarren number (slope of the bank to the steepness of the incident waves):

$$I_r = \frac{\tan\beta}{\sqrt{2\pi H_i/(1.3gT_z^2)}} \qquad \text{Equation 2.63}$$

Where:

T_z = Wave period = $0.581(\frac{FU_{10}{}^2}{g^3})^{0.25}$, with F = the fetch and U_{10} = the wind speed at a height of 10 m above mean water level.

Escarameia (1998), however, recommends that laboratory tests be conducted to determine the wave characteristics of cellular blocks. Waves are not part of the scope of this study.

2.2.5.4 Rooseboom & van Vuuren (2013)

According to Rooseboom & van Vuuren (2013), the settling velocity in water of loose concrete block revetments should be greater than the following:

$$V_{ss} \geq \frac{\sqrt{gDS_f}}{0.12} \qquad \text{Equation 2.64}$$

Where:

D = Depth of flow (m)

Knowing that $V^* = \sqrt{gDS_f}$, Rooseboom & van Vuuren (2013) equates the Movability Number (V^*/V_{ss}) of ACB's to 0.12, for particle Reynolds numbers ($R_e{}^*$) larger than 13.

For this thesis, the settling velocity of Armorflex blocks was determined experimentally. Refer to Section 3.3.2 for experimental procedure followed.

2.3 Riprap and Reno-Mattresses

Riprap and Reno-mattresses have similar characteristics. Riprap consists of sized and graded rocks and is widely used for erosion protection of embankments. Reno-mattresses, also

known as rock mattresses, are relatively thin, flexible rectangular wire cages filled with rock. The wires are generally high-quality galvanised steel wire to ensure longevity in terms of corrosion protection. The wires can be coated with PVC on request or, alternatively, stainless steel wires can be used. The corrosion protection of the wires is especially required in industrial- or mining environments. Reno-mattresses, like riprap, are flexible and permeable. Riprap structures are generally the most cost-effective revetment if a suitable nearby quarry is available. Generally, Reno-mattresses are used where the available rocks are too small in size than what is deemed acceptable for use as riprap (Jansen van Vuuren, Rooseboom & Kruger, 2013). Rock in Reno-mattresses, however, should still be designed hydraulically to prevent segregation and failure. Also, based on critical bed shear stress, the median rock diameter in mattresses must be 79% of the riprap rock diameter, which is relatively large (Stoffberg, 2005).

Figure 2-15 and Figure 2-16 are photographs of riprap and Reno-mattresses being used for erosion protection of stormwater canals. Photographs taken and supplied by Malherbe (2019).

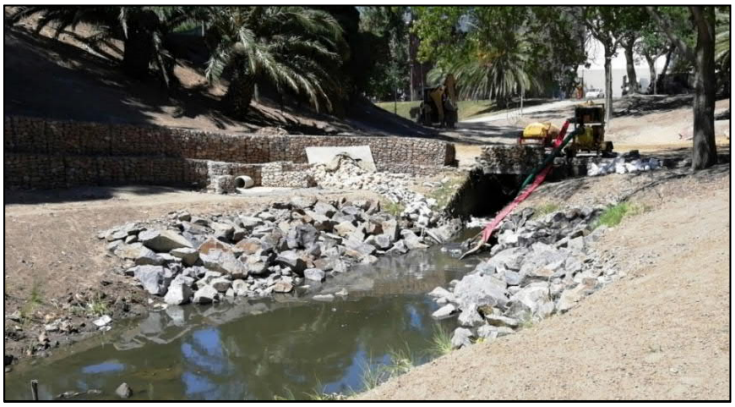

Figure 2-15: Riprap used on embankments at Elizabeth Park, Bellville, Cape Town (Malherbe, 2019a)

Figure 2-16: Reno-mattresses downstream of gabion weir at Elizabeth Park, Bellville, Cape Town (Malherbe, 2019b)

Reno-mattresses are known as being high maintenance revetments as debris transported down a channel may get caught in the wires. Labourers doing maintenance on the revetments may unknowingly move or displace rocks or damage the wires of the Reno-mattresses, which could possibly lead to rocks being dislodged from the structure during flood events (Sclafani, 2010).

Riprap has more flexibility than Reno-mattresses as riprap particles may move individually to conform to changes in the subgrade. Reno-mattresses, however, are more rigid, which poses a greater risk to catastrophic failure than riprap (Jansen van Vuuren *et al.*, 2013). Thus, Jansen van Vuuren *et al.* (2013) recommends Reno-mattresses for use in small streams only.

2.3.1 Physical characteristics of riprap and Reno-mattresses

This section includes a discussion on the physical characteristics specific to riprap and Reno-mattresses. This section is intended to be read in conjunction with Section 2.1.2 as the physical characteristics previously discussed also influence incipient motion conditions of rock revetments.

2.3.1.1 Rock size

The ability of riprap to resist a certain flow is a function of the stone size, the hydraulic gradient and the discharge. The size distribution of riprap is one of the most important design parameters (Simons & Sentürk, 1992). Table 2-17 presents the size classification of riprap.

Table 2-17: Riprap size classification (Simons & Sentürk, 1992)

Rock size (mm)	Classification
4000 – 2000	Very large boulders
2000 – 1000	Large boulders
1000 – 500	Medium boulders
500 – 250	Small boulders
250 - 130	Large cobbles

For Reno-mattresses, it is obvious that the designed rock size should be larger than the openings in the mesh wire to prevent rocks from washing out of the wire cage, which could expose the subgrade.

2.3.1.2 Rock grading

Riprap forms a stable attack surface of its top layer when well graded. A good grading ensures the interlocking of individual particles and maximum internal friction (Annandale, 2006).

Simons & Sentürk (1992) published a grading method that is still widely accepted today and is presented by the following three equations:

$$d_{100} \geq 2d_{50} \quad \text{Equation 2.65}$$

$$d_{20} \geq 0.5d_{50} \quad \text{Equation 2.66}$$

$$d_{min} \geq 0.2d_{50} \quad \text{Equation 2.67}$$

The grading width, f_g, can either be narrow, wide or very wide, as given in Table 2-18. CIRIA *et al.* (2007) recommend a wide grading for riprap structures.

Table 2-18: Grading width (CIRIA *et al.*, 2007)

Grading width, f_g	d_{85}/d_{15}
Narrow	< 1.5
Wide	1.5 – 2.5
Very wide	2.5 – 5.0

The grading guideline by Simons & Sentürk (1992), if interpolated linearly, relates to a grading width (d_{85}/d_{15}) of 3.6, which falls in the "very wide" category. Thus, Simons & Sentürk (1992) recommends a wider grading width than CIRIA *et al.* (2007).

For riprap exposed to overtopping flow conditions, Przedwojski *et al.* (1995) recommends that $d_{60}/d_{10} \geq 2.15$. The US Army Corps of Engineers presented the following equations, similar to those presented by Simons & Sentürk (1992), for riprap design:

$$1.26d_{50} \leq d_{100} \leq 2d_{50} \quad \text{Equation 2.68}$$

$$0.74d_{50} \leq d_{15} \leq d_{50} \quad \text{Equation 2.69}$$

The performance of riprap and Reno-mattresses is highly dependent on the underlying granular filter layers. Filters are typically designed that the particles in the lower layer are sized as to prevent them from penetrating the upper layer, in effect preventing the washing out of the base material below the filter. The fact that the design of filters is independent of hydraulic loading, which is often times very difficult to determine (CIRIA *et al.*, 2007; Przedwojski *et al.*, 1995), keeps the design simple.

The following uniformity criterion is applicable to granular filters, as presented by CIRIA *et al.* (2007) and Przedwojski *et al.* (1995):

$$d_{60}/d_{10} < 10 \quad \text{Equation 2.70}$$

To ensure a stable interface between two granular filter layers, Przedwojski *et al.* (1995) recommends the following retention criterion, with the base and filter material denoted as b and f, respectively:

$$d_{15f}/d_{85b} \geq 2.15 \qquad \text{Equation 2.71}$$

2.3.1.3 Rock density

For stability calculations, the density of the rock used in riprap or Reno-mattresses is an important parameter. An adequate estimate for riprap density is in the order of 2650 kg/m³ (CIRIA *et al.*, 2007; Annandale, 2006; Przedwojski *et al.*, 1995; Simons & Sentürk, 1992). However, for design purposes CIRIA *et al.* (2007) recommends using the apparent rock density (ρ_{app}):

$$\rho_{app} = \rho_r(1 - p) + \rho_w p S_r \qquad \text{Equation 2.72}$$

Where:

ρ_r = Rock density (kg/m³)

p = Porosity of rock particle = pore volume/total volume

S_r = Degree of saturation = volume of water in pores/volume of pores.

Langmaak (2013) argues that there are no other references cited that mention ρ_{app}. He poses the argument that there is not enough time for water to fill all the voids in structures that are submerged only for short periods at a time. Therefore, p ≈ 0, and hence $\rho_{app} \approx \rho_r$.

2.3.1.4 Layer thicknesses of riprap and Reno-mattresses

Many researchers such as Langmaak (2013), Maynord *et al.* (1989) and Stoffberg (2005) recommend a riprap structure layer thickness $t > 2d_{50}$, but never less than 200 mm. Rooseboom & van Vuuren (2013) proposes a minimum thickness of $1.5d_{50}$, but also never less than 200 mm. Jansen van Vuuren *et al.* (2013), on the other hand, recommends that the layer thickness should never be less than the greater of d_{100}, $1.5d_{50}$ or 300 mm. For underwater installations, Jansen van Vuuren *et al.* (2013) recommends that layer thicknesses be increased by 50% to account for uncertainties during installation.

According to Stoffberg (2005), the layer thickness of Reno-mattresses are typically based on $2d_{50}$, rounded up to the next standard Reno-mattress available. Standard mat thicknesses available are 170 mm, 230 mm and 300 mm. Dimensions of standard Reno-mattresses available are given in Table 2-19.

Table 2-19: Standard sizes of Reno-mattresses (Gabion Baskets, 2019; Maccaferri, 2015)

Length (m)	Width (m)	Thickness (m)	Plan area (m²)	Volume (m³)
2	1	0.3	2	0.6
3	1	0.3	3	0.9
4	1	0.3	4	1.2
6	2	0.17	12	2.04
6	2	0.23	12	2.76
6	2	0.3	12	3.6

A model and prototype study conducted by Simons, Chen, Swenson and Simons, Li & Associates (1984) at the CSU, showed that required layer thicknesses of riprap can in some cases be 1.5 to 3 times the required layer thickness of Reno-mattresses. This indicates that the wire mesh is a major contributor to the stability of Reno-mattresses (Stoffberg, 2005). Reference is made to Table 2-22 which presents a comparison between required riprap- and Reno-mattress thicknesses, according to the CSU study (1984).

2.3.2 Design guidelines

Even though there has been extensive research conducted on the performance of riprap and Reno-mattress revetments, there remains uncertainty in its design for turbulent and non-uniform conditions. Generally, laboratory studies are performed for such project specific conditions, or overly conservative designs are proposed, leading to unnecessary expense (Langmaak, 2013). Some commonly used and accepted design methods are summarised in the following sections.

2.3.2.1 Escarameia & May (1992) and Escarameia's (1995) design equation

The design equation presented by Escarameia & May (1992) and Escarameia (1995) in Section 2.2.5.1 as Equation 2.57 (given again as Equation 2.73) is also applicable to the design of riprap structures:

$$d_{n50} = C_r \frac{V_b^2}{2g\Delta} \qquad \text{Equation 2.73}$$

Where:

C_r = 12.3r – 0.2 (for armourstone) (CIRIA *et al.*, 2007)

The same requirements listed in Section 2.2.5.1 need to be met to use Equation 2.73. This method is difficult to apply in practice due to the difficulty of quantifying turbulence intensity r. Langmaak (2013) proved this design equation to yield adequate results, although it is extremely sensitive to errors made in the estimation of the bed velocity. This method relies on

the experience and interpretation of the design engineer, which could be troublesome (Langmaak, 2013).

2.3.2.2 Pilarczyk's (1995) design equation

Pilarczyk's (1995) design equation, given as Equation 2.58 in Section 2.2.5.2 and again as Equation 2.74, could also be used for the design of riprap and gabion revetments (Pilarczyk, 1995):

$$d_{n50} = \frac{\varphi_s}{\Delta}\frac{0.035}{\psi_c}K_T^2 K_h(\psi_s{}^2)^{-1}\frac{V^2}{2g} \qquad \text{Equation 2.74}$$

Recommended values for the stability correction factor, φ_s, are given in Table 2-20.

Table 2-20: Recommended values for stability correction factor (CIRIA et al., 2007)

Hydraulic condition	Recommended φ_s
Exposed edges of gabions	1
Exposed edges of riprap/armourstone	1.5
Continuous rock protection	0.75

2.3.2.3 General Design Equation (CIRIA et al., 2007)

By using the equation of Izbash & Khaldre (1970) as a base and incorporating the Shields's parameter for critical shear stress, CIRIA *et al.* (2007) developed the equation referred to as the "General Design Equation":

$$\frac{V^2/2g}{\Delta d} = k_\beta k_\gamma K_t^{-2} K_w^{-1} \Lambda_h \psi_{cr} \qquad \text{Equation 2.75}$$

Where:

K_w = Wave amplification factor

CIRIA *et al.* (2007) recommends the following critical Shields's parameters (ψ_{cr}):

- 0.030 – 0.035 for the critical point where particles begin to move; and
- 0.050 – 0.055 for limited movement of particles.

A laboratory study conducted by Langmaak (2013) showed a large discrepancy between the results obtained in his study and the prediction of the General Design Equation. Langmaak (2013) stated that Pilarczyk's (1995) design equation yields more consistent results than the General Design Equation.

2.3.2.4 Shields's design criteria (Rooseboom & van Vuuren, 2013)

The criteria presented by Rooseboom & van Vuuren (2013) are used by many South African Engineers for the design of riprap and Reno-mattress revetment structures. Rooseboom & van Vuuren (2013) simplified Shields's approach for uniform flow conditions and presented an expression that can be used for bed stability calculations for non-cohesive particles larger than 6 mm, with a relative density of 2650 kg/m³:

$$d_{50} > 11DS_0 \qquad \text{Equation 2.76}$$

The rock diameter required to protect the side slopes of channels and rivers against erosion can be calculated using the following equation (Rooseboom & van Vuuren, 2013):

$$d_{50} > \frac{8.3DS_0}{\cos\gamma\sqrt{1-\frac{tan^2\gamma}{tan^2\varphi}}} \qquad \text{Equation 2.77}$$

Where:

γ = Side slope of channel or river normal to flow (degrees from horizontal)

φ = Angle of repose of the rock particles (degrees).

The derivation of Equation 2.76 uses a relatively high Shields's parameter of 0.056. Langmaak (2013), however, argues that this method may yield too small rock sizes, which could result in an underdesigned structure.

2.3.2.5 Liu's design criteria

Jansen van Vuuren *et al.* (2013) disagrees with Shields's theory, stating that particle size cannot be used as a means of measuring the transportability of non-cohesive particles and that particle settling velocity should be used. Jansen van Vuuren *et al.* (2013) therefore recommends the equations presented in Section 2.1.3.4 for design purposes (Jansen van Vuuren *et al.*, 2013). As a result, Stoffberg (2005) and Langmaak (2013) aimed to apply the stream power-based incipient motion studies of Rooseboom (1992) and Armitage (2002) to define incipient motion conditions for riprap and Reno-mattresses. Their findings are presented in this section, while Section 4.5 compares the incipient motion conditions of riprap and Reno-mattresses with those of Armorflex, as developed in this study.

a) Stoffberg (2005)

Stoffberg (2005) analysed the results from hydraulic tests conducted on Reno-mattresses by Simons, Chen, Swenson and Simons, Li & Associates (1984) at the CSU. Table 2-21 presents the critical velocities for various mattress thicknesses determined through the study conducted at the CSU. Also given in Table 2-21 are the results from a study conducted by Agostini &

Papetti (Simons *et al.*, 1984), which is included for comparison. Stoffberg (2005) mentioned that the limiting velocities suggested by Agostini & Papetti (Simons *et al.*, 1984) were all lower than the velocities suggested by the CSU study for Fr<1.5, particularly for 150 mm and 230 mm thick mattresses. Agostini & Papetti's design criteria therefore result in thicker mattress linings than that required when using the CSU criteria (Stoffberg, 2005).

Table 2-22 shows the critical shear stress required to initiate movement of standard Reno-mattresses as well as the corresponding layer thickness of riprap required at this shear stress value (Simons *et al.*, 1984). Shields's parameters, ψ, used in the CSU study were 0.1 for Reno-mattresses and 0.047 for riprap (Stoffberg, 2005).

Table 2-21: Critical velocities for standard Reno-mattress thicknesses

Reno-mattress thickness (mm)	V_{cr} (m/s) determined by the CSU study (Simons *et al.*, 1984)		Suggested V_{cr} (m/s) values by Agostini & Papetti (Simons *et al.*, 1984)
	Fr < 1.5	Fr > 3	
150	4.420	3.688	1.798
230	4.694	3.962	3.597
300	4.999	4.206	4.511
450	5.578	4.755	5.395

Table 2-22: Required thickness of Reno-mattresses as determined through the CSU study (1984) compared to riprap thicknesses (Stoffberg, 2005)

Shear stress (kg/m²)	Required layer thickness (mm)	
	Reno-mattresses	Riprap
17.09	150	432
19.53	230	508
22.45	300	584
26.85	450	711

Stoffberg (2005) finally calculated Movability Numbers for all tests conducted by Simons *et al.* (1984), which are presented in Table 2-23. The table includes Stoffberg's suggested Movability Numbers for Reno-mattresses and riprap, based on the results obtained.

Table 2-23: Movability Numbers using stream power theory (Stoffberg, 2005)

Layer thickness (mm)	Movability Numbers	
	Reno-mattress	Riprap
150	0.168	0.127
230	0.171	0.127
300	0.171	0.149
450	0.165	0.15
Average	0.169	0.138
Suggested	**0.165**	**0.13**

Even though Stoffberg (2005) recommended Liu's stream power approach for riprap and Reno-mattresses placed at steep slopes in turbulent flow conditions, his results also showed good correlation to Shields's theory. Stoffberg (2005) thus recommended the following design guidelines for riprap and Reno-mattress revetments:

Riprap design guidelines:

- Shields's theory and Liu's stream power theory holds for ψ = 0.056 and $\frac{V^*}{V_{ss}}$ = 0.130 for $R_e{}^*$ > 13, respectively.
- For turbulent conditions or around bends, apply a safety factor of 1.5 to the calculated d_{50}: $d_{50_{increased}}$ = 1.5d_{50} = 1.5(11DS_0) = 16.5DS_0.

Reno-mattresses design guidelines:

- Shields's theory and stream power theory holds for ψ = 0.090 and $\frac{V^*}{V_{ss}}$ = 0.165 for $R_e{}^*$ > 13, respectively.
- d_{50} = 7DS_0
- For turbulent conditions or around bends, apply safety factor of 1.5 to calculated d_{50}: $d_{50_{increased}}$ = 1.5d_{50} = 1.5(7DS_0) = 10.5DS_0, but not smaller than the largest mesh opening (100 mm).

Stoffberg (2005) did not, however, determine the drag coefficient experimentally but assumed a value of 0.4.

b) Langmaak (2013)

Langmaak (2013) performed large scale laboratory tests on riprap to determine the dimensionless Movability Number at large particle Reynolds numbers. Langmaak (2013)

proved that Liu's theory holds for riprap placed on steep slopes, exposed to non-uniform, high turbulent flow conditions.

Langmaak (2013) found that the success of Liu's theory is extremely reliable on the correct determination of settling velocity. He therefore determined the drag coefficient experimentally rather than working off assumptions. His results showed a drag coefficient of 1.66, which differs substantially to the 0.4 assumed by Stoffberg (2005). Langmaak (2013) furthermore recommended that settling velocity should be calculated using d_{90} to consider the hiding effects of a non-uniform riprap bed.

Langmaak (2013) found that for riprap, graded as stipulated by Simons & Sentürk (1992) in Section 2.3.1.2, Liu's critical Movability Number can be taken as 0.18 for design purposes, which is close to the 0.17 recommended by Armitage (2002).

2.4 Conclusions drawn from the Literature Study

The literature study presented an investigation into incipient motion theory, with emphasis put on Liu's stream power approach. An in-depth study of Armorflex blocks and its physical characteristics, installation guidelines, previous hydraulic testing and design guidelines was conducted as it is the subject of this thesis. The literature study concluded with a section on the incipient motion criteria of riprap and Reno-mattresses, two common revetment alternatives to Armorflex. The following main conclusions were drawn from the literature study:

- Incipient motion theory is reasonably well understood. Three of the most widely used single-parameter approaches to determining incipient motion of non-cohesive particles are critical flow velocity, Shields's critical bed shear stress and Liu's stream power approach.
- Critical flow velocity is not a suitable parameter to use for defining incipient motion. Average flow velocity is, although easy to measure, not a suitable parameter to use for predicting incipient motion as it does not sufficiently represent the flow conditions in the vicinity of the particle under consideration. On the other hand, local flow velocity in the vicinity of the particle under investigation is extremely difficult, if not impossible to determine.
- Shields claimed that particle movement is uniquely determined by shear stress, which is in fact not the case (Yang, 1973). Shields uses median particle diameter to describe incipient motion, while Rooseboom (1992) is of the opinion that settling velocity is a more suitable parameter.

- Liu's stream power approach is the preferred method for defining the incipient motion of particles exposed to flowing water. Liu's method assumes uniform flow conditions.
- In using Movability Number as a means of defining incipient motion, the determination of the settling velocity of the particle under consideration is of critical importance and needs to be done accurately. Langmaak (2013) stressed the importance of accurately determining the settling velocity when investigating the incipient motion conditions of irregular shaped particles.
- From previous hydraulic testing, the incipient motion conditions of Armorflex have typically been expressed in terms of limiting flow velocity and/or limiting bed shear stress. Armorflex incipient motion criteria have not been provided in terms of Movability Number in the past.
- Previous Armorflex hydraulic testing has been conducted in Europe and the United States of America. The specific Armorflex blocks tested are not identical to the Armorflex 140 and Armorflex 180 that are available in South Africa.
- Concern is expressed over the lack of limiting flow characteristic design guidelines available from Armorflex manufacturers. Technicrete (2016) presents a maximum desired slope of 1V:1.5H and limiting flow velocities of 3.5 and 5.5 m/s for Armorflex 140 and 180, respectively. No reference is made to flow depth, hydraulic radius, shear stress, Froude number, or Movability Number. Contech Construction Products inc. (Armortec Incorporated, 1981) presents flow velocity and hydraulic radius at various bed slopes as limiting flow parameters of Armorflex class 30 (similar to Armorflex 180, but not identical). Armortec Erosion Control Systems (Koutsourais, 1994) presented a limiting flow velocity of 4.5 m/s and a limiting shear stress of 73.4 kg/m² for Armorflex class 30, based on flume studies conducted by Clopper (1989).
- The shear stress-based theories for defining the incipient motion of riprap and Reno-mattresses are currently the most reliable. Stream power methods such as the Movability Number approach were shown to be valuable in determining the incipient motion conditions of riprap and Reno-mattresses on steep slopes and exposed to turbulent overtopping flows. Stoffberg (2005) presented Movability Numbers of 0.13 and 0.165 for riprap and Reno-mattresses, respectively, while Langmaak (2013) argued that a Movability Number of 0.18 can be used for the design of riprap.

3. PHYSICAL MODEL STUDY

Several tests were conducted in an undistorted physical model to determine the incipient motion conditions of Armorflex 140 and 180 blocks on steep slopes. All tests and experiments were conducted in the Hydraulics Laboratory at the University of Stellenbosch.

This section comprises an investigation into the scale effects of the hydraulic model, the manufacturing of the scaled blocks, the experimental determination of the drag coefficient of the blocks, the setting up of the hydraulic tests and the testing procedure itself.

3.1 Hydraulic modelling

A scaled model in hydraulic engineering aims to simulate the direct physical conditions in the same medium as in the prototype. To achieve the desired similarity between model and prototype, certain scaling laws need to be satisfied.

The hydraulic laboratory had a discharge capacity of just under 600 L/s. Given the flow limitation, a scale model study was undertaken to investigate the incipient motion of the blocks under hydraulic loading. A half-width channel cross-section was used, assuming symmetry with the aim to decrease the effects of scaling.

3.1.1 Scale theory and physical model scale laws

The type of flow present in a hydraulic model depicts which dimensionless group is used. Some widely used dimensionless groups are the following (Pettersson & Pettersson, 2011):

- Reynolds number (ratio of inertia and viscous forces)
- Froude number (ratio of inertia and gravitational forces)
- Mach number (ratio of fluid velocity to the local sonic velocity).

As this thesis investigates free surface flow conditions, inertial and gravitational forces govern the flow. Therefore, the Froudian similarity law (i.e. Froude number remains constant) was adopted to convert model values into scale prototype values. Table 3-1 shows the model-to-prototype scaling rations used, as prescribed by the Froudian similarity law.

In most model studies, even geometrically similar models, some sort of scale distortion and/or scale effects on the flow exist. Therefore, results from model studies either enhance or reduce the safety of the prototype structure (Novak, et al., 2014).

Table 3-1: Prototype-to-model multiplication factor with the Froudian similarity law

Variable	Prototype-to-model multiplication factor
Dimensions or length (m)	λ
Area (m²)	λ^2
Volume (m³)	λ^3
Velocity (m/s)	$\sqrt{\lambda}$
Flow rate (m³/s)	$\lambda^{2.5}$
Shear stress (kg/m²)	λ
Mass (kg)	λ^3

According to Novak *et al.* (2014), the main scale effects are model roughness and the model approach conditions associated with turbulent boundary layer development, cavitation effects, surface tension effects and aeration- and vortex-formation problems. However, with a high enough Reynolds number, some of these effects can be minimised. According to Novak *et al.* (2014), open channel flow models should have Reynolds numbers above $10^{3.5}$ – $10^{4.5}$ in order to avoid scale effects. In addition, Novak *et al.* (2014) recommends a minimum flow depth of 0.03 m to avoid surface tension effects.

3.1.2 Model scale effects

The selected scale for this model study was 1:3. Therefore, λ in Table 3-1 is equal to 3. To prove that the scale- and surface tension effects of the model study are minimised, the criteria of Novak *et al.* (2014) for open channel flow models was investigated. For each test conducted, flow depth readings were recorded at 0.5 m intervals along the centreline of the test section, with the readings were corrected for bed slope. The Reynolds number was determined using Equation 3.1 (van Vuuren & Rooseboom, 2013).

$$R_e = \frac{VR}{\nu} \qquad \text{Equation 3.1}$$

Where:

V = Average velocity (m/s) = Q/A

R = Hydraulic radius (m) = A/P, where P = wetted perimeter (m).

Figure 3-1 and Figure 3-2 show the flow depths and Reynolds numbers at the point of incipient motion in the model tests conducted. The results show that Tests 9a and 9b had a flow depth slightly lower than the required 0.03 m recommended by Novak *et al.* (2014). Figure 3-2 shows that the model's Reynolds numbers were all well above the minimum of $10^{4.5}$, satisfying the

scale effects criteria of Novak *et al.* (2014). All results were therefore deemed representative of the prototype.

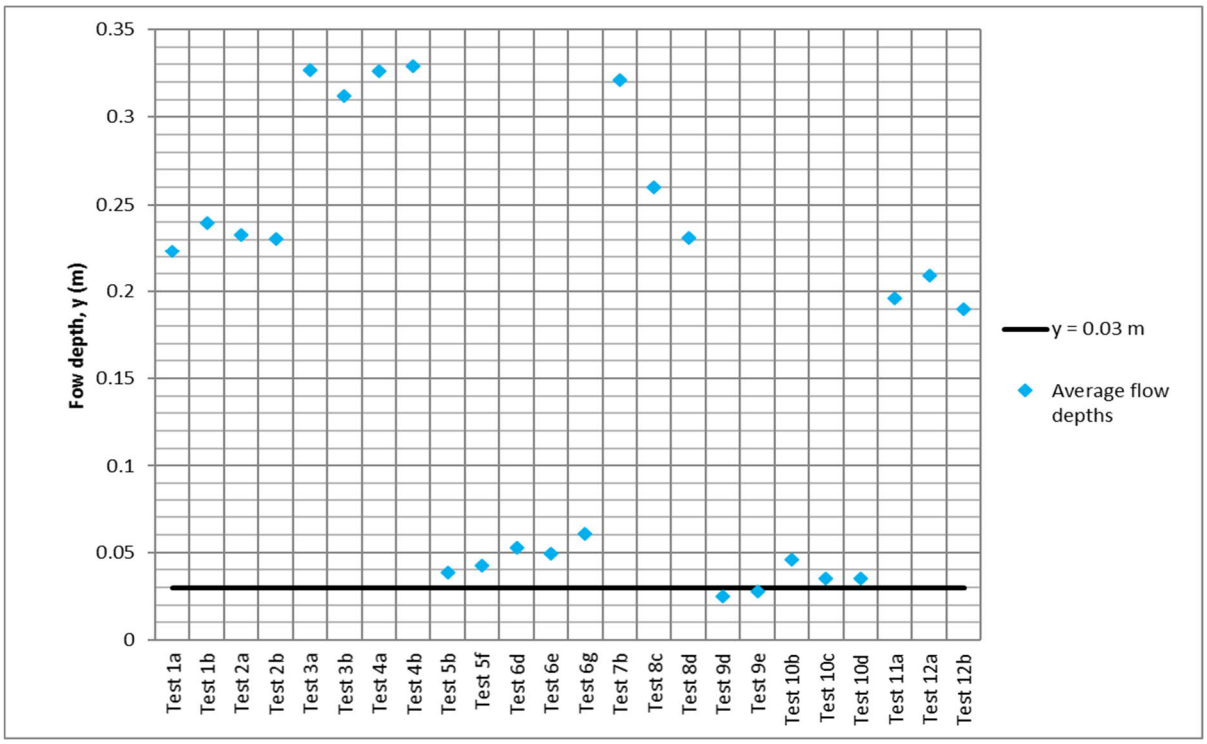

Figure 3-1: Flow depths at incipient motion in model tests conducted

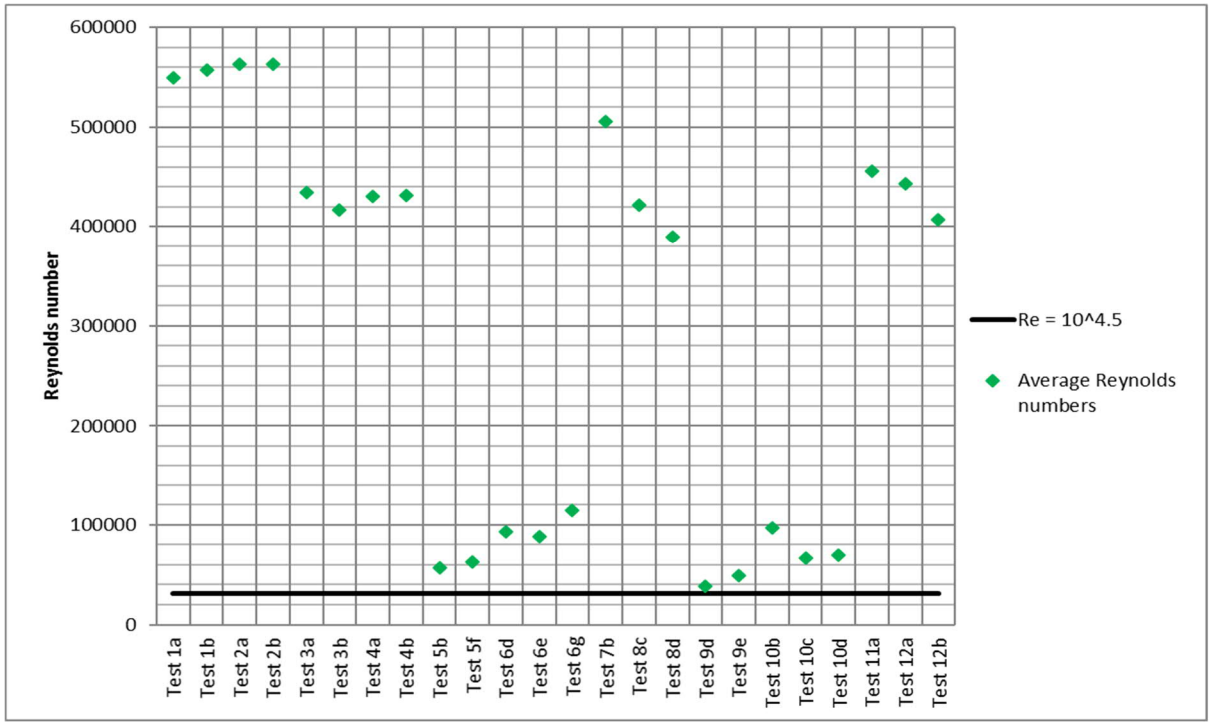

Figure 3-2: Reynolds numbers at incipient motion in model tests conducted

Modelling a half-width channel as a means of representing a full width prototype channel, some limitations to the model study can be expected. One of these limitations is the determination of the wetted perimeter P. Figure 3-3 and Figure 3-4 schematically show flow velocity contours inside a full- and half-width trapezoidal channel. Closer to the channel bed and sides, flow velocity reduces due to increased roughness from the walls. In the half-width channel, the influence of the smooth wall A'B' is assumed negligibly small compared to the rougher wall B'C'D' where Armorflex is installed. In doing so, however, its influence is ascribed to wall B'C'D' in the process. The optimum Manning's n value determined in Section 4.2 would therefore differ slightly from that if a full-width channel had been modelled.

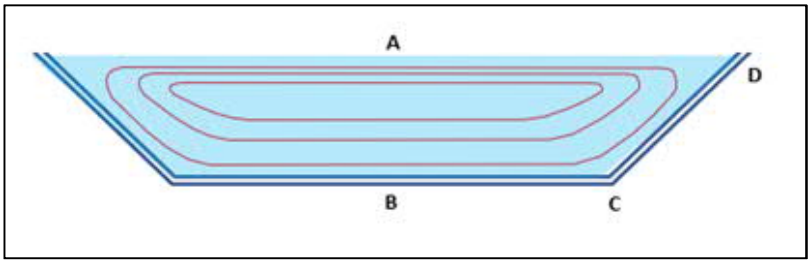

Figure 3-3: Full-width trapezoidal channel cross-section

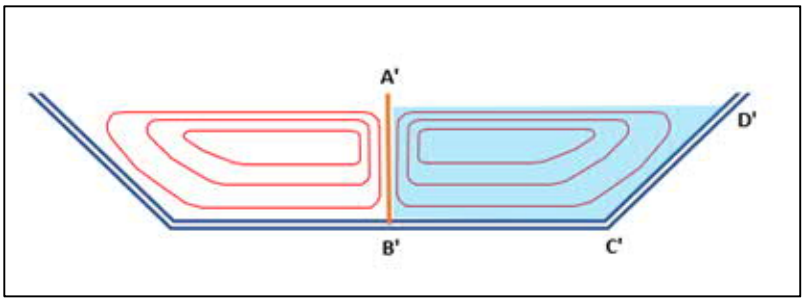

Figure 3-4: Half-width trapezoidal channel cross-section

3.2 Manufacturing of the Armorflex model blocks

As volume is the most important parameter that controls, with the mass density, the mass of the unit and in effect its stability, high quality moulds had to be manufactured to ensure precise and consistent block dimensions and shape. For each Armorflex block type, thirty-six soft polyurethane moulds were manufactured. Figure 3-5 shows the manufactured moulds of the Armorflex 140 and Armorflex 180 model blocks. After casting more than 30 sets of blocks, the moulds showed no signs of deformation.

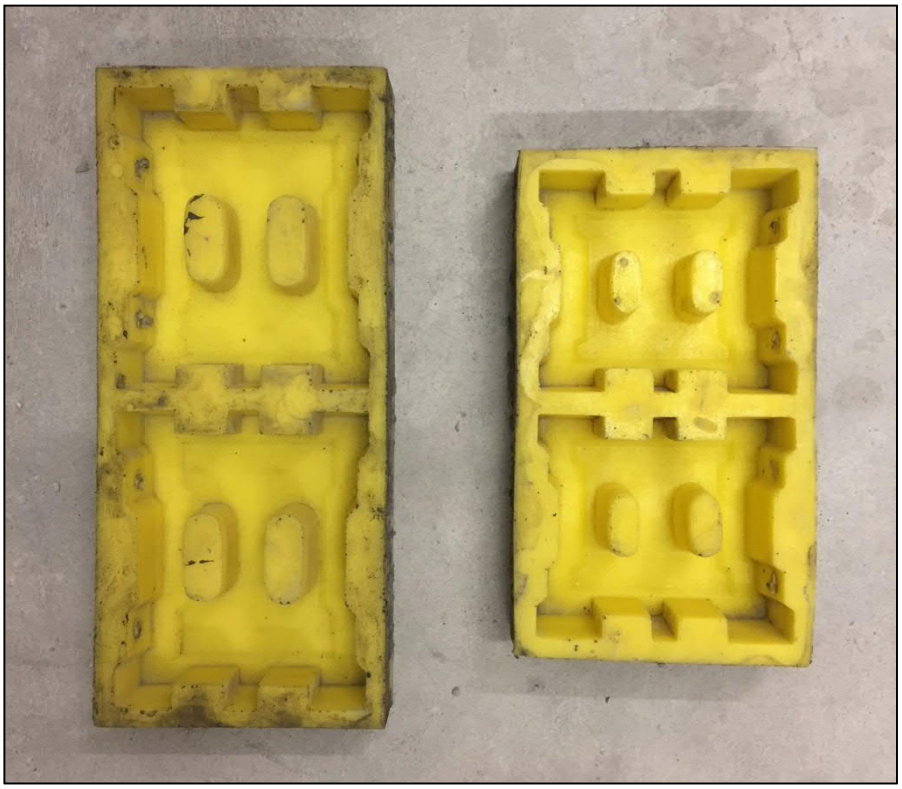

Figure 3-5: Armorflex 140 (left) and Armorflex 180 (right) soft polyurethane moulds

The model blocks were manufactured using a high strength mortar mix design of sand, cement, water and a viscosity modifying agent (Chryso Aquaberton). A water-cement ratio of 0.5 was used, contributing to an average 28-day concrete cube strength of 39.4 MPa. After casting, the blocks were left to set in a climate-controlled room for an average of two days before demoulding.

Figure 3-6 and Figure 3-7 show plan views of the prototype and model scale Armorflex 140 and 180 blocks, respectively. The model blocks were manufactured without holes for cables/wires, as it proved to be impractical at a scale of 1:3. As per Section 2.2.3, the effect of cables on the stability of ACB revetments is uncertain. Some researchers (Clopper, 1989; NCMA, 2010) disregard the effect of cables on system stability, while others (Escarameia, 1995, 1998) show a difference in performance between cabled- and loose concrete block revetments.

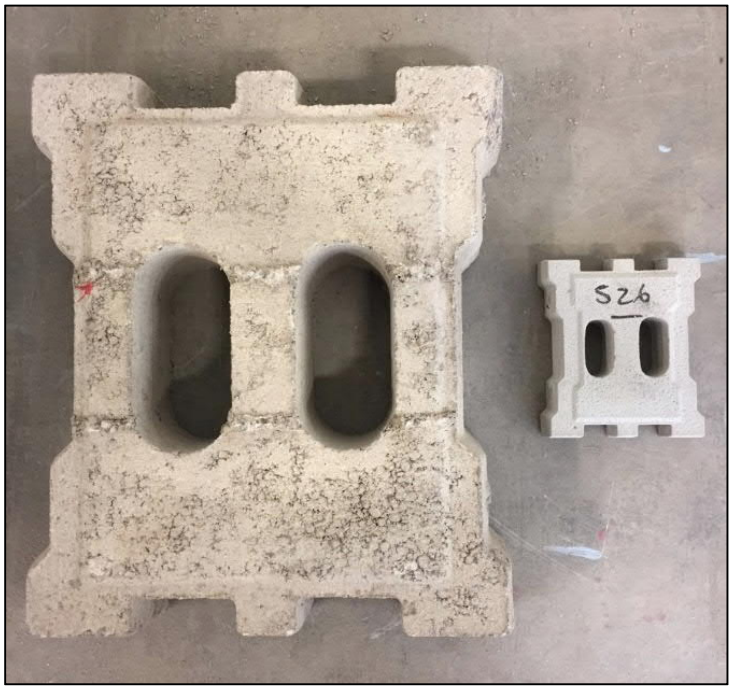

Figure 3-6: Armorflex 140 prototype and 1:3 scale model blocks

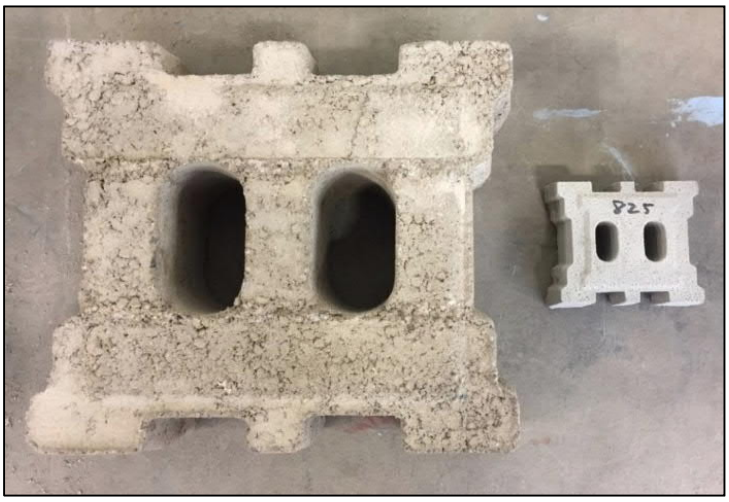

Figure 3-7: Armorflex 180 prototype and 1:3 scale model blocks

3.2.1 Weight of model blocks

According to Technicrete (2016), the average prototype block weights of Armorflex 140 and 180 are 17.5 kg and 16.4 kg, respectively. However, the weight of the sample blocks provided by Technicrete differs from the average weights stated in their product brochure. Table 3-2 shows the discrepancy in weight, proposing that a big tolerance may exist in terms of block volume, unit weight and possibly concrete density in the manufacturing process of Armorflex blocks.

Table 3-2: Variance in weight of Armorflex blocks

Block type	Average weight (Technicrete, 2016)	Actual weight of block provided by Technicrete	Variance from product brochure (Technicrete, 2016)
Armorflex 140	17.5 kg	19.37 kg	+1.87 kg (10.7%)
Armorflex 180	16.4 kg	17.66 kg	+1.26 kg (7.7%)

Another manufacturer of Armorflex 180 in South Africa, INCA Concrete Products, states that the dry mass average of 6 samples should not be less than 16.4 kg, with no block weighing less than 15.25 kg (INCA Concrete Products, 2018). A lower weight limit variance of ±7% is thus adopted. No upper weight limit is provided by the manufacturer.

To set up an allowable weight range for the scaled blocks used in this model study, a 7% variance from the average weight stated by Technicrete (2016) was adopted. Table 3-3 presents the block weight envelope for both prototype and model scale Armorflex blocks.

Each block was numbered before being weighed using a calibrated digital scale (Digi DS-788 with a 6/15 kg capacity and a scale interval of 2/5 g). Blocks that fell outside the unit weight envelope of Table 3-3 were rejected and discarded.

Table 3-3: Block weight range adopted for model study

Prototype scale	Armorflex 140	Armorflex 180
Upper weight limit (kg)	18.73	17.55
Average weight (kg)	17.5	16.4
Lower weight limit (kg)	16.27	15.25
Model scale	**Armorflex 140**	**Armorflex 180**
Upper weight limit (kg)	0.694	0.650
Average weight (kg)	0.648	0.607
Lower weight limit (kg)	0.603	0.565

Table 3-4 provides some statistics in terms of the unit weight of all blocks manufactured for the study. The average unit weight of the scaled Armorflex 140 blocks differed by a mere +0.66% from the average weight specified by Technicrete (2016), while that of the scaled Armorflex 180 blocks varied by -2.13% from the average weight specified by Technicrete (2016).

Table 3-4: Statistics on unit weights of all blocks used in the model study

	Armorflex 140		Armorflex 180	
No. of blocks manufactured	635		935	
No. of eligible blocks based on weight	606		845	
Eligible blocks weight envelope	**Weight (kg)**	**Variance from design**	**Weight (kg)**	**Variance from design**
Minimum weight	0.607	-6.35%	0.565	-6.98%
Average weight	0.652	0.66%	0.594	-2.13%
Maximum weight	0.693	6.92%	0.638	5.04%

3.2.2 Density of model blocks

The density of the Armorflex 140 and 180 model blocks were determined using the known equation of mass divided by volume. To determine the volume of each block type, a simple water displacement test was conducted on a sample of 30 randomly selected blocks of each type. When immersing a block into a half-filled cylinder with known diameter, the volume of water displaced is equal to the volume of the block.

The calculated densities of the sample of scaled Armorflex 140 and 180 blocks are presented in “Appendix B: Scale Armorflex concrete densities” as Table B- 1 and Table B- 2, respectively. Figure 3-8 and Figure 3-9 shows the distribution plot for the densities of the Armorflex 140 and 180 model blocks. The samples of Armorflex 140 and Armorflex 180 blocks had average concrete densities of 1921.9 kg/m^3 and 1920.8 kg/m^3, respectively. The variance in block volume is ascribed to human error during the casting of the moulds. The two block types had standard deviations of 60.7 kg/m^3 and 44.8 kg/m^3, respectively.

An average concrete density of 1921.4 kg/m^3 was adopted and used in all further calculations. For concrete, this density is strikingly low given that INCA Concrete Products (2018) claim that Armorflex blocks are manufactured using concrete with density no less than 2100 kg/m^3. The difference in concrete density was primarily ascribed to a possible safety factor incorporated by the manufacturers of Armorflex to ensure that the minimum unit weight criteria are comfortably met. This could perhaps explain why the weight of the sample blocks provided by Technicrete was significantly higher than the average block weights stated in Technicrete's (2016) product brochure.

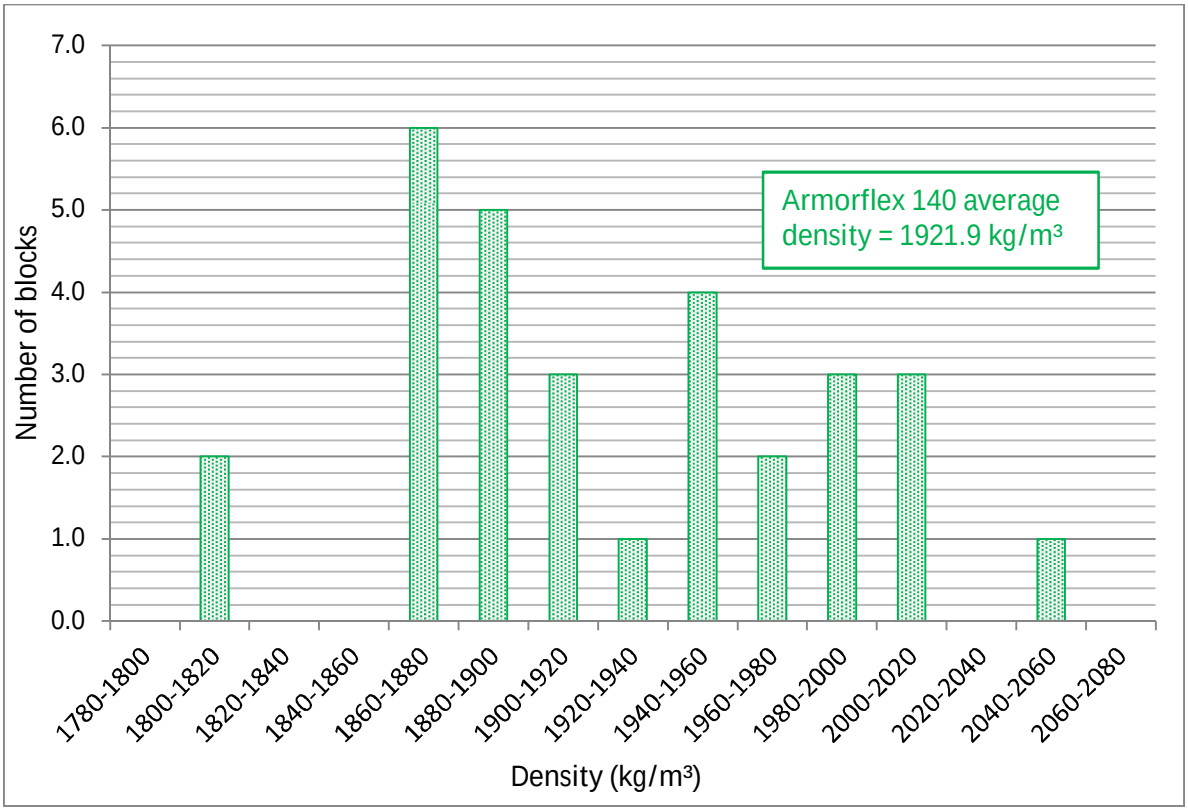

Figure 3-8: Distribution of Armorflex 140 model block densities

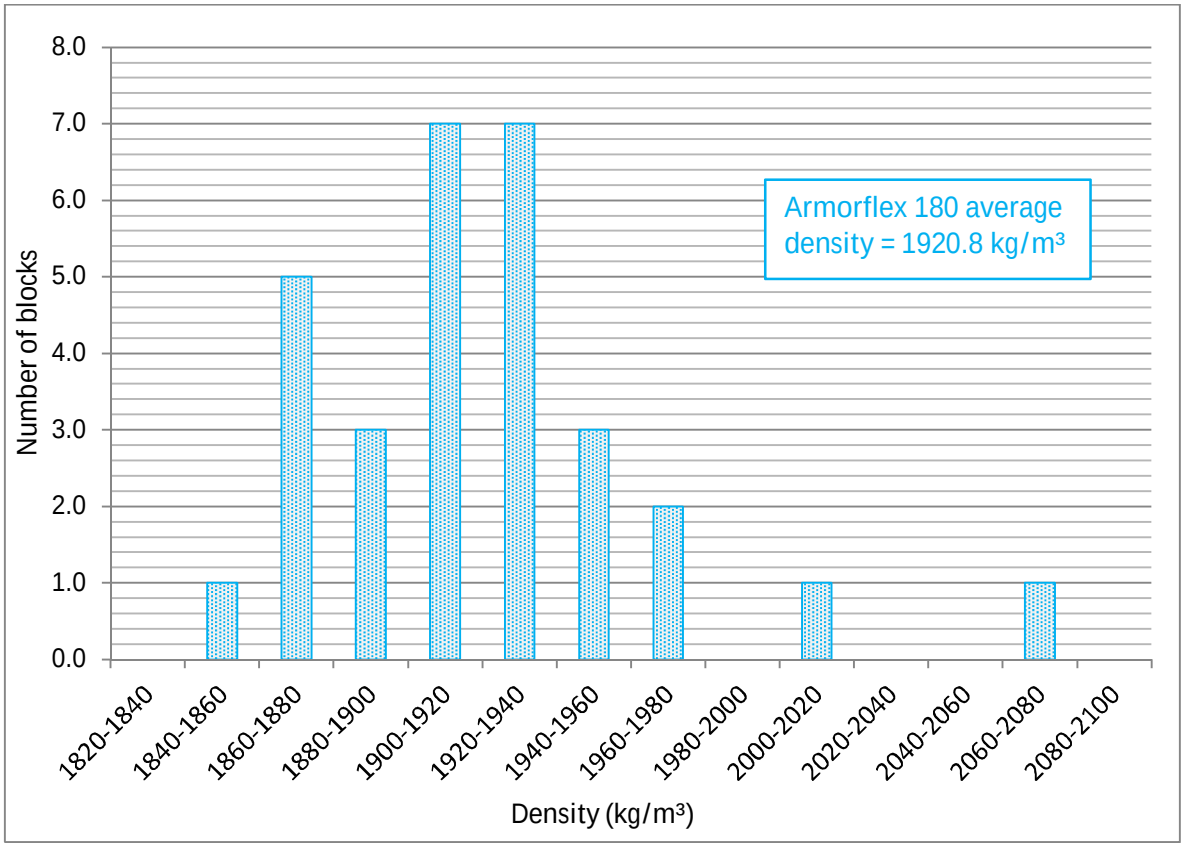

Figure 3-9: Distribution of Armorflex 140 model block densities

3.3 Experimental determination of drag coefficient for block settling velocity

To utilise the Liu Diagram for analysing incipient motion conditions of Armorflex blocks, the settling velocity of both block types were required. Settling velocity, discussed in Section 2.1.2.4, is represented by Equation 3.2:

$$V_{ss} = \sqrt{\frac{4}{3}\left(\frac{\rho_s - \rho}{\rho}\right)\frac{gd}{C_D}} \qquad \text{Equation 3.2}$$

This section details the determination of the following parameters to solve Equation 3.2:

- Particle size, d (representative particle size in the case of Armorflex);
- Settling Velocity, V_{ss}; and
- Drag coefficient, C_D.

3.3.1 Determination of a representative particle size d

Equation 3.2 calls for a particle size d, which generally refers to a specific sieve size. Due to the shape of an Armorflex block, however, a representative sphere diameter was determined instead.

Literature on the determination of a representative sphere diameter shows how many theoretical approaches assume a specific particle orientation during free-fall conditions. However, in order to remain impartial to particle orientation during free-fall, a volume-equivalent sphere diameter d_V (i.e. the diameter of a sphere with equal volume as the particle) was determined, as given by Equation 3.3 (Pabst & Gregorova, 2007). The volume-equivalent sphere diameters calculated for both model block types are presented in Table 3-5.

$$d_V = \left(\frac{6}{\pi}V_{block}\right)^{1/3} \qquad \text{Equation 3.3}$$

Where:

V_{block} = Volume of Armorflex block (m³).

Table 3-5: Volume-equivalent sphere diameter of Armorflex 140 and 180 model blocks

Block type	Average volume of model scale blocks, V_{block} (m³)	Volume-equivalent model sphere diameter, d_V (m)
Armorflex 140	0.00034	0.0864
Armorflex 180	0.00031	0.0836

3.3.2 Experimental determination of the settling velocity of Armorflex blocks

3.3.2.1 Settling velocity test structure

The settling velocity of the blocks was determined experimentally in a 5.55 m high steel tank in the hydraulics laboratory of the University of Stellenbosch. The tank had a diameter of 1.5 m and was filled with water to its brim. Figure 3-10 shows the steel tank with its dimensions.

When released from a stationary position, particles initially accelerate before reaching terminal velocity at a certain distance. The tank had an inspection window at a depth of 1 m from the top of the tank, as shown in Figure 3-10. However, the inside walls of the tank were completely rusted, colouring the water to such an extent that the blocks could not be seen passing the window after being dropped. Figure 3-11 shows the rusted inner walls of the empty tank prior to initial filling.

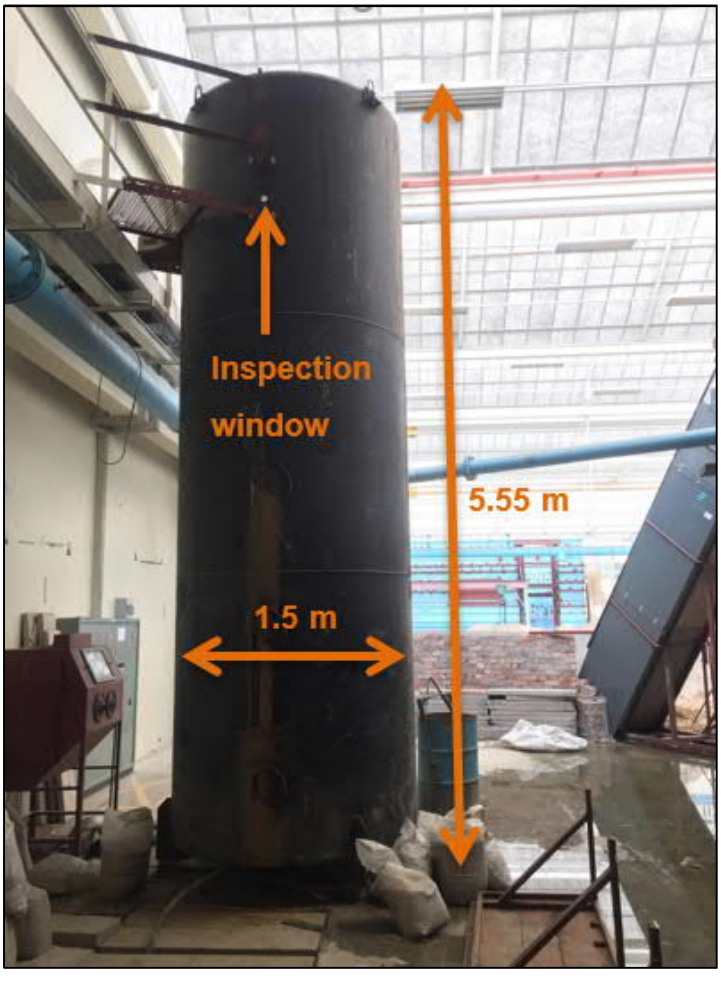

Figure 3-10: Steel tank used to determine the settling velocity experimentally

Figure 3-11: Rusted inner walls of steel tank

With the aim of mitigating the poor visibility through the inspection window, a steel plate, suspended by four nylon ropes, was lowered to a depth of 1.9 m below the surface of the water. A vertical distance of 1.9 m was assumed to be sufficient for the blocks to reach terminal velocity. With a video camera recording, blocks were released from a stationary position just under the surface of the water. As the blocks hit the steel plate, the slight movement of the nylon ropes was visible on the video recordings. The time difference between the point of release and the visible movement of the ropes was recorded. A total of 30 samples of each block type were tested and an average time was obtained.

The video camera used could record 60 frames per second, which meant that a maximum error of 0.033 seconds (duration between two consecutive frames) could be associated with the time difference recorded.

The steel plate was then removed and the tests repeated, with the blocks now falling the full height of the tank (5.55 m). Since the tank is made of steel, the sound of the blocks hitting the bottom was clearly audible on the video recordings, which made time recordings easy.

Since the height difference remained constant (5.55 – 1.9 = 3.65 m), the settling velocity could be calculated by dividing the height difference by the time it took each block to fall 3.65 m, as given in Equation 3.4.

$$V_{ss} = \frac{3.65}{\text{Time difference (5.55 m fall)} - \text{time difference (1.9 m fall)}} \quad \text{Equation 3.4}$$

Not all tested blocks yielded viable results. Results from blocks that made contact with the tank sides or crossbars were disregarded. A total of 21 Armorflex 140 blocks and 24 Armorflex 180 blocks yielded viable results. Figure 3-12 and Figure 3-13 present the distribution of the viable results of Armorflex 140 and 180 samples tested, with Table 3-6 presenting the averages.

Table 3-6: Settling velocity of Armorflex 140 and 180 blocks

Block type	Average time difference recorded (s)			Average V_{ss} (m/s)
	Fall = 1.9 m	Fall = 5.55 m	Fall = 3.65 m	
Armorflex 140	3.534	9.774	6.240	0.585
Armorflex 180	3.194	8.578	5.384	0.678

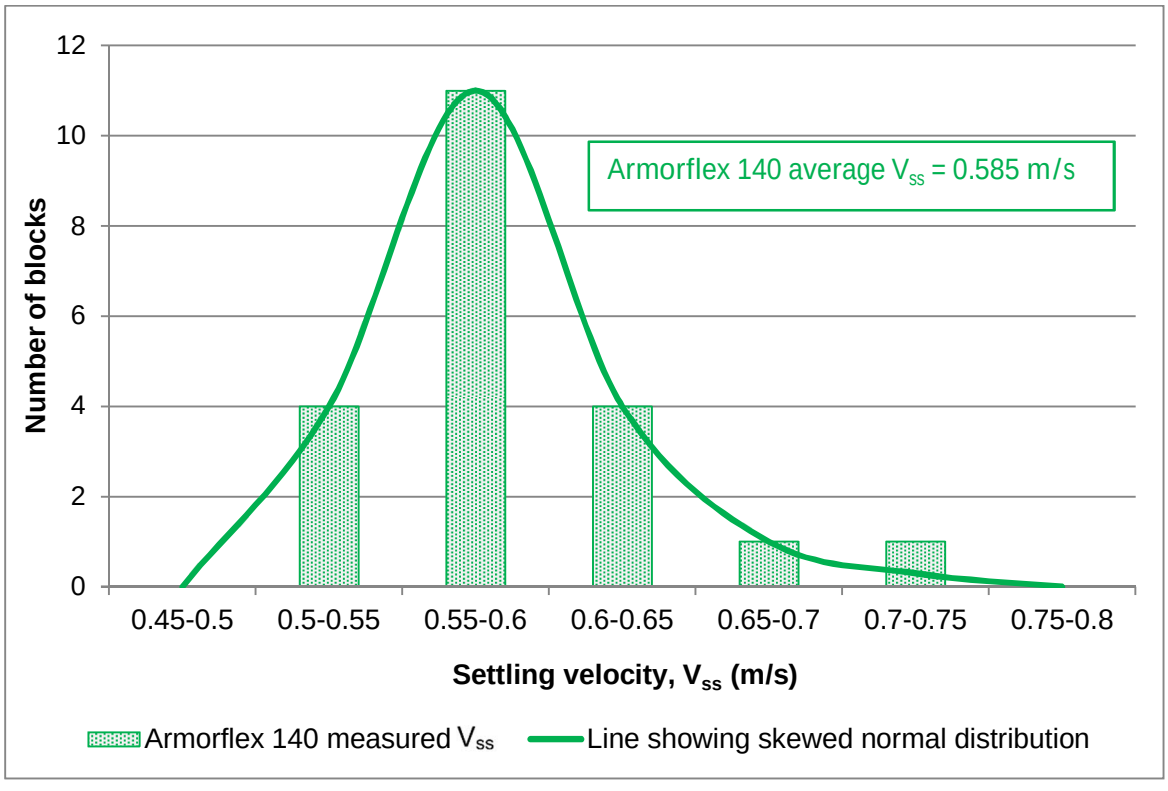

Figure 3-12: Skewed normal distribution of V_{ss} of Armorflex 140 samples

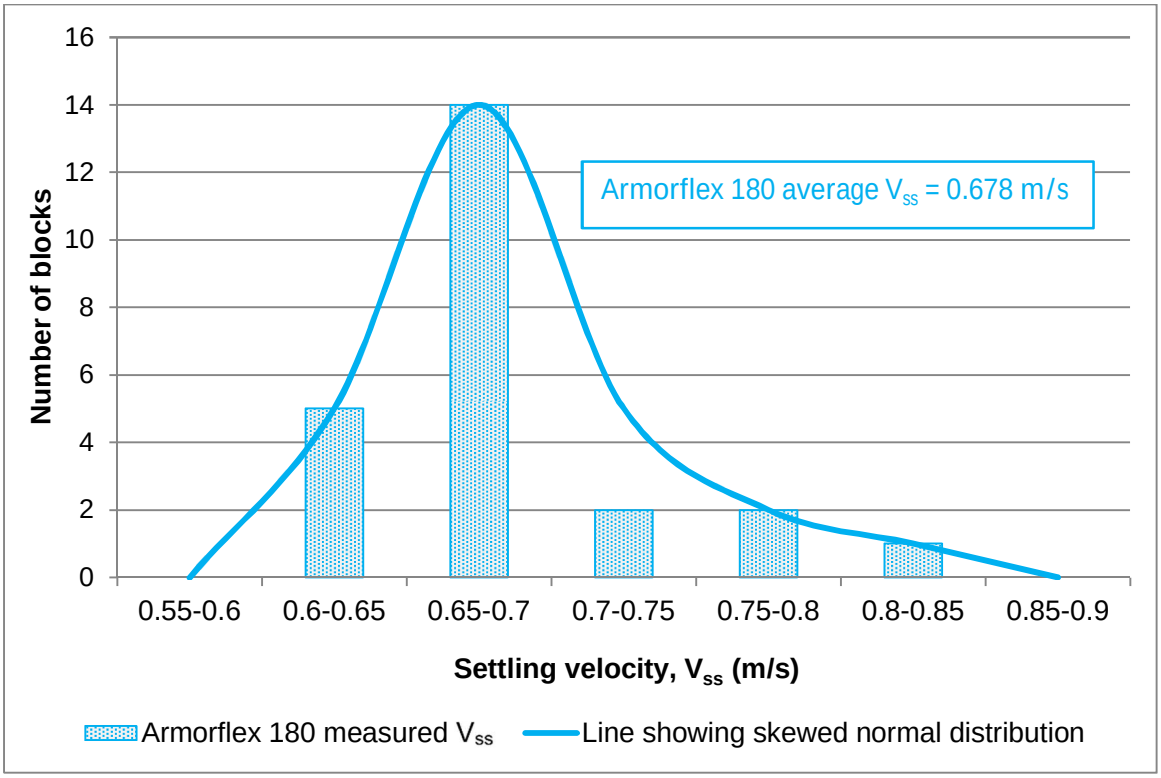

Figure 3-13: Skewed normal distribution of V_{ss} of Armorflex 180 samples

3.3.3 Determination of the drag coefficient of Armorflex model blocks

With d_V and V_{ss} known, the drag coefficient could be determined by solving Equation 3.2. Average drag coefficient values of 3.045 and 2.191 were determined for Armorflex 140 and Armorflex 180, respectively.

3.4 Test channel setup

3.4.1 Test channel layout

The rectangular channel used for the model study was constructed with brick walls, 23 m long (measured from inlet pipe to the end of channel), 1.2 m deep and 0.935 m wide. Figure 3-15 schematically shows the test channel setup inside the hydraulic laboratory. Water was pumped through a 600 mm ND mild steel pipeline, through the calibrated flow meter and into the stilling basin at the upstream end of the test channel. An in-line gate vale controlled the flow. Downstream of the stilling basin, hollow bricks were stacked on top of one another to straighten the flow and prevent waves from entering the approach channel, forcing the flow to be uniform. The position of the weir was selected as chainage 0 (CH 0 m), with the 6 m long Armorflex test section starting 3 m downstream from the weir at CH 3 m and ending at CH 9 m. No tailwater gate was used to control flow depths in the model, thus allowing water to flow freely into the downstream catchpit.

The flow was measured using an electromagnetic FLOWMETRIX SAFMAG flow meter (Figure 3-14) that was installed into the 600 mm ND inlet pipeline conveying flow into the test channel stilling basin. The SAFMAG flow meter accurately measured flow rates with an approximate error of 0.0005 m³/s.

Figure 3-14: Electromagnetic FLOWMETRIX SAFMAG flow meter display

Tests were conducted on three different bed slopes (1:30, 1:20 and 1:10), after which a side slope of 1V:1.5H was added to each bed slope. Six bed slope test channels and six side slope test channels were thus set up given the two types of Armorflex blocks investigated (12 test setups in total). Typical cross-sections of the constructed channels for the bed slope tests and side slope tests are shown in Figure 3-16 and Figure 3-17, respectively. A side slope of 1V:1.5H was investigated as it is Technicrete's (2016) recommended maximum desired slope.

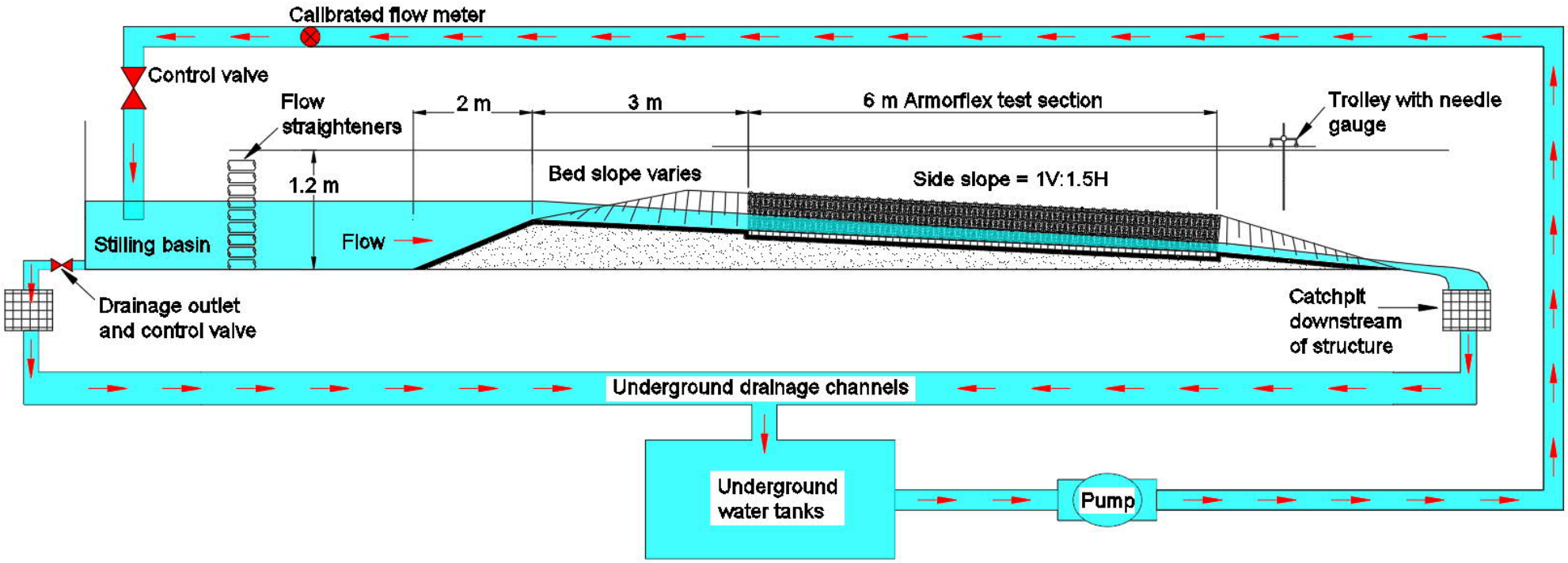

Figure 3-15: **Test channel layout in the hydraulics laboratory (not to scale)**

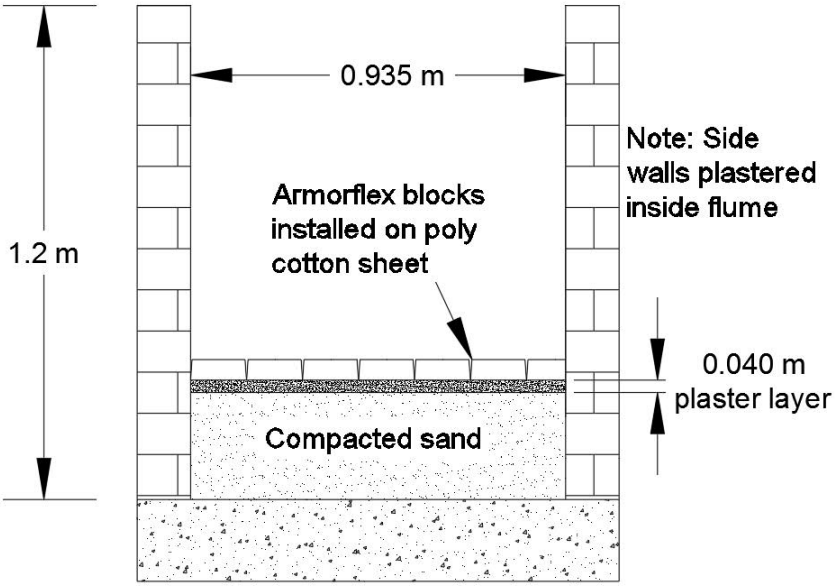

Figure 3-16: Bed slope tests: Typical cross-section through test section (not to scale)

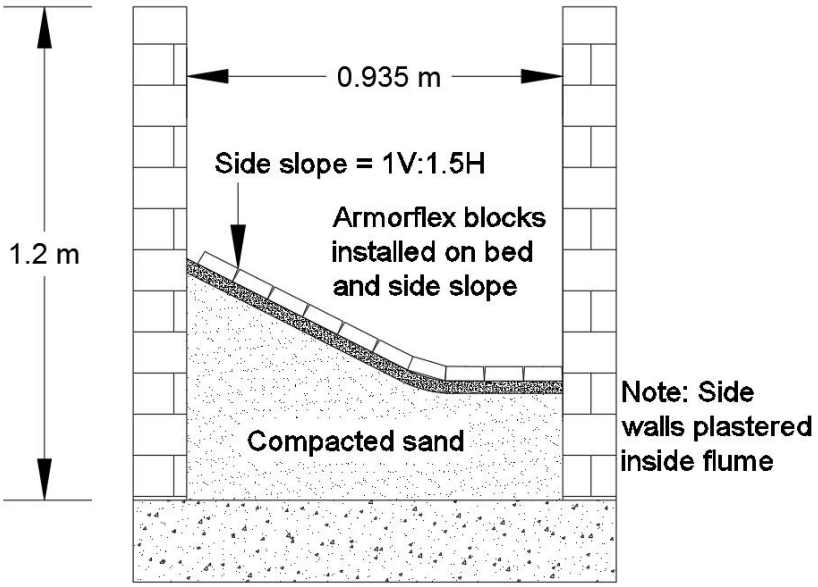

Figure 3-17: Side slope tests: Typical cross-section through test section (not to scale)

3.4.2 Foundation preparation prior to block installation

The channel bed and side slopes were constructed with sand, compacted by hand, and topped with a 40 mm cement plaster layer. Apart from ensuring a smooth and even plastered bed, no other subgrade preparation was required prior to the installation of the filter layer and the Armorflex blocks itself. The rigid bed eliminated the possibility of the foundation eroding and

ultimately resulting in block failure. It was deemed that results obtained on a rigid bed would be similar to those obtained from tests on erodible beds given the erodible bed and filters remain stable. Testing on the rigid bed seemed to be more practical given the number of tests that had to be conducted. Erodible bed would have required constant maintenance and reconstruction every time block failure occurred. A sand bed also has the problem of some flow going through the sand.

A step equal to the height of the blocks was formed at the upstream and downstream ends of the test section to form an even bed throughout the flume length. By “sinking” the test section into the bed, a smooth transition of flow into the test section was promoted. The step in the channel can be seen in Figure 3-15. The step on the downstream end of the test section also served as a means of preventing the blocks from sliding downstream under hydraulic loading.

The side slopes of the half-trapezoidal channels were set out using 6.4 mm thick Masonite templates, cut to form the desired 1V:1.5H side slope, and a radius of 0.203 m (equivalent to a full scale minimum radius of 0.61 m) at the toe of each template. This radius corresponds to the minimum radius recommended by the original manufacturer Nicolon Corporation. The templates were spaced at 1 m intervals and levelled using a dumpy level. The close spacing between adjacent templates allowed for accurate construction of the slope. Figure 3-18 shows the channel with the Masonite templates installed, prior to the filling of the sand, while Figure 3-19 shows the side slope with the compacted sand infill prior to the concrete topping.

Figure 3-20 shows the completed rigid embankment with concrete topping. Prior to block installation, a permeable poly cotton sheet was installed along the length of the test section to represent a scaled geotextile filter layer. Initially, two 3 m long sheets were installed, overlapping in the centre of the channel. The overlap was ± 40 mm, which is much less than the required 303 mm (910 mm full scale) as prescribed in the installation guide of Armortec (2016). Block failure was found to occur repeatedly where the sheets overlapped, confirming that the length of the overlap between geotextile sheets is critical. The results from the tests conducted with the faulty filter layer were therefore not assessed and the fabric was replaced with a single 6 m long sheet with no overlaps. Figure 3-21 shows the poly cotton sheet installed for one of the bed slope tests conducted.

Figure 3-18: Installation of templates for the side slope

Figure 3-19: Sand infill prior to concrete topping

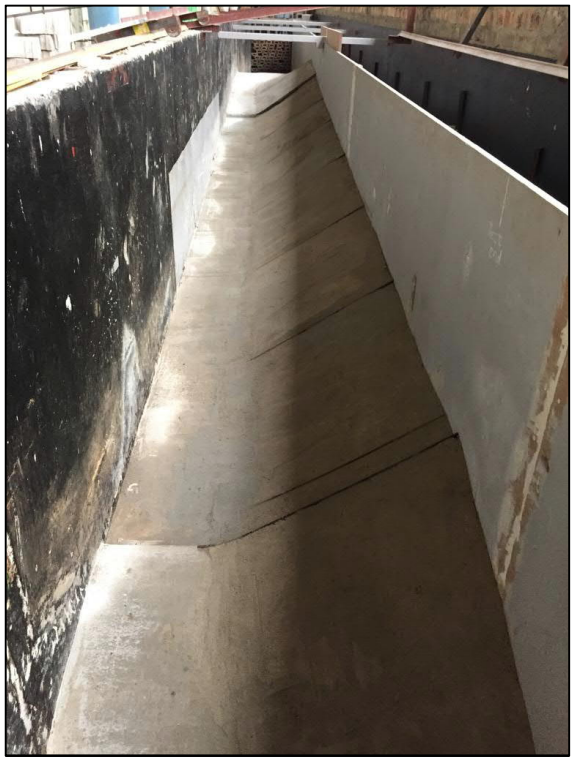

Figure 3-20: Rigid side slope constructed with concrete topping

Figure 3-21: Installed permeable poly cotton sheet

3.4.3 Installation of Armorflex block units

The scaled Armorflex blocks were installed in accordance with the recommendations of Armortec (2016b), from the downstream end proceeding in an upstream direction in the test section. The scaled units were not connected with wires or cables. Therefore, blocks had to be hand-packed one by one. Figure 3-22 and Figure 3-23 show Armorflex 140 blocks installed for the bed slope and side slope tests, respectively. The packing orientation relative to flow direction is indicated by a blue arrow.

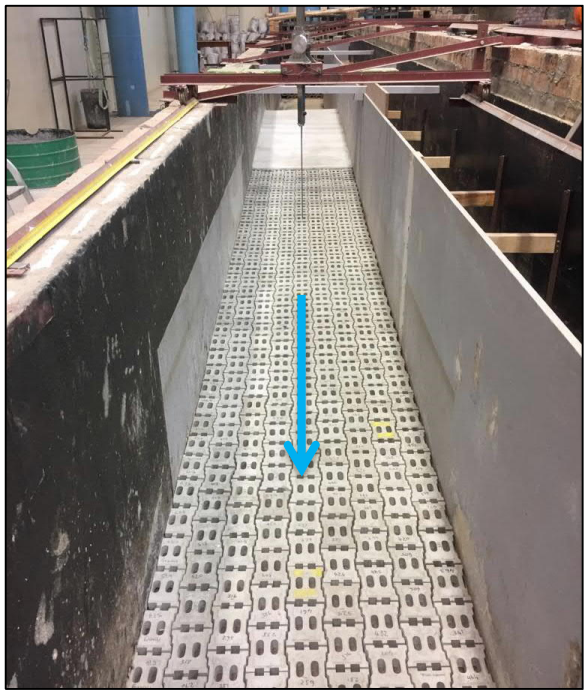

Figure 3-22: Installed Armorflex 140 blocks for tests on bed slope

Figure 3-23: Installed Armorflex 140 blocks for tests on side slope

The column of blocks against the symmetry wall (left side wall in Figure 3-22) had to be cut to fit into the test channel. SikaFlex was used to glue the cut blocks to the channel side and underlying cotton sheet to prevent failure. Additionally, the first three rows of blocks at the upstream end and last three rows at the downstream end were also glued to the floor, preventing failure to occur in these areas.

After the blocks were installed, the structure was visually inspected for blocks projecting more than the allowed maximum of 4.2 mm (12.7 mm full scale) as recommended by Nicolon Corporation. The structure was also inspected for blocks not tightly packed or with no contact with adjacent blocks.

3.5 Testing procedure

3.5.1 Definition of incipient motion for model study

Incipient motion of the Armorflex model blocks was defined as the loss of solid contact between one or more blocks and the foundation bed, i.e. the point at which one or more blocks are lifted out of plane. This definition is in accordance with the ASTM's (2008a) first condition of what can be used as guidance for blocks reaching their stability threshold. As the foundation bed was rigid and non-erodible, the loss of soil beneath the filter layer and the mass slumping/sliding of the foundation was not possible.

3.5.2 Test scenarios

The following four test scenarios were investigated:

i. Armorflex 140 installed on bed slopes;
ii. Armorflex 140 installed on side slopes;
iii. Armorflex 180 installed on bed slopes; and
iv. Armorflex 180 installed on side slopes.

Each test scenario was broken up in three parts in terms of the specific bed slope, that being either 1:10, 1:20 or 1:30, resulting in a total of 12 different test channel setups. Each test was repeated several times to investigate the repeatability of the results obtained. In total, as presented in Table 3-8 and Table 3-9, 39 tests were conducted, of which 24 rendered viable results for data analyses. The tests were referenced using a three-part code, with the first part referring to channel bed slope, the second to channel side slope and the third to the block type. Table 3-7 lists the 12 test channel setups investigated.

Table 3-7: List of tests conducted

Test No	Test code (bed slope_side slope_block type)	Bed slope	Side slope	Block type
1	30_0_140	1:30	0*	Armorflex 140
2	30_0_180	1:30	0*	Armorflex 180
3	30_1.5_140	1:30	1:1.5	Armorflex 140
4	30_1.5_180	1:30	1:1.5	Armorflex 180
5	20_0_140	1:20	0*	Armorflex 140
6	20_0_180	1:20	0*	Armorflex 180
7	20_1.5_140	1:20	1:1.5	Armorflex 140

Test No	Test code (bed slope_side slope_block type)	Bed slope	Side slope	Block type
8	20_1.5_180	1:20	1:1.5	Armorflex 180
9	10_0_140	1:10	0*	Armorflex 140
10	10_0_180	1:10	0*	Armorflex 180
11	10_1.5_140	1:10	1:1.5	Armorflex 140
12	10_1.5_180	1:10	1:1.5	Armorflex 180

* *0 denotes that the channel was tested without a side slope*

3.5.3 Methodology followed

Upon completion of the visual inspection of the blocks as described in Section 3.4.3, the test section was surveyed using a dumpy level, with bed levels (i.e. the top of block levels) recorded at 500 mm intervals along the centreline of the revetment.

At the start of each test, a small flow, typically in the range of 30-50 L/s, was initially released over the revetment. This initial low flow was released to identify projecting blocks. Projecting blocks would typically result in local turbulence in the area. In such a case the subgrade would be inspected for anything that could cause the block to protrude.

The flow was then increased at a slow rate of about 5-10 L/s per minute to prevent flow surges from entering the test section. The structure was carefully observed from the top of the channel until incipient motion (lifting of a block or group of blocks out of plane) was observed. The flow at failure was recorded before being terminated. Once fully drained, the test section was repacked, evaluated again at low flows, and finally retested. Only now, the flow was increased to a flow rate just less than that at which failure initially occurred. The flow was slowly increased at a rate of ±10 L/s per 5 minutes, with water surface elevation measurements recorded at each goal discharge, until failure was observed. At failure, water surface elevations upstream of the point of failure were recorded. The flow at which block movement was observed is referred to as Q_m. The test would then be repeated to investigate the consistency of results. As mentioned in Section 2.1.4, no slope adjustment factor was applied to the results obtained from the model study.

3.5.4 Data collection

The data collected for each hydraulic test included embankment elevation, water-surface elevation (WSE), position of block failure and flow rate at incipient motion. Flow rate was read off from the laboratory's calibrated flow meter. Embankment and water surface elevations were measured at 0.5 m intervals along the channel centreline using two needle gauges

attached to a trolley moving on a rail along the length of the channel. However, only the WSE readings upstream of the point of block failure could be used in the analyses of the collected data because of the sudden increased turbulence and change in flow conditions effected downstream of the point of block failure. Figure 3-24 shows blocks lifted out of plane during “Test 9e: 10_0_140”. The figure shows the increased turbulence and change in flow conditions downstream of the point of block failure.

The test channel walls were non-transparent, which meant that the blocks could only be monitored for movement from the top. The Armorflex structure had to be constantly monitored as block movement would not always result in catastrophic failure only. There were cases in which blocks were lifted out of plane without completely dislodging from the structure. At greater flow depths, however, the visual monitoring of blocks for slight movement was challenging and, in most cases, only catastrophic failure of the revetment could be recorded as the point of incipient motion. Figure 3-25 shows the general washing away of a section of the block structure downstream of the point of initial failure during “Test 3a: 30_1.5_140”. For side slope tests, the blocks on the bed were fixed to the underlying poly cotton sheet to prevent failure.

Figure 3-24: Block failure on channel bed during Test 9e: 10_0_140

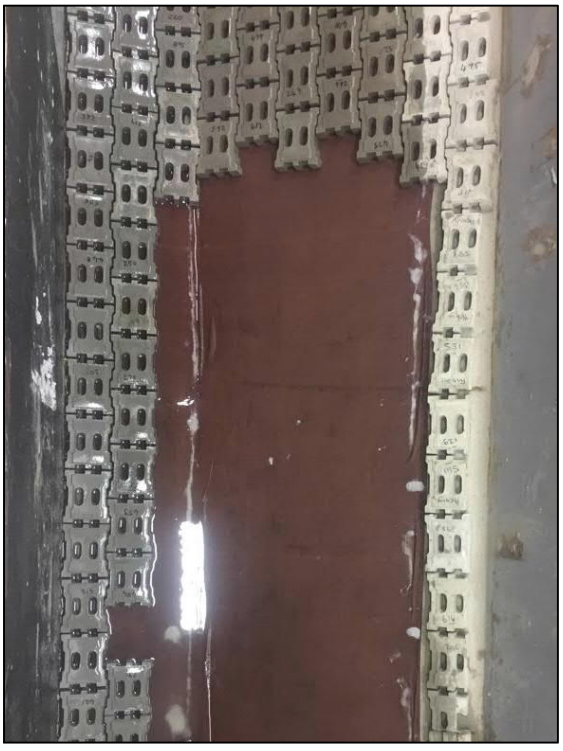

Figure 3-25: Catastrophic failure on side slope following initial block movement

All tests were recorded with a video camera set up at the downstream end of the test channel. Figure 3-26 shows the position of the video camera relative to the test channel. The video recordings were secured as a backup to view at a later stage in case the movement of a block was not observed during the test.

The high turbulence of flow in the test channel made WSE readings challenging to capture accurately. In an attempt to correct possible errors made during the recording of the WSE's, a linear trendline of the observed WSE data points was plotted, effectively obtaining a representative WSE at each measurement station upstream of the point of failure. Flow depths were calculated as the difference between the bed elevation and the representative WSE at a specific measurement station. To compensate for the bed slope, as recommended by ASTM (2008a), flow depths were multiplied by the cosine of the respective as-built bed slope angle.

The obtained data could then be analysed to determine critical values for flow velocity, shear stress, Froude number, shear velocity, Shields's parameter and ultimately Movability Number. The analyses of the collected data are presented in Section 4, and includes the determination of an optimum Manning's n value for each test conducted as recommended by ASTM (2008b).

Figure 3-26: Video camera set up at downstream end of test channel

3.6 Findings and conclusions drawn from the physical model study

Table 3-8 and Table 3-9 present the observed results from all tests conducted on Armorflex 140 and Armorflex 180, respectively. Only the tests marked with a green shading had enough recorded data to be analysed, which is included in Section 4. In many tests, as denoted by "No WSE readings" in Table 3-8 and Table 3-9, catastrophic failure of the blocks occurred before flow depth measurements could be recorded. In such cases only the flow rate at block failure and the position of block failure could be recorded. In other cases, as denoted by "insufficient readings u/s of failure" in Table 3-8 and Table 3-9, catastrophic failure of block structure occurred while flow depth measurements were being recorded. In Test 7a, block failure was observed at CH 4 m (1 m from the start of the test section). The readings taken upstream of the point of failure in this test were therefore deemed insufficient. Furthermore, in terms of the position of failure, 76% of all failures were observed between chainages 5.5 m and 7.5 m in the test section.

The tables show fair consistency/repeatability in terms of the flow rate at which block failure was observed. The maximum flow rate available in the hydraulics laboratory of just under 0.6 m³/s was achieved before block failure could be initiated during Test 2. For the side slope tests, the maximum flow depth inside the test channel became the limiting factor, resulting in Tests 4, 7b and 11 not achieving block failure before running out of depth.

Table 3-8: Results for all tests conducted on Armorflex 140 blocks

Test no	Test code	Bed slope (V:H)	Side slope (V:H)	Q_m (m³/s)	Position of failure d/s of weir	Notes/system condition
Bed slope tests:						
Test 1a	30_0_140_i	1:30	N/A	0.580	CH7	Unstable
Test 1b	30_0_140_ii	1:30	N/A	0.589	CH6.5	Unstable
Test 5a	*20_0_140_i*	*1:20*	*N/A*	*0.070*	*CH6*	*Unstable – No WSE readings*
Test 5b	20_0_140_ii	1:20	N/A	0.060	CH6	Unstable
Test 5c	*20_0_140_iii*	*1:20*	*N/A*	*0.074*	*CH5*	*Unstable – No WSE readings*
Test 5d	*20_0_140_iv*	*1:20*	*N/A*	*0.068*	*CH5.6*	*Unstable – No WSE readings*
Test 5e	*20_0_140_v*	*1:20*	*N/A*	*0.070*	*CH6*	*Insufficient readings u/s of failure*

Test no	Test code	Bed slope (V:H)	Side slope (V:H)	Q_m (m^3/s)	Position of failure d/s of weir	Notes/system condition
Test 5f	20_0_140_vi	1:20	N/A	0.066	CH6	Unstable
Test 9a	*10_0_140_i*	*1:10*	*N/A*	*0.046*	*CH8*	*Unstable – No WSE readings*
Test 9b	*10_0_140_ii*	*1:10*	*N/A*	*0.062*	*CH7*	*Unstable – No WSE readings*
Test 9c	*10_0_140_iii*	*1:10*	*N/A*	*0.049*	*CH7.5*	*Unstable – No WSE readings*
Test 9d	10_0_140_iv	1:10	N/A	0.041	CH5 & CH7	Unstable
Test 9e	10_0_140_v	1:10	N/A	0.052	CH5 & CH8	Unstable
Side slope tests:						
Test 3a	30_1.5_140_i	1:30	1:1.5	0.451	CH7.5	Unstable
Test 3b	30_1.5_140_ii	1:30	1:1.5	0.420	CH7.5	Unstable
Test 7a	*20_1.5_140_i*	*1:20*	*1:1.5*	*0.378*	*CH4*	*Unstable – Failure 1 m from start of test section. No viable readings*
Test 7b	20_1.5_140_ii	1:20	1:1.5	0.526	DNF*	Stable – No failure at maximum depth in test channel
Test 11a	10_1.5_140_i	1:10	1:1.5	0.349	DNF	Stable – No failure at maximum depth in test channel

** DNF stands for "Did Not Fail".*
"Unstable" denotes that block movement was observed.
"Stable" denotes that no block movement was observed, i.e. DNF (Did not fail).

Table 3-9: Results for all tests conducted on Armorflex 180 blocks

Test no	Test code	Bed slope (V:H)	Side slope (V:H)	Q_m (m^3/s)	Position of failure d/s of weir	Notes/system condition
Bed slope tests:						
Test 2a	30_0_180_i	1:30	N/A	0.595	DNF*	Stable – No failure at maximum Q in lab
Test 2b	30_0_180_ii	1:30	N/A	0.595	DNF	Stable – No failure at maximum Q in lab
Test 6a	*20_0_180_i*	*1:20*	*N/A*	*0.121*	*CH7*	*Unstable – No WSE readings*

Test no	Test code	Bed slope (V:H)	Side slope (V:H)	Qm (m^3/s)	Position of failure d/s of weir	Notes/system condition
Test 6b	*20_0_180_ii*	*1:20*	*N/A*	*0.150*	*CH7*	*Unstable – No WSE readings*
Test 6c	*20_0_180_iii*	*1:20*	*N/A*	*0.120*	*CH8*	*Unstable – No WSE readings*
Test 6d	20_0_180_iv	1:20	N/A	0.099	CH7	Unstable
Test 6e	20_0_180_v	1:20	N/A	0.093	CH7	Unstable
Test 6f	*20_0_180_vi*	*1:20*	*N/A*	*0.107*	*CH6*	*Unstable – No WSE readings*
Test 6g	20_0_180_vii	1:20	N/A	0.121	CH8	Unstable
Test 10a	*10_0_180_i*	*1:10*	*N/A*	*0.050*	*CH4*	*Unstable – No WSE readings*
Test 10b	10_0_180_ii	1:10	N/A	0.103	CH6 & CH7	Unstable
Test 10c	10_0_180_iii	1:10	N/A	0.070	CH7	Unstable
Test 10d	10_0_180_iv	1:10	N/A	0.074	CH7	Unstable
Side slope tests:						
Test 4a	30_1.5_180_i	1:30	1:1.5	0.453	DNF	Stable – No failure at maximum depth in test channel
Test 4b	30_1.5_180_ii	1:30	1:1.5	0.456	DNF	Stable – No failure at maximum depth in test channel
Test 8a	*20_1.5_180_i*	*1:20*	*1:1.5*	*0.300*	*CH6.9*	*Unstable – No WSE readings*
Test 8b	*20_1.5_180_ii*	*1:20*	*1:1.5*	*0.415*	*CH6.5*	*Unstable – Insufficient readings u/s of failure*
Test 8c	20_1.5_180_iii	1:20	1:1.5	0.379	CH7.5	Unstable
Test 8d	20_1.5_180_iv	1:20	1:1.5	0.326	CH7.5	Unstable
Test 12a	10_1.5_180_i	1:10	1:1.5	0.351	CH7	Unstable
Test 12b	10_1.5_180_ii	1:10	1:1.5	0.305	CH7.5	Unstable

** DNF stands for "Did Not Fail".*
"Unstable" denotes that block movement was observed.
"Stable" denotes that no block movement was observed, i.e. DNF (Did not fail).

The following conclusions were drawn from the physical model study of Armorflex on steep bed and side slopes:

- Block installation is critical and should be done from the downstream end moving upstream. Blocks require contact with adjacent blocks, which increases the friction

between individual units and keeps it locked down into the structure. Blocks that are not tightly packed within the block matrix seem to lift out of plane prematurely.

- Blocks installed on the bed slope are less stable than those installed on the side slope. This can be expected as local flow velocities in the vicinity of the blocks on the side slope are small compared to that experienced by the blocks on the bed. Therefore, in the half-trapezoidal channel tests, the blocks on the bed had to be fixed to the underlying poly cotton sheet to prevent it from failing before the blocks on the side slope. Furthermore, the additional load from blocks “resting” on each other on a side slope may possibly result in increased stability of blocks.
- Clean water needs to be used for the hydraulic testing of loose Armorflex blocks. The laboratory refilled the tanks with clean water only after Tests 1 and 2 were already completed. Upon removing the blocks from the channel after Tests 1 and 2, it was found that sand particles had been deposited in between the blocks, reinforcing the system by increasing the friction between adjacent blocks. This resulted in postponed block failure in Test 1 and no failure in Test 2.
- At high flows, block movement typically resulted in the washing away of blocks downstream of the point of initial movement.
- At lower flows, single units would be lifted out of plane without resulting in the catastrophic failure of the structure downstream. In some cases, blocks lifted out of plane without completely dislodging from the structure.
- Only WSE measurements upstream of the point of block failure could be recorded because of the increased turbulence downstream of the point of failure.
- The overlap length of the underlying geotextile filter layer is critical. The installation of the geotextile filter should be done in accordance with the installation guide of Armortec (2016).

4. PHYSICAL MODEL DATA ANALYSIS

This section presents the analysis of the data collected in the laboratory model study and the discussion of the results obtained from the study. This section provides incipient motion criteria for Armorflex revetment systems in terms of critical flow parameters and concludes with a summary of the findings.

4.1 Laboratory data

The data obtained from each test in the model study is set out in numerical and graphical formats in “Appendix C: Laboratory results” as C1 and C2, respectively. The data and graphs present the bed elevations as well as the observed and representative water surface elevations (WSE’s) at incipient motion inside the 6 m long test section between CH 3 m and CH 9 m. The graphs also show the chainage(s) at which block failure was observed. WSE’s downstream from the point of failure were disregarded due to the increased turbulence and change in flow patterns in the area.

Flow depths normal to the embankment were determined using the as-built bed slope instead of the designed bed slope. Table 4-1 presents the designed bed- and side slopes versus as-built bed- and side slopes.

Table 4-1: Designed versus as-built bed- and side slopes

Designed bed slope S_o (V:H)	As-built bed slope S_o (V:H)
1:10	1:10.22
1:20	1:20.33
1:30	1:32.64
Designed side slope (V:H)	**As-built side slope (V:H)**
1:1.5	1:1.576

The tables in Appendix C1 present the bed level readings, observed WSE readings, observed flow depths and the representative WSE’s and flow depths obtained from the plotted linear trendline. The data is presented graphically in Appendix C2, with the blue and green lines respectively indicating the observed and representative WSE at incipient motion. The position of initial block failure is indicated by a red marker on the bed elevation plot. The data is presented in model scale and not prototype.

4.2 Analysis of collected data

Collected data from the laboratory tests were analysed to determine typical flow parameters such as hydraulic radius, cross-sectional average flow velocity, Froude number, shear stress and Shields's parameter at each measurement station upstream of the point of block failure. The analysis also included the determination of the optimal Manning's n value that best represents the observed data of each test. As the main aim of this study is developing design guidelines in terms of Liu's Movability Number, parameters required to plot the laboratory test results on Liu's Diagram are presented. Findings and conclusions drawn from the data analyses are listed, which includes the comparison of laboratory results with design guidelines of Armorflex manufacturers. The laboratory results are also compared to design guidelines for riprap and Reno-mattresses in terms of Movability Number.

4.2.1 Typical flow parameters at Q_m

This section presents the critical flow characteristics at failure in each test. Generally, the critical flow conditions are those present in the vicinity of the position of failure. For this study the flow conditions at the measurement station just upstream of the point of block failure were assumed to represent the critical flow conditions resulting in failure. Where no failure was observed, the station with the highest Movability Number was taken as the most critical station not resulting in failure. "Appendix C3: Typical flow parameters at Qm" includes tables that present the flow parameters at each measurement station upstream of the point of failure in the test section, with the critical station highlighted in red shading.

With the flow depth measured at each station, the flow velocity V could be calculated as the section-averaged velocity at each measurement station using the known equation of Q/A. The Energy Grade Line (EGL) elevation was calculated using Equation 2.52, from which a local EGL slope could be determined at each measurement station. Shear stress was calculated with Equation 2.53 and Shields's parameter with Equation 2.10. The Froude number was determined using the known equation $Fr = V/\sqrt{gd_m}$, where d_m denotes the hydraulic mean depth, which is the ratio of flow area over the width at the water surface (A/B).

Table 4-2 and Table 4-3 present the flow characteristics at the critical measurement station for each of the tests conducted on Armorflex 140 and Armorflex 180, respectively.

Table 4-2: Critical flow characteristics at Q_m for all Armorflex 140 bed- and side slope tests

Test no	Test code	Q_m (m^3/s)	y (m)	R (m)	V_{cr} (m/s)	EGL (m)	Fr	Local EGL slope (m/m)	Shear stress (kg/m^2)	Shields's parameter	System condition
Bed slope tests:											
Test 1a	30_0_140_i	0.580	0.223	0.223	2.788	0.805	1.887	0.030	65.526	0.084	Unstable*
Test 1b	30_0_140_ii	0.589	0.232	0.232	2.718	0.810	1.802	0.021	47.547	0.061	Unstable
Test 5b	20_0_140_ii	0.060	0.040	0.040	1.614	0.498	2.586	0.055	21.270	0.027	Unstable
Test 5f	20_0_140_vi	0.066	0.043	0.043	1.636	0.526	2.514	0.053	22.542	0.029	Unstable
Test 9d	10_0_140_iv	0.041	0.024	0.024	1.872	0.731	3.899	0.092	21.298	0.027	Unstable
Test 9e	10_0_140_v	0.052	0.027	0.027	2.043	0.769	3.954	0.100	26.686	0.034	Unstable
Side slope tests:											
Test 3a	30_1.5_140_i	0.451	0.311	0.194	2.609	0.805	1.792	0.015	45.837	0.059	Unstable
Test 3b	30_1.5_140_ii	0.420	0.299	0.188	2.579	0.785	1.803	0.017	49.660	0.064	Unstable
Test 7b	20_1.5_140_ii	0.526	0.311	0.194	3.043	1.092	2.091	0.022	65.879	0.084	Stable**
Test 11a	10_1.5_140_i	0.349	0.182	0.127	4.241	1.317	3.645	0.061	109.380	0.140	Stable

** "Unstable" denotes that block movement was observed.*

*** "Stable" denotes that no block movement was observed, i.e. DNF (Did not fail).*

Table 4-3: Critical flow characteristics at Q_m for all Armorflex 180 bed- and side slope tests

Test no	Test code	Q_m (m^3/s)	y (m)	R (m)	V_{cr} (m/s)	EGL (m)	Fr	Local EGL slope (m/m)	Shear stress (kg/m^2)	Shields's parameter	System condition
Bed slope tests:											
Test 2a	30_0_180_i	0.595	0.219	0.219	2.913	0.804	1.989	0.024	52.195	0.069	Stable**
Test 2b	30_0_180_ii	0.595	0.218	0.218	2.921	0.805	1.998	0.027	57.474	0.076	Stable
Test 6d	20_0_180_iv	0.099	0.054	0.054	1.947	0.549	2.673	0.050	26.660	0.035	Unstable*
Test 6e	20_0_180_v	0.093	0.051	0.051	1.964	0.549	2.785	0.049	24.371	0.032	Unstable
Test 6g	20_0_180_vii	0.121	0.060	0.060	2.170	0.553	2.834	0.038	22.208	0.029	Unstable
Test 10b	10_0_180_ii	0.103	0.042	0.042	2.612	0.861	4.065	0.059	24.490	0.032	Unstable
Test 10c	10_0_180_iii	0.070	0.032	0.032	2.370	0.702	4.246	0.093	28.944	0.038	Unstable
Test 10d	10_0_180_iv	0.074	0.032	0.032	2.491	0.732	4.474	0.087	26.895	0.036	Unstable
Side slope tests:											
Test 4a	30_1.5_180_i	0.453	0.321	0.199	2.499	0.805	1.694	0.031	97.840	0.129	Stable
Test 4b	30_1.5_180_ii	0.456	0.324	0.200	2.484	0.804	1.678	0.031	99.655	0.132	Stable
Test 8c	20_1.5_180_iii	0.379	0.243	0.159	3.117	1.021	2.376	0.017	39.508	0.052	Unstable
Test 8d	20_1.5_180_iv	0.326	0.220	0.148	3.056	0.979	2.423	0.031	66.574	0.088	Unstable
Test 12a	10_1.5_180_i	0.351	0.194	0.134	3.903	1.294	3.262	0.051	96.287	0.127	Unstable
Test 12b	10_1.5_180_ii	0.305	0.176	0.124	3.871	1.263	3.372	0.054	92.280	0.122	Unstable

** "Unstable" denotes that block movement was observed.*

*** "Stable" denotes that no block movement was observed, i.e. DNF (Did not fail).*

4.2.2 Optimal Manning's n value

The method presented by ASTM (2008b) in Section 2.2.3.7 was used to determine the optimal Manning's n value that best represents the data observed in each test. Figure 4-1 and Figure 4-2 graphically present the optimal Manning's n values that minimised the objective functions in all Armorflex 140 and Armorflex 180 tests, respectively. Also indicated on each graph is the typical Manning's n value range of 0.025 – 0.035 for Armorflex blocks as stated by Technicrete (2016).

The graphs indicate that the majority of tests had a Manning's n roughness value outside the range specified by Technicrete (2016). The average Manning's n values for Armorflex 140 blocks on bed- and side slopes were 0.017 and 0.024, respectively. For Armorflex 180 blocks installed on bed- and side slopes, the average Manning's n values were 0.015 and 0.022, respectively. These averages are shown on the graphs.

The difference in roughness values between prototype and scaled model blocks could be attributed to differences in the block manufacturing process. Prototype Armorflex blocks are typically dry-packed and hydraulically compressed in the mould, whereas the model blocks were wet-cast into soft polyurethane moulds. The surface finish on the wet-cast concrete blocks were smooth and even, while that of the dry-packed prototype blocks were more textured, resembling the surface finish of a paving brick. Reference is made to Figure 3-6 and Figure 3-7 that show the difference in surface finish between the prototype Armorflex blocks and the model blocks.

Another possible cause of the low roughness values is that the tests were conducted under controlled laboratory conditions, meaning no debris or foreign materials could influence the roughness parameter, whereas field measurements might be affected in such a way.

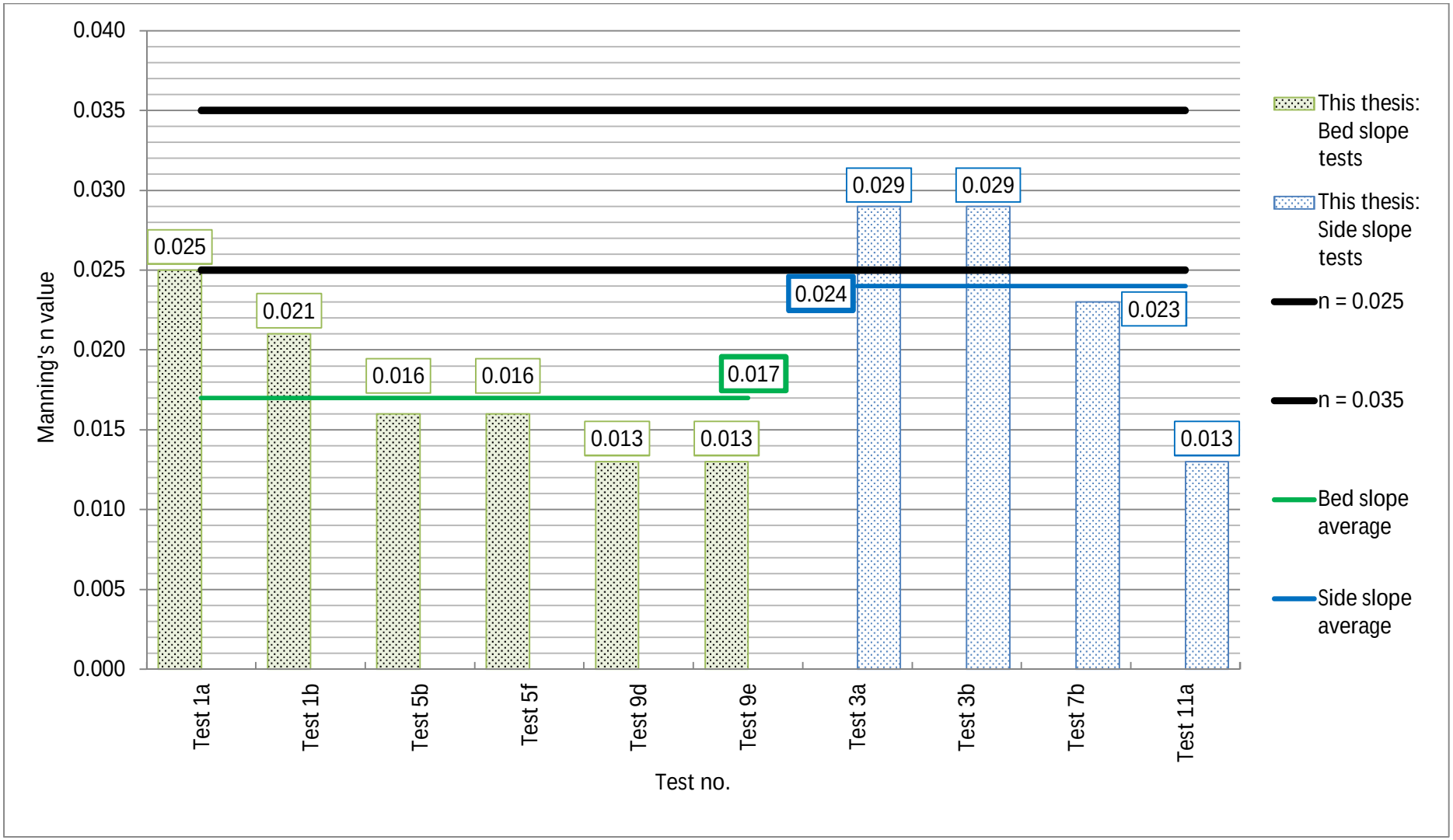

Figure 4-1: Optimal Manning's n value for Armorflex 140 tests

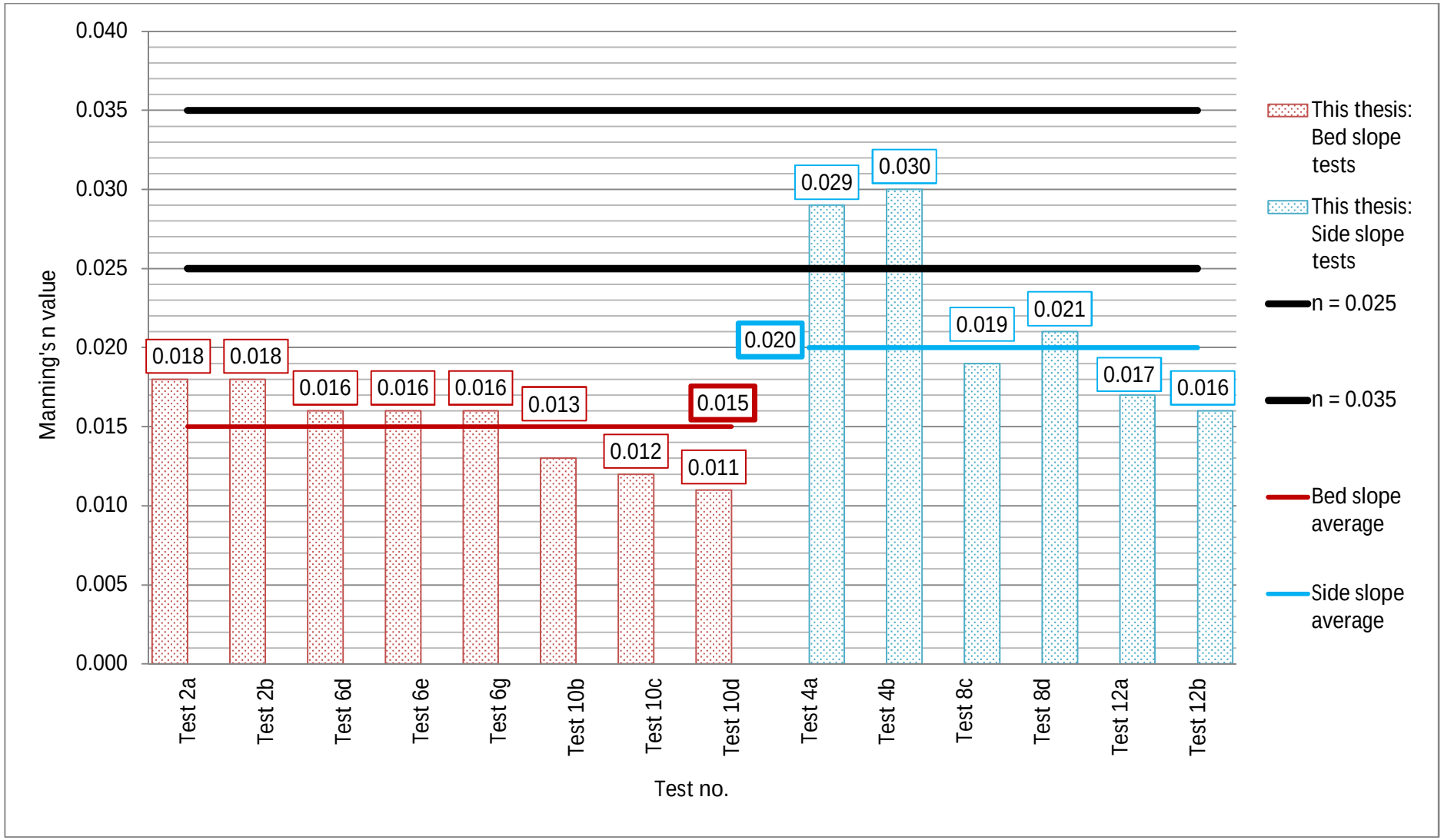

Figure 4-2: Optimal Manning's n value for Armorflex 180 tests

4.2.3 Liu Diagram parameters

The collected data from the laboratory tests was used to determine the parameters of the Liu Diagram to investigate whether it can be used to determine the incipient motion conditions of Armorflex blocks in channelized applications.

Liu's Diagram plots the Movability Number (V^*/V_{ss}) against the particle Reynolds number. With settling velocity of both Armorflex block types already determined in the experiments described in Section 3.3.2, shear velocity and particle Reynolds number had to be determined using the laboratory data.

Even though Liu assumed uniform flow conditions ($S_o = S_f$), S_f was calculated as the local energy grade line (EGL) slope at the measurement station just upstream to where failure occurred. With S_f determined, shear velocity could be calculated using Equation 2.9, with particle Reynolds number calculated using Equation 2.5. The kinematic viscosity of water was assumed as 1.13×10^{-6} m²/s in the calculation of the particle Reynolds number, even though no water temperature measurements were taken in the laboratory.

Table 4-4 and Table 4-5 present the processed data required to plot the results from the laboratory tests on the Liu Diagram for Armorflex 140 and Armorflex 180, respectively.

Studying the analysed data of all tests conducted on Armorflex 140 and 180, it was apparent that the unclean water used in Tests 1 and 2 had a stabilising effect on the structure, causing it to either fail late (Test 1), or not fail at all (Test 2). It was noted in Section 3.6 that upon removing the blocks after the completion of Tests 1 and 2, blocks were difficult to remove by hand. It was noticed that sand particles had been deposited in between adjacent blocks, reinforcing the structure by increasing the friction between neighbouring blocks.

Tests 1 and 2 were still included in the sections following this one, but the results were not be used for defining the flow conditions at incipient motion of Armorflex blocks.

Table 4-4: Liu Diagram parameters for Armorflex 140 tests

Test no	Test code	V_{ss} (m/s)	S_f (m/m)	V* (m/s)	Movability Number	Re*
Bed slope tests:						
Test 1a	30_0_140_i	0.585	0.030	0.256	0.438	19 572.24
Test 1b	30_0_140_ii	0.585	0.021	0.218	0.373	16 672.37
Test 5b	20_0_140_ii	0.585	0.055	0.146	0.249	11 151.13

Test no	Test code	V_{ss} (m/s)	S_f (m/m)	V* (m/s)	Movability Number	Re*
Test 5f	20_0_140_vi	0.585	0.053	0.150	0.257	11 479.76
Test 9d	10_0_140_iv	0.585	0.092	0.146	0.249	11 158.42
Test 9e	10_0_140_v	0.585	0.100	0.163	0.279	12 490.52
Side slope tests:						
Test 3a	30_1.5_140_i	0.585	0.015	0.214	0.366	16 369.71
Test 3b	30_1.5_140_ii	0.585	0.017	0.223	0.381	17 038.79
Test 7b**	20_1.5_140_ii	0.585	0.022	0.257	0.439	19 624.95
Test 11a**	10_1.5_140_i	0.585	0.061	0.331	0.565	25 287.46

***Did Not Fail at maximum flow depth in flume.*

Table 4-5: Liu Diagram parameters for Armorflex 180 tests

Test no	Test code	V_{ss} (m/s)	S_f (m/m)	V* (m/s)	Movability Number	Re*
Bed slope tests:						
Test 2a*	30_0_180_i	0.678	0.024	0.228	0.337	16 902.17
Test 2b*	30_0_180_ii	0.678	0.027	0.240	0.354	17 736.34
Test 6d	20_0_180_iv	0.678	0.050	0.163	0.241	12 079.67
Test 6e	20_0_180_v	0.678	0.049	0.156	0.230	11 549.53
Test 6g	20_0_180_vii	0.678	0.038	0.149	0.220	11 025.17
Test 10b	10_0_180_ii	0.678	0.059	0.156	0.231	11 577.79
Test 10c	10_0_180_iii	0.678	0.093	0.170	0.251	12 586.64
Test 10d	10_0_180_iv	0.678	0.087	0.164	0.242	12 132.83
Side slope tests:						
Test 4a**	30_1.5_180_i	0.678	0.031	0.313	0.461	23 141.17
Test 4b**	30_1.5_180_ii	0.678	0.031	0.316	0.466	23 354.90
Test 8c	20_1.5_180_iii	0.678	0.017	0.199	0.293	14 705.21
Test 8d	20_1.5_180_iv	0.678	0.031	0.258	0.381	19 088.90
Test 12a	10_1.5_180_i	0.678	0.051	0.310	0.458	22 956.76
Test 12b	10_1.5_180_ii	0.678	0.054	0.304	0.448	22 474.07

**Did Not Fail at maximum flow rate of laboratory.*

***Did Not Fail at maximum flow depth in flume.*

4.3 Incipient motion criteria for Armorflex

This section provides criteria defining the incipient motion conditions of Armorflex 140 and 180 blocks tested on bed- and side slopes. The analysed data from the physical model tests were used to express the point of incipient motion for each of the four test scenarios investigated in terms of the following parameters:

- Critical flow velocity, V_{cr};
- Critical shear stress, τ_{cr};
- Critical Froude number, F_r; and
- Movability Number.

Where applicable, the findings were compared to those from previous hydraulic performance testing. The limiting flow characteristics presented in this section are full scale values, converted from the model scale values using the Froudian similarity law, which is given in Table 3-1.

The results presented in this section, specifically the design criteria in terms of Movability Number, were used to develop a Microsoft Excel model that will assist designers in designing safe Armorflex-lined channels. The Excel model can be found on the CD that is attached to this thesis. Figure D- 1 in “Appendix D: Microsoft Excel model” is a print screen image of the calculation sheet of the Armorflex design spreadsheet. The output of the model is either a stable or unstable design, together with a safety factor. It is, however, recommended that the designer of the revetment apply a suitable safety factor to the design.

4.3.1 Incipient motion criteria in terms of critical flow velocity

Figure 4-3 and Figure 4-4 graphically present the critical flow velocities of Armorflex 140 and 180, respectively. By neglecting Tests 1 and 2, the graphs show a general trend of increasing critical flow velocity as the bed slope increases, regardless of whether blocks were installed on the bed- or side slopes.

Table 4-6 presents the range of critical flow velocities that produced failure in each of the four test scenarios. The velocities not producing failure were not included. The table also provides a suggested flow velocity to represent the critical flow velocity for each test scenario.

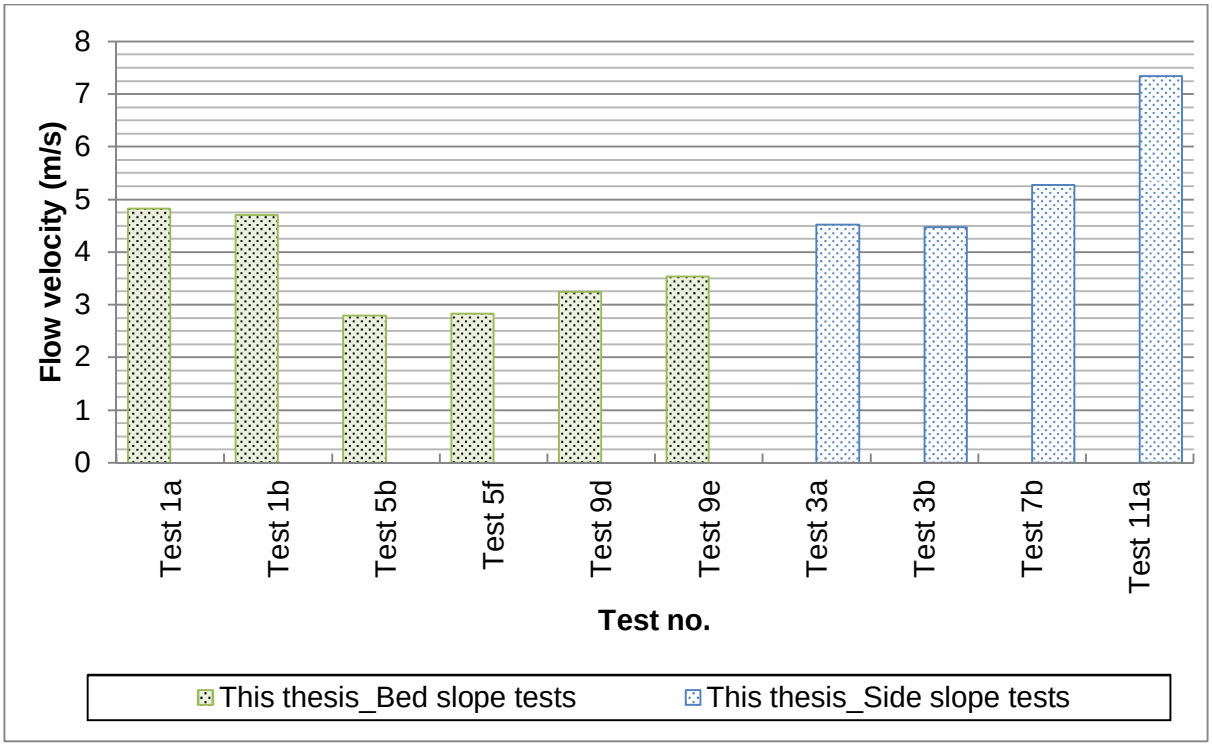

Figure 4-3: Armorflex 140 critical flow velocities

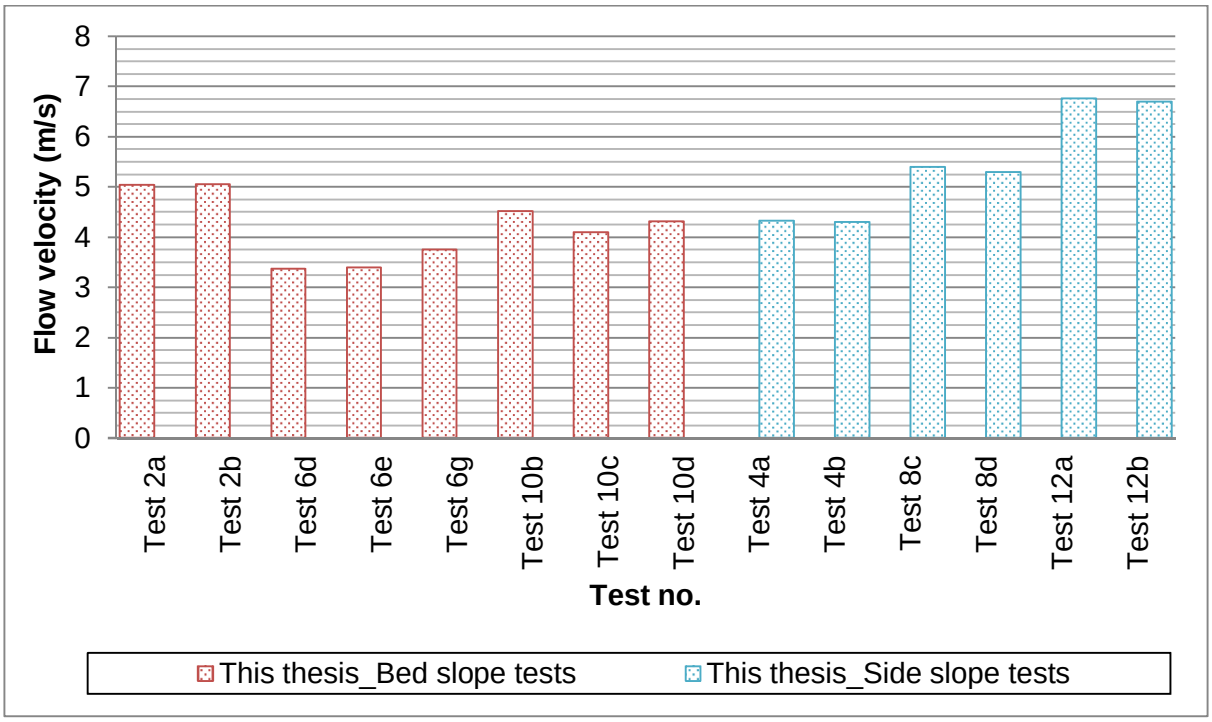

Figure 4-4: Armorflex 180 critical flow velocities

Table 4-6: Suggested critical flow velocities for Armorflex 140 and 180

Test scenario	V_{cr} range observed (m/s)	Suggested V_{cr} (m/s)
Armorflex 140 on bed slope	2.795 – 3.538	2.7
Armorflex 140 on side slope	4.467 – 4.518	4.4
Armorflex 180 on bed slope	3.373 – 4.525	3.3
Armorflex 180 on side slope	5.293 – 6.759	5.2

The blocks were tested without screeding the structure with topsoil and filling the voids with material. It was therefore expected that the limiting flow velocities at failure would be much lower than that obtained in the CIRIA embankment testing of Armorflex class 30S as presented by Clopper & Chen (1988). The critical velocities suggested for Armorflex 180 correspond reasonably well with the Armorflex class 30 critical flow velocity range of 3.7 – 4.6 m/s obtained from the FHWA overtopping flow study conducted by Clopper & Chen (1988). The performance testing of Armorflex class 30S by the CSU in 2000 produced a similar critical flow velocity of 3.7 m/s.

4.3.2 Incipient motion criteria in terms of critical shear stress

Figure 4-5 and Figure 4-6 graphically illustrate the critical shear stress at the point of incipient motion in each test conducted on Armorflex 140 and 180. By neglecting Tests 1 and 2, the critical shear stress of Armorflex 140 and Armorflex 180 installed on bed slopes are similar, seeming nearly impartial to changes in bed slope grade from 1H:20H to 1V:10H. The side slope tests 4a, 4b, 7b and 11a did not achieve block failure. Only Tests 3a and 3b could be used to define incipient motion conditions of Armorflex 140 on side slopes, while Tests 8 and 12 could be used for Armorflex 180.

Table 4-7 presents the range of critical shear stress at failure in each of the four test scenarios as well as a suggested shear stress value to represent the critical shear stress for each test scenario.

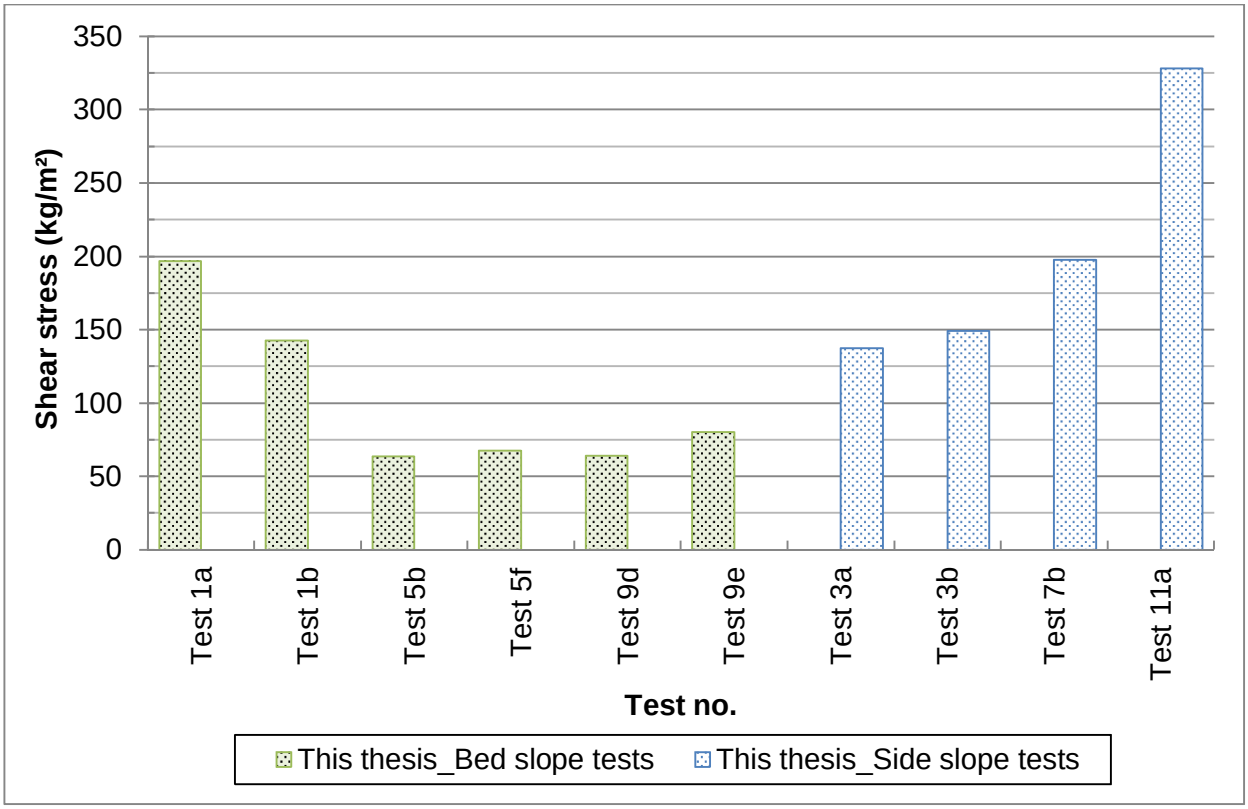

Figure 4-5: Armorflex 140 critical shear stress

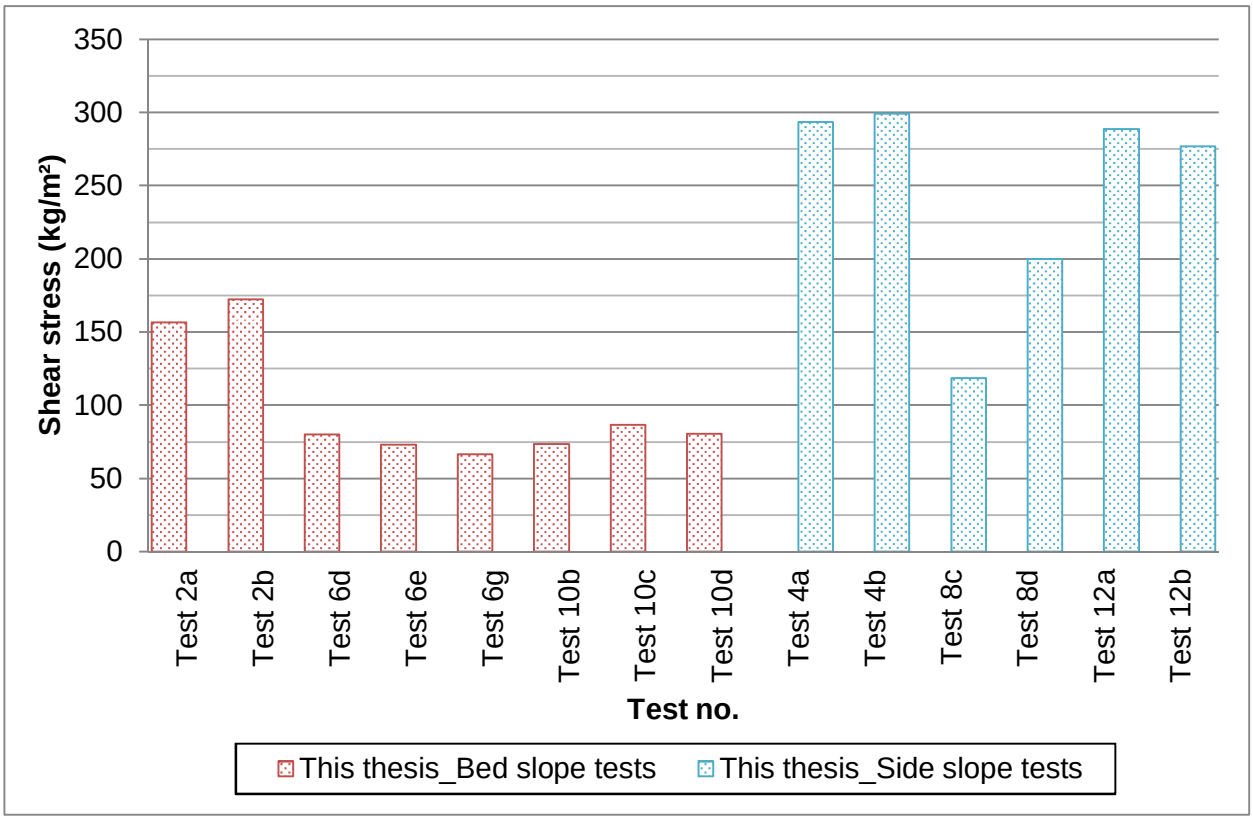

Figure 4-6: Armorflex 180 critical shear stress

Table 4-7: Suggested critical shear stress for Armorflex 140 and 180

Test scenario	Observed range of τ_{cr} (kg/m²)	Suggested τ_{cr} (kg/m²)
Armorflex 140 on bed slope	63.81 – 80.06	63.8
Armorflex 140 on side slope	137.51 – 148.98	137.5
Armorflex 180 on bed slope	66.62 – 86.83	66.6
Armorflex 180 on side slope	118.52 – 288.86	118.5

Armorflex blocks installed on side slopes in a wide trapezoidal channel fails at higher shear stress values than blocks installed on bed slopes. The FHWA overtopping flow study conducted by Clopper & Chen (1988) presented a critical bed shear stress range of 58.6 – 97.7 kg/m² for Armorflex class 30 blocks, which is similar to the results shown in Table 4-7. The suggested critical shear stress values are, however, less than the 144 – 192 kg/m² critical shear stress range given by Clopper (1989) for Armorflex class 30 blocks. On the other hand, the results from Table 4-7 show significantly higher critical shear stress values than the 19.5 kg/m² obtained in the performance testing of Armorflex class 30S by the CSU in 2000.

4.3.3 Incipient motion criteria in terms of critical Froude number

Froude number is used as a parameter to define incipient motion conditions to compare the findings from this study to the results from relevant previous performance testing of Armorflex. Figure 4-7 and Figure 4-8 illustrate the Froude number at the point of incipient motion in each test conducted on Armorflex 140 and 180. The graphs show that all test failures occurred under supercritical flow conditions, Fr > 1. This means that the actual flow depths measured were below the critical flow depth in each test. By disregarding Tests 1 and 2, failure of Armorflex 140 blocks installed on bed slopes were observed at Froude numbers between 2.51 and 3.95, while failures on side slopes occurred at Froude numbers of 1.79 and 1.80. No failure was observed in Tests 7b and 11a even though high Froude numbers of 2.09 and 3.64 were respectively calculated at the highest flow possible in both tests. Armorflex 180 blocks installed on bed slopes failed at Froude numbers ranging from 2.67 to 4.47, while side slope failures occurred at Froude numbers between 2.38 and 3.37. No failure was observed in Tests 4a and 4b.

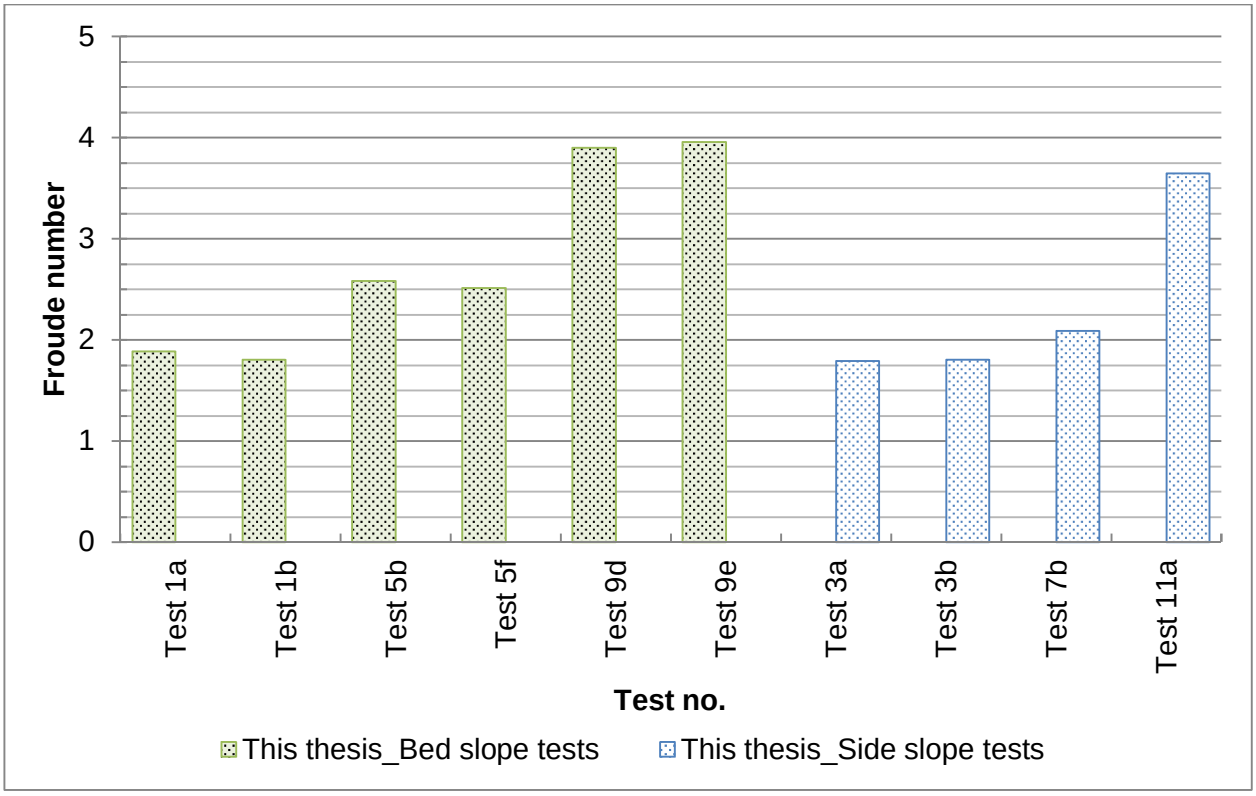

Figure 4-7: Armorflex 140 critical Froude number

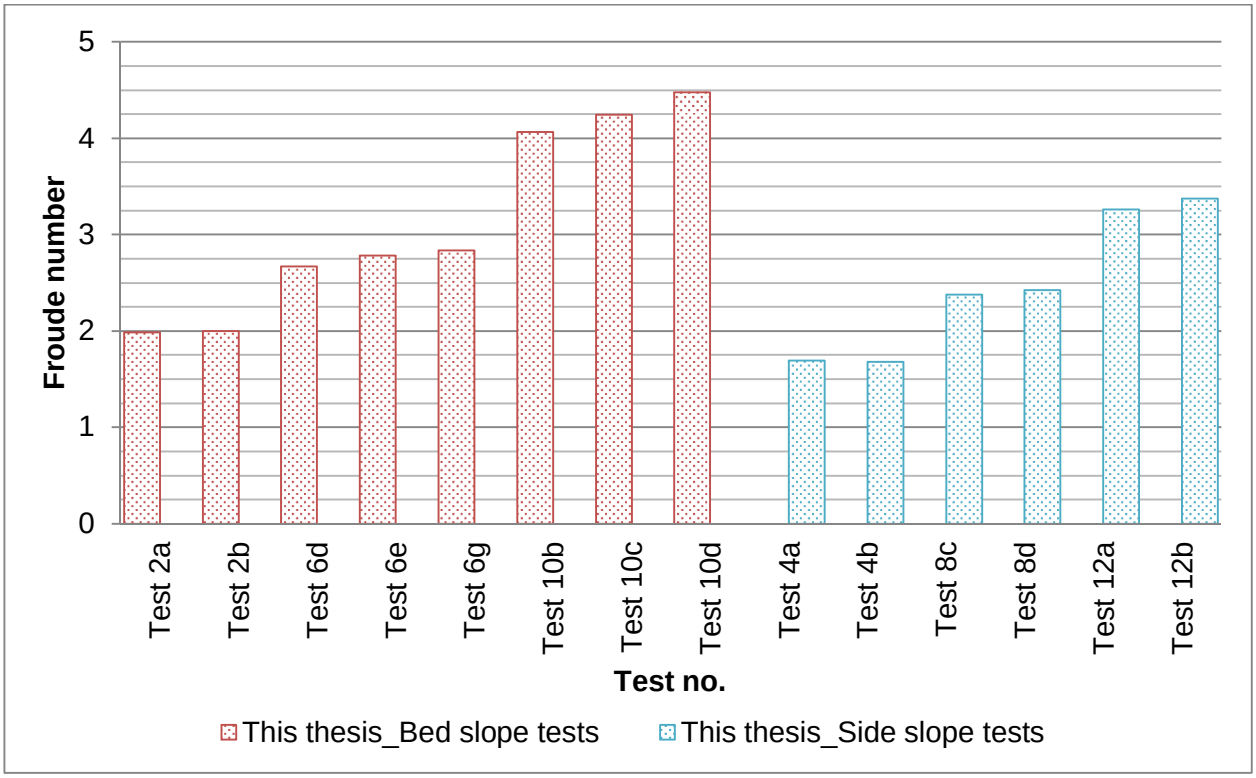

Figure 4-8: Armorflex 180 critical Froude number

Table 4-8 presents the range of critical Froude number at failure in each of the four test scenarios, as well as a suggested Froude number to represent the critical Froude number for each test scenario.

Table 4-8: Suggested critical Froude numbers for Armorflex 140 and 180

Test scenario	Range of Froude numbers	Suggested Froude number
Armorflex 140 on bed slope	2.51 – 3.95	2.50
Armorflex 140 on side slope	1.79 – 1.80	1.75
Armorflex 180 on bed slope	2.67 – 4.47	2.65
Armorflex 180 on side slope	2.38 – 3.37	2.35

For cabled Armorflex blocks (with the cables tightly- to moderately tensioned) tested under rapid flow conditions, Escarameia (1995) presented a critical Froude number range of 2.27 – 2.68. This range corresponds well to the results presented in Table 4-8, apart from Armorflex 140 blocks on side slopes.

4.3.4 Incipient motion criteria in terms of Movability Number

When using Movability Number as the parameter of defining the point of incipient motion, a fine line exists between recommending an underdesigned system and an overdesigned, expensive system. In other words, if a high Movability Number is wrongfully recommended for design purposes, less conservative designs are the result, which could lead to premature failure of the specified revetment. On the other hand, if a small Movability Number is wrongfully recommended, it may lead to structures being overdesigned, which can be an unnecessary expense.

Given the few data points available for each of the four test scenarios, a general trend of results could not be regarded to aid in judging whether the lowest achieved Movability Number is an outlier. Therefore, to ensure a safe design, the lowest value was recommended to define the point of incipient motion, adopting a 100% probability of exceedance value approach.

The parameters of the Liu Diagram, presented in Section 4.2.3, were used to plot the Movability Number versus particle Reynolds number for each of the following four test scenarios investigated, as presented in Figure 4-9 to Figure 4-12. Figure 4-13 presents the plot for all blocks and all cases on one graph. Illustrated in Figure 4-13, side slope test results plot higher on the Liu Diagram than bed slope test results. This verifies the observation listed in Section 3.6 that blocks installed on bed slopes are less stable than blocks installed on a side slope of 1V:1.5H.

All test data points plotted above the higher 0.17 Movability Number defined by Armitage (2002), with all scenarios showing a trend of increasing Movability Number with increasing particle Reynolds number. Rooseboom & van Vuuren (2013) equates the Movability Number of loose articulating concrete blocks (such as Armorflex) to 0.12, for particle Reynolds numbers (R_e^*) larger than 13. According to the results from this study, Rooseboom & van Vuuren's (2013) recommended Movability Number of 0.12 is considered conservative for design purposes.

4.3.4.1 Armorflex 140 installed on a bed slope

The Movability Number values for the Armorflex 140 bed slope tests varies between 0.249 (Tests 5b and 9d) to 0.438 (Test 1a). It is however clear from Figure 4-9 that Tests 1a and 1b showed Movability Numbers considerably higher than the other Movability Numbers achieved for bed slope tests. This supports the author's claim that the use of unclean water during Tests 1 and 2 resulted in an increased stability of the structure. Results from Tests 1a and 1b were therefore discarded, changing the range of Movability Numbers to 0.249 – 0.279 (Test 9e). A Movability Number of 0.249 is therefore recommended for design purposes for Armorflex 140 installed on bed slopes.

4.3.4.2 Armorflex 140 installed in a trapezoidal channel on a side slope

No failure was observed during Tests 7a and 11a, which meant only Tests 3a and 3b could be regarded for this scenario. Therefore, Movability Number values for the Armorflex 140 side slope tests that achieved failure ranges between 0.366 in Test 3a to 0.381 in Test 3b. The recommended Movability Number for Armorflex 140 installed on a side slope in a trapezoidal channel is 0.366. However, given that only two viable test results were obtained, there is a high possibility that the Movability Number recommended is an outlier.

By dividing the recommended Movability Number for Armorflex 140 blocks on side slopes by the Movability Number for Armorflex 140 blocks on bed slopes, a dimensionless stability factor of 1.47 is obtained.

4.3.4.3 Armorflex 180 installed on a bed slope

The Movability Numbers for the Armorflex 180 bed slope tests ranges between 0.220 (Test 6g) to 0.354 (Test 2b), even though no failure was achieved in Tests 2a and 2b. However, considering that Test 2, as with Test 1, was tested with unclean water, the stability of the blocks was compromised and the test results were discarded, changing the maximum Movability Number for the range of viable test results to 0.251, achieved in Test 10c. The

recommended Movability Number for design purposes for Armorflex 180 blocks installed on bed slopes is 0.220.

4.3.4.4 Armorflex 180 installed in a trapezoidal channel on a side slope

Tests 4a and 4b produced no failure of Armorflex 180 blocks installed on the 1V:1.5H side slope. Therefore, the only viable results that could be regarded for the determination of design guidelines in terms of Movability Numbers were those of Tests 8c, 8d, 12a and 12b. The Movability Number values obtained in these tests ranged between 0.293 (Test 8c) to 0.458 (Test 12a). Investigating the Liu Diagram for this test scenario in Figure 4-12, it could be a fair assumption that the low Movability Number achieved in Test 8c is an outlier, and that the Movability Number of 0.381 from Test 8d should rather be used as the recommended value for design purposes. Considering the few data points available, the more conservative Movability Number of 0.293 is recommended for design purposes.

By dividing the recommended Movability Number for Armorflex 180 blocks on side slopes by the Movability Number for Armorflex 180 blocks on bed slopes, a dimensionless stability factor of 1.33 is obtained.

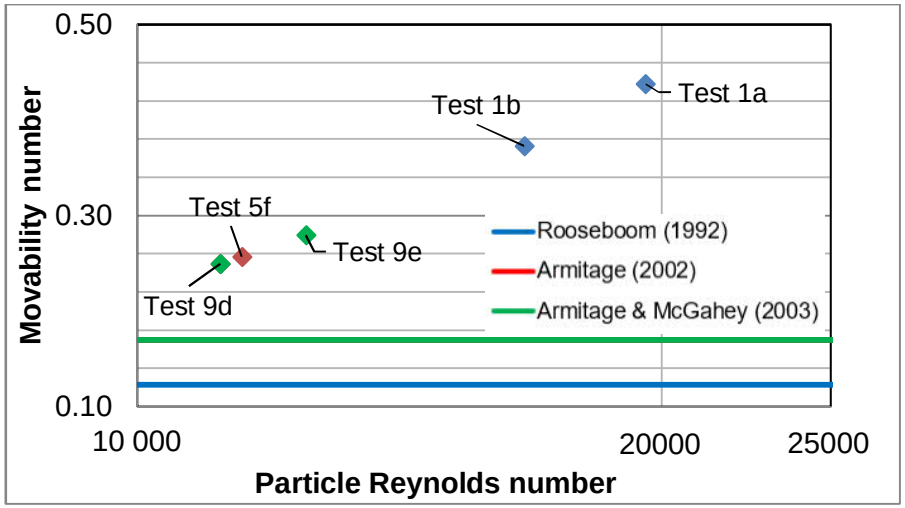

Figure 4-9: **Liu Diagram for bed slope tests on Armorflex 140 blocks**

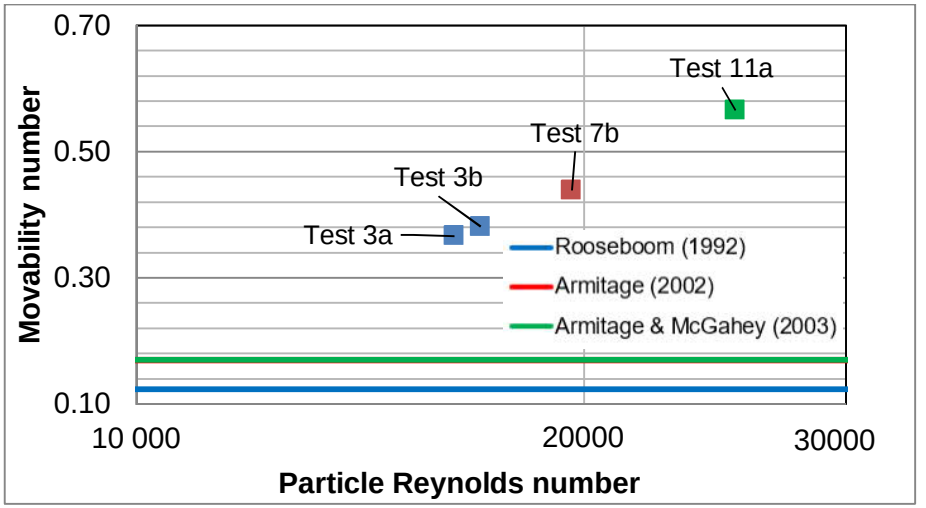

Figure 4-10: **Liu Diagram for side slope tests on Armorflex 140 blocks**

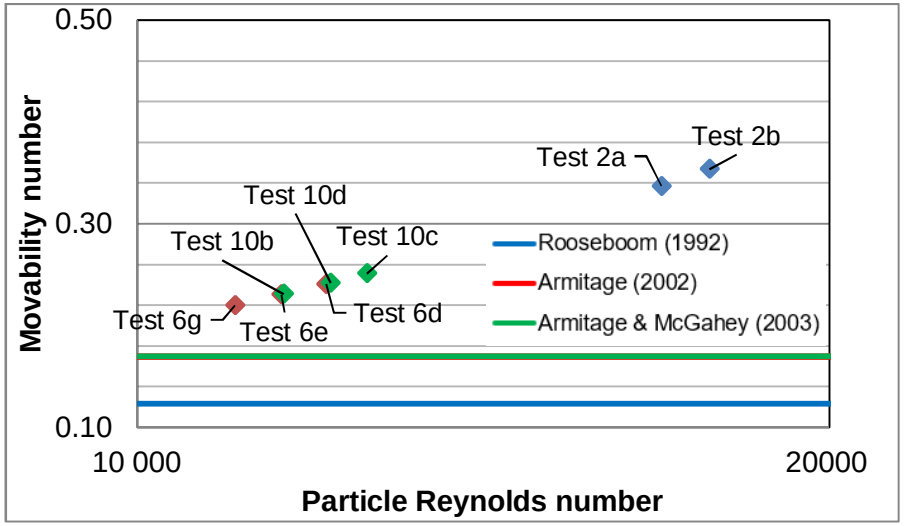

Figure 4-11: **Liu Diagram for bed slope tests on Armorflex 180 blocks**

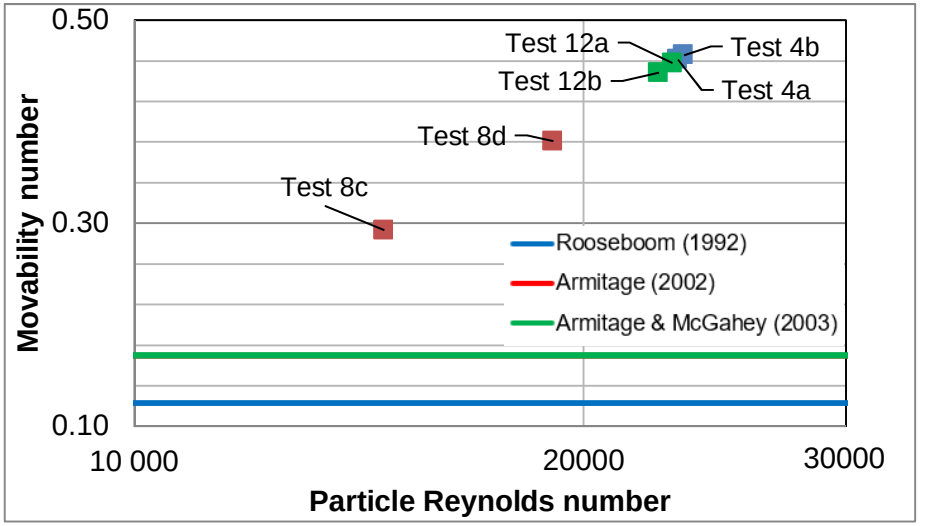

Figure 4-12: **Liu Diagram for side slope tests on Armorflex 180 blocks**

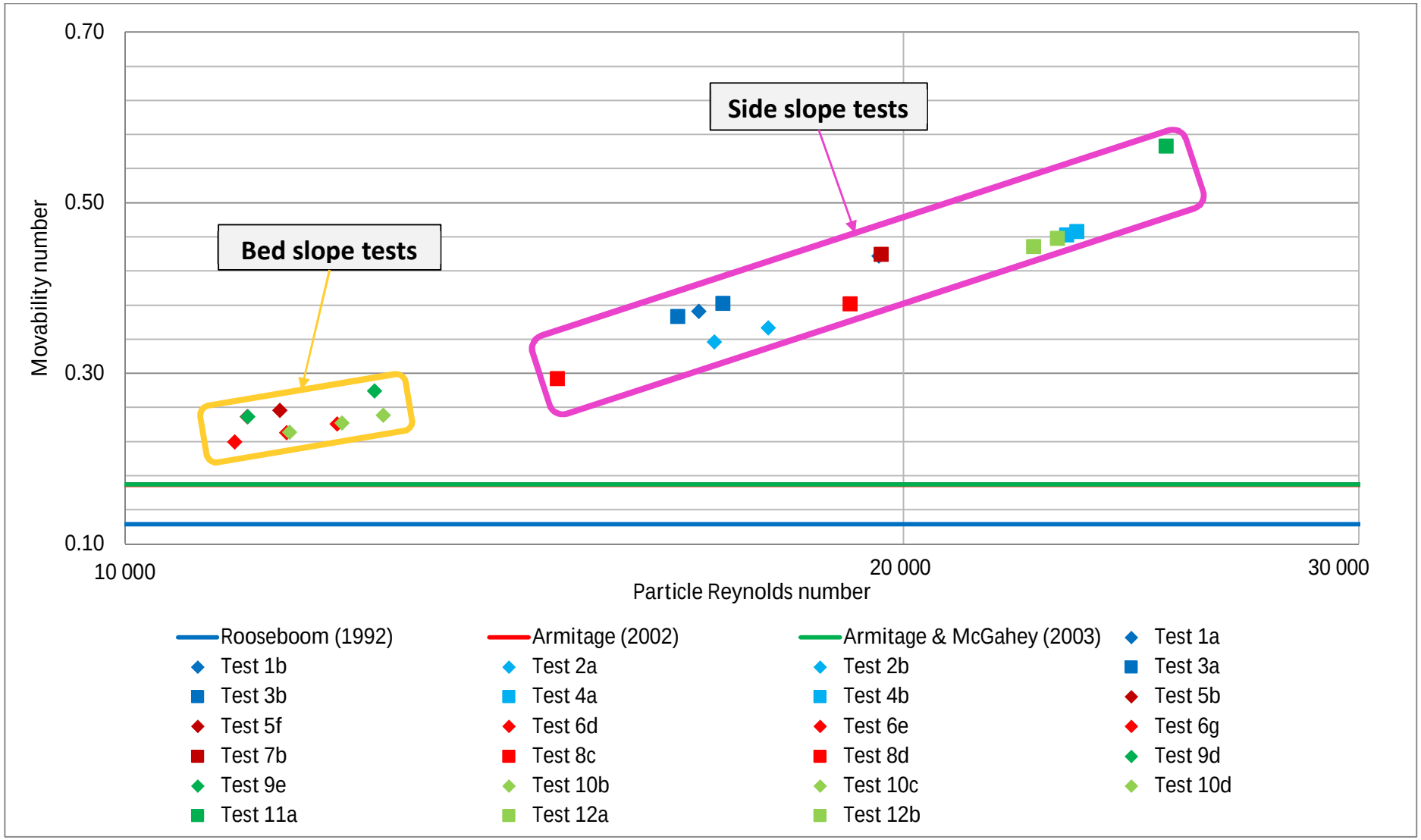

Figure 4-13: Liu Diagram for all blocks and all cases

4.4 Comparison of findings to Armorflex manufacturer design guidelines

4.4.1.1 Technicrete

Figure 4-14 graphically presents the suggested critical flow velocities of the different test scenarios, as presented in Section 4.3.1, as well as Technicrete's (2016) specified limiting flow velocities of 3.5 m/s and 5.5 m/s for Armorflex 140 and 180, respectively.

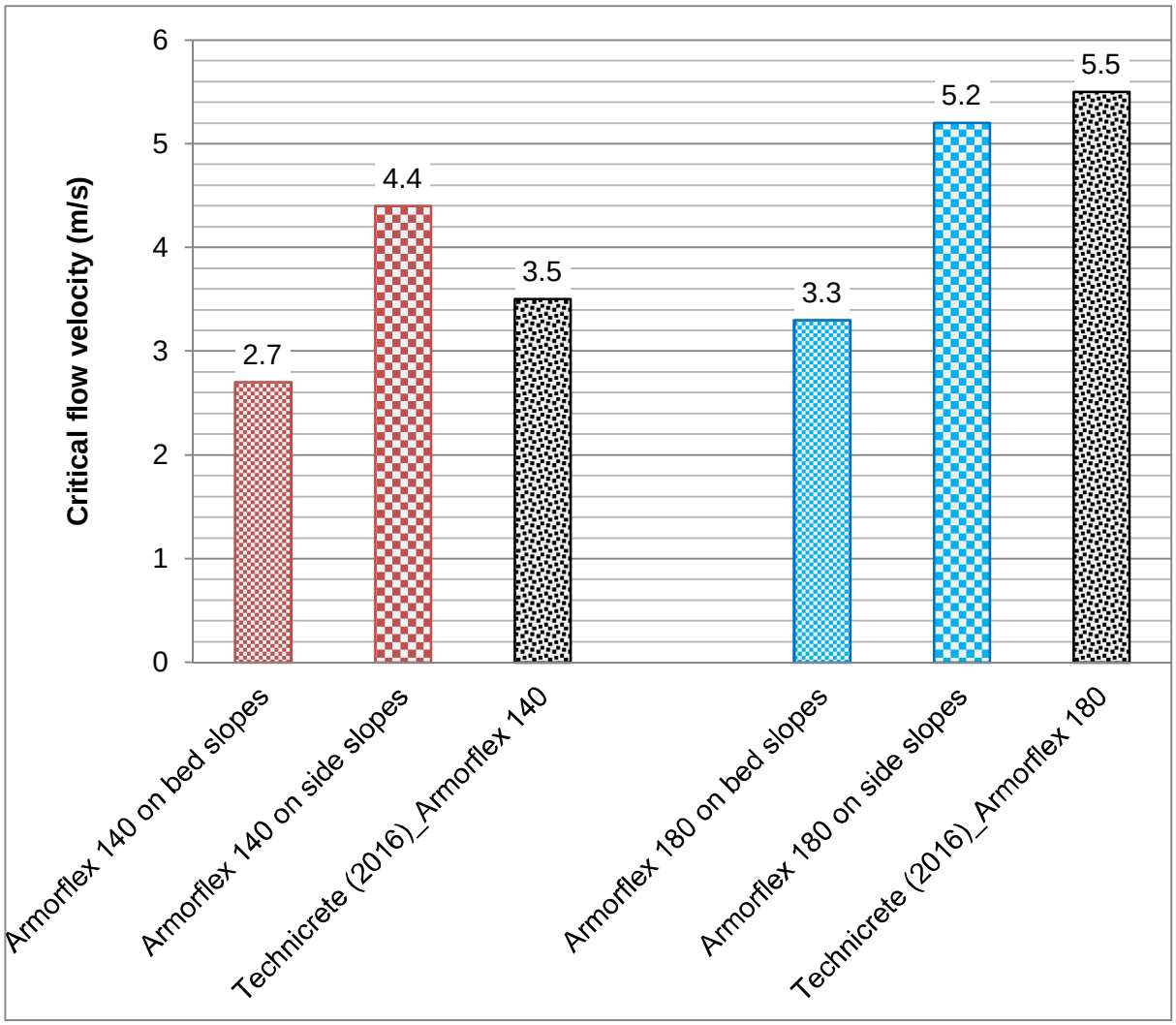

Figure 4-14: Suggested critical flow velocity for Armorflex blocks versus Technicrete (2016) guideline

Figure 4-14 shows that Technicrete's 3.5 m/s limiting flow velocity for Armorflex 140 blocks may be an overestimation for blocks installed on bed slopes, while the critical velocity achieved on side slopes was greater than the 3.5 m/s limiting flow velocity. Armorflex 180's bed slope- and side slope tests resulted in suggested critical flow velocities lower than Technicrete's limiting flow velocity of 5.5 m/s. According to incipient motion theory, flow velocity is not a suitable parameter for defining incipient motion conditions of non-cohesive particles.

Therefore, Technicrete's (2016) guidelines of the capabilities of Armorflex 140 and 180 blocks in terms of flow velocity alone cannot be used to assist and guide a design engineer in designing a safe and stable Armorflex lined structure for given flow conditions.

4.4.1.2 Contech Construction Products inc.

Contech (Armortec Incorporated, 1981) provides design guidelines for Armorflex class 30 as presented in Section 2.2.4.1, which are defined in terms of flow velocity, hydraulic radius, bed slope and shear stress. Even though Armorflex class 30 is similar only to Armorflex 180, the results for Armorflex 140 are also included in this comparison.

Figure 4-15 presents the flow velocities achieved at the point of incipient motion in all tests conducted, plotted with the design guideline of Contech (Armortec Incorporated, 1981) for Armorflex class 30 at various bed slopes. In contrast to the comparison of the results to the design guidelines of Technicrete (2016), no critical flow velocities plotted lower than the limiting flow velocity at the respective bed slope stated by Contech. Even though it could be said that the guideline of Contech (Armortec Incorporated, 1981) seems to be conservative, flow velocity still remains an unsuitable parameter for defining incipient motion.

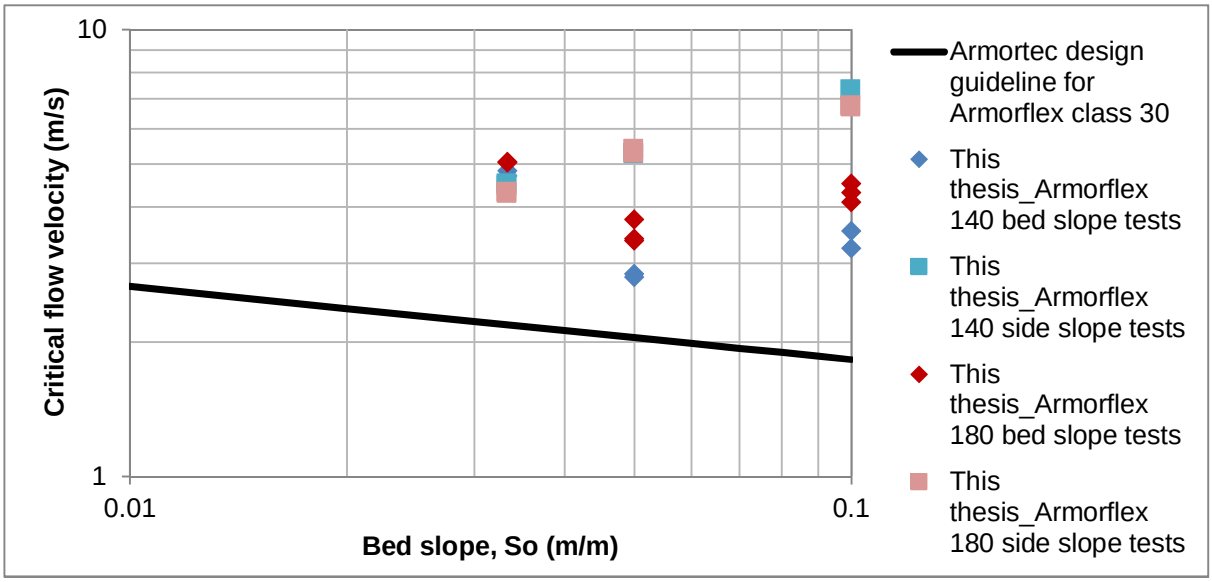

Figure 4-15: Armorflex 140 and 180 limiting flow velocities at tested bed slopes

Figure 4-16 presents the hydraulic radius at the point of incipient motion in all tests conducted, plotted with the recommended values of Contech (Armortec Incorporated, 1981) for Armorflex class 30 at various bed slopes. Interpreting this graph, it was clear that blocks installed on side slopes are more stable than blocks installed on bed slopes. The Armorflex 140 and Armorflex 180 tests carried out on side slopes of 1:20 and 1:10 plotted above the limiting hydraulic radius recommended by Armortec Incorporated (1981), while all other test results plotted below the

design values of Contech (Armortec Incorporated, 1981). This raises concern for using hydraulic radius as a parameter of defining the incipient motion conditions of Armorflex blocks.

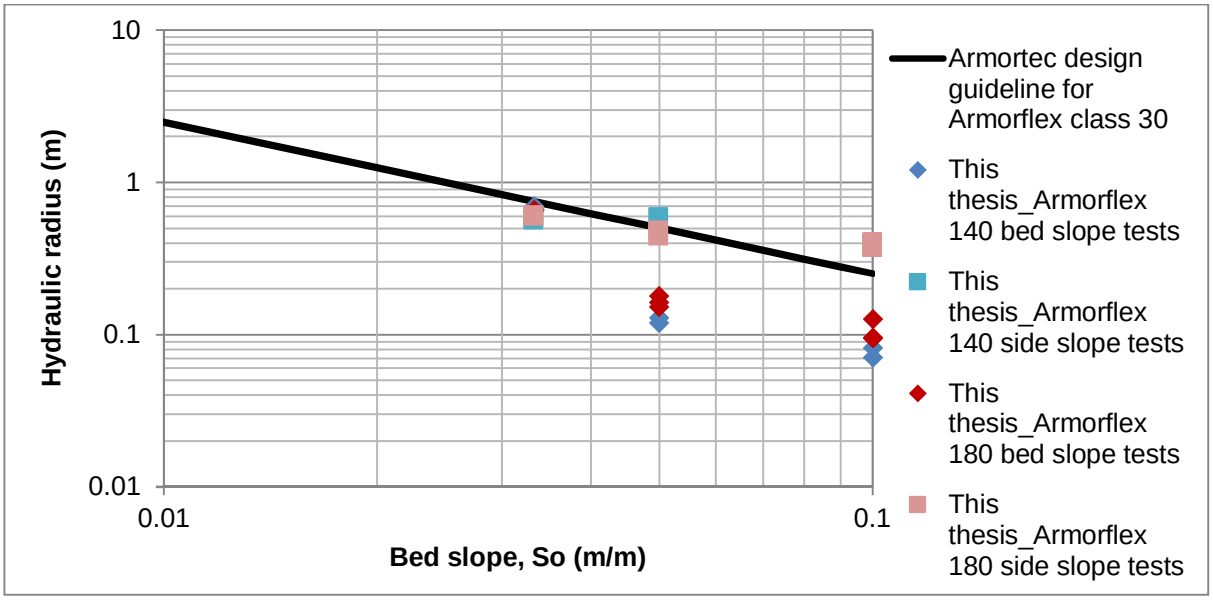

Figure 4-16: Armorflex 140 and 180 hydraulic radius at tested bed slopes

Figure 4-17 presents the suggested critical shear stresses for the four test scenarios investigated in this study versus the critical shear stress of Armorflex class 30 of 73.4 kg/m² as presented by Armortec Erosion Control Systems (Koutsourais, 1994).

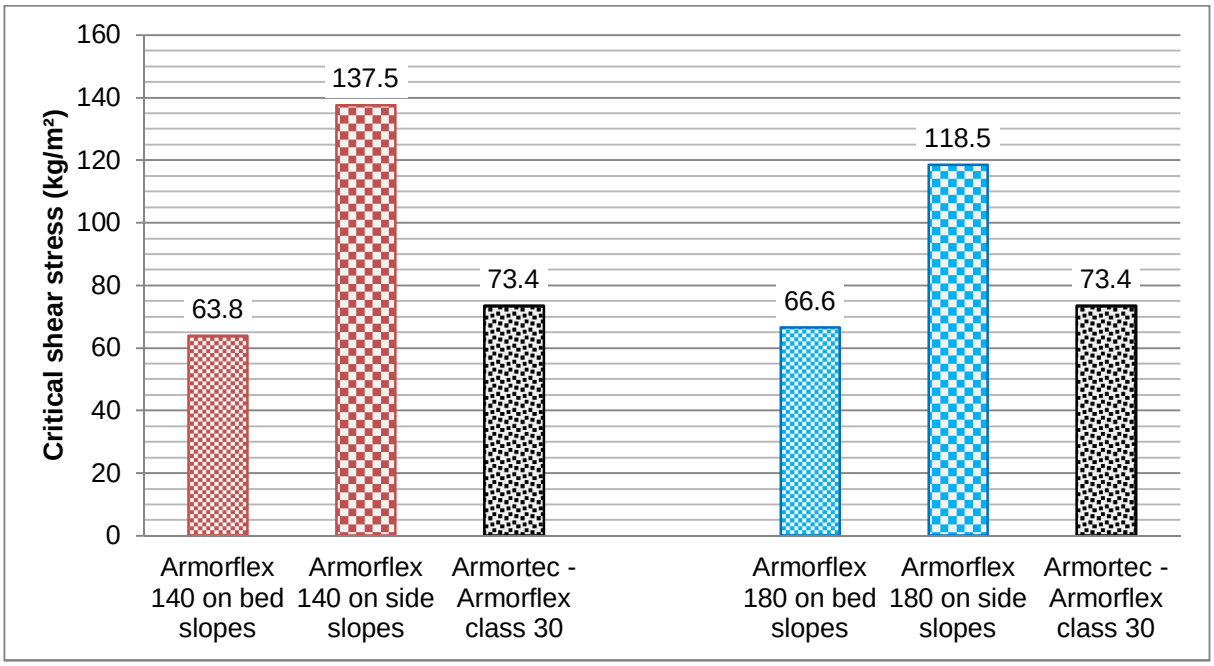

Figure 4-17: Suggested critical shear stress for Armorflex blocks versus Armortec's critical shear stress for Armorflex class 30 (Koutsourais, 1994)

The suggested critical bed shear stresses for the bed slope tests on Armorflex 140 and Armorflex 180 compare reasonably well to the proposed value of 73.4 kg/m². The suggested critical shear stress values for blocks installed on channel side slopes are close to two times the critical values suggested for blocks installed on bed slopes, and much greater than the limiting shear stress of 73.4 kg/m² specified by Koutsourais (1994) for Armorflex class 30 blocks.

4.5 Comparison of results to incipient motion criteria for riprap and Reno-mattresses

The incipient motion criteria for riprap and Reno-mattresses are compared to those recommended in this study for Armorflex 140 and 180. The literature study showed that the incipient motion criteria for riprap and Reno-mattresses have been thoroughly investigated by many researchers, being mainly presented in terms of critical flow velocity and critical shear stress. However, Stoffberg (2005) and Langmaak (2013) managed to apply the stream power-based incipient motion studies of Rooseboom (1992) and Armitage (2002) to define incipient motion conditions for riprap and Reno-mattresses.

Stoffberg (2005), basing his findings on tests conducted by Simons *et al.* (1984), presented suggested Movability Numbers of 0.13 and 0.165 for riprap and Reno-mattresses, respectively.

Langmaak (2013), on the other hand, found that for riprap, graded as stipulated by Simons & Sentürk (1992) in Section 2.3.1.2, a critical Movability Number of 0.18 can be used for design purposes, which is close to the 0.17 recommended by Armitage (2002).

Figure 4-18 shows how the Movability Numbers for riprap and Reno-mattresses, as suggested by Stoffberg (2005) and Langmaak (2013), compare with those suggested in this study for Armorflex 140 and 180. The graph shows that the Movability Numbers defining incipient motion of different Armorflex blocks are higher than the Movability Numbers suggested for riprap and Reno-mattresses. Unlike riprap and Reno-mattresses, Armorflex has no material smaller than the design weight that can be dislodged by the forces of flowing water, subsequently, undermining the larger material (Armortec Incorporated, 1981).

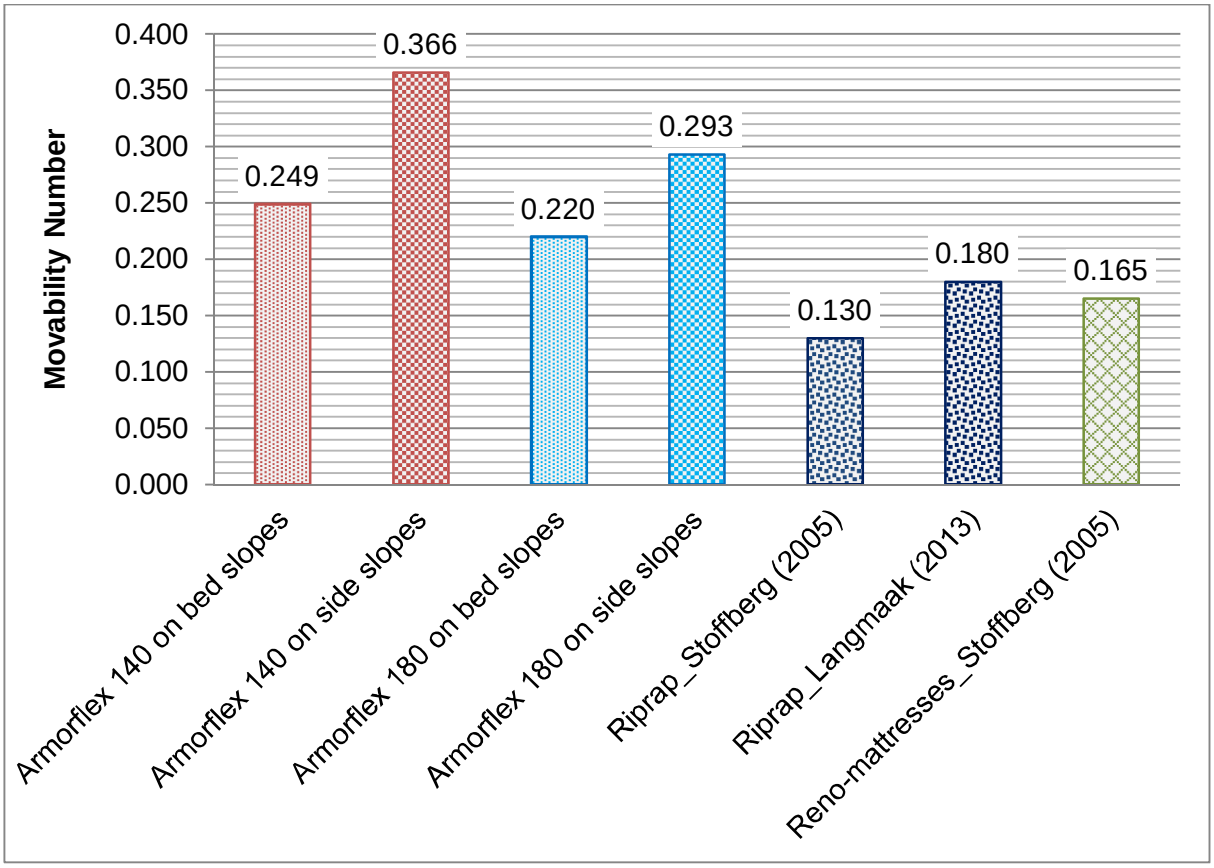

Figure 4-18: Suggested Movability Numbers of Armorflex, riprap and Reno-mattresses

Stoffberg (2005) presents critical flow velocities for various Reno-mattress thicknesses by analysing the results from hydraulic tests conducted at the CSU on Reno-mattresses by Simons, Chen, Swenson and Simons, Li & Associates (1984). Stoffberg (2005) also included the more conservative recommended critical flow velocities by Agostini & Papetti (Simons *et al.*, 1984) for the standard mattress thicknesses, which is given in Table 2-22. The critical flow velocities and Froude numbers observed during the performance testing of Armorflex blocks were used to estimate the recommended mattress thicknesses using the guide presented by Stoffberg (2005). Table 4-9 and Table 4-10 present the estimated mattress thicknesses for the critical flow conditions observed in all tests conducted on Armorflex 140 and 180, respectively.

Table 4-9: Armorflex 140 critical flow velocities, Fr and estimated Reno-mattress thicknesses

Test no	Test code	V_{cr} for Armorflex 140 (m/s)	Fr	Estimated required mattress thickness (mm)	
				CSU study (Simons *et al.*, 1984)	Agostini & Papetti (Simons *et al.*, 1984)
Bed slope tests:					
Test 1a	30_0_140_i	4.829	1.887	N/A*	450
Test 1b	30_0_140_ii	4.708	1.802	N/A	450
Test 5b	20_0_140_ii	2.795	2.586	N/A	230
Test 5f	20_0_140_vi	2.834	2.514	N/A	230
Test 9d	10_0_140_iv	3.242	3.899	150	230
Test 9e	10_0_140_v	3.538	3.954	150	230
Side slope tests:					
Test 3a	30_1.5_140_i	4.518	1.792	N/A	450
Test 3b	30_1.5_140_ii	4.467	1.803	N/A	300
Test 7b	20_1.5_140_ii	5.271	2.091	N/A	450
Test 11a	10_1.5_140_i	7.346	3.645	N/A	N/A

** N/A denotes that either the flow velocity or Froude number is outside the scope of study of the CSU and/or Agostini & Papetti.*

Table 4-10: Armorflex 180 critical flow velocities, Fr and estimated Reno-mattress thicknesses

Test no	Test code	V_{cr} for Armorflex 180 (m/s)	Fr	Estimated required mattress thickness (mm)	
				CSU study (Simons *et al.*, 1984)	Agostini & Papetti (Simons *et al.*, 1984)
Bed slope tests:					
Test 2a	30_0_180_i	5.045	1.989	N/A*	450
Test 2b	30_0_180_ii	5.060	1.998	N/A	450
Test 6d	20_0_180_iv	3.373	2.673	N/A	230
Test 6e	20_0_180_v	3.402	2.785	N/A	230
Test 6g	20_0_180_vii	3.759	2.834	N/A	300
Test 10b	10_0_180_ii	4.525	4.065	450	450
Test 10c	10_0_180_iii	4.105	4.246	300	300
Test 10d	10_0_180_iv	4.315	4.474	450	300

Test no	Test code	Vcr for Armorflex 180 (m/s)	Fr	Estimated required mattress thickness (mm)	
				CSU study (Simons et al., 1984)	Agostini & Papetti (Simons et al., 1984)
Side slope tests:					
Test 4a	30_1.5_180_i	4.328	1.694	N/A	300
Test 4b	30_1.5_180_ii	4.302	1.678	N/A	300
Test 8c	20_1.5_180_iii	5.400	2.376	N/A	N/A
Test 8d	20_1.5_180_iv	5.293	2.423	N/A	450
Test 12a	10_1.5_180_i	6.759	3.262	N/A	N/A
Test 12b	10_1.5_180_ii	6.705	3.372	N/A	N/A

** N/A denotes that either the flow velocity or Froude number is outside the scope of study of the CSU and Agostini & Papetti.*

4.6 Summary of findings

This section provides a summary of the findings from the analysis and interpretation of the results.

The calculated optimal Manning's n values for Armorflex blocks installed on bed slopes were considerably lower than the Technicrete (2016) specified range of 0.025 – 0.035. For the bed slope tests, optimal Manning's n values of 0.017 and 0.015 were determined for Armorflex 140 and Armorflex 180, respectively. For the side slope tests, optimal Manning's n values of 0.024 and 0.022 were determined for Armorflex 140 and Armorflex 180, respectively.

The results from Tests 1 and 2 showed the stabilising effect of sand particles between adjacent blocks. It is therefore expected that block structures screeded with topsoil or gravel are more stable than structures not screeded with material. The gravel increases the friction between neighbouring blocks, causing an interlocking effect, which in turn increases the stability of the block structure.

The study showed that Liu's Movability Number can be used to define the critical point of incipient motion for Armorflex blocks. Table 4-11 presents the critical flow conditions suggested for Armorflex blocks installed on bed- and side slopes, with Movability Number recommended for design purposes. All parameters show that Armorflex blocks installed on side slopes are generally more stable than blocks installed on bed slopes. In terms of Liu's

Movability Number, Armorflex 140 and Armorflex 180 blocks installed on side slopes are respectively 1.47 and 1.33 times more stable than when installed on bed slopes.

Table 4-11: Critical flow parameters at incipient motion of Armorflex 140 and Armorflex 180

Block type and scenario	V_{cr} (m/s)	τ_{cr} (kg/m²)	F_r	Movability Number
Armorflex 140 on bed slopes	2.7	63.8	2.50	0.249
Armorflex 140 on side slopes	4.4	137.5	1.75	0.366
Armorflex 180 on bed slopes	3.3	66.6	2.65	0.220
Armorflex 180 on side slopes	5.2	118.5	2.35	0.293

The critical shear stresses of Armorflex 140 and 180 compare well with the results from the FHWA overtopping flow study conducted by Clopper & Chen (1988), which presented a critical bed shear stress range of 58.6 – 97.7 kg/m² for Armorflex class 30 blocks. The suggested critical bed shear stress for Armorflex blocks on bed slopes compares reasonably well to the limiting bed shear stress of 73.4 kg/m² presented by Armortec Erosion Control Systems (Koutsourais, 1994). The critical shear stress values for blocks installed on channel side slopes are close to two times that for blocks installed on bed slopes, and much greater than the limiting shear stress of 73.4 kg/m² specified by Koutsourais (1994).

The critical Froude numbers determined for the four test scenarios correspond well with the findings from the study by Escarameia (1995), apart from the critical Froude number suggested for Armorflex 140 on side slopes. Given that only the two side slope tests conducted on the 1V:10H bed slope achieved failure (Tests 3a and 3b), the results obtained may be outliers and not representative of the true conditions of failure.

The recommended Movability Numbers for Armorflex 140 and 180 are all greater than the 0.12 recommended by Rooseboom & van Vuuren (2013). Rooseboom & van Vuuren's (2013) criteria is therefore considered conservative for design of ACB revetments. The recommended Movability Numbers for Armorflex blocks are also greater than the Movability Numbers recommended for riprap and Reno-mattresses.

The respective critical flow velocities of 2.7 m/s and 3.3 m/s obtained in this study for Armorflex 140 and Armorflex 180 on bed slopes propose that Technicrete's (2016) respective limiting flow velocities of 3.5 m/s and 5.5 m/s are overestimations. In contrast, Contech's (Armortec Incorporated, 1981) guideline seems conservative in that this study had no block failures at flow velocities lower than those specified by Armortec Incorporated (1981). However, according to incipient motion theory, it is understood that average flow velocity is not a suitable

parameter to use to define incipient motion conditions. Therefore, the limiting flow velocity guidelines of Technicrete (2016) and Contech (Armortec Incorporated, 1981) are unsuitable and deemed insufficient for guiding design engineers in the design of safe and stable Armorflex lined structures for given flow conditions.

5. CONCLUSIONS

This section presents the general conclusions drawn from the Armorflex physical hydraulic model study and the data analysis.

Given that the main aim of the study was to present incipient motion conditions of Armorflex 140 and 180 blocks in terms of Liu's (1957) Movability Number, the accurate determination of block settling velocity was critical. The settling velocity of Armorflex 140 and 180 model scale blocks was determined experimentally in the hydraulics laboratory. Average settling velocities of 0.585 m/s (1.013 m/s prototype) and 0.678 m/s (1.174 m/s prototype) were determined for Armorflex 140 and Armorflex 180, respectively.

The uniform, puzzle-like shape of Armorflex blocks makes installation easy, even without cables linking the blocks together. The way in which the blocks interlock with one another makes faulty installation easy to pick up during an inspection on site. Given the uniform shape of the blocks, projecting blocks are easily identified after installation. For loose block installation, packing should commence from the downstream end, ensuring each block is in contact with neighbouring blocks.

Drag forces instantly move a block downstream once it gets dislodged clear of neighbouring blocks. At high flows, once a block is lifted out of plane, the general washing away of blocks downstream of the point of initial block movement was observed. To limit the extent of damage in the field, anchor beams can be cast at specific intervals (as specified by the designer), restricting the area in which failure can occur. For cabled Armorflex systems, intermediate anchoring is recommended. Y-fencing bars are driven into the ground at 2 m spacing through the block openings before encasing it with concrete.

Researchers propose that a designed filter layer be installed between a well-prepared subgrade and the blocks. The filter can either be a granular- or geotextile filter. The filter should permit seepage to occur freely, while preventing fines from washing out from underneath the structure.

This study showed the importance of maintaining the recommended overlap length of a geotextile filter. Armortec (2016) recommends an overlap length of 910 mm. During the initial tests conducted, the filter layer that was used had an insufficient overlap length. Block failure continuously occurred at the position where the overlap was. The results of these tests were discarded and the filter replaced.

Armorflex structures screeded with topsoil or gravel are more stable than Armorflex structures not screeded with any material. The screed material enhances the stability of the structure by increasing the friction between neighbouring blocks, causing an interlocking effect.

From the literature study, average flow velocity is not a suitable parameter for defining the point of incipient motion of Armorflex. The limiting flow conditions of Armorflex presented by Technicrete (2016) and Contech (Armortec Incorporated, 1981) in terms of flow velocities are not suitable design guidelines.

The Movability Numbers recommended for design of Armorflex 140 installed on bed and side slopes are 0.249 and 0.366, respectively, while those for Armorflex 180 installed on bed and side slopes are 0.220 and 0.293, respectively. No safety factor has been applied to the recommended Movability Numbers. It is recommended that the designer of the revetment applies a suitable safety factor in the design. All recommended Movability Numbers are greater than Rooseboom & van Vuuren's (2013) proposed Movability Number of 0.12, rendering Rooseboom & van Vuuren's (2013) criteria conservative in design. The recommended Movability Numbers are also greater than those recommended for riprap and Reno-mattresses. Unlike riprap and Reno-mattresses, Armorflex has no particles smaller than the design weight than can be washed away by forces of flowing water, undermining the larger particles (Armortec Incorporated, 1981).

In a wide trapezoidal channel, Armorflex blocks installed on a side slope of 1V:1.5H are more stable than blocks installed on a bed slope. Dimensionless stability factors of 1.47 and 1.33 can respectively be applied to the Movability Numbers of Armorflex 140 and 180 blocks installed on bed slopes to determine the Movability Numbers of the blocks on side slopes. Blocks installed on channel side slopes experience smaller local flow velocities than those on the bed. Furthermore, the additional load from blocks resting on top of each other on a side slope could possibly have a stabilising effect.

6. RECOMMENDATIONS FOR FUTURE STUDIES

This section presents recommended experiments and future studies on Armorflex blocks in channelized applications.

In this thesis, the hydraulic performance of Armorflex blocks in supercritical flow conditions was investigated (Fr > 1). A study is required to determine the incipient motion conditions of Armorflex blocks in subcritical flow conditions (Fr < 1).

Given that this study investigated the incipient motion conditions of Armorflex blocks in a straight channel only, further research in this field is recommended whereby sharp bends in the horizontal alignment of ACB channels are taken into account.

As settling velocity is a critical parameter in any Movability Number analysis, the accurate determination thereof is crucial. It may be an interesting experiment to determine the settling velocity of prototype Armorflex blocks and to compare the findings with the settling velocities determined in this study.

The Movability Numbers presented in this thesis have not been adjusted with slope correction factors. To consider the effect of the respective slopes on incipient motion conditions, the angle of repose of Armorflex blocks is required. It is recommended that future incipient motion studies determine the angle of repose of Armorflex.

The results from this study showed that blocks installed on a side slope of 1V:1.5H are more stable than blocks installed on a bed slope ranging between 1V:30H and 1V:10H. An investigation is required to determine the optimum side slope of Armorflex blocks in channelized applications.

As a general recommendation for future studies on Armorflex blocks, clean water should be used in the hydraulic tests. Using dirty water may cause sand particles to be transported in between adjacent blocks, increasing the friction between the blocks and in effect, increasing the stability of the structure.

7. REFERENCES

Abt, S.R. & Johnson, T.L. 1991. Riprap design for overtopping flow. *Journal of hydraulic engineering*. 117(8):959–972.

Abt, S.R., Leech, J.R., Thornton, C.I. & Lipscomb, C.M. 2001. Articulated concrete block stability testing. *Journal of the American Water Resources Association*. 37(1):27–34.

Annandale, G.W. 2006. *Scour Technology: Mechanics and Engineering practice*. New York: McGraw-Hill.

Armitage, N.P. 2002. *A unit stream power model for the prediction of local scour*.

Armitage, N. & McGahey, C. 2003. A unit stream power model for the prediction of local scour in rivers. *Water Research Commission. WRC Report*. (1098/1):3.

Armortec. 2016a. *Armorflex Brochure [online]. Available from http://www.armortec.co.uk/downloads/Armorflex.pdf [Accessed 18 April 2016]*.

Armortec. 2016b. *Armorflex Installation Guide [online]. Available from https://www.conteches.com/technical-guides/search?filter=PNNA22FI91/ [Accessed 22 August 2016]*.

Armortec Erosion Control Solutions. 2002. *Armorflex Design Manual [online]. Available from http://www.superiorconcretemn.com/Media/GeoLink/flexmanual.pdf/[Accessed 19 April 2016]*.

Armortec Incorporated. 1981. *Armorflex erosion control system: Bank and channel protection. Technical bulletin BC-1*. Georgia.

ASTM. 2008a. *Standard test method for performance testing of articulating concrete block (ACB) revetment systems for hydraulic stability in open channel flow. D7277-08*. West Conshohocken, Pennsylvania: ASTM International.

ASTM. 2008b. *Standard guide for analysis and interpretation of test data for articulating concrete block (ACB) revetment systems in open channel flow. D7276-08*. West Conshohocken, Pennsylvania: ASTM International.

Bagnold, R.A. 1960. *Sediment discharge and stream power: A preliminary announcement*. Vol. 421. Washington: U.S. Department of the Interior.

Bouvard, M. 1992. *Mobile barrages and intakes on sediment transporting rivers*. AA Balkema, Brookfield.

Brink, C. 2004. Bend diversion to minimise sediment intake. University of Stellenbosch.

Christian, H.E. 1988. *Streambank erosion and bank stabilization. Reduction of sediment entrainment: Its trapping and flushing*. USA, Littleton: Water Resources Publications.

CIRIA, CUR & CETMEF. 2007. *The Rock Manual. The use of rock in hydraulic engineering (2nd edition)*. C683, CIRIA, London.

City of Tshwane. 2018. *Armorflex Typical Standard Details [online]. Available from http://www.tshwane.gov.za/sites/residents/Services/Documents/STD012_sh1of1.pdf/ [Accessed 18 March 2018]*.

Clopper, P.E. 1989. *Hydraulic stability of articulating concrete block revetment systems during overtopping flow. Report no. FHWA-RD-89-199*.

Clopper, P.E. 1991. *Protecting embankment dams with concrete block systems*.

Clopper, P.E. & Chen, Y.H. 1988. *Minimizing embankment damage during overtopping flow. Report no. FHWA/RD-88/181*.

Concha, F. 2009. Settling velocities of particulate systems. *KONA Powder and Particle Journal*. 27:18–37.

Cox, A.L. 2010. Moment stability analysis method for determining safety factors for articulating concrete blcks. Colorado State University.

Escarameia, M. 1995. *Channel protection - Gabion mattresses and concrete blocks. Report SR 427*.

Escarameia, M. 1998. *River and channel revetments: A design manual*. London: Thomas Telford Publications.

Escarameia, M. & May, R.W.. 1992. *Channel protection: Turbulence downstream of structures. Report SR 313*. London.

Gabion Baskets. 2019. *Gabions and River Mattresses. Available from https://www.gabionbaskets.co.za/gabions-and-river-mattresses/#. [Accessed 25 March 2019]*.

Graf, W.H. 1971. *Hydraulics of Sediment Transport. Series in Water Resources and*

Environmental Engineering. McGraw-Hill Inc, New York, USA.

Graf, W.H. 1998. *Fluvial hydraulics: Flow and transport processes in channels of simple geometry*. Chichester, United Kingdom: John Wiley & Sons.

Henderson, F.M. 1966. *Open channel flow*. New York: Macmillan Publishing Co., Inc.

Hewlett, H., Boorman, L. & Bramley, M. 1987. *Design of reinforced grass waterways. In CIRIA Technical Report*. London.

INCA Concrete Products. 2018. *Armorflex Brochure [online]. Available from https://www.specifile.co.za/brochure/inca-concrete-armorflex-erosion-control-system/ [Accessed 11 June 2018]*.

Izbash, S. V & Khaldre, K.Y. 1970. *Hydraulics of river channel closure*. London: Butterworths.

Jansen van Vuuren, A., Rooseboom, A. & Kruger, E. 2013. Drainage manual. 6th edition. Chapter 8 - Bridges and major culverts. In The South African National Roads Agency SOC Ltd *Drainage manual*.

Julien, P.Y. 2010. *Erosion and sedimentation*. 2nd ed. ed. Cambridge ; New York: Cambridge University Press.

Julien, P.Y. & Anthony, D.J. 2002. Bed load motion and grain sorting in a meandering stream. *Journal of Hydraulic Research*. 40(2):125–133.

Koutsourais, M. 1994. *Armortec Concrete Erosion Control Systems: A study of articulated concrete blocks designed to protect embankment dams*. Industrial Fabrics Association International.

Kramer, H. 1935. Sand mixtures and sand movement in fluvial model. *Transactions of the American Society of Civil Engineers*. 100(1):798–838.

Langmaak, K.R. 2013. Incipient motion of riprap on steep slopes. University of Stellenbosch.

Leech, J.R., Abt, S.R., Thornton, C.I. & Combs, P.G. 1999. Developing confidence in concrete revetment products for bank stabilization. *Journal of the American Water Resources Association*. 35(4):877–885.

Leidersdorf, C.B., Gadd, P.E. & McDougal, W.G. 1988. Articulated concrete mat slope protection. In *Coastal Engineering*. 2400–2415.

Lipscomb, C.., Thornton, C.I., Abt, S.R. & Leech, J.R. 2001. Performance of Articulated

Concrete Blocks in Vegetated and Un-vegetated Conditions. *Land and Water*. 45(4).

Liu, H.K. 1957. Mechanics of sediment-ripple formation. *Journal of the Hydraulics Division*. 83(2):1–23.

Maccaferri. 2015. *Reno Mattresses: Technical Data Sheet. [online]. Available from https://www.geofabrics.co/sites/default/files/technicaldata/tds-reno-mattress.pdf*.

Malherbe, I. 2019a.

Malherbe, I. 2019b.

Maynord, S.T., Ruff, J.F. & Abt, S.R. 1989. Riprap design. *Journal of Hydraulic Engineering*. 115(7):937–949.

National Concrete Masonry Association. 2010. *Design manual for articulating concrete block (ACB) revetment systems. Second edition*. Herndon, Virginia: NCMA Publications.

National Concrete Masonry Association. 2011. *Articulating concrete block revetment design - Factor of safety method. TEK 11-12A*. NCMA Publications.

Nicolon Corporation. n.d. *Armorflex Design Manual: Designing stable channels with Armorflex articulated concrete block revetment systems*.

Novak, P., Moffat, A.I.B., Nalluri, C. & Narayanan, R. 2014. *Hydraulic structures*. CRC Press.

Pabst, W. & Gregorova, E. 2007. *Characterization of particles and particle systems*.

Pacheco-Ceballos, R. 1983. Energy losses and shear stresses in channel bends. *Journal of Hydraulic Engineering*. 109(6):881–896.

Pettersson, H. & Pettersson, J. 2011. Safety Evaluation of the Plunge Pool and the Downstream River of the Baihetan Hydropower Station Using Model Experiments. Linköping University.

Pilarczyk, K.W. 1984. Closing of estauries, tidal inlets and dike breaches. *The closure of tidal basins*. 2:13.

Pilarczyk, K.W. 1995. *Simplified unification of stability formulae for revetments under current and wave attack*. John Wiley and Sons: Chichester, United Kingdom.

Prandtl, L. 1925. Über die ausgebildete turbulenz (investigations on turbulent flow). *Z. Angew. Math. Mech*. 5:136–139.

Przedwojski, B., Błażejewski, R. & Pilarczyk, K.W. 1995. *River training techniques: Fundamentals, design and applications*. AA Balkema.

Raudkivi, A.J. 1998. Loose boundary hydraulics, A. A. Balkema, Rotterdam, The Netherlands.

Robinson, K.M., Rice, C.E. & Kadavy, K.C. 1998. Design of rock chutes. *Transactions of the ASAE*. 41(3):621.

Rooseboom, A. 1974. *Open channel fluid mechanics. Technical report No. 62*. Pretoria: Department of Environment Affairs.

Rooseboom, A. 1992. *Sediment transport in rivers and reservoirs: A southern African perspective*. (WRC report ; no. 297/1/92). Stellenbosch: Sigma Beta.

Rooseboom, A. & van Vuuren, S. 2013. Drainage manual. 6th edition. Chapter 5 - Surface drainage. In The South African National Roads Agency SOC Ltd *Drainage manual*.

Scholl, B.B.N., Thornton, C.I. & King, B. 2010. *Articulated Concrete Block Design. Professional development series*.

Schweiger, P.G. & Holderbaum, R.E. 2001. *The ABC's of ACB's: An assessment of articulating concrete blocks for embankment overtopping protection*.

Sclafani, P. 2010. Methodology for predicting maximum velocity and shear stress in a sinuous channel with bendway weirs using 1-D HEC-RAS modeling results. Colorado State University.

Shields, A. 1936. Application of similarity principles and turbulence research to bed-load movement. California Institute of Technology, Pasadena, California.

Simons, D.B. & Sentürk, F. 1976. *Sediment transport technology. Fort Collins, Colorado, USA*. Water Resources Publications.

Simons, D.B. & Sentürk, F. 1992. *Sediment transport technology: Water and sediment dynamics. Littleton, Colorado*. Water Resources Publications.

Simons, D.B., Chen, Y.H., Swenson, L.J. & Simons, Li & Associates, I. 1984. *Hydraulic test to develop design criteria for the use of reno mattresses. Prepared by the Civil Engineering Department, Engineering Research Centre, Colorado State University, Fort Collins, Colorado*.

Stevens, M.A. & Simons, D.B. 1971. Stability analysis for coarse granular material on slopes.

River mechanics. 1:11–17.

Stoffberg, F. 2005. Evaluation of the incipient motion criteria for rock in reno mattresses and rip rap. University of Stellenbosch.

Technicrete. 2016. *Armorflex Brochure [online]. Available from http://www.technicrete.co.za/product-category/erosion-protection/ [Accessed 11 April 2016]*.

Thornton, C.I. 2015. *Articulating Concrete Block Testing Summary*.

U.S. Army Corps of Engineers. 1981. *The streambank erosion control evaluation and demonstration act of 1974, Section 32, Public Law 93-251, Final Report to Congress*.

Vanoni, V.A. 1975. Sedimentation engineering, ASCE manuals and reports on engineering practice - No. 54. *American Society of Civil Engineers, New York, NY*.

van Vuuren, S. & Rooseboom, A. 2013. Drainage manual. 6th edition. Chapter 4 - Hydraulic calculations. In The South African National Roads Agency SOC Ltd *Drainage manual*.

van der Walt, S.C. 2005. Mathematical modelling of sediment transport dynamics in the Berg River considering current and future water resources. University of Stellenbosch.

Yang, C.T. 1973. Incipient motion and sediment transport. *Journal of the Hydraulics Division*. 99(10):1679–1704.

APPENDIX A: MOMENT STABILITY ANALYSES OF ACB'S

Table A- 1 lists the definition of variables used in the safety factor derivations of Clopper (1991) and the NCMA (2010).

Table A- 1: Symbols used in the safety factor derivations of Clopper (1991) and the NCMA (2010)

Definition	Symbol used	
	Clopper (1991)	NCMA (2010)
Cross-section taken along block rotation path	A – A	
Coefficient of the weight force acting in the direction normal to the side-slope plane	-	a_θ
Drag force (kg)	F_D	
Lift force (kg)	F_L	
Submerged weight of block (kg)	W_s	
One-half of the block height (m)	l_1	
Block length measured from the block centre to the block corner (m)	l_2	
Moment arm for the drag force component along the path of motion (m)	l_3	
Moment arm for the lift force (m)	l_4	
Point of rotation	O	
Block rotation angle measured in the side-slope plane (degrees)	β	
Angle between the drag force and the block rotation path measured in the side-slope plane (degrees)	δ	
Resulting angle of the combined weight force components acting in the side-slope plane measured from a vertical line projected onto the side-slope plane (degrees)	-	θ
Bed-slope angle (degrees)	λ	θ_0
Side-slope angle (degrees)	θ	θ_1

A1: Method by Nicolon Corporation (n.d.)

Nicolon adopted the safety factor method of Clopper (1991) for the design of Armorflex revetments. Figure A- 1 illustrates the forces acting on a rectangular armour unit resting on a channel side slope.

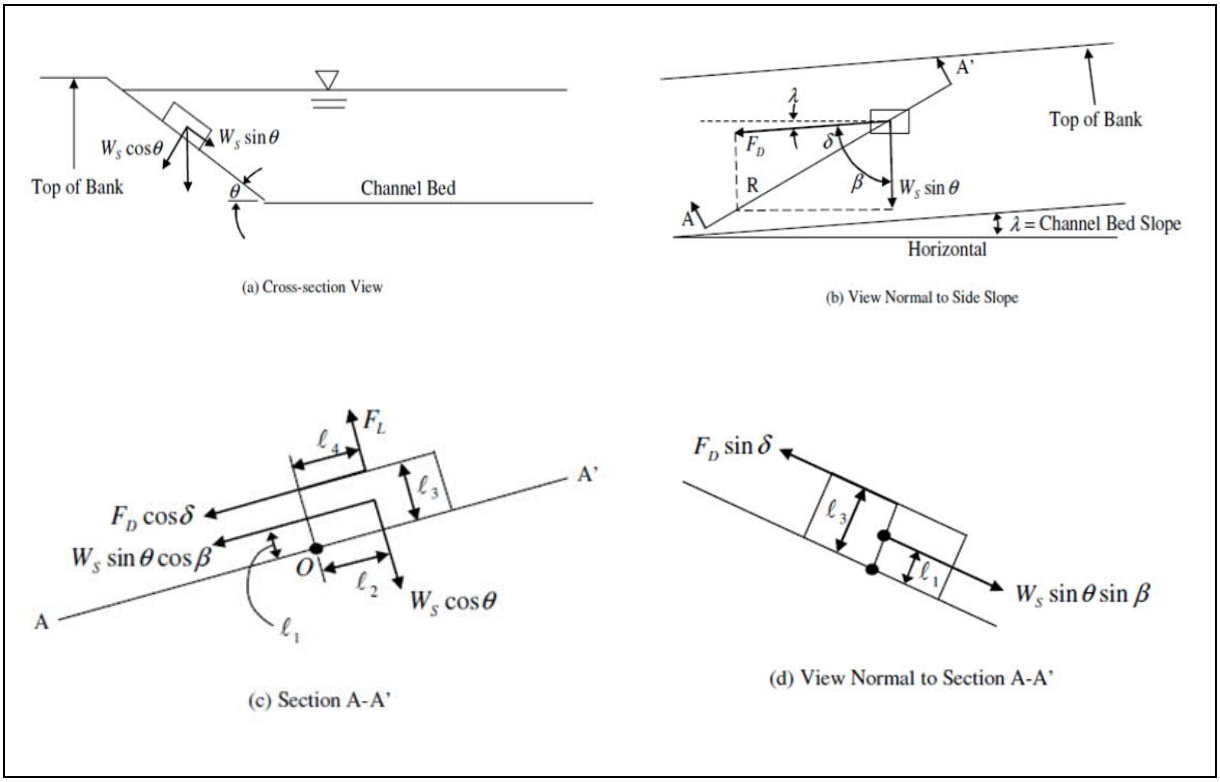

Figure A- 1: Symbols used in the safety factor derivations of Clopper (1991) and the NCMA (2010)

As illustrated by Figure A- 1(a), the weight force component parallel and perpendicular to the side-slope plane is $W_s\sin\theta$ and $W_s\cos\theta$, respectively, when accounting only for the side slope and assuming that the bed slope is horizontal.

Figure A- 1(b) illustrates that the forces acting on a rectangular armor unit include the drag force F_D, and a component of the submerged weight force W_s. The drag force acts in the direction of the streamline velocity vector, deviating from the horizontal at an angle λ. According to Clopper (1991), motion initiates along the vector R, located at an angle β from the vertical line projected on the side-slope plane.

Figure A- 1(c) shows that the forces acting within a cross-section A-A, taken along vector R, include the following:

- $W_s\cos\theta$: The weight force acting perpendicular into the side-slope plane;
- F_L: The lift force acting perpendicular out of the side-slope plane;
- $F_d\cos\delta$: The drag force component acting along cross-section A-A; and
- $W_s\sin\theta\cos\beta$: The submerged weight force component along cross-section A-A parallel to the side-slope plane.

The design manual of Nicolon defined the moment arm for drag force (l_3) as 0.8 times the block thickness and not the full block thickness as used in the designs of Clopper (1991) and the Armortec Erosion Control Solutions.

Taking moments about point O, Clopper (1991) derived the following safety factor equation for channelized conditions:

$$SF = \frac{(l_2/l_1)\cos\theta}{\sin\theta\cos\beta + (l_2/l_1)\eta'} \qquad \text{Equation A.1}$$

Where:

η' = Stability number on a channel side slope = $\frac{l_3 F_D \cos\delta}{l_2 W_s} + \frac{l_4 F_L}{l_2 W_s}$

Clopper (1991) included expressions to take into account additional lift- and drag forces. These forces may occur when blocks are not installed properly. The additional forces due to the impact of the flow against the projecting face of a block are determined by Equation A.2. According to *Nicolon*, the projecting height of Armorflex blocks should never exceed 12.7 mm.

$$F_D' = F_L' = C_D \rho (\Delta Z) w V^2 \qquad \text{Equation A.2}$$

Where:

F_D' = Additional drag force (kg)

F_L' = Additional lift force (kg)

C_D = Drag force coefficient, taken as 0.5

ΔZ = Height of the projecting surface normal to the direction of flow (m)

w = Width of the projecting surface normal to the direction of flow (m).

For projecting blocks, the safety factor equation for channelized conditions yields:

$$SF = \frac{(l_2/l_1)\cos\theta}{\sin\theta\cos\beta + (l_2/l_1)\eta' + \frac{l_3 F_D' \sin(\lambda+\beta)}{l_1 W_s} + \frac{l_4 F_L'}{l_1 W_s}} \qquad \text{Equation A.3}$$

A2: Method by Contech Construction Products inc.

Contech Construction Products inc. (Armortec Erosion Control Solutions) adopted the method presented by the NCMA (2010) for the design of Armorflex. The NCMA (2010) combined the methods of Julien (2010) and Julien and Anthony (2002) and included modifications to account for block geometry.

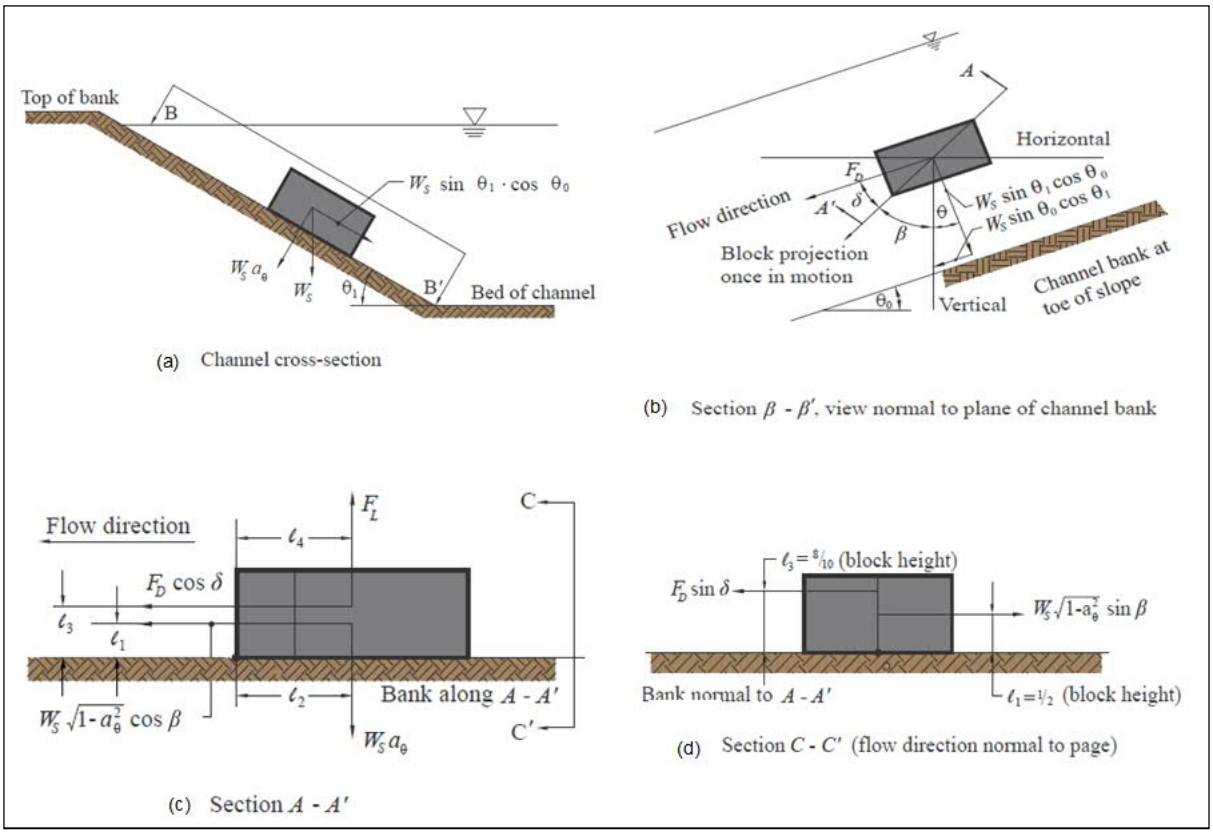

Figure A- 2: Force diagrams (adapted from NCMA, 2010)

Figure A- 2(a) and Figure A- 2(b) illustrate that the forces acting on a block include a drag force F_D, and a component of the submerged weight force F_s. The streamline velocity vector deviates from the horizontal at an angle θ_0. Two weight force components act in this plane, with a combination of the two producing a single weight force acting at an angle θ from a vertical line projected on the side-slope plane. Julien (2010) defined the two weight force components as $F_s\sin\theta_1$ and $F_s\sin\theta_0$ while Julien and Anthony (2002) defined it as $F_s\cos\theta_1\sin\theta_0$ and $F_s\cos\theta_0\sin\theta_1$. The NCMA (2010) used the definition by Julien (2010) to develop an expression for a_θ and the definition by Julien and Anthony (2002) to develop an expression for θ. These expressions are presented as Equation A.4 and Equation A.5, respectively.

$$a_\theta = \sqrt{\cos^2\theta_1 - \sin^2\theta_0} \qquad \text{Equation A.4}$$

$$\theta = \tan^{-1}\left(\frac{\cos\theta_1\sin\theta_0}{\cos\theta_0\sin\theta_1}\right) \qquad \text{Equation A.5}$$

When a block starts to move, it follows a path at an angle β from a vertical line projected on the side-slope plane. Figure A- 2(b) shows the angle β as the combined force vectors F_D, $F_s\sin\theta_1\cos\theta_0$ and $F_s\sin\theta_0\cos\theta_1$.

Figure A- 2(c) shows the forces acting within a cross-section A-A, taken along the movement path of the block. The forces include:

- $F_s a_\theta$: The weight force acting perpendicular into the side-slope plane;
- F_L: The lift force acting perpendicular out of the side-slope plane;
- $F_D \cos\delta$: The drag force component acting along cross-section A-A; and
- $F_s\sqrt{1-a_\theta{}^2}\cos\beta$: The submerged weight force component along cross-section A-A parallel to the side-slope plane.

Like Nicolon, the NCMA (2010) expressed the moment arm for drag force (l_3) as 0.8 times the block thickness. Taking moments about point O, the NCMA (2010) derived the following safety factor equation for channelized conditions:

$$SF = \frac{a_\theta (l_2/l_1)}{\sqrt{1-a_\theta{}^2}\cos\beta + \eta'(l_2/l_1)} \qquad \text{Equation A.6}$$

The NCMA (2010) included expressions that take into account additional lift- and drag forces attributed to the projection of an individual block above adjacent blocks (refer to Equation A.2). For projecting blocks, the safety factor equation for channelized conditions yields:

$$SF = \frac{(l_2/l_1)a_\theta}{\sqrt{1-a_\theta{}^2}\cos\beta + \eta'(l_2/l_1) + \frac{l_3 F_D{}' \sin(\theta_0+\beta)}{l_1 F_S} + \frac{l_4 F_L{}'}{l_1 F_S}} \qquad \text{Equation A.7}$$

In 2011, the NCMA published the TEK 11-12A (2011) as an addendum to NCMA (2010), which included improvements in terms of the assumptions made with regards to alignment of flow. The NCMA (2010) assumes flow parallel to the block, meaning the drag force is calculated using the block width. However, in practice the flow is not necessarily aligned with the sides of the block. Because of the uncertainty, TEK 11-12A (2011) recommends that the diagonal distance of the block, $2l_2$, be used instead of the width of the block when calculating the safety factor.

A3: Extrapolation of results

ASTM (2008a) requires that ACB's be tested at steep slopes, typically 1V:2H. Moment stability analyses, i.e. factor of safety methods, require the shear stress on a horizontal surface to be calculated. Additionally, calculating critical bed shear stress on project specific bed slopes is advantageous. Extrapolation of shear stress results from a tested bed slope to more mild slopes is possible, as presented in Equation A.8.

$$\tau_{cr,\beta_U} = \tau_{cr,\beta_T} \cdot \left(\frac{l_2\cos\beta_U - l_1\sin\beta_U}{l_2\cos\beta_T - l_1\sin\beta_T}\right) \qquad \text{Equation A.8}$$

Where:

τ_{cr,β_U} = Critical shear stress for untested bed slope (kg/m²)

τ_{cr,β_T} = Critical shear stress for tested bed slope (kg/m²)

β_U = Untested bed slope (degrees)

β_T = Tested bed slope (degrees)

l_x = Block specific moment arms (m).

The same principle can be used to extrapolate results within a block class in terms of block thickness. Equation A.9 should only be used to extrapolate up in thickness.

$$\tau_{cr,U} = \tau_{cr,T} \cdot \left(\frac{W_{S,U} l_{2U}}{W_{S,T} l_{2T}} \cdot \frac{l_{3T} + l_{4T}}{l_{3U} + l_{4U}}\right) \quad \text{Equation A.9}$$

Where:

$\tau_{cr,U}$ = Critical shear stress for untested block (kg/m²)

$\tau_{cr,T}$ = Critical shear stress for tested block (kg/m²)

$W_{S,U}$ = Submerged weight of untested block (kg)

$W_{S,T}$ = Submerged weight of tested block (kg)

l_{xT} and l_{xU} = Moment arms of tested and untested block, respectively (m).

Using Equation A.8 and Equation A.9, Nicolon, Contech (*Armortec Erosion Control Solutions)* and the CSU extrapolated results to determine a set of design criteria for various Armorflex block classes. These design values are given in Table A- 2. The moment arms and the critical shear stresses in Table A- 2 assume blocks to be orientated with the long axis parallel to the flow.

It is interesting to note that the design values presented by Armorflex manufacturers are considerably higher than those extrapolated by CSU. For many block classes, CSU's critical shear stresses are up to 30% lower than that claimed by Armorflex manufacturers.

Table A- 2: Extrapolated safety factor equation variables

Armorflex block class	Weight (kg)	Submerged weight, W_s (kg)	τ_{cr} (kg/m²) on 0˚ bed slope		
			Nicolon Corporation (n.d.)	Armortec Erosion Control Solutions (2002)	CSU (Thornton, 2015)
30S	15.4	9.0	73.2	70.3	25.4
45S	17.8	11.1	87.9	87.4	30.3
50S	19.0	13.0	97.6	92.8	29.8
55S	22.8	15.1	112.3	107.9	35.6
40	26.8	16.9	121.1	109.4	54.7

Armorflex block class	Weight (kg)	Submerged weight, W_s (kg)	τ_{cr} (kg/m²) on 0˚ bed slope		
			Nicolon Corporation (n.d.)	Armortec Erosion Control Solutions (2002)	CSU (Thornton, 2015)
45	32.3	20.6	147.9	133.3	65.9
50	34.6	21.7	154.8	130.0	66.4
55	41.5	26.4	188.9	157.2	79.6
60	42.3	27.5	196.8	151.4	76.7
70	51.7	34.2	244.1	173.3	86.4
75	50.8	33.8	241.7	186.5	90.8
85	61.5	41.3	292.9	209.9	103.0
40L	44.1	21.2	-	126.0	71.3
45L	49.5	25.5	-	151.4	106.9
50L	49.5	27.4	-	148.9	107.9
55L	62.7	32.8	-	181.6	128.4
60L	-	34.0	-	173.8	-
70L	79.2	40.8	-	199.2	144.0
75L	-	40.8	-	210.9	-
85L	94.0	49.3	-	237.8	171.4
40T	26.4	25.5	-	155.3	122.1
50T	34.2	32.8	-	180.2	148.9
60T	42.4	40.8	-	205.6	171.9
70T	49.4	49.3	-	227.0	188.0

A4: Design steps

Contech recommend the following steps for designing Armorflex:

Step 1: Determine an acceptable target SF

$$SF_T = S \cdot F_B \cdot X_C \cdot X_M \qquad \text{Equation A.10}$$

Where:

SF_T = Target safety factor

SF_B = Base safety factor

X_C = Multiplier based on consequence of failure

X_M = Multiplier based on hydraulic model uncertainty.

Table A- 3 presents values of SF_B, X_C and X_M, all being dependent on site specific conditions.

SF_T is dependent on the complexity of the model and design. If the design is complex but the model is simple, SF_T would be higher. If the design is simple and the model is complex, SF_T would be lower. If the site conditions are well known and the installation conditions are well controlled, SF_T could be as low as 1.2 (Scholl *et al.*, 2010).

Table A- 3: Values of SF_B, X_C and X_M (Scholl *et al.*, 2010)

Base factor of safety, SF_B	
Application	**SF_B**
Channel bed/bank	1.2 – 1.4
Bridge pier/abutment	1.5 – 1.7
Overtopping spillway	1.8 – 2.0

Consequence of failure multiplier, X_C	
Consequence of failure	**X_C**
Low	1.0 – 1.2
Medium	1.3 – 1.5
High	1.6 – 1.8
Extreme or loss of life	1.9 – 2.0

Multiplier based on hydraulic model uncertainty, X_M	
Hydraulic model	**X_M**
Deterministic	1.0 – 1.3
Empirical or stochastic	1.4 – 1.7
Estimates	1.8 – 2.0

Step 2: Calculate design shear stress

Cox (2010) deems it more accurate to use hydraulic radius, R, associated with the roughened perimeter instead of flow depth when calculating the boundary shear stress:

$$\tau_{des} = \rho g R S_f \qquad \text{Equation A.11}$$

Step 3: Obtain properties of appropriate ACB's

The required block properties include the following:

- Specific gravity of block material;
- Moment arms;
- Submerged weight of block;
- Design shear stress;

- Critical shear stress on a horizontal surface;
- Maximum test velocity (design velocity); and
- Test bed slope.

Step 4: Calculate the SF for all appropriate ACB systems

Refer to the SF equations derived by Clopper (1991) and the NCMA (2010) in Appendix A1 and A2, respectively.

Step 5: Decide on appropriate product

An appropriate ACB product is selected with reference to SF_T. Once an appropriate block has been selected, the extent of the revetment should be determined, both longitudinally and vertically, according to the installation guidelines given in Section 2.2.2.

APPENDIX B: SCALE ARMORFLEX CONCRETE DENSITIES

Table B- 1: Average density of scaled Armorflex 140 blocks

Test no.	Block unit no.	Mass (kg)	Volume (m^3)	ρ (kg/m^3)	Average ρ (kg/m^3)
1	603	0.643	0.00032	1989.1	
2	331	0.661	0.00032	2044.7	
3	252	0.641	0.00035	1810.4	
4	302	0.665	0.00034	1963.6	
5	461	0.646	0.00034	1907.5	
6	635	0.631	0.00034	1863.2	
7	460	0.647	0.00032	2001.4	
8	527	0.689	0.00035	1946.0	
9	224	0.644	0.00035	1818.9	
10	195	0.681	0.00034	2010.8	
11	10	0.63	0.00034	1860.3	
12	236	0.671	0.00034	1981.3	
13	380	0.637	0.00034	1880.9	
14	351	0.63	0.00034	1860.3	
15	459	0.634	0.00034	1872.1	1921.9
16	458	0.649	0.00034	1916.4	
17	151	0.638	0.00034	1883.9	
18	16	0.653	0.00032	2020.0	
19	141	0.638	0.00034	1883.9	
20	131	0.629	0.00032	1945.7	
21	110	0.67	0.00035	1892.3	
22	378	0.635	0.00034	1875.0	
23	619	0.641	0.00032	1982.9	
24	185	0.662	0.00034	1954.7	
25	142	0.632	0.00034	1866.2	
26	53	0.652	0.00034	1925.2	
27	8	0.615	0.00032	1902.4	
28	220	0.66	0.00034	1948.8	
29	47	0.666	0.00034	1966.6	

Test no.	Block unit no.	Mass (kg)	Volume (m³)	ρ (kg/m³)	Average ρ (kg/m³)
30	422	0.667	0.00035	1883.9	

Table B- 2: Average density of scaled Armorflex 180 blocks

Test no.	Block unit no.	Mass (kg)	Volume (m³)	ρ (kg/m³)	Average ρ (kg/m³)
1	18	0.572	0.00029	1955.7	1920.8
2	90	0.592	0.00031	1922.9	
3	611	0.619	0.00031	2010.5	
4	60	0.572	0.00028	2064.3	
5	50	0.578	0.00031	1877.4	
6	661	0.589	0.00031	1913.1	
7	118	0.567	0.00029	1938.6	
8	113	0.576	0.00031	1870.9	
9	950	0.603	0.00031	1958.6	
10	696	0.617	0.00032	1908.6	
11	94	0.575	0.00029	1965.9	
12	709	0.586	0.00031	1903.4	
13	783	0.595	0.00031	1932.6	
14	730	0.617	0.00032	1908.6	
15	92	0.567	0.00029	1938.6	
16	674	0.616	0.00032	1905.5	
17	809	0.581	0.00031	1887.1	
18	671	0.595	0.00031	1932.6	
19	146	0.575	0.00031	1867.6	
20	199	0.574	0.00029	1962.5	
21	477	0.589	0.00031	1913.1	
22	472	0.592	0.00031	1922.9	
23	368	0.576	0.00031	1870.9	
24	119	0.584	0.00031	1896.9	
25	191	0.57	0.00029	1948.8	
26	76	0.594	0.00031	1929.3	
27	732	0.605	0.00032	1871.5	
28	183	0.581	0.00031	1887.1	

Test	Block unit no.	Mass (kg)	Volume (m^3)	ρ (kg/m^3)	Average ρ (kg/m^3)
29	168	0.569	0.00031	1848.1	
30	398	0.588	0.00031	1909.9	

APPENDIX C: LABORATORY RESULTS

C1: Numerical survey data

Table C1- 1: Bed- and water levels for Test 1a: 30_0_140_i

CH (m)	Bed levels		Water level readings @Qm (mm)	Flow depth @Qm (m)	Longitudinal flow depth @Qm (m)	Observed WSE (m)	Representative longitudinal flow depth @Qm (m)	Representative WSE (m)
	Bed level reading (mm)	Bed elevation (m)						
-2		0.000						
0		0.400						
3		0.313						
3.5	416.5	0.286					0.222	0.509
4	395.0	0.267	619.13	0.224	0.224	0.491	0.226	0.492
4.5	394.0	0.255	617.00	0.223	0.223	0.478	0.221	0.475
5	376.5	0.236	599.50	0.223	0.223	0.458	0.223	0.459
5.6	724.0	0.215	501.00	0.223	0.223	0.438	0.223	0.439
6	744.0	0.202	520.84	0.223	0.223	0.425	0.224	0.426
6.5	756.5	0.186	533.72	0.223	0.223	0.409	0.223	0.409

CH (m)	Bed levels		Water level readings @Qm (mm)	Flow depth @Q_m (m)	Longitudinal flow depth @Q_m (m)	Observed WSE (m)	Representative longitudinal flow depth @Qm (m)	Representative WSE (m)
	Bed level reading (mm)	Bed elevation (m)						
7	775.0	0.171						
7.5	787.0	0.153						
8	801.5	0.134						
8.5	814.5	0.116						
9	826.5	0.099						
10		0.000						

Table C1- 2: Bed- and water levels for Test 1b: 30_0_140_ii

CH (m)	Bed levels		Water level readings @Qm (mm)	Flow depth @Q_m (m)	Longitudinal flow depth @Q_m (m)	Observed WSE (m)	Representative longitudinal flow depth @Qm (m)	Representative WSE (m)
	Bed level reading (mm)	Bed elevation (m)						
-2		0.000						
0		0.400						
3		0.313						

CH (m)	Bed levels		CH (m)	Flow depth @Qm (m)	Longitudinal flow depth @Qm (m)	Observed WSE (m)	Representative longitudinal flow depth @Qm (m)	Representative WSE (m)
	Bed level reading (mm)	Bed elevation (m)						
3.5	416.5	0.286					0.247	0.534
4	395.0	0.267	632.25	0.237	0.237	0.504	0.247	0.514
4.5	394.0	0.255	641.98	0.248	0.248	0.503	0.239	0.494
5	376.5	0.236	630.25	0.254	0.254	0.489	0.238	0.474
5.6	724.0	0.215	493.08	0.231	0.231	0.446	0.234	0.450
6	744.0	0.202	526.79	0.217	0.217	0.419	0.232	0.434
6.5	756.5	0.186						
7	775.0	0.171						
7.5	787.0	0.153						
8	801.5	0.134						
8.5	814.5	0.116						
9	826.5	0.099						
10		0.000						

Table C1- 3: Bed- and water levels for Test 2a: 30_0_180_i_DNF

CH (m)	Bed levels		Water level readings @Qm (mm)	Flow depth @Q_m (m)	Longitudinal flow depth @Q_m (m)	Observed WSE (m)	Representative longitudinal flow depth @Qm (m)	Representative WSE (m)
	Bed level reading (mm)	Bed elevation (m)						
-2		0.000						
0		0.400						
3		0.313						
3.5	425	0.286					0.250	0.536
4	402	0.267	639.25	0.237	0.237	0.504	0.249	0.516
4.5	400	0.255	647.98	0.248	0.248	0.503	0.240	0.495
5	384.5	0.236	638.25	0.254	0.254	0.489	0.239	0.474
5.6	711.5	0.215	480.58	0.231	0.231	0.446	0.234	0.450
6	736	0.202	518.79	0.217	0.217	0.419	0.231	0.433
6.5	748	0.186	529.63	0.218	0.218	0.405	0.226	0.412
7	767	0.171	531.91	0.235	0.235	0.406	0.221	0.392
7.5	781	0.153	562.17	0.219	0.219	0.371	0.219	0.371
8	795	0.134	582.65	0.212	0.212	0.346	0.216	0.351

CH (m)	Bed levels		Water level readings @Qm (mm)	Flow depth @Q_m (m)	Longitudinal flow depth @Q_m (m)	Observed WSE (m)	Representative longitudinal flow depth @Qm (m)	Representative WSE (m)
	Bed level reading (mm)	Bed elevation (m)						
8.5	809	0.116						
9	814.5	0.099						
10		0.000						

Table C1- 4: Bed- and water levels for Test 2b: 30_0_180_ii_DNF

CH (m)	Bed levels		Water level readings @Qm (mm)	Flow depth @Q_m (m)	Longitudinal flow depth @Q_m (m)	Observed WSE (m)	Representative longitudinal flow depth @Qm (m)	Representative WSE (m)
	Bed level reading (mm)	Bed elevation (m)						
-2		0.000						
0		0.400						
3		0.313						
3.5	425	0.286					0.246	0.532
4	402	0.267	635.38	0.233	0.233	0.500	0.245	0.512
4.5	400	0.255	646.36	0.246	0.246	0.501	0.237	0.492

CH (m)	Bed levels		Water level readings @Qm (mm)	Flow depth @Qm (m)	Longitudinal flow depth @Qm (m)	Observed WSE (m)	Representative longitudinal flow depth @Qm (m)	Representative WSE (m)
	Bed level reading (mm)	Bed elevation (m)						
5	384.5	0.236	637.84	0.253	0.253	0.489	0.236	0.472
5.6	711.5	0.215	482.39	0.229	0.229	0.444	0.232	0.447
6	736	0.202	520.79	0.215	0.215	0.417	0.229	0.431
6.5	748	0.186	532.67	0.215	0.215	0.402	0.225	0.411
7	767	0.171	534.05	0.233	0.233	0.404	0.220	0.391
7.5	781	0.153	558.81	0.222	0.222	0.375	0.218	0.371
8	795	0.134	583.00	0.212	0.212	0.346	0.216	0.350
8.5	809	0.116						
9	814.5	0.099						
10		0.000						

Table C1- 5: Bed- and water levels for Test 3a: 30_1.5_140_i

CH (m)	Bed levels		Water level readings @Qm (mm)	Flow depth @Q_m (m)	Longitudinal flow depth @Q_m (m)	Observed WSE (m)	Representative longitudinal flow depth @Qm (m)	Representative WSE (m)
	Bed level reading (mm)	Bed elevation (m)						
-2		0.100						
0		0.400						
3		0.300						
3.5	416.5	0.276	768.00	0.352	0.351	0.627	0.343	0.619
4	395	0.254	745.00	0.350	0.350	0.604	0.342	0.596
4.5	394	0.238	725.00	0.331	0.331	0.569	0.335	0.573
5	376.5	0.221	692.50	0.316	0.316	0.537	0.329	0.550
5.6	724	0.202	413.00	0.311	0.311	0.513	0.320	0.523
6	744	0.188	432.50	0.312	0.311	0.499	0.316	0.504
6.5	756.5	0.165	436.50	0.320	0.320	0.485	0.316	0.481
7	775	0.147	452.00	0.323	0.323	0.470	0.311	0.458
7.5	787	0.133						
8	801.5	0.117						

CH (m)	Bed levels		Water level readings @Qm (mm)	Flow depth @Q_m (m)	Longitudinal flow depth @Q_m (m)	Observed WSE (m)	Representative longitudinal flow depth @Qm (m)	Representative WSE (m)
	Bed level reading (mm)	Bed elevation (m)						
8.5	814.5	0.106						
9	826.5	0.091						
10		0.000						

Table C1- 6: Bed- and water levels for Test 3b: 30_1.5_140_ii

CH (m)	Bed levels		Water level readings @Qm (mm)	Flow depth @Q_m (m)	Longitudinal flow depth @Q_m (m)	Observed WSE (m)	Representative longitudinal flow depth @Qm (m)	Representative WSE (m)
	Bed level reading (mm)	Bed elevation (m)						
-2		0.100						
0		0.400						
3		0.300						
3.5	416.5	0.276	750.00	0.334	0.333	0.609	0.326	0.602
4	395	0.254	727.00	0.332	0.332	0.586	0.326	0.580
4.5	394	0.238	709.00	0.315	0.315	0.553	0.320	0.558

CH (m)	Bed levels		Water level readings @Qm (mm)	Flow depth @Qm (m)	Longitudinal flow depth @Qm (m)	Observed WSE (m)	Representative longitudinal flow depth @Qm (m)	Representative WSE (m)
	Bed level reading (mm)	Bed elevation (m)						
5	376.5	0.221	681.00	0.305	0.304	0.525	0.314	0.535
5.6	724	0.202	425.00	0.299	0.299	0.501	0.306	0.508
6	744	0.188	444.50	0.300	0.299	0.487	0.302	0.490
6.5	756.5	0.165	447.50	0.309	0.309	0.474	0.303	0.468
7	775	0.147	470.00	0.305	0.305	0.452	0.299	0.446
7.5	787	0.133						
8	801.5	0.117						
8.5	814.5	0.106						
9	826.5	0.091						
10		0.000						

Table C1- 7: Bed- and water levels for Test 4a: 30_1.5_180_i_DNF

CH (m)	Bed levels		Water level readings @Qm (mm)	Flow depth @Q_m (m)	Longitudinal flow depth @Q_m (m)	Observed WSE (m)	Representative longitudinal flow depth @Qm (m)	Representative WSE (m)
	Bed level reading (mm)	Bed elevation (m)						
-2		0.100						
0		0.400						
3		0.3						
3.5	425	0.276	780.00	0.355	0.355	0.631	0.349	0.625
4	402	0.254	758.00	0.356	0.356	0.610	0.348	0.602
4.5	400	0.238	740.50	0.341	0.340	0.578	0.341	0.579
5	384.5	0.221	710.00	0.326	0.325	0.546	0.335	0.556
5.6	711.5	0.2024	399.00	0.313	0.312	0.515	0.326	0.528
6	736	0.188	421.00	0.315	0.315	0.503	0.322	0.510
6.5	748	0.165	425.50	0.323	0.322	0.487	0.321	0.486
7	767	0.147	442.00	0.325	0.325	0.472	0.316	0.463
7.5	781	0.133						
8	795	0.117						

CH (m)	Bed levels		Water level readings @Qm (mm)	Flow depth @Q_m (m)	Longitudinal flow depth @Q_m (m)	Observed WSE (m)	Representative longitudinal flow depth @Qm (m)	Representative WSE (m)
	Bed level reading (mm)	Bed elevation (m)						
8.5	809	0.106						
9	814.5	0.091						
10		0						

Table C1- 8: Bed- and water levels for Test 4b: 30_1.5_180_ii_DNF

CH (m)	Bed levels		Water level readings @Qm (mm)	Flow depth @Q_m (m)	Longitudinal flow depth @Q_m (m)	Observed WSE (m)	Representative longitudinal flow depth @Qm (m)	Representative WSE (m)
	Bed level reading (mm)	Bed elevation (m)						
-2		0.000						
0		0.4						
3		0.3						
3.5	425	0.276	784.50	0.360	0.359	0.635	0.352	0.628
4	402	0.254	760.00	0.358	0.358	0.612	0.351	0.605
4.5	400	0.238	744.00	0.344	0.344	0.582	0.344	0.582

CH (m)	Bed levels		Water level readings @Qm (mm)	Flow depth @Qm (m)	Longitudinal flow depth @Qm (m)	Observed WSE (m)	Representative longitudinal flow depth @Qm (m)	Representative WSE (m)
	Bed level reading (mm)	Bed elevation (m)						
5	384.5	0.221	710.00	0.326	0.325	0.546	0.338	0.559
5.6	711.5	0.206	397.00	0.315	0.314	0.517	0.328	0.531
6	736	0.188	417.50	0.319	0.318	0.506	0.324	0.512
6.5	748	0.165	422.50	0.326	0.325	0.490	0.324	0.489
7	767	0.147	437.00	0.330	0.330	0.477	0.319	0.466
7.5	781	0.133						
8	795	0.117						
8.5	809	0.106						
9	814.5	0.091						
10		0						

Table C1- 9: Bed- and water levels for Test 5b: 20_0_140_ii

CH (m)	Bed levels		Water level readings @Qm (mm)	Flow depth @Q_m (m)	Longitudinal flow depth @Q_m (m)	Observed WSE (m)	Representative longitudinal flow depth @Qm (m)	Representative WSE (m)
	Bed level reading (mm)	Bed elevation (m)						
-2		0.100						
0		0.650						
3		0.475						
3.5	513	0.451					0.037	0.488
4	477	0.427	513	0.036	0.036	0.463	0.037	0.464
4.5	444	0.402	481	0.037	0.037	0.438	0.038	0.440
5	420	0.376	461	0.041	0.041	0.417	0.039	0.415
5.6	665	0.346	625	0.040	0.040	0.386	0.039	0.385
6	683	0.326	643	0.040	0.040	0.366	0.040	0.366
6.5	712	0.302						
7	732	0.277						
7.5	747	0.254						
8	777	0.230						

CH (m)	Bed levels		Water level readings @Qm (mm)	Flow depth @Q_m (m)	Longitudinal flow depth @Q_m (m)	Observed WSE (m)	Representative longitudinal flow depth @Qm (m)	Representative WSE (m)
	Bed level reading (mm)	Bed elevation (m)						
8.5	804	0.206						
9	821	0.181						
10		0.100						

Table C1- 10: Bed- and water levels for Test 5f: 20_0_140_vi

CH (m)	Bed levels		Water level readings @Qm (mm)	Flow depth @Q_m (m)	Longitudinal flow depth @Q_m (m)	Observed WSE (m)	Representative longitudinal flow depth @Qm (m)	Representative WSE (m)
	Bed level reading (mm)	Bed elevation (m)						
-2		0.000						
0		0.650						
3		0.475						
3.5	513	0.451					0.042	0.493
4	477	0.427	518	0.041	0.041	0.468	0.041	0.468
4.5	444	0.402	485	0.041	0.041	0.442	0.042	0.444

CH (m)	Bed levels		Water level readings @Qm (mm)	Flow depth @Qm (m)	Longitudinal flow depth @Qm (m)	Observed WSE (m)	Representative longitudinal flow depth @Qm (m)	Representative WSE (m)
	Bed level reading (mm)	Bed elevation (m)						
5	420	0.376	465	0.045	0.045	0.421	0.043	0.419
5.6	665	0.346	623	0.042	0.042	0.388	0.043	0.389
6	683	0.326						
6.5	712	0.302						
7	732	0.277						
7.5	747	0.254						
8	777	0.230						
8.5	804	0.206						
9	821	0.181						
10		0.100						

Table C1- 11: Bed- and water levels for Test 6d: 20_0_180_iv

CH (m)	Bed levels		Water level readings @Qm (mm)	Flow depth @Q_m (m)	Longitudinal flow depth @Q_m (m)	Observed WSE (m)	Representative longitudinal flow depth @Qm (m)	Representative WSE (m)
	Bed level reading (mm)	Bed elevation (m)						
-2		0.100						
0		0.650						
3		0.475						
3.5	528	0.451					0.051	0.502
4	489	0.427	540	0.051	0.051	0.478	0.051	0.478
4.5	453	0.402	504	0.051	0.051	0.452	0.052	0.453
5	432	0.376	485	0.053	0.053	0.429	0.053	0.429
5.6	653	0.346	603	0.050	0.050	0.396	0.054	0.400
6	671	0.326	612	0.059	0.059	0.385	0.054	0.380
6.5	693	0.302	641	0.052	0.052	0.353	0.054	0.356
7	724	0.277						
7.5	736	0.254						
8	770	0.230						

CH (m)	Bed levels		Water level readings @Qm (mm)	Flow depth @Q_m (m)	Longitudinal flow depth @Q_m (m)	Observed WSE (m)	Representative longitudinal flow depth @Qm (m)	Representative WSE (m)
	Bed level reading (mm)	Bed elevation (m)						
8.5	796	0.206						
9	814	0.181						
10		0.100						

Table C1- 12: Bed- and water levels for Test 6e: 20_0_180_v

CH (m)	Bed levels		Water level readings @Qm (mm)	Flow depth @Q_m (m)	Longitudinal flow depth @Q_m (m)	Observed WSE (m)	Representative longitudinal flow depth @Qm (m)	Representative WSE (m)
	Bed level reading (mm)	Bed elevation (m)						
-2		0.000						
0		0.650						
3		0.475						
3.5	528	0.451					0.048	0.499
4	489	0.427	537.00	0.048	0.048	0.475	0.048	0.475
4.5	453	0.402	500.50	0.048	0.047	0.449	0.049	0.450

CH (m)	Bed levels		Water level readings @Qm (mm)	Flow depth @Qm (m)	Longitudinal flow depth @Qm (m)	Observed WSE (m)	Representative longitudinal flow depth @Qm (m)	Representative WSE (m)
	Bed level reading (mm)	Bed elevation (m)						
5	432	0.376	483.00	0.051	0.051	0.427	0.050	0.426
5.6	653	0.346	603.50	0.050	0.049	0.395	0.050	0.396
6	671	0.326	619.00	0.052	0.052	0.378	0.051	0.377
6.5	693	0.302	643.00	0.050	0.050	0.351	0.051	0.352
7	724	0.277	670.00	0.054				
7.5	736	0.254	677.00	0.059				
8	770	0.230	715.00	0.055				
8.5	796	0.206	744.00	0.052				
9	814	0.181	763.00	0.051				
10		0.100						

Table C1- 13: Bed- and water levels for Test 6g: 20_0_180_vii

CH (m)	Bed levels		Water level readings @Qm (mm)	Flow depth @Q_m (m)	Longitudinal flow depth @Q_m (m)	Observed WSE (m)	Representative longitudinal flow depth @Qm (m)	Representative WSE (m)
	Bed level reading (mm)	Bed elevation (m)						
-2		0.000						
0		0.650						
3		0.475						
3.5	528	0.451	590.00	0.062	0.062	0.513	0.060	0.511
4	489	0.427	549.00	0.060	0.060	0.487	0.060	0.487
4.5	453	0.402	513.50	0.061	0.060	0.462	0.060	0.462
5	432	0.376	492.00	0.060	0.060	0.436	0.061	0.437
5.6	653	0.346	595.00	0.058	0.058	0.404	0.061	0.407
6	671	0.326	608.00	0.063	0.063	0.389	0.061	0.388
6.5	693	0.302	632.50	0.061	0.060	0.362	0.061	0.363
7	724	0.277	663.00	0.061	0.061	0.338	0.061	0.338
7.5	736	0.254	674.00	0.062	0.062	0.315	0.060	0.313
8	770	0.230						

CH (m)	Bed levels		Water level readings @Qm (mm)	Flow depth @Q_m (m)	Longitudinal flow depth @Q_m (m)	Observed WSE (m)	Representative longitudinal flow depth @Qm (m)	Representative WSE (m)
	Bed level reading (mm)	Bed elevation (m)						
8.5	796	0.206						
9	814	0.181						
10		0.100						

Table C1- 14: Bed- and water levels for Test 7b: 20_1.5_140_ii_DNF

CH (m)	Bed levels		Water level readings @Qm (mm)	Flow depth @Q_m (m)	Longitudinal flow depth @Q_m (m)	Observed WSE (m)	Representative longitudinal flow depth @Qm (m)	Representative WSE (m)
	Bed level reading (mm)	Bed elevation (m)						
-2		0.000						
0		0.650						
3		0.495						
3.5	524	0.467					0.352	0.819
4	480	0.438	826.50	0.347	0.346	0.784	0.348	0.786
4.5	451	0.415	785.00	0.334	0.334	0.748	0.338	0.753

CH (m)	Bed levels		Water level readings @Qm (mm)	Flow depth @Qm (m)	Longitudinal flow depth @Qm (m)	Observed WSE (m)	Representative longitudinal flow depth @Qm (m)	Representative WSE (m)
	Bed level reading (mm)	Bed elevation (m)						
5	424.5	0.391	757.00	0.333	0.332	0.723	0.329	0.720
5.6	661.5	0.359	336.00	0.326	0.325	0.684	0.321	0.680
6	679.5	0.337	354.50	0.325	0.325	0.662	0.316	0.653
6.5	703.5	0.309	391.50	0.312	0.312	0.621	0.311	0.620
7	729.5	0.281	433.00	0.297	0.296	0.577	0.306	0.587
7.5	748.5	0.255						
8	777.5	0.229						
8.5	802.5	0.205						
9	822.5	0.181						
10		0.100						

Table C1- 15: Bed- and water levels for Test 8c: 20_1.5_180_iii

CH (m)	Bed levels		Water level readings @Qm (mm)	Flow depth @Q_m (m)	Longitudinal flow depth @Q_m (m)	Observed WSE (m)	Representative longitudinal flow depth @Qm (m)	Representative WSE (m)
	Bed level reading (mm)	Bed elevation (m)						
-2		0.000						
0		0.650						
3		0.495						
3.5	532	0.467					0.280	0.746
4	489	0.438					0.277	0.715
4.5	459	0.415					0.269	0.683
5	432.5	0.391					0.261	0.652
5.6	654.5	0.359					0.255	0.614
6	672	0.337	418.5	0.2535	0.253	0.590	0.252	0.589
6.5	694.5	0.310	450.5	0.244	0.244	0.554	0.247	0.557
7	719	0.283	474.5	0.2445	0.244	0.527	0.243	0.526
7.5	742.5	0.261						
8	770	0.238						

CH (m)	Bed levels		Water level readings @Qm (mm)	Flow depth @Q_m (m)	Longitudinal flow depth @Q_m (m)	Observed WSE (m)	Representative longitudinal flow depth @Qm (m)	Representative WSE (m)
	Bed level reading (mm)	Bed elevation (m)						
8.5	795	0.214						
9	816	0.189						
10		0.100						

Table C1- 16: Bed- and water levels for Test 8d: 20_1.5_180_iv

CH (m)	Bed levels		Water level readings @Qm (mm)	Flow depth @Q_m (m)	Longitudinal flow depth @Q_m (m)	Observed WSE (m)	Representative longitudinal flow depth @Qm (m)	Representative WSE (m)
	Bed level reading (mm)	Bed elevation (m)						
-2		0.000						
0		0.650						
3		0.495						
3.5	532	0.467					0.243	0.710
4	489	0.438					0.242	0.680
4.5	459	0.415					0.236	0.651

CH (m)	Bed levels		Water level readings @Qm (mm)	Flow depth @Qm (m)	Longitudinal flow depth @Qm (m)	Observed WSE (m)	Representative longitudinal flow depth @Qm (m)	Representative WSE (m)
	Bed level reading (mm)	Bed elevation (m)						
5	432.5	0.391					0.230	0.621
5.6	654.5	0.359					0.227	0.586
6	672	0.337	447	0.225	0.225	0.562	0.225	0.562
6.5	694.5	0.310	470	0.2245	0.224	0.534	0.223	0.533
7	719	0.283	499	0.22	0.220	0.503	0.220	0.503
7.5	742.5	0.261						
8	770	0.238						
8.5	795	0.214						
9	816	0.189						
10		0.100						

Table C1- 17: Bed- and water levels for Test 9d: 10_0_140_iv

CH (m)	Bed levels		Water level readings @Qm (mm)	Flow depth @Q_m (m)	Longitudinal flow depth @Q_m (m)	Observed WSE (m)	Representative longitudinal flow depth @Qm (m)	Representative WSE (m)
	Bed level reading (mm)	Bed elevation (m)						
-2		0.100						
0	692	1.000						
3	972	0.720						
3.5	1021	0.671	732.0	0.028	0.028	0.699	0.026	0.697
4	1068	0.624	681.5	0.0225	0.022	0.646	0.025	0.649
4.5	1116	0.576	635.0	0.024	0.024	0.600	0.025	0.601
5	1163	0.529	588.0	0.025	0.025	0.554	0.024	0.553
5.6	1211	0.471						
6	1259	0.433						
6.5	1307	0.385						
7	1353	0.339						
7.5	1411	0.281						
8	1460	0.232						

CH (m)	Bed levels		Water level readings @Qm (mm)	Flow depth @Q_m (m)	Longitudinal flow depth @Q_m (m)	Observed WSE (m)	Representative longitudinal flow depth @Qm (m)	Representative WSE (m)
	Bed level reading (mm)	Bed elevation (m)						
8.5	1510	0.182						
9	1571	0.121						
10		0.000						

Table C1- 18: Bed- and water levels for Test 9e: 10_0_140_v

CH (m)	Bed levels		Water level readings @Qm (mm)	Flow depth @Q_m (m)	Longitudinal flow depth @Q_m (m)	Observed WSE (m)	Representative longitudinal flow depth @Qm (m)	Representative WSE (m)
	Bed level reading (mm)	Bed elevation (m)						
-2	0	0.100						
0	692	1.000						
3	972	0.720						
3.5	1021	0.671	738.0	0.028	0.028	0.699	0.029	0.700
4	1068	0.624	688.5	0.030	0.029	0.653	0.028	0.652
4.5	1116	0.576	639.0	0.028	0.028	0.604	0.028	0.604

CH (m)	Bed levels		Water level readings @Qm (mm)	Flow depth @Qm (m)	Longitudinal flow depth @Qm (m)	Observed WSE (m)	Representative longitudinal flow depth @Qm (m)	Representative WSE (m)
	Bed level reading (mm)	Bed elevation (m)						
5	1163	0.529	590.0	0.027	0.027	0.556	0.027	0.556
5.6	1211	0.471						
6	1259	0.433						
6.5	1307	0.385						
7	1353	0.339						
7.5	1411	0.281						
8	1460	0.232						
8.5	1510	0.182						
9	1571	0.121						
10		0.000						

Table C1- 19: Bed- and water levels for Test 10b: 10_0_180_ii

CH (m)	Bed levels		Water level readings @Qm (mm)	Flow depth @Q_m (m)	Longitudinal flow depth @Q_m (m)	Observed WSE (m)	Representative longitudinal flow depth @Qm (m)	Representative WSE (m)
	Bed level reading (mm)	Bed elevation (m)						
-2		0.100						
0	692	1.000						
3	972	0.720						
3.5	1021	0.671	762.0	0.047	0.047	0.718	0.049	0.720
4	1068	0.624	714.0	0.049	0.049	0.673	0.047	0.671
4.5	1116	0.576	667.0	0.047	0.047	0.623	0.046	0.622
5	1163	0.529	618.5	0.047	0.046	0.575	0.044	0.573
5.6	1211	0.471	502.5	0.040	0.039	0.511	0.042	0.514
6	1259	0.433						
6.5	1308	0.384						
7	1353	0.339						
7.5	1411	0.281						
8	1460	0.232						

CH (m)	Bed levels		Water level readings @Qm (mm)	Flow depth @Q_m (m)	Longitudinal flow depth @Q_m (m)	Observed WSE (m)	Representative longitudinal flow depth @Qm (m)	Representative WSE (m)
	Bed level reading (mm)	Bed elevation (m)						
8.5	1510	0.182						
9	1571	0.121						
10		0.000						

Table C1- 20: Bed- and water levels for Test 10c: 10_0_180_iii

CH (m)	Bed levels		Water level readings @Qm (mm)	Flow depth @Q_m (m)	Longitudinal flow depth @Q_m (m)	Observed WSE (m)	Representative longitudinal flow depth @Qm (m)	Representative WSE (m)
	Bed level reading (mm)	Bed elevation (m)						
-2		0.100						
0	692	1.000						
3	972	0.720						
3.5	1021	0.671	753.0	0.038	0.038	0.709	0.040	0.711
4	1068	0.624	703.5	0.039	0.038	0.662	0.038	0.662
4.5	1116	0.576	658.0	0.038	0.038	0.614	0.036	0.612

CH (m)	Bed levels		Water level readings @Qm (mm)	Flow depth @Qm (m)	Longitudinal flow depth @Qm (m)	Observed WSE (m)	Representative longitudinal flow depth @Qm (m)	Representative WSE (m)
	Bed level reading (mm)	Bed elevation (m)						
5	1163	0.529	608.5	0.037	0.036	0.565	0.034	0.563
5.6	1211	0.471	511.5	0.031	0.030	0.502	0.033	0.504
6	1259	0.433	552.0	0.032	0.031	0.464	0.032	0.465
6.5	1308	0.384	595.0	0.033	0.032	0.416	0.032	0.416
7	1353	0.339						
7.5	1411	0.281						
8	1460	0.232						
8.5	1510	0.182						
9	1571	0.121						
10		0.000						

Table C1- 21: Bed- and water levels for Test 10d: 10_0_180_iv

CH (m)	Bed levels		Water level readings @Qm (mm)	Flow depth @Q_m (m)	Longitudinal flow depth @Q_m (m)	Observed WSE (m)	Representative longitudinal flow depth @Qm (m)	Representative WSE (m)
	Bed level reading (mm)	Bed elevation (m)						
-2		0.100						
0	692	1.000						
3	972	0.720						
3.5	1021	0.671	753.0	0.038	0.038	0.709	0.040	0.711
4	1068	0.624	704.0	0.039	0.039	0.663	0.038	0.662
4.5	1116	0.576	658.0	0.038	0.038	0.614	0.037	0.613
5	1163	0.529	610.0	0.038	0.038	0.567	0.035	0.564
5.6	1211	0.471	509.5	0.033	0.032	0.504	0.033	0.504
6	1259	0.433	553.5	0.030	0.030	0.463	0.032	0.465
6.5	1308	0.384	596.0	0.032	0.031	0.415	0.032	0.416
7	1353	0.339						
7.5	1411	0.281						
8	1460	0.232						

CH (m)	Bed levels		Water level readings @Qm (mm)	Flow depth @Q_m (m)	Longitudinal flow depth @Q_m (m)	Observed WSE (m)	Representative longitudinal flow depth @Qm (m)	Representative WSE (m)
	Bed level reading (mm)	Bed elevation (m)						
8.5	1510	0.182						
9	1571	0.121						
10		0.000						

Table C1- 22: Bed- and water levels for Test 11a: 10_1.5_140_i_DNF

CH (m)	Bed levels		Water level readings @Qm (mm)	Flow depth @Q_m (m)	Longitudinal flow depth @Q_m (m)	Observed WSE (m)	Representative longitudinal flow depth @Qm (m)	Representative WSE (m)
	Bed level reading (mm)	Bed elevation (m)						
-2		0.100						
0	647	1.000						
3	927	0.720						
3.5	974	0.673	925.5	0.217	0.215	0.888	0.221	0.894
4	1022	0.625	869.0	0.210	0.209	0.834	0.214	0.839
4.5	1070	0.577	827.0	0.216	0.215	0.792	0.208	0.785

CH (m)	Bed levels		Water level readings @Qm (mm)	Flow depth @Qm (m)	Longitudinal flow depth @Qm (m)	Observed WSE (m)	Representative longitudinal flow depth @Qm (m)	Representative WSE (m)
	Bed level reading (mm)	Bed elevation (m)						
5	1120	0.527	776.5	0.216	0.214	0.741	0.203	0.730
5.6	1180	0.467	352.0	0.201	0.199	0.666	0.197	0.664
6	1220	0.427	397.0	0.193	0.192	0.619	0.193	0.620
6.5	1271	0.376	447.5	0.189	0.188	0.564	0.189	0.565
7	1323	0.324	499.5	0.185	0.184	0.508	0.186	0.510
7.5	1375	0.272	559.0	0.183	0.182	0.454	0.183	0.455
8	1428	0.219	618.5	0.178	0.177	0.396	0.182	0.401
8.5	1478	0.169						
9	1525	0.122						
10		0.000						

Table C1- 23: Bed- and water levels for Test 12a: 10_1.5_180_i

CH (m)	Bed levels		Water level readings @Qm (mm)	Flow depth @Q_m (m)	Longitudinal flow depth @Q_m (m)	Observed WSE (m)	Representative longitudinal flow depth @Qm (m)	Representative WSE (m)
	Bed level reading (mm)	Bed elevation (m)						
-2		0.100						
0	647	1.000						
3	927	0.720						
3.5	974	0.673	937.0	0.221	0.219	0.892	0.229	0.902
4	1022	0.625	885.0	0.219	0.217	0.842	0.222	0.847
4.5	1070	0.577	855.0	0.237	0.236	0.813	0.215	0.792
5	1120	0.527	785.0	0.214	0.213	0.740	0.211	0.738
5.6	1180	0.467	341.0	0.204	0.203	0.670	0.205	0.672
6	1220	0.427	388.5	0.199	0.197	0.624	0.201	0.628
6.5	1271	0.376	435.0	0.196	0.195	0.571	0.197	0.573
7	1323	0.324	485.0	0.194	0.193	0.517	0.194	0.518
7.5	1375	0.272						
8	1428	0.219						

CH (m)	Bed levels		Water level readings @Qm (mm)	Flow depth @Q_m (m)	Longitudinal flow depth @Q_m (m)	Observed WSE (m)	Representative longitudinal flow depth @Qm (m)	Representative WSE (m)
	Bed level reading (mm)	Bed elevation (m)						
8.5	1478	0.169						
9	1525	0.122						
10		0.000						

Table C1- 24: Bed- and water levels for Test 12b: 10_1.5_180_ii

CH (m)	Bed levels		Water level readings @Qm (mm)	Flow depth @Q_m (m)	Longitudinal flow depth @Q_m (m)	Observed WSE (m)	Representative longitudinal flow depth @Qm (m)	Representative WSE (m)
	Bed level reading (mm)	Bed elevation (m)						
-2		0.100						
0	647	1.000						
3	927	0.720						
3.5	974	0.673	918.5	0.202	0.201	0.874	0.208	0.881
4	1022	0.625	876.5	0.210	0.209	0.834	0.202	0.827
4.5	1070	0.577	823.0	0.205	0.204	0.781	0.195	0.772

CH (m)	Bed levels		Water level readings @Qm (mm)	Flow depth @Qm (m)	Longitudinal flow depth @Qm (m)	Observed WSE (m)	Representative longitudinal flow depth @Qm (m)	Representative WSE (m)
	Bed level reading (mm)	Bed elevation (m)						
5	1120	0.527	759.0	0.188	0.187	0.714	0.191	0.718
5.6	1180	0.467	363.0	0.182	0.181	0.648	0.185	0.652
6	1220	0.427	406.5	0.181	0.180	0.607	0.182	0.609
6.5	1271	0.376	450.5	0.181	0.180	0.556	0.178	0.554
7	1323	0.324	500.5	0.179	0.178	0.502	0.176	0.500
7.5	1375	0.272						
8	1428	0.219						
8.5	1478	0.169						
9	1525	0.122						
10		0.000						

C2: Graphical survey data

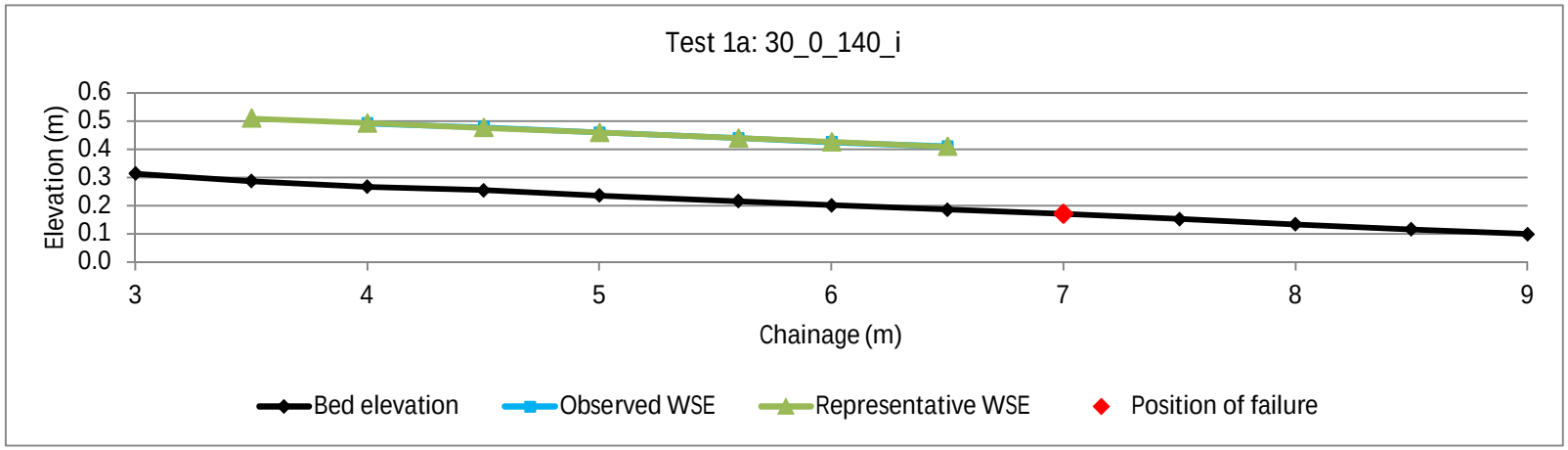

Figure C2- 1: Bed- and water-surface elevation for Test 1a: 30_0_140_i

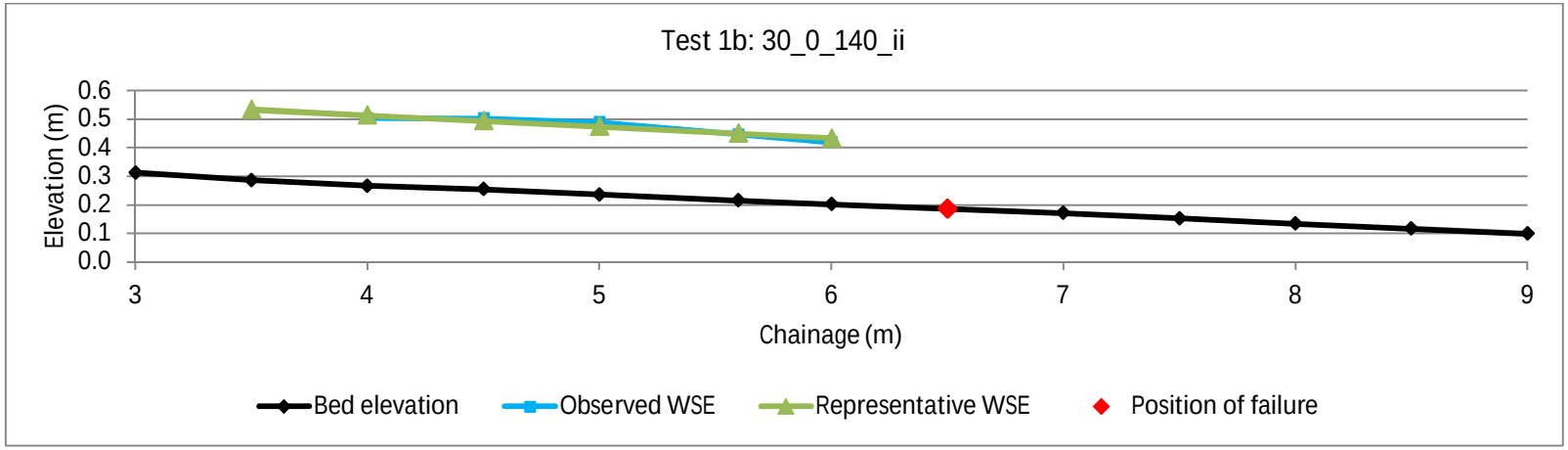

Figure C2- 2: Bed- and water-surface elevation for Test 1b: 30_0_140_ii

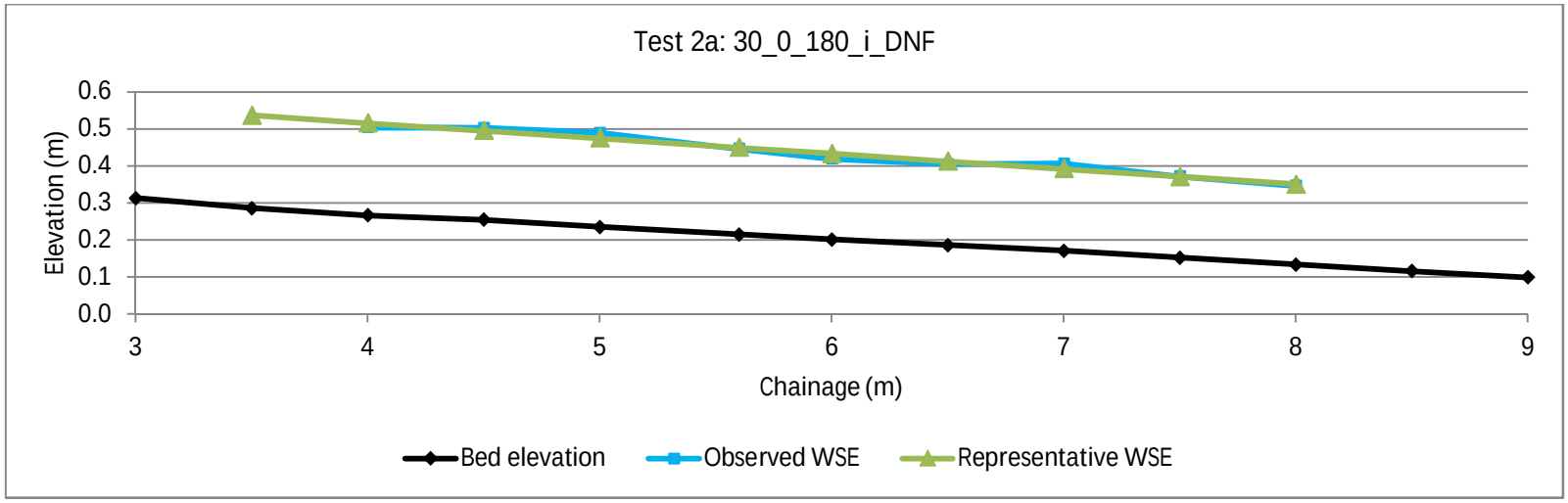

Figure C2- 3: Bed- and water-surface elevation for Test 2a: 30_0_180_i_DNF

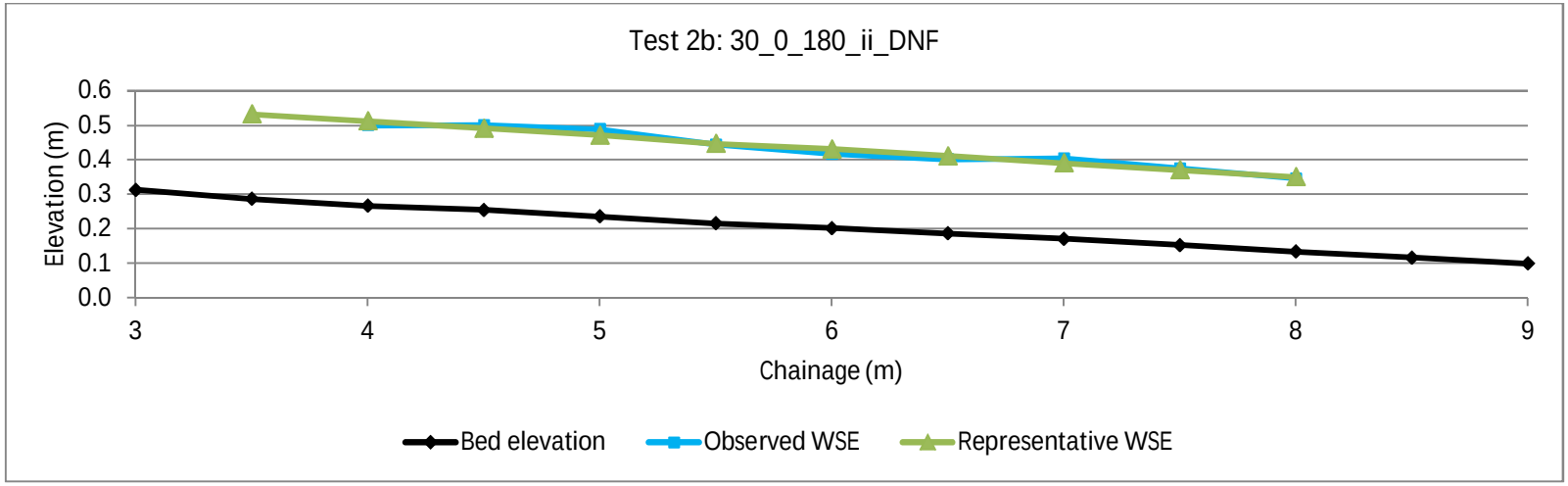

Figure C2- 4: Bed- and water-surface elevation for Test 2b: 30_0_180_ii_DNF

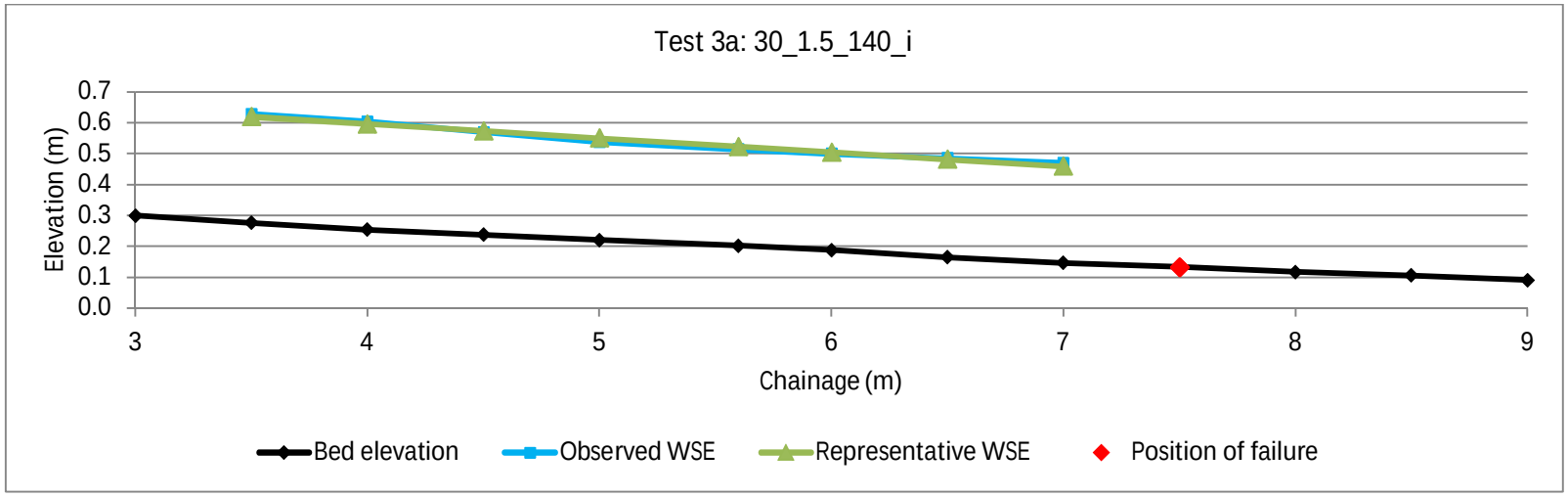

Figure C2- 5: Bed- and water-surface elevation for Test 3a: 30_1.5_140_i

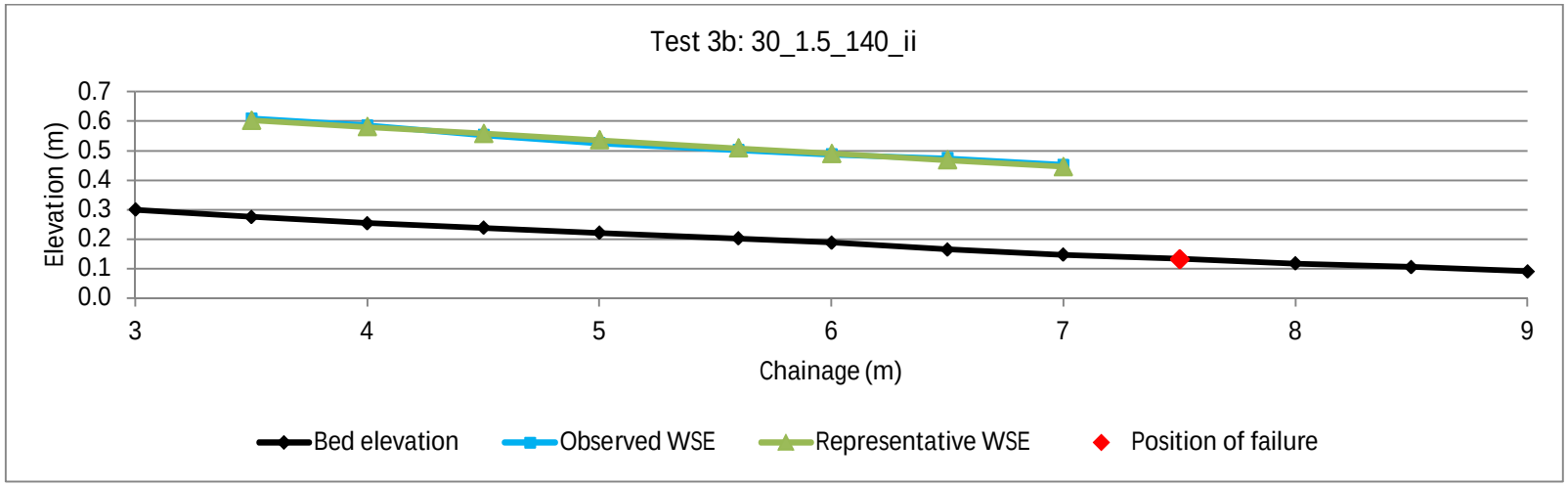

Figure C2- 6: Bed- and water-surface elevation for Test 3b: 30_1.5_140_ii

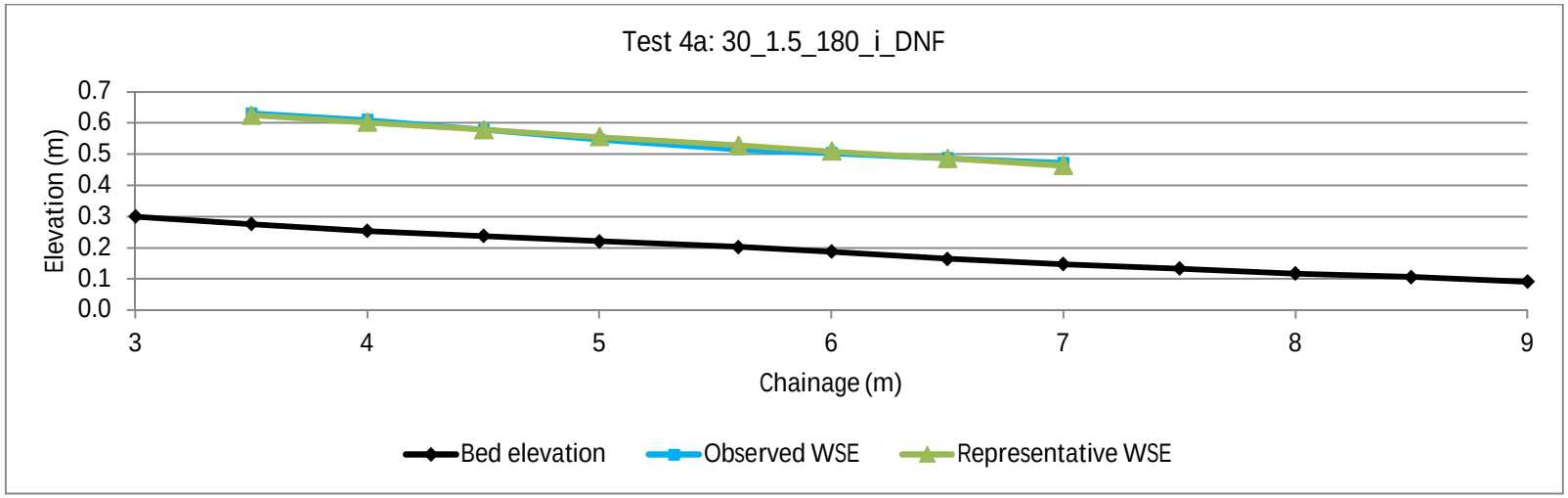

Figure C2- 7: Bed- and water-surface elevation for Test 4a: 30_1.5_180_i_DNF

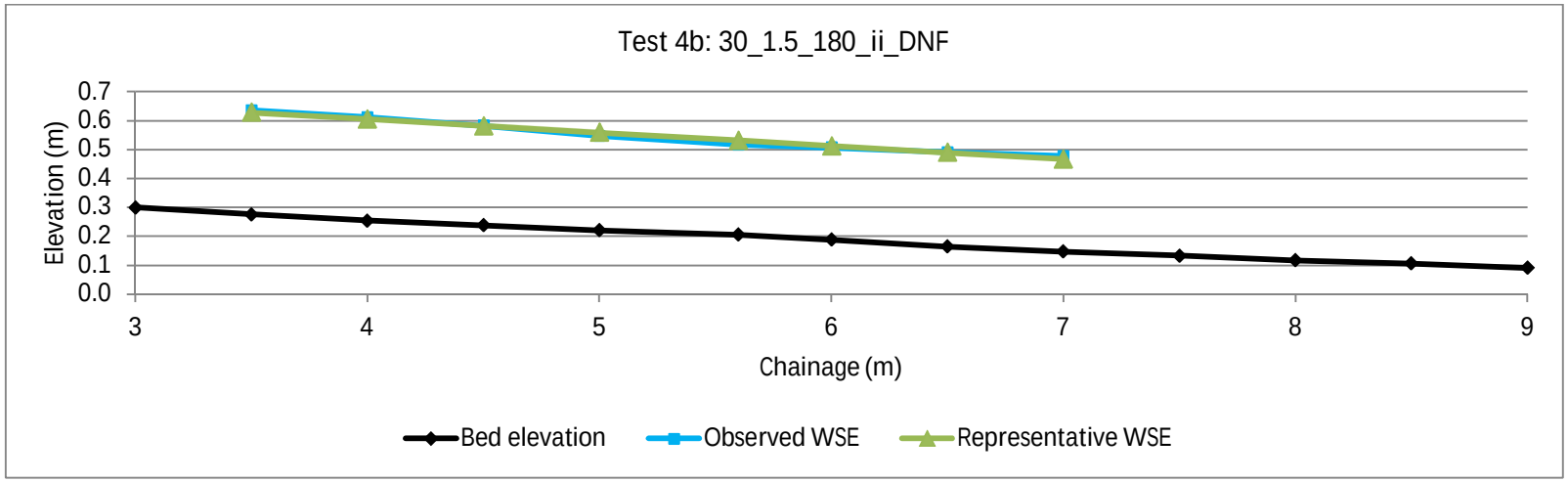

Figure C2- 8: Bed- and water-surface elevation for Test 4b: 30_1.5_180_ii_DNF

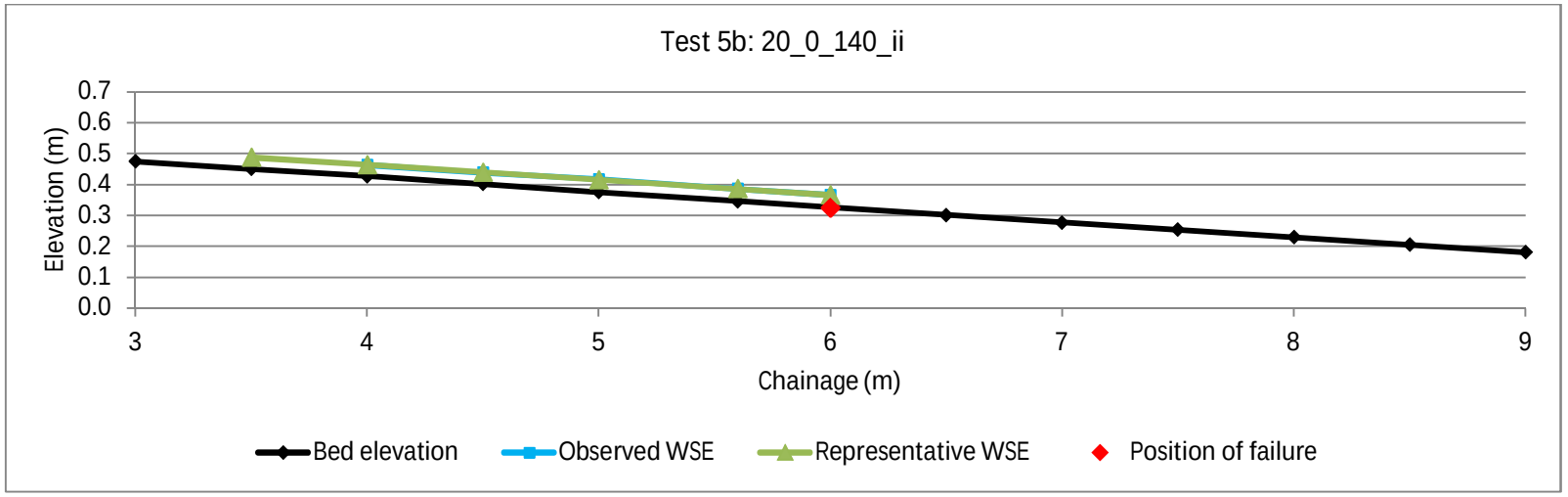

Figure C2- 9: Bed- and water-surface elevation for Test 5b: 20_0_140_ii

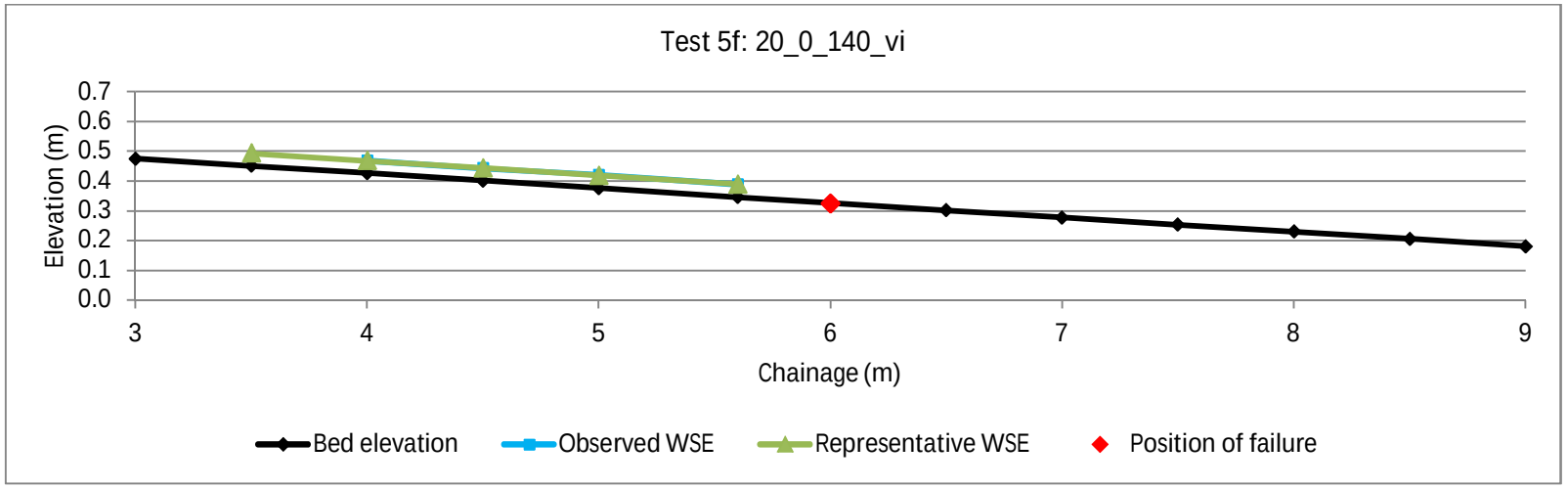

Figure C2- 10: Bed- and water-surface elevation for Test 5f: 20_0_140_vi

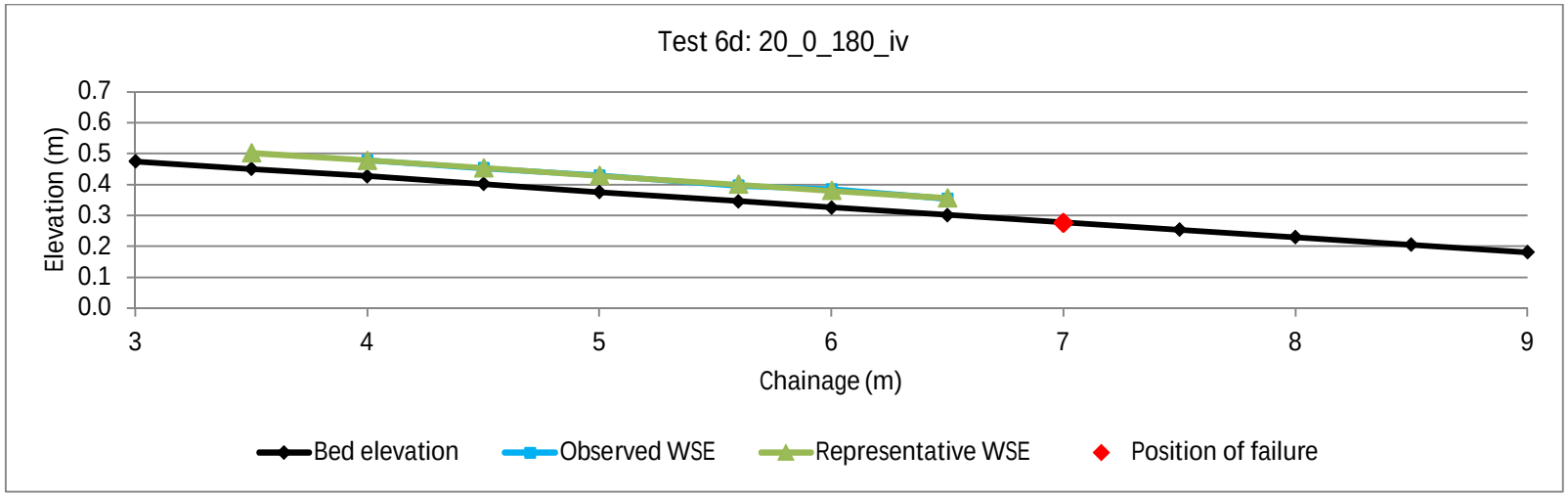

Figure C2- 11: Bed- and water-surface elevation for Test 6d: 20_0_180_iv

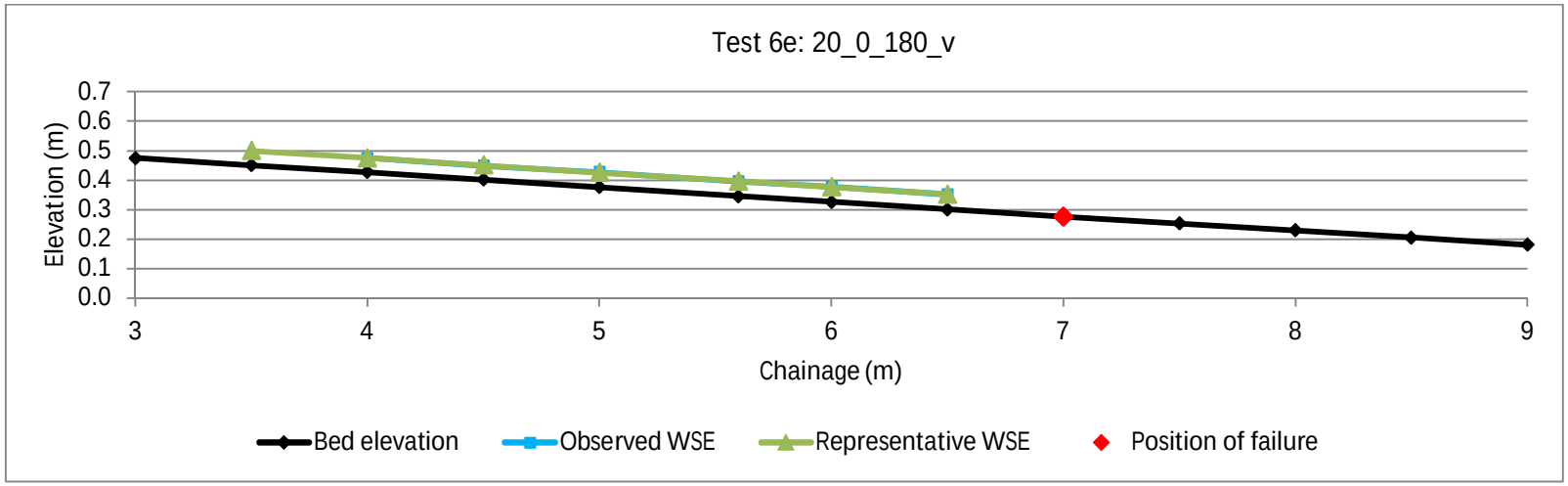

Figure C2- 12: Bed- and water-surface elevation for Test 6e: 20_0_180_v

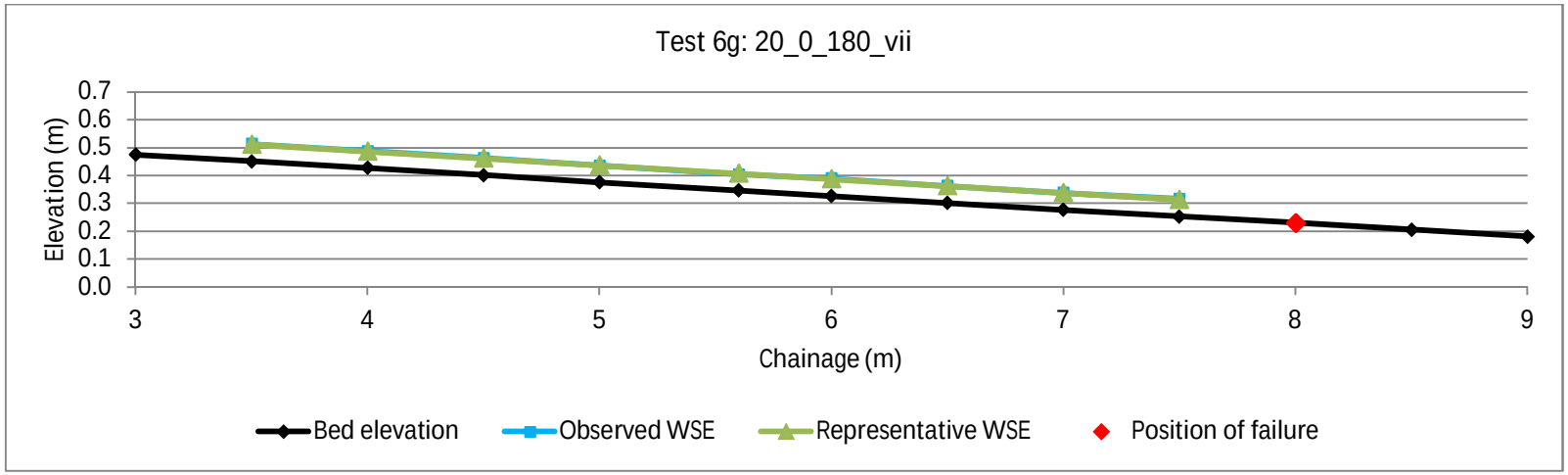

Figure C2- 13: Bed- and water-surface elevation for Test 6g: 20_0_180_vii

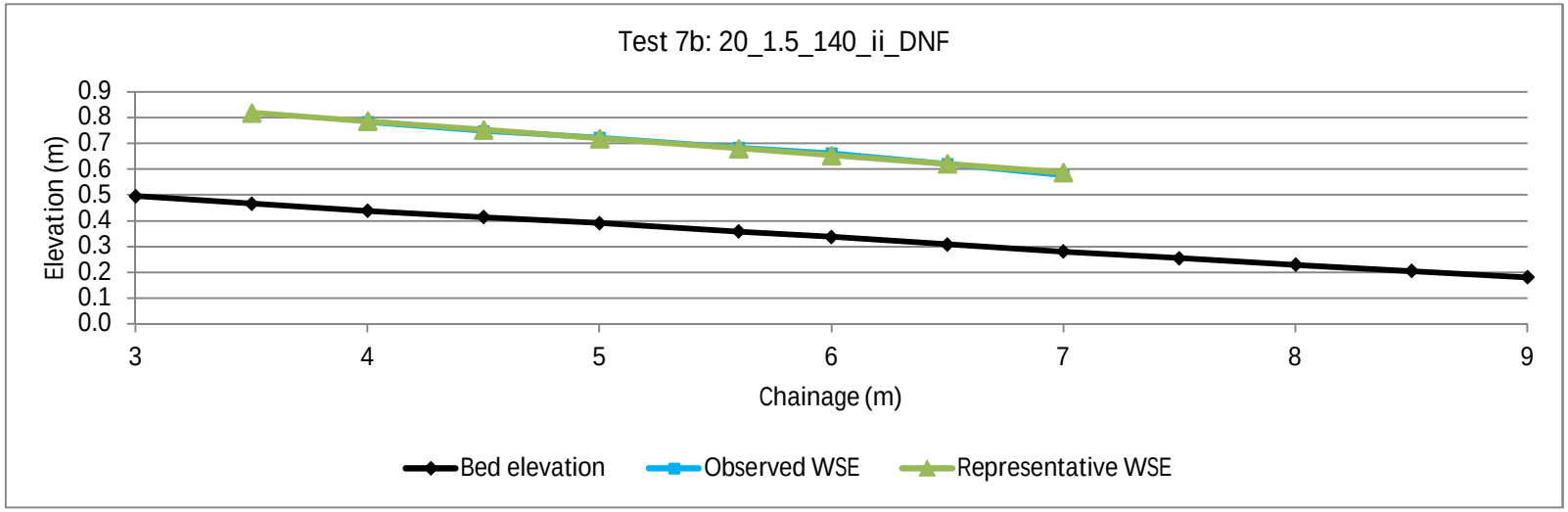

Figure C2- 14: Bed- and water-surface elevation for Test 7b: 20_1.5_140_ii_DNF

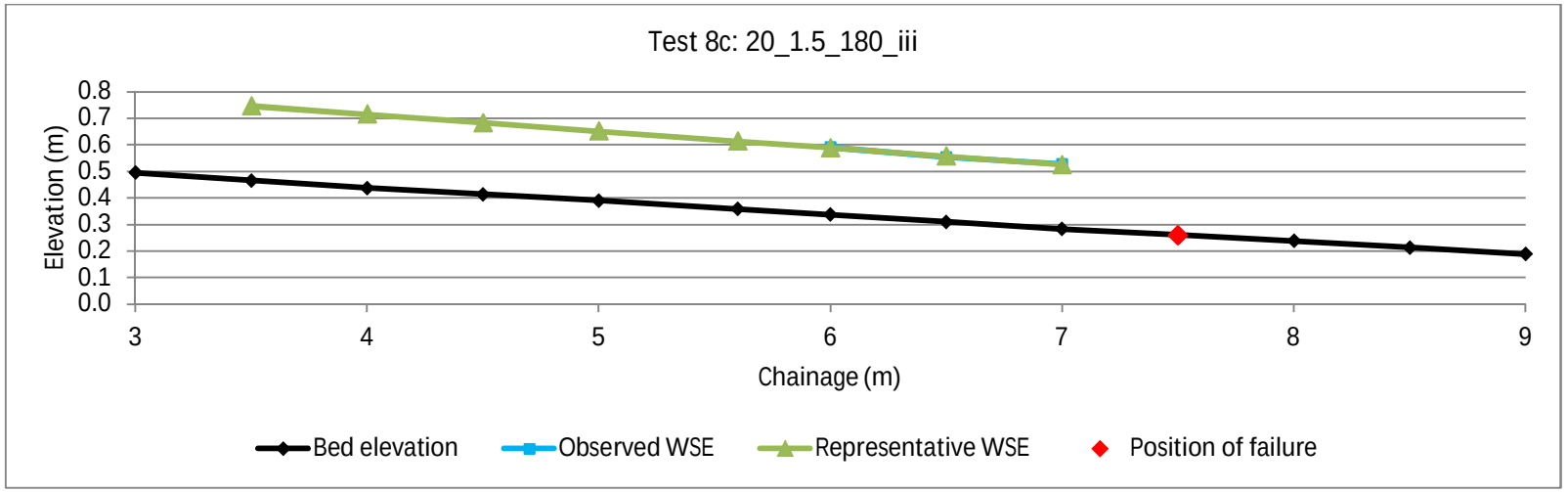

Figure C2- 15: Bed- and water-surface elevation for Test 8c: 20_1.5_180_iii

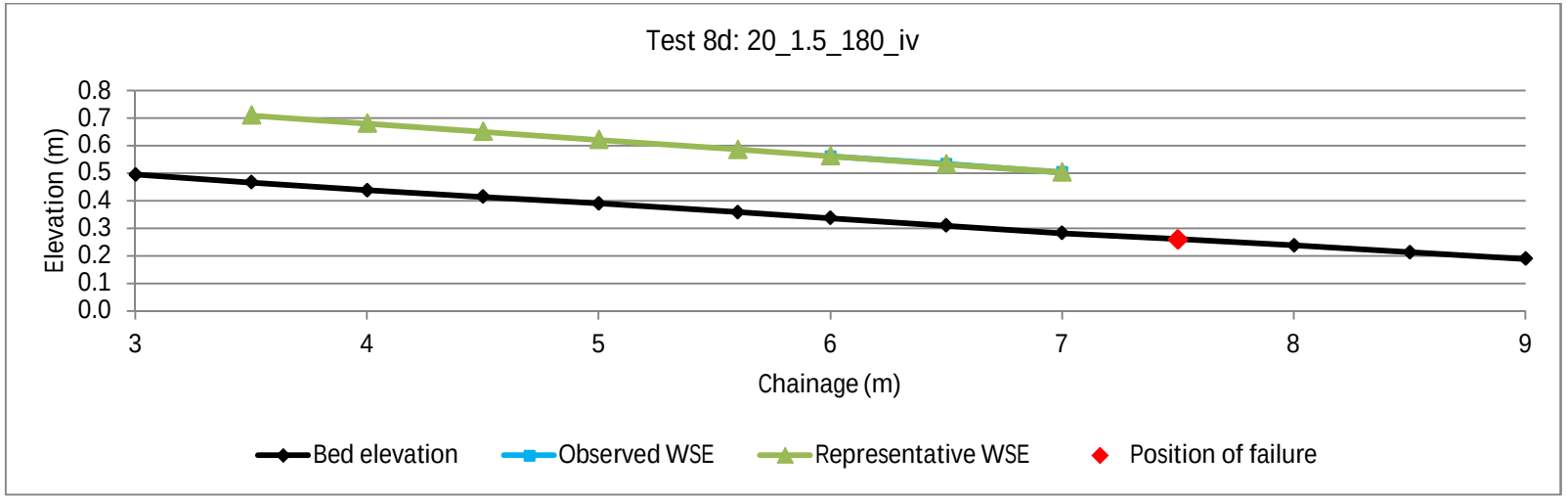

Figure C2- 16: Bed- and water-surface elevation for Test 8d: 20_1.5_180_iv

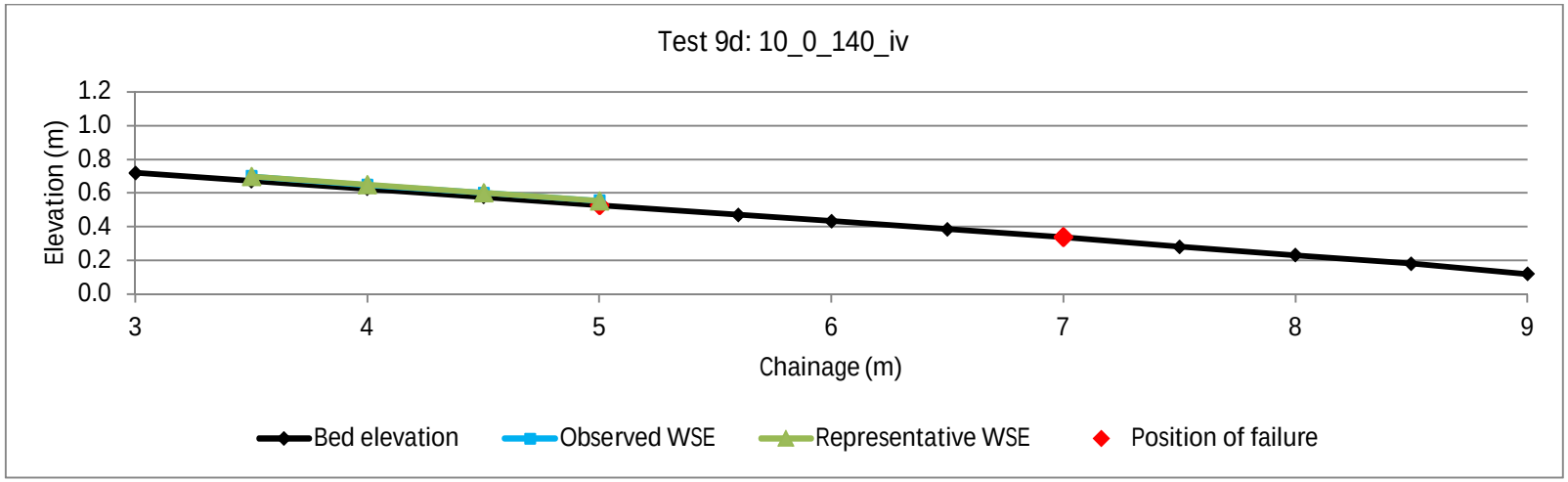

Figure C2- 17: Bed- and water-surface elevation for Test 9d: 10_0_140_iv

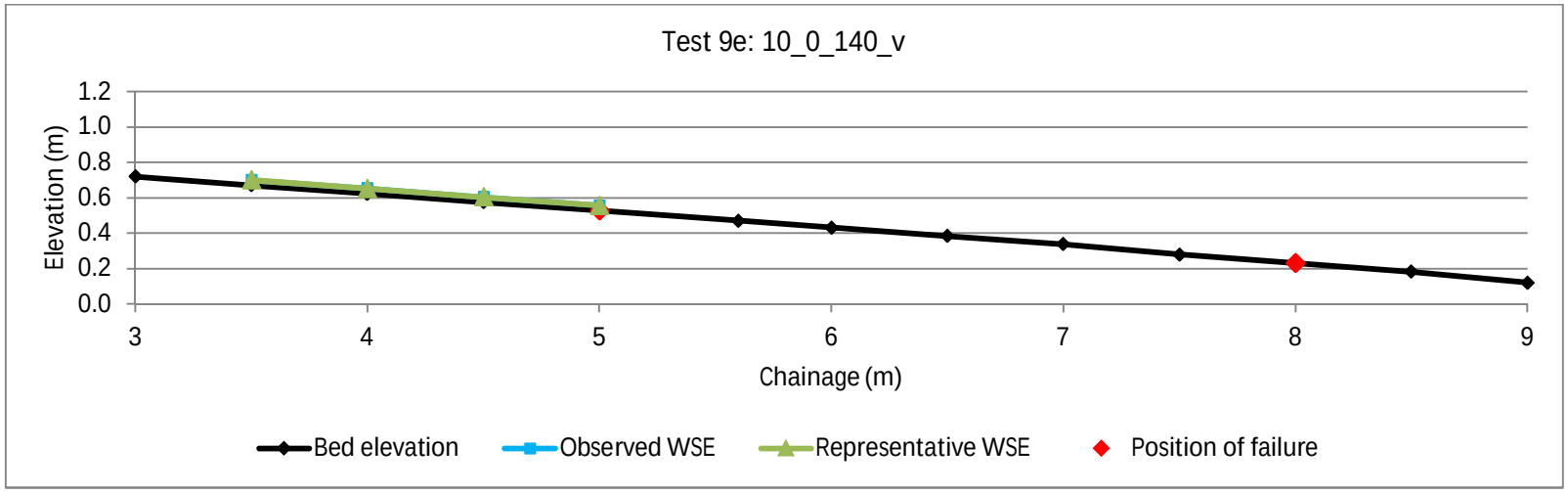

Figure C2- 18: Bed- and water-surface elevation for Test 9e: 10_0_140_v

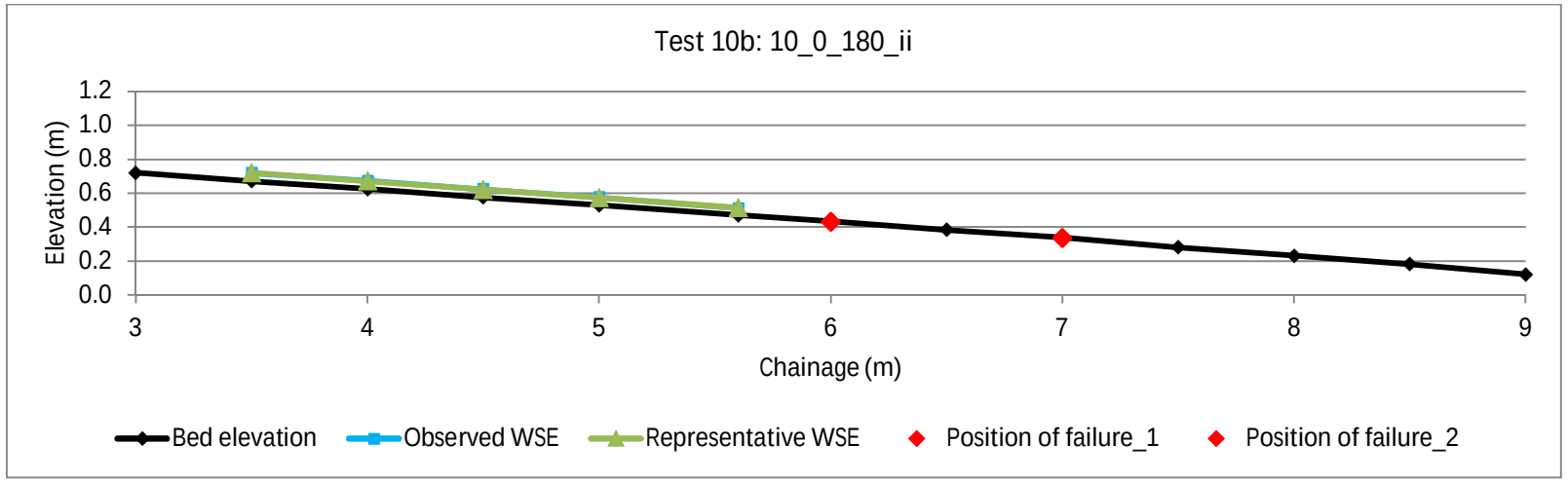

Figure C2- 19: Bed- and water-surface elevation for Test 10b: 10_0_180_ii

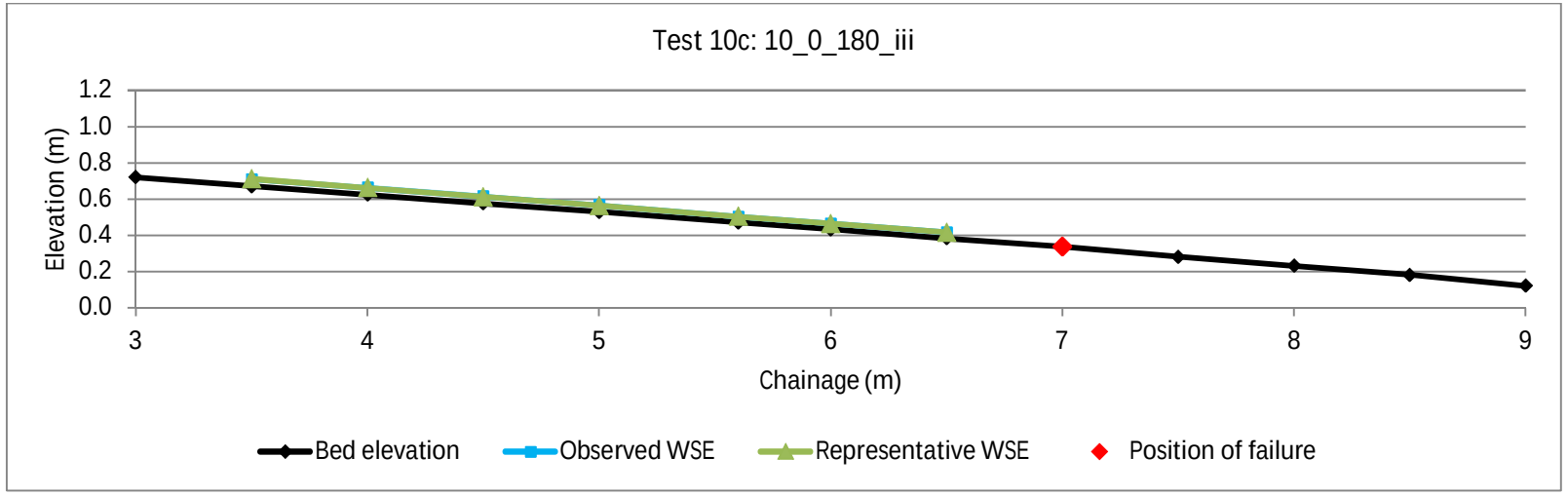

Figure C2- 20: Bed- and water-surface elevation for Test 10c: 10_0_180_iii

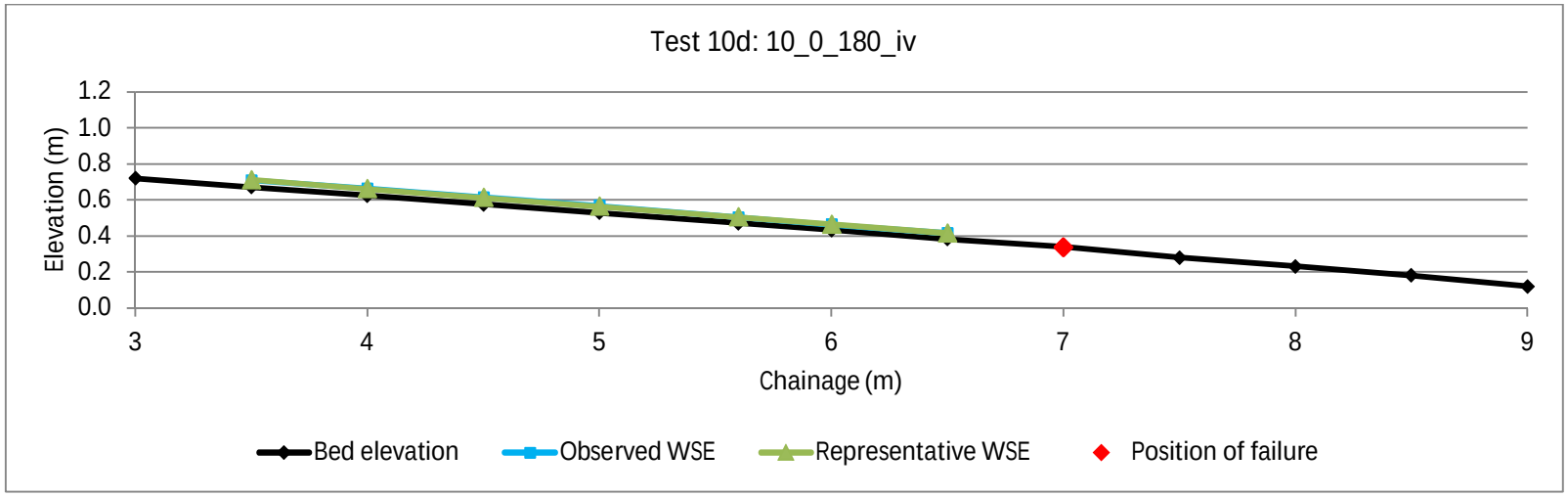

Figure C2- 21: Bed- and water-surface elevation for Test 10d: 10_0_180_iv

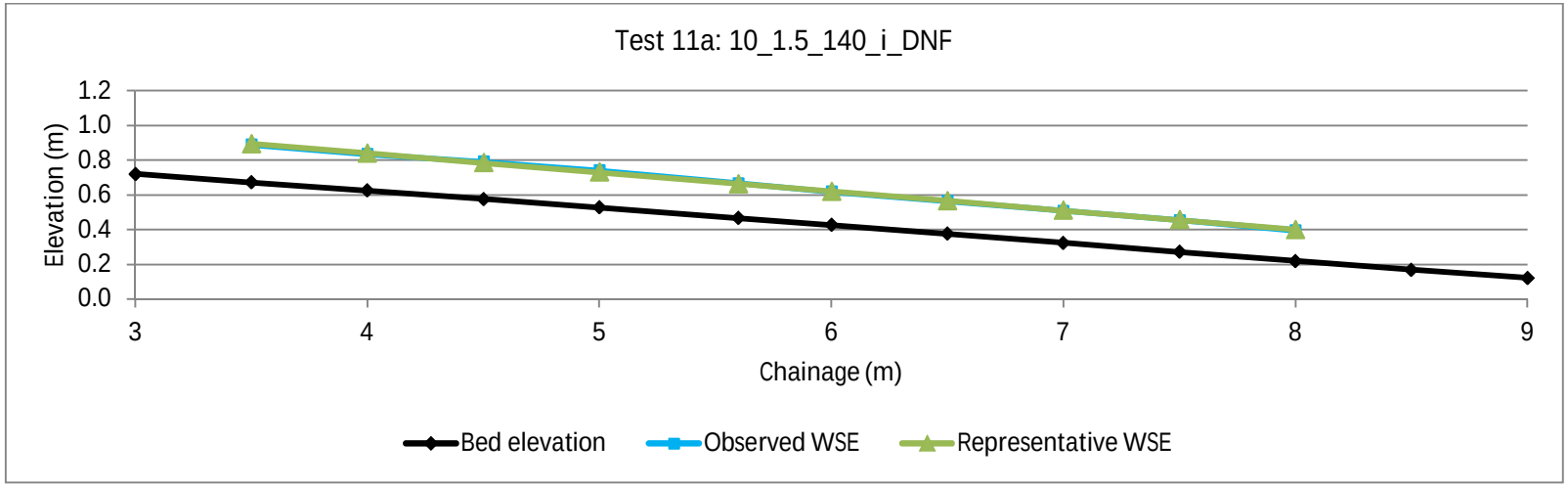

Figure C2- 22: Bed- and water-surface elevation for Test 11a: 10_1.5_140_i_DNF

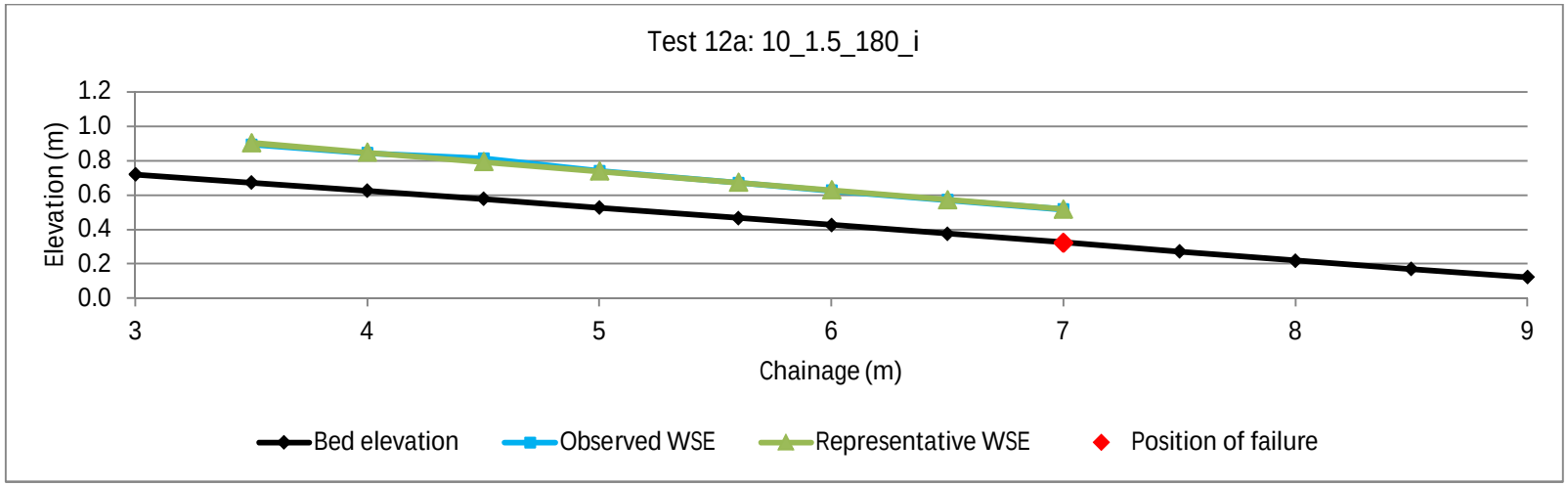

Figure C2- 23: Bed- and water-surface elevation for Test 12a: 10_1.5_180_i

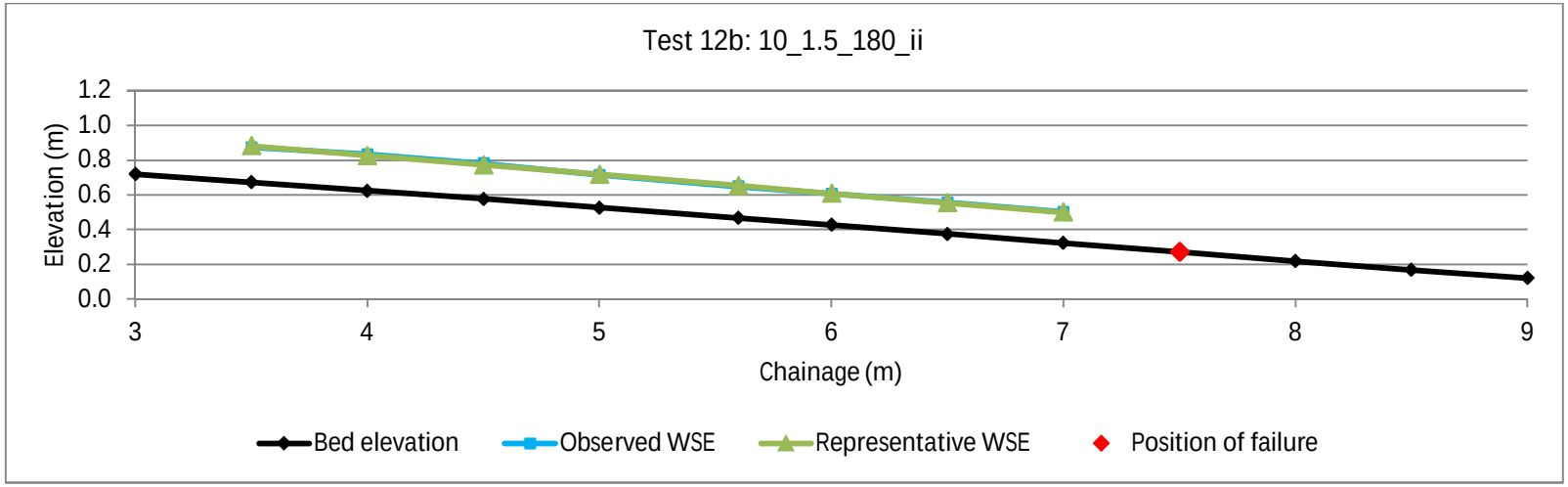

Figure C2- 24: Bed- and water-surface elevation for Test 12b: 10_1.5_180_ii

C3: Typical flow parameters at Q_m

Table C3- 1: Flow parameters at Q_m for Test 1a: 30_0_140_i

Q_m	0.580 m³/s							
CH (m)	y (m)	R (m)	V (m/s)	EGL (m)	Fr	Local EGL slope (m/m)	Shear stress τ (kg/m²)	Shields's parameter ψ
3.5	0.222	0.222	2.791	0.906	1.890	N/A	N/A	N/A
4	0.226	0.226	2.751	0.878	1.849	0.028	61.283	0.078
4.5	0.221	0.221	2.811	0.878	1.910	0.025	54.499	0.070
5	0.223	0.223	2.779	0.853	1.878	0.029	62.560	0.080
5.6	0.223	0.223	2.778	0.832	1.876	0.029	62.605	0.080
6	0.224	0.224	2.772	0.817	1.871	0.030	65.898	0.084
6.5	0.223	0.223	2.788	0.805	1.887	0.030	65.526	0.084

Table C3- 2: Flow parameters at Q_m for Test 1b: 30_0_140_ii

Q_m	0.589 m³/s							
CH (m)	y (m)	R (m)	V (m/s)	EGL (m)	Fr	Local EGL slope (m/m)	Shear stress τ (kg/m²)	Shields's parameter ψ
3.5	0.247	0.247	2.550	0.865	1.638	N/A	N/A	N/A
4	0.247	0.247	2.551	0.845	1.639	0.017	40.436	0.052
4.5	0.239	0.239	2.639	0.848	1.724	0.017	39.100	0.050
5	0.238	0.238	2.648	0.831	1.733	0.017	38.536	0.049
5.6	0.234	0.234	2.692	0.819	1.776	0.021	48.009	0.061
6	0.232	0.232	2.718	0.810	1.802	0.021	47.547	0.061

Table C3- 3: Flow parameters at Q_m for Test 2a: 30_0_180_i_DNF

Q_m	0.595 m³/s							
CH (m)	y (m)	R (m)	V (m/s)	EGL (m)	Fr	Local EGL slope (m/m)	Shear stress τ (kg/m²)	Shields's parameter ψ
3.5	0.250	0.250	2.548	0.867	1.627	N/A	N/A	N/A
4	0.249	0.249	2.555	0.848	1.634	0.014	35.406	0.047
4.5	0.240	0.240	2.649	0.853	1.725	0.012	27.958	0.037

CH (m)	y (m)	R (m)	V (m/s)	EGL (m)	Fr	Local EGL slope (m/m)	Shear stress τ (kg/m²)	Shields's parameter ψ
5	0.239	0.239	2.666	0.837	1.742	0.014	32.424	0.043
5.6	0.234	0.234	2.719	0.826	1.794	0.018	40.741	0.054
6	0.231	0.231	2.751	0.819	1.826	0.019	42.270	0.056
6.5	0.226	0.226	2.815	0.816	1.890	0.019	41.309	0.055
7	0.221	0.221	0.221	2.884	0.816	1.960	0.025	53.129
7.5	0.219	0.219	0.219	2.913	0.804	1.989	0.024	52.195
8	0.216	0.216	0.216	2.941	0.791	2.019	0.024	51.685

Table C3- 4: Flow parameters at Q_m for Test 2b: 30_0_180_ii_DNF

Q_m	0.595 m³/s							
CH (m)	y (m)	R (m)	V (m/s)	EGL (m)	Fr	Local EGL slope (m/m)	Shear stress τ (kg/m²)	Shields's parameter ψ
3.5	0.246	0.246	2.592	0.874	1.669	N/A	N/A	N/A
4	0.245	0.245	2.595	0.855	1.672	0.015	35.982	0.048
4.5	0.237	0.237	2.686	0.859	1.762	0.012	28.795	0.038
5	0.236	0.236	2.699	0.843	1.774	0.015	33.821	0.045
5.6	0.232	0.232	2.746	0.832	1.821	0.019	43.295	0.057
6	0.229	0.229	2.775	0.824	1.850	0.020	45.242	0.060
6.5	0.225	0.225	2.835	0.820	1.910	0.020	44.293	0.059
7	0.220	0.220	2.899	0.819	1.975	0.027	58.142	0.077
7.5	0.218	0.218	2.921	0.805	1.998	0.027	57.474	0.076
8	0.216	0.216	2.944	0.792	2.021	0.027	57.029	0.075

Table C3- 5: Flow parameters at Q_m for Test 3a: 30_1.5_140_i

Q_m	0.451 m³/s							
CH (m)	y (m)	R (m)	V (m/s)	EGL (m)	Fr	Local EGL slope (m/m)	Shear stress τ (kg/m²)	Shields's parameter ψ
3.5	0.343	0.209	2.266	0.881	1.496	N/A	N/A	N/A
4	0.342	0.209	2.275	0.860	1.504	0.013	44.404	0.057

CH (m)	y (m)	R (m)	V (m/s)	EGL (m)	Fr	Local EGL slope (m/m)	Shear stress τ (kg/m²)	Shields's parameter ψ
4.5	0.335	0.206	2.345	0.853	1.563	0.015	47.791	0.061
5	0.329	0.203	2.407	0.845	1.616	0.016	51.156	0.066
5.6	0.320	0.198	2.505	0.842	1.701	0.017	52.051	0.067
6	0.316	0.196	2.550	0.836	1.741	0.017	51.407	0.066
6.5	0.316	0.196	2.550	0.813	1.741	0.015	46.565	0.060
7	0.311	0.194	2.609	0.805	1.792	0.015	45.837	0.059

Table C3- 6: Flow parameters at Q_m for Test 3b: 30_1.5_140_ii

Q_m	0.420 m³/s							
CH (m)	y (m)	R (m)	V (m/s)	EGL (m)	Fr	Local EGL slope (m/m)	Shear stress τ (kg/m²)	Shields's parameter ψ
3.5	0.326	0.201	2.268	0.865	1.528	N/A	N/A	N/A
4	0.326	0.201	2.272	0.843	1.532	0.014	43.590	0.056
4.5	0.320	0.198	2.339	0.836	1.590	0.015	47.439	0.061
5	0.314	0.195	2.397	0.828	1.641	0.017	51.263	0.066
5.6	0.306	0.191	2.491	0.825	1.724	0.018	54.245	0.069
6	0.302	0.190	2.533	0.817	1.761	0.018	53.621	0.069
6.5	0.303	0.190	2.526	0.793	1.755	0.017	50.392	0.065
7	0.299	0.188	2.579	0.785	1.803	0.017	49.660	0.064

Table C3- 7: Flow parameters at Q_m for Test 4a: 30_1.5_180_i_DNF

Q_m	0.453 m³/s							
CH (m)	y (m)	R (m)	V (m/s)	EGL (m)	Fr	Local EGL slope (m/m)	Shear stress τ (kg/m²)	Shields's parameter ψ
3.5	0.349	0.212	2.218	0.876	1.454	N/A	N/A	N/A
4	0.348	0.212	2.228	0.855	1.462	0.015	50.334	0.067
4.5	0.341	0.208	2.296	0.847	1.520	0.016	53.379	0.071
5	0.335	0.205	2.357	0.839	1.572	0.017	56.425	0.075
5.6	0.326	0.201	2.453	0.835	1.655	0.017	54.897	0.073
6	0.322	0.199	2.498	0.828	1.694	0.023	71.727	0.095

CH (m)	y (m)	R (m)	V (m/s)	EGL (m)	Fr	Local EGL slope (m/m)	Shear stress τ (kg/m²)	Shields's parameter ψ
6.5	0.321	0.199	2.499	0.805	1.694	0.031	97.840	0.129
7	0.316	0.197	2.557	0.797	1.745	0.031	96.303	0.127

Table C3- 8: Flow parameters at Q_m for Test 4b: 30_1.5_180_ii_DNF

Q_m	0.456 m³/s							
CH (m)	y (m)	R (m)	V (m/s)	EGL (m)	Fr	Local EGL slope (m/m)	Shear stress τ (kg/m²)	Shields's parameter ψ
3.5	0.352	0.214	2.207	0.876	1.442	N/A	N/A	N/A
4	0.351	0.213	2.217	0.855	1.450	0.015	52.625	0.070
4.5	0.344	0.210	2.284	0.847	1.506	0.017	55.621	0.074
5	0.338	0.207	2.344	0.839	1.558	0.018	58.625	0.078
5.6	0.328	0.202	2.439	0.834	1.639	0.018	59.065	0.078
6	0.324	0.200	2.483	0.827	1.677	0.023	73.763	0.098
6.5	0.324	0.200	2.484	0.804	1.678	0.031	99.655	0.132
7	0.319	0.198	2.541	0.795	1.728	0.031	98.104	0.130

Table C3- 9: Flow parameters at Q_m for Test 5b: 20_0_140_ii

Q_m	0.060 m³/s							
CH (m)	y (m)	R (m)	V (m/s)	EGL (m)	Fr	Local EGL slope (m/m)	Shear stress τ (kg/m²)	Shields's parameter ψ
3.5	0.037	0.037	1.748	0.643	2.915	N/A	N/A	N/A
4	0.037	0.037	1.727	0.616	2.862	0.059	21.480	0.028
4.5	0.038	0.038	1.686	0.584	2.761	0.063	23.463	0.030
5	0.039	0.039	1.647	0.553	2.666	0.058	22.236	0.028
5.6	0.039	0.039	1.627	0.520	2.617	0.055	21.137	0.027
6	0.040	0.040	1.614	0.498	2.586	0.055	21.270	0.027

Table C3- 10: Flow parameters at Q_m for Test 5f: 20_0_140_vi

Q_m	0.066 m³/s							
CH (m)	y (m)	R (m)	V (m/s)	EGL (m)	Fr	Local EGL slope (m/m)	Shear stress τ (kg/m²)	Shields's parameter ψ
3.5	0.042	0.042	1.685	0.638	2.629	N/A	N/A	N/A
4	0.041	0.041	1.714	0.618	2.696	0.050	20.244	0.026
4.5	0.042	0.042	1.681	0.588	2.619	0.060	24.879	0.032
5	0.043	0.043	1.650	0.558	2.546	0.056	23.657	0.030
5.6	0.043	0.043	1.636	0.526	2.514	0.053	22.542	0.029

Table C3- 11: Flow parameters at Q_m for Test 6d: 20_0_180_iv

Q_m	0.099 m³/s							
CH (m)	y (m)	R (m)	V (m/s)	EGL (m)	Fr	Local EGL slope (m/m)	Shear stress τ (kg/m²)	Shields's parameter ψ
3.5	0.051	0.051	2.066	0.719	2.920	N/A	N/A	N/A
4	0.051	0.051	2.082	0.699	2.955	0.055	27.127	0.036
4.5	0.052	0.052	2.038	0.665	2.861	0.059	29.678	0.039
5	0.053	0.053	1.995	0.632	2.772	0.062	31.939	0.042
5.6	0.054	0.054	1.968	0.597	2.717	0.058	30.304	0.040
6	0.054	0.054	1.951	0.574	2.680	0.053	28.330	0.037
6.5	0.054	0.054	1.947	0.549	2.673	0.050	26.660	0.035

Table C3- 12: Flow parameters at Q_m for Test 6e: 20_0_180_v

Q_m	0.093 m³/s							
CH (m)	y (m)	R (m)	V (m/s)	EGL (m)	Fr	Local EGL slope (m/m)	Shear stress τ (kg/m²)	Shields's parameter ψ
3.5	0.048	0.048	2.066	0.717	3.004	N/A	N/A	N/A
4	0.048	0.048	2.087	0.697	3.052	0.053	25.008	0.033
4.5	0.049	0.049	2.045	0.663	2.958	0.067	31.777	0.042
5	0.050	0.050	2.003	0.630	2.869	0.061	29.803	0.039
5.6	0.050	0.050	1.980	0.596	2.818	0.057	28.122	0.037

CH (m)	y (m)	R (m)	V (m/s)	EGL (m)	Fr	Local EGL slope (m/m)	Shear stress τ (kg/m²)	Shields's parameter ψ
6	0.051	0.051	1.964	0.573	2.785	0.052	26.106	0.035
6.5	0.051	0.051	1.964	0.549	2.785	0.049	24.371	0.032

Table C3- 13: Flow parameters at Q_m for Test 6g: 20_0_180_vii

Q_m	0.121 m³/s							
CH (m)	y (m)	R (m)	V (m/s)	EGL (m)	Fr	Local EGL slope (m/m)	Shear stress τ (kg/m²)	Shields's parameter ψ
3.5	0.060	0.060	2.152	0.747	2.799	N/A	N/A	N/A
4	0.060	0.060	2.179	0.729	2.852	0.050	28.893	0.038
4.5	0.060	0.060	2.152	0.698	2.799	0.061	36.206	0.048
5	0.061	0.061	2.126	0.667	2.748	0.057	33.983	0.045
5.6	0.061	0.061	2.115	0.635	2.728	0.053	32.009	0.042
6	0.061	0.061	2.108	0.614	2.714	0.049	29.614	0.039
6.5	0.061	0.061	2.117	0.591	2.731	0.046	27.502	0.036
7	0.061	0.061	2.126	0.568	2.748	0.041	24.250	0.032
7.5	0.060	0.060	2.170	0.553	2.834	0.038	22.208	0.029

Table C3- 14: Flow parameters at Q_m for Test 7b: 20_1.5_140_ii_DNF

Q_m	0.526 m³/s							
CH (m)	y (m)	R (m)	V (m/s)	EGL (m)	Fr	Local EGL slope (m/m)	Shear stress τ (kg/m²)	Shields's parameter ψ
3.5	0.352	0.214	2.540	1.148	1.658	N/A	N/A	N/A
4	0.348	0.212	2.590	1.128	1.699	0.016	55.947	0.072
4.5	0.338	0.207	2.698	1.124	1.791	0.016	54.403	0.070
5	0.329	0.202	2.814	1.123	1.890	0.018	56.837	0.073
5.6	0.321	0.199	2.907	1.111	1.972	0.019	61.109	0.078
6	0.316	0.197	2.972	1.104	2.029	0.020	63.537	0.081
6.5	0.311	0.194	3.043	1.092	2.091	0.022	65.879	0.084
7	0.306	0.191	3.116	1.082	2.156	0.022	64.800	0.083

Table C3- 15: Flow parameters at Q_m for Test 8c: 20_1.5_180_iii

Q_m	0.379 m³/s							
CH (m)	y (m)	R (m)	V (m/s)	EGL (m)	Fr	Local EGL slope (m/m)	Shear stress τ (kg/m²)	Shields's parameter ψ
3.5	0.280	0.178	2.556	1.079	1.836	N/A	N/A	N/A
4	0.277	0.177	2.595	1.058	1.873	0.004	10.214	0.014
4.5	0.269	0.173	2.705	1.056	1.976	0.009	22.593	0.030
5	0.261	0.169	2.822	1.057	2.088	0.014	36.718	0.049
5.6	0.255	0.166	2.906	1.044	2.168	0.017	41.595	0.055
6	0.252	0.164	2.964	1.036	2.225	0.018	44.744	0.059
6.5	0.247	0.162	3.039	1.028	2.298	0.018	43.943	0.058
7	0.243	0.159	3.117	1.021	2.376	0.017	39.508	0.052

Table C3- 16: Flow parameters at Q_m for Test 8d: 20_1.5_180_iv

Q_m	0.326 m³/s							
CH (m)	y (m)	R (m)	V (m/s)	EGL (m)	Fr	Local EGL slope (m/m)	Shear stress τ (kg/m²)	Shields's parameter ψ
3.5	0.243	0.160	2.667	1.072	2.029	N/A	N/A	N/A
4	0.242	0.159	2.682	1.047	2.044	0.007	15.526	0.021
4.5	0.236	0.156	2.777	1.044	2.138	0.015	34.841	0.046
5	0.230	0.153	2.876	1.043	2.239	0.020	44.276	0.059
5.6	0.227	0.151	2.928	1.023	2.292	0.024	52.465	0.069
6	0.225	0.150	2.964	1.010	2.328	0.031	69.050	0.091
6.5	0.223	0.149	3.009	0.994	2.375	0.032	69.498	0.092
7	0.220	0.148	3.056	0.979	2.423	0.031	66.574	0.088

Table C3- 17: Flow parameters at Q_m for Test 9d: 10_0_140_iv

Q_m	0.041 m³/s							
CH (m)	y (m)	R (m)	V (m/s)	EGL (m)	Fr	Local EGL slope (m/m)	Shear stress τ (kg/m²)	Shields's parameter ψ
3.5	0.026	0.026	1.695	0.843	3.360	N/A	N/A	N/A

CH (m)	y (m)	R (m)	V (m/s)	EGL (m)	Fr	Local EGL slope (m/m)	Shear stress τ (kg/m²)	Shields's parameter ψ
4	0.025	0.025	1.774	0.809	3.596	0.069	16.665	0.021
4.5	0.025	0.025	1.785	0.763	3.629	0.078	18.877	0.024
5	0.024	0.024	1.872	0.731	3.899	0.092	21.298	0.027

Table C3- 18: Flow parameters at Q_m for Test 9e: 10_0_140_v

Q_m	0052 m³/s							
CH (m)	y (m)	R (m)	V (m/s)	EGL (m)	Fr	Local EGL slope (m/m)	Shear stress τ (kg/m²)	Shields's parameter ψ
3.5	0.029	0.029	1.933	0.890	3.639	N/A	N/A	N/A
4	0.028	0.028	1.991	0.854	3.807	0.072	19.747	0.025
4.5	0.028	0.028	1.981	0.804	3.776	0.085	23.434	0.030
5	0.027	0.027	2.043	0.769	3.954	0.100	26.686	0.034

Table C3- 19: Flow parameters at Q_m for Test 10b: 10_0_180_ii

Q_m	0.103 m³/s							
CH (m)	y (m)	R (m)	V (m/s)	EGL (m)	Fr	Local EGL slope (m/m)	Shear stress τ (kg/m²)	Shields's parameter ψ
3.5	0.049	0.049	2.229	0.973	3.203	N/A	N/A	N/A
4	0.047	0.047	2.335	0.949	3.435	0.049	22.629	0.030
4.5	0.046	0.046	2.399	0.915	3.577	0.052	23.431	0.031
5	0.044	0.044	2.522	0.897	3.857	0.049	20.912	0.028
5.6	0.042	0.042	2.612	0.861	4.065	0.059	24.490	0.032

Table C3- 20: Flow parameters at Q_m for Test 10c: 10_0_180_iii

Q_m	0.070 m³/s							
CH (m)	y (m)	R (m)	V (m/s)	EGL (m)	Fr	Local EGL slope (m/m)	Shear stress τ (kg/m²)	Shields's parameter ψ
3.5	0.040	0.040	1.898	0.894	3.043	N/A	N/A	N/A
4	0.038	0.038	2.006	0.867	3.308	0.055	20.234	0.027

CH (m)	y (m)	R (m)	V (m/s)	EGL (m)	Fr	Local EGL slope (m/m)	Shear stress τ (kg/m²)	Shields's parameter ψ
4.5	0.036	0.036	2.070	0.831	3.466	0.057	20.252	0.027
5	0.034	0.034	2.200	0.810	3.798	0.057	19.054	0.025
5.6	0.033	0.033	2.293	0.772	4.040	0.061	19.783	0.026
6	0.032	0.032	2.359	0.748	4.216	0.078	24.378	0.032
6.5	0.032	0.032	2.370	0.702	4.246	0.093	28.944	0.038

Table C3- 21: Flow parameters at Q_m for Test 10d: 10_0_180_iv

Q_m	0.074 m³/s							
CH (m)	y (m)	R (m)	V (m/s)	EGL (m)	Fr	Local EGL slope (m/m)	Shear stress τ (kg/m²)	Shields's parameter ψ
3.5	0.040	0.040	1.948	0.905	3.095	N/A	N/A	N/A
4	0.038	0.038	2.066	0.880	3.379	0.050	18.862	0.025
4.5	0.037	0.037	2.139	0.846	3.560	0.051	18.349	0.024
5	0.035	0.035	2.282	0.829	3.922	0.056	18.859	0.025
5.6	0.033	0.033	2.390	0.795	4.204	0.056	18.006	0.024
6	0.032	0.032	2.468	0.775	4.411	0.071	22.091	0.029
6.5	0.032	0.032	2.491	0.732	4.474	0.087	26.895	0.036

Table C3- 22: Flow parameters at Q_m for Test 11a: 10_1.5_140_i

Q_m	0.349 m³/s							
CH (m)	y (m)	R (m)	V (m/s)	EGL (m)	Fr	Local EGL slope (m/m)	Shear stress τ (kg/m²)	Shields's parameter ψ
3.5	0.221	0.148	3.256	1.435	2.578	N/A	N/A	N/A
4	0.214	0.145	3.398	1.428	2.725	0.008	16.116	0.021
4.5	0.208	0.141	3.551	1.427	2.886	0.014	27.846	0.036
5	0.203	0.138	3.665	1.414	3.009	0.014	27.196	0.035
5.6	0.197	0.135	3.811	1.404	3.166	0.018	34.354	0.044
6	0.193	0.133	3.913	1.400	3.279	0.019	36.600	0.047
6.5	0.189	0.131	4.019	1.388	3.396	0.033	61.388	0.079

CH (m)	y (m)	R (m)	V (m/s)	EGL (m)	Fr	Local EGL slope (m/m)	Shear stress τ (kg/m²)	Shields's parameter ψ
7	0.186	0.129	4.101	1.367	3.487	0.040	73.762	0.094
7.5	0.183	0.128	4.185	1.348	3.581	0.050	89.905	0.115
8	0.182	0.127	4.241	1.317	3.645	0.061	109.380	0.140

Table C3- 23: Flow parameters at Q_m for Test 12a: 10_1.5_180_i

Q_m	0.351 m³/s							
CH (m)	y (m)	R (m)	V (m/s)	EGL (m)	Fr	Local EGL slope (m/m)	Shear stress τ (kg/m²)	Shields's parameter ψ
3.5	0.229	0.152	3.121	1.399	2.436	N/A	N/A	N/A
4	0.222	0.149	3.253	1.387	2.571	0.019	41.272	0.055
4.5	0.215	0.145	3.395	1.380	2.717	0.025	51.845	0.069
5	0.211	0.143	3.501	1.362	2.829	0.031	64.630	0.086
5.6	0.205	0.139	3.635	1.345	2.972	0.031	62.843	0.083
6	0.201	0.137	3.730	1.337	3.074	0.034	67.810	0.090
6.5	0.197	0.135	3.828	1.320	3.180	0.042	82.105	0.109
7	0.194	0.134	3.903	1.294	3.262	0.051	96.287	0.127

Table C3- 24: Flow parameters at Q_m for Test 12b: 10_1.5_180_ii

Q_m	0.305 m³/s							
CH (m)	y (m)	R (m)	V (m/s)	EGL (m)	Fr	Local EGL slope (m/m)	Shear stress τ (kg/m²)	Shields's parameter ψ
3.5	0.208	0.141	3.090	1.368	2.508	N/A	N/A	N/A
4	0.202	0.138	3.225	1.357	2.652	0.017	34.262	0.045
4.5	0.195	0.134	3.369	1.351	2.809	0.024	45.176	0.060
5	0.191	0.132	3.475	1.333	2.926	0.031	58.399	0.077
5.6	0.185	0.129	3.610	1.316	3.075	0.031	56.747	0.075
6	0.182	0.127	3.704	1.308	3.182	0.036	63.655	0.084
6.5	0.178	0.125	3.800	1.290	3.291	0.045	78.011	0.103
7	0.176	0.124	3.871	1.263	3.372	0.054	92.280	0.122

APPENDIX D: MICROSOFT EXCEL MODEL

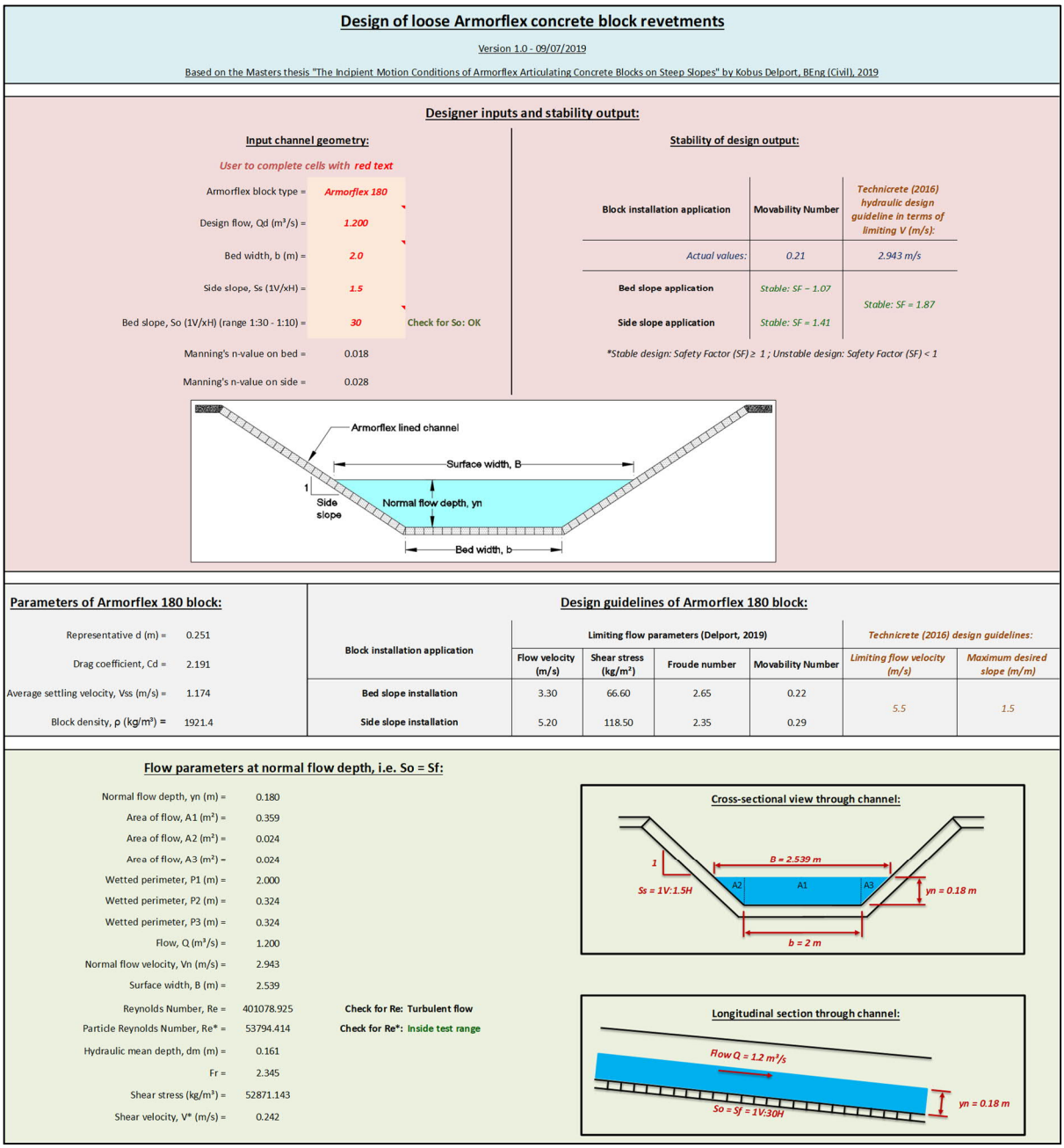

Figure D- 1: Snip image of the calculation sheet of the Microsoft Excel Armorflex design model